

DISS. ETH NO. 26601

**Molecular mechanism of Arrestin-3 Recruitment and Activation by G  
Protein-Coupled Receptors**

A thesis submitted to attain the degree of  
DOCTOR OF SCIENCES of ETH ZURICH  
(Dr. sc. ETH Zürich)

Presented by

**Benoît Meger**

Doctor of Pharmacy (PharmD), University of Montpellier, France  
Master of Science (MSc), University of Nîmes, France

Born on 29.08.1992

Citizen of France

Accepted on the recommendation of  
Prof. Gebhard Schertler, examiner  
Dr. Maria Waldhoer, scientific co-supervisor  
Dr. Philipp Berger, scientific co-supervisor  
Prof. Sabine Werner, co-examiner

2020



# Content

Acknowledgements.....	1
Abbreviations.....	2
Summary.....	3
Résumé .....	4
<b>INTRODUCTION .....</b>	<b>6</b>
A. G protein Coupled Receptors.....	6
B. G proteins .....	6
C. Arrestin .....	8
C.1. Visual and $\beta$ arrestins.....	8
C.2. Arrestin structure.....	8
C.3. Arrestin activation.....	9
C.4. The role of arrestins in GPCR trafficking .....	11
C.5. The role of arrestins in regulating GPCR signaling .....	11
C.6. Arrestin scaffold function .....	12
D. GPCR activation .....	13
D.1. Core activation of a GPCR upon ligand activation.....	13
D.2. Phosphorylation of the carboxy-terminus of GPCRs by GPCR Related Kinases .....	13
D.3. The GPCR-arrestin interface .....	15
D.4. Biased signaling.....	18
E. Aim of thesis .....	19
<b>CHAPTER 1 – An alanine scan on arrestin-3 for assessing the requirements of arrestin-3 recruitment to the <math>\beta</math>2-adrenergic receptor.....</b>	<b>22</b>
<b>Material and methods .....</b>	<b>22</b>
1.1. PCR-driven mutagenesis .....	22
1.2. Alanine arrestin-3 mutant screening by split nanoluciferase.....	25
1.2.1. Cell transfection.....	26
1.2.2. EGFP fluorescence and split nanoluc assay .....	28
1.2.3. Data analysis.....	29
1.3. Bioluminescence Resonance Energy Transfer (BRET) assay.....	30
1.3.1. Cell transfection.....	31
1.3.2. BRET measurement.....	32
1.3.3. Data analysis .....	32
<b>Results .....</b>	<b>34</b>
1.4. Alanine scan approach for the recruitment of arrestin-3 to $\beta$ 2AR.....	34

1.4.1. Large-scale screening of single point alanine mutants of arrestin-3 .....	34
1.4.2. Ligand screen of “red-line” mutants by split nanoluc .....	36
1.5. Validation of arrestin-3 alanine mutant split nanoluc results by a BRET assay .....	40
Discussion, chapter 1 .....	42
 CHAPTER 2 – Engineered arrestins for the stabilization of $\beta$ 1-adrenergic receptor variants .....	48
Material and methods .....	48
2.1. Combined alanine mutants of arrestin-3 .....	48
2.2. Variants of the turkey $\beta$ 1-adrenergic receptor .....	49
Results .....	50
2.4. Recruitment of single point pre-activated mutants to the $\beta$ 2-adrenergic receptor .....	50
2.5. Recruitment of combined arrestin-3 mutants to the $\beta$ 2-adrenergic receptor and variants of the $\beta$ 1-adrenergic receptor .....	52
Discussion, chapter 2 .....	56
 CHAPTER 3 – Recruitment of arrestin 1/2/3 and constrained arrestin-3 mutants to rhodopsin by centrifugal pull-downs .....	58
Material and methods .....	58
3.1. Design of di-cysteine and glycine mutants of arrestin-3 .....	58
3.1.1. Constrained arrestin-3 mutants and cloning .....	59
3.2.2. Expression of arrestin-3 mutants in <i>Escherichia Coli</i> .....	62
3.2.3. Purification of arrestin-3 mutants .....	64
3.2. Limited trypsin digestion of arrestin-3 mutants .....	68
3.3. Circular dichroism .....	69
3.4. Mass spectrometry .....	70
3.4.1. Crosslinking efficiency of constrained arrestin-3 mutants .....	70
3.4.2. Phosphorylation state of PROS membrane preparations .....	71
3.5. Centrifugal pull-down assays .....	72
3.5.1. Preparation of Rod Outer Segment (ROS) membranes .....	73
3.5.2. Centrifugal pull-downs .....	73
3.5.3. Data analysis .....	74
Results .....	74
3.6. Purification of arrestin-3 di-cysteine and glycine mutants .....	75
3.6.1. Optimization of arrestin-3 purification .....	75
3.6.2. Expression of arrestin-3 mutants .....	77
3.7. Protein characterization of di-cysteine and glycine mutants .....	78
3.7.1. Limited trypsinization of arrestin-3 mutants .....	78
3.7.2. Thermal stability of arrestin-3 mutants by circular dichroism .....	80

3.7.3. Mass spectrometry.....	83
3.8. Phosphorylation state of PROS membrane preparations.....	88
3.9. Centrifugal pull-downs.....	90
3.9.1. Salt screening on arrestin-3.....	90
3.9.2. Comparison of arrestin 1/2/3.....	92
3.9.3. Arrestin-3 di-cysteine mutants: receptor titrations.....	98
Discussion, chapter 3.....	103
CONCLUSION.....	108
APPENDIX.....	110
REFERENCES.....	120
CURRICULUM VITAE.....	131

## **Publication**

- Patent EP19153159: “ $\beta$ -arrestin mutants”, January 2019, Benoit Meger, Mirjam Zimmermann, Martin Konrad Ostermaier, Maria Waldhoer, Philipp Berger.

## **Acknowledgements**

To my sister Laura, for her joie-de-vivre, her great spirit and her contagious laugh.

To Jonathan, and his indefectible support in all the highs and lows of life.

To my parents, who gave me all the tools I needed to achieve my goals.

To my grandparents, who's presence in my life is more precious than ever.

To my PSI colleagues and friends, who were always present for me both in and out of the lab.

To Anaïs, Bastien, Tinu, Agnès & Blandine, for their constant support from very far away.

To Maria Waldhoer, Philipp Berger and Martha Sommer, for their mentorship and advice.

To Prof. Gebhard Schertler, to have trusted me throughout this project.

## Abbreviations

<b>AP-2</b>	Adaptor Protein 2
<b>Arr1/2/3</b>	Arrestin-1, -2 or -3
<b>AUC</b>	Area Under Curve
<b>β1AR/ β2AR</b>	β <sub>1</sub> or β <sub>2</sub> -adrenergic Receptor
<b>B6/B44</b>	turkey β1AR variants
<b>BRET</b>	Bioluminescence Resonance Emission Transfer
<b>CAAX</b>	Protein prenylation motif
<b>CMV</b>	CytoMegalovirus promoter
<b>DTT</b>	1,4-DiThioThreitol
<b>EGFP</b>	Engineered Green Fluorescent Protein
<b>ERK1/2</b>	Extracellular signal-Regulated Kinases 1 and 2
<b>ESI-ToF</b>	ElectroSpray ionization-Time Of Flight mass spectrometry
<b>ExpGFP</b>	(mutant over WT) GFP fluorescence ratio
<b>GPCRs</b>	G protein Coupled Receptors
<b>GRK</b>	GPCR-Related Kinase
<b>HEK293</b>	Human Embryonic Kidney cells
<b>HPLC-MS</b>	High Performance Liquid Chromatography-Mass Spectrometry
<b>IAA</b>	Iodoacetamide
<b>IC<sub>50</sub></b>	Half maximal Inhibitory Concentration
<b>ICL</b>	IntraCellular Loop
<b>IMAC</b>	Immobilized Metal Affinity Chromatography
<b>MAPK</b>	Mitogen Activated Protein Kinase
<b>MW</b>	Molecular Weight
<b>OpS</b>	Opsin
<b>PCR</b>	Polymerase Chain Reaction
<b>pEC<sub>50</sub></b>	log (half maximal Effective Concentration)
<b>R<sub>AUC</sub></b>	(WT over mutant) AUC ratio
<b>Rluc8</b>	Renilla luciferase 8
<b>ROS/PROS</b>	Rod Outer Segment/ Phosphorylated ROS
<b>SCAR3</b>	Split nanoluC ARrestin 3 cell line
<b>SDS-PAGE</b>	Sodium Dodecyl Sulfate–PolyAcrylamide Gel Electrophoresis
<b>Split nanoluc</b>	Split nanoluciferase assay (Promega)
<b>TCEP</b>	Tris(2-CarboxyEthyl)Phosphine
<b>TM</b>	TransMembrane domain

## Summary

Arrestins are 45-47 kDa cytosolic proteins that constitute a family of 4 members in mammals and are important regulators of G protein-coupled receptor (GPCR) signaling. Arrestins play key roles in desensitizing GPCRs to G protein coupling, and some arrestins also regulate GPCR internalization and cellular trafficking. Arrestin-1 and arrestin-4 are primarily expressed in the retina and regulate the activity of the opsins, the light-sensitive GPCRs involved in photo-transduction in the rod and cone cells. Arrestin-2 and arrestin-3, the so-called “ $\beta$ -arrestins”, are ubiquitously expressed and regulate hundreds of different GPCRs. Over the past three decades, the mechanisms of arrestin recruitment and activation by GPCRs have mainly been investigated through structural and mutagenesis studies of arrestin-1. Due to their high structural and sequence similarity, the other arrestins were assumed to operate in a similar manner as arrestin-1, although more recent studies suggest significant mechanistic and functional differences between the different arrestins. Currently the molecular processes behind arrestin-2/3/4 recruitment and activation by GPCRs is not as well understood as for arrestin-1. This thesis aims at filling this gap in knowledge, specifically regarding the molecular mechanisms underlying the recruitment and activation of the human arrestin-3 to several GPCRs.

The first part of the thesis reports on the recruitment of arrestin-3 mutants, derived from an alanine-scan library, to the human  $\beta$ 2-adrenergic receptor ( $\beta$ 2AR) in living cells. A novel split-nanoluciferase assay was employed, which is based on protein-fragment complementation and has several advantages over other currently available reporter enzyme strategies. The objectives were to i) validate this new split nanoluc approach and ii) to assess possible new binding modes of arrestin-3 to the  $\beta$ 2AR. However, technical limitations of the split nanoluc assay made the assay inconclusive.

The second part of this thesis describes double and triple alanine mutants of arrestin-3, which were anticipated to simultaneously disrupt the polar core and the three-element interaction, two structural elements important in stabilizing the basal arrestin conformation. The mutants I386A+T299A and I386A+T299A+R166A in particular formed stable complexes with the  $\beta$ 1-adrenergic receptor. The results from this study are part of the patent EP19153159 application “ $\beta$ -arrestin mutants” filed in January 2019.

The third part of this thesis describes a targeted mutagenesis approach, whereby key structural features of arrestin-3 involved in GPCR recruitment and arrestin activation were constrained by intramolecular cysteine crosslinking or inactivated by glycine mutations. After extensive characterization by mass spectrometry, circular dichroism and limited trypsin digest, the recruitment of different arrestins and constrained mutants of arrestin-3 to various activated states of rhodopsin were assessed by centrifugal pull-down analysis. In comparison to arrestin-1, the phosphorylated receptor C-terminus and phospholipid membrane play a more significant role in the recruitment of arrestin-2 and arrestin-3 to rhodopsin. Spontaneous intramolecular crosslinking in arrestin-3 was found to be particularly efficient for the restriction of loop movements. Restraining inter-domain rotation, a hallmark of arrestin activation, had the most dramatic effect on the recruitment of arrestin-3 to phosphorylated and light-activated rhodopsin.



## Résumé

Les arrestines sont des protéines cytosoliques de 45 à 47 kDa qui constituent une famille de 4 membres chez les mammifères. Les arrestines ont un rôle régulateur sur les voies de signalisation associées aux récepteurs couplés aux protéines G (RCPG) où elles participent à la désensibilisation de ces derniers vis-à-vis des protéines G. Certaines arrestines sont également impliquées dans l'internalisation et le trafic cellulaire des RCPGs. Les arrestines-1 et -4 sont principalement exprimées dans les cellules dites cônes et bâtonnets de la rétine et régule l'activité des opsines, RCPGs impliqués dans la photo-transduction. Les arrestines -2 et -3, autrement appelées  $\beta$ -arrestines, sont ubiquitairement exprimées et régulent l'activité de centaines de RCPGs. Depuis trois décennies, les mécanismes de recrutement aux RCPGs et d'activation de l'arrestine ont été exploré à travers des études structurales et de mutagenèse effectuées sur l'arrestine-1. À cause de la grande similarité séquentielle et structurale entre arrestines, ces mécanismes ont été présumés comparable, malgré l'émergence de récentes études soulignant des différences mécanistiques et fonctionnelles entre arrestines. Actuellement, les processus moléculaires régissant le recrutement des arrestines 2/3/4 par les RCPGs ne sont toujours pas clairement élucidés, contrairement à l'arrestine-1. Cette thèse vise à explorer ces questions à travers les mécanismes moléculaires impliqués dans le recrutement et l'activation de l'arrestine-3 humaine par plusieurs RCPGs.

La première partie de cette thèse est consacrée au recrutement de mutants alanine de l'arrestine-3 par le récepteur  $\beta$ 2-adrenergique (R $\beta$ 2A) *in cellulo*. Pour cela, une nouvelle méthode d'analyse appelée split nanoluciferase a été employée. Ce dosage est basé sur la complémentation de fragments protéiques et possède plusieurs avantages sur les autres stratégies de révélation enzymatique en vigueur. Les objectifs de ce projet furent de i) valider le dosage split nanoluc et ii) de détecter de nouveaux modes d'interaction de l'arrestin-3 avec le R $\beta$ 2A. Cependant, les limitations techniques de cette méthode n'ont pas permis de conclure sur ce dernier objectif.

La seconde partie de cette thèse se concentre sur l'utilisation de mutants di-alanine et tri-alanine de l'arrestine-3, visant à déstabiliser les poches d'acides aminés appelés « polar core » et « three-element interaction », deux éléments stabilisateurs de l'arrestin-3 favorisant le maintien de la protéine dans son état basal. Les mutants I386A+T299A and I386A+T299A+R166A en particulier ont permis la formation de complexes stables avec le récepteur  $\beta$ 1-adrenergique. Les résultats de cette étude ont été inclus dans la soumission d'un brevet européen (EP19153159 "β-arrestin mutants") en Janvier 2019.

La troisième partie de cette thèse fait état d'une approche de mutagenèse ciblée dans laquelle des éléments structuraux de l'arrestine-3 possiblement impliqués dans le recrutement aux RCPGs et dans l'activation de l'arrestine, furent contraints par l'introduction de ponts disulfures intramoléculaires ou par mutations glycine. Après une caractérisation par spectrométrie de masse, dichroïsme circulaire et trypsinisation limitée, le recrutement par plusieurs états d'activation de la rhodopsin de différentes arrestines ainsi que des mutants de l'arrestin-3 structurellement contraints ont été étudiés par précipitation. Comparés à l'arrestine-1, l'extrémité phosphorylée C-terminale de la rhodopsine et les phospholipides de la membrane plasmique jouent un rôle plus prépondérant dans le recrutement de l'arrestine-2 et -3 par la rhodopsine. La formation de ponts disulfures spontanés fut particulièrement efficace dans la restriction des régions flexibles de l'arrestine. La restriction de la rotation inter-domaine de l'arrestin-3, une étape cruciale pour l'activation de la protéine, eut l'effet le plus drastique sur le recrutement de l'arrestine-3 par la rhodopsin phosphorylée et stimulée par la lumière.



# INTRODUCTION

## A. G protein Coupled Receptors

From bacteria to complex eukaryotes, cellular organisms need to sense their environment for nutrition, adaptation, communication and other critical functions. G protein Coupled Receptors (GPCRs) constitute a large family of membrane receptors and represent around 2% of the encoded genome in humans. They are known to cover a majority of vital functions from light absorption to hormone recognition<sup>1,2</sup> and as such embody a great source of pharmacological targets. This superfamily of receptors is composed of class A (Rhodopsin-like receptors), class B (secretin and adhesion receptors), class C (glutamate receptors) and so-called frizzled GPCRs<sup>1</sup>. Located at the plasma membrane of cells, GPCRs (figure 1) are generally composed of an N-terminal sequence facing the environment, seven transmembrane  $\alpha$ -helices (TM), three intra- (ICL) and three extracellular loops, a cytosolic  $\alpha$ -helix (helix 8) and a more or less structured carboxy-terminus facing the cytoplasm. The size and functional relevance of each region vary dramatically across receptors<sup>3</sup>.

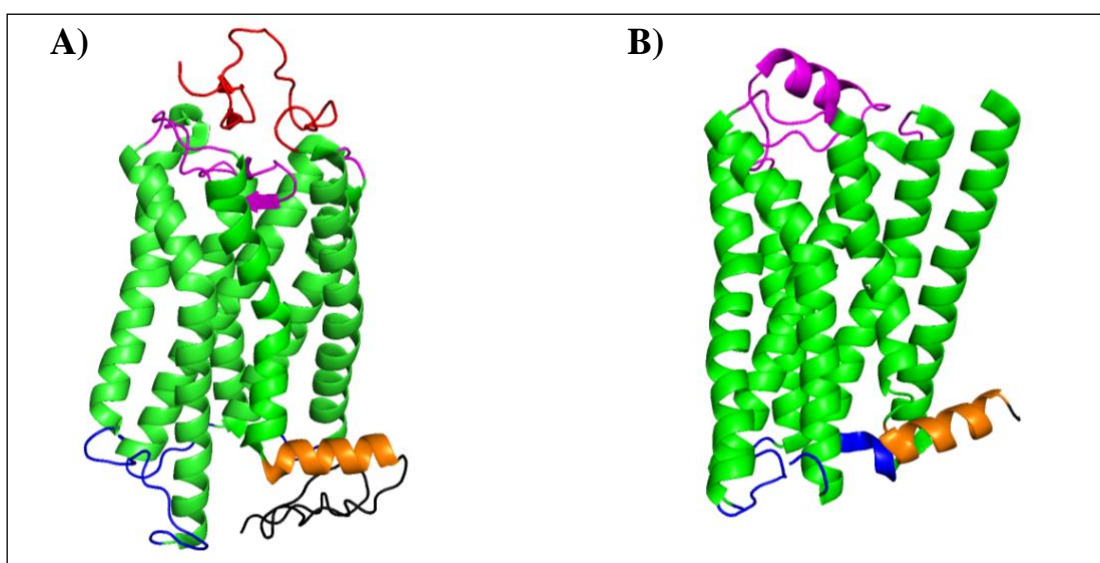


**Figure 1.** Structures of A) bovine rhodopsin<sup>4</sup> (PDB 2G87) and B) the human  $\beta$ 2-adrenergic receptors<sup>5</sup> (PDB 6PS4). Red: N-terminal region; green: transmembrane  $\alpha$ -helices; magenta: extracellular loops; blue: intracellular loops; orange: cytoplasmic  $\alpha$ -helix and black: C-tail.

## B. G proteins

In the early 1970s, heterotrimeric G proteins were discovered as the main signaling partners of GPCRs (figure 2) and their mechanism of activation has been well-described since then<sup>6,7</sup>. Upon GPCR stimulation, G proteins are recruited to the receptor as a tri-complex, consisting of the subunits  $G\alpha$ ,  $G\beta$

and  $G\gamma$ ). The GPCR-G protein interaction triggers the exchange of Guanosine Di-Phosphate (GDP) by Guanosine Tri-Phosphate (GTP) in the  $G\alpha$  subunit, which leads to the dissociation of the GTP-bound  $G\alpha$  subunit from  $G\beta\gamma$ . In its free form, GTP-bound  $G\alpha$  activates ( $G_{\alpha s}$  = stimulatory G protein) or inactivates ( $G_{\alpha i}$  = inhibitory G protein) nearby adenylyl cyclases (ACs), which leads to an increase (with  $G_{\alpha s}$ ) or decrease (with  $G_{\alpha i}$ ) in cyclic Adenosine Mono Phosphate (cAMP). Then, the GTPase activity of  $G\alpha$  terminates the signaling event, allowing the re-association of the tri-complex  $G\alpha\beta\gamma$  in its nucleotide-free form with the GPCR<sup>8</sup>. The activated G protein signaling cascade is specific of the  $G\alpha$  subtype involved. The subtypes  $G_{\alpha s}$ ,  $G_{\alpha i}$ ,  $G_{\alpha q}$  and  $G_{\alpha_{12/13}}$  constitute the four families of  $G\alpha$  proteins and are highly conserved among species. The preference of GPCRs towards certain G protein subtypes has been numerously reported. For example, the  $\beta$ 2-adrenergic receptor ( $\beta$ 2AR) couples primarily to  $G_{\alpha s}$  but also to  $G_{\alpha i}$ <sup>9</sup>, whereas the D2 dopamine receptor couples mainly to  $G_{\alpha i}$ <sup>10</sup>. The exact mechanism behind this functional selectivity has not been clearly elucidated, but is suggested to be dependent on structural differences among GPCRs, ligand specificity and the dynamic nature of GPCR activated conformations. Additionally, an allosteric effect between G proteins and ligands has been reported by structural<sup>8,11</sup> and functional<sup>12</sup> studies, suggesting that G protein coupling increases ligand affinity to  $\beta$ 2AR by stabilizing the receptor in a “closed” conformation that restricts ligand access to its binding pocket.

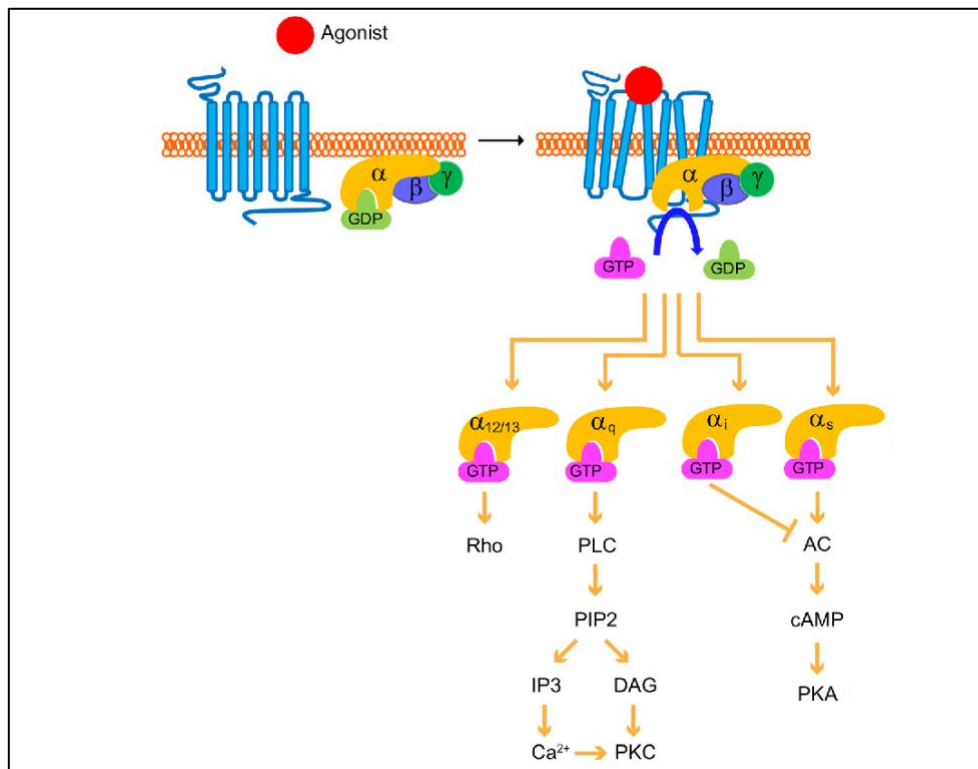


**Figure 2.** Schematic representation of the four main G protein pathways.  $\alpha$ ,  $\beta$ ,  $\gamma$ : G protein subunits. The four  $G\alpha$  subtypes are represented:  $G_{\alpha s}$  (stimulatory),  $G_{\alpha i}$  (inhibitory),  $G_{\alpha q}$  and  $G_{12/13}$ . AC: adenylyl cyclase. cAMP: cyclic adenosine monophosphate. PKA: Protein kinase A. PLC: phospholipase C. PIP2: phosphatidylinositol 4,5-bisphosphate. DAG: diacylglycerol. IP3: inositol triphosphate. PKC: protein kinase C. Rho: Ras homologous proteins. Image adapted from Wang *et al.*, 2018<sup>13</sup>.

## C. Arrestin

### C.1. Visual and $\beta$ arrestins

Arrestins are cytoplasmic proteins recruited to stimulated GPCRs. The arrestin family is composed of four highly conserved members in vertebrates (table 1):

- Arrestin-1 (or visual arrestins) and arrestin-4 are almost entirely expressed in rod and cone photoreceptor cells of the retina. In nature, arrestin-1 couples to rhodopsin, a light sensitive GPCR. Arrestin-1 is the preferred arrestin in terms of recruitment to rhodopsin<sup>12-14</sup>, although in vitro studies proved that arrestin-1 is also capable to recognize other GPCRs<sup>16</sup>. A naturally occurring splice variant of arrestin-1 (called p44) is also involved in the termination of phototransduction<sup>17-19</sup>.
- Arrestin-2 and arrestin-3 (or  $\beta$ arrestins) are ubiquitously expressed in tissues and are recruited to GPCRs, often with a noticeable preference for arrestin-2 or arrestin-3. For example, the beta-adrenergic receptor family favors coupling to arrestin-3<sup>20,21</sup>, whereas the ghrelin receptor prioritizes arrestin-2<sup>22</sup>. Interestingly, the expression ratio of arrestin-1 versus arrestin-2 varies dramatically across tissues, which in itself is thought to regulate GPCR signaling<sup>16</sup>.

		Bovine	Human		
		Arrestin-1	Arrestin-1	Arrestin-2	Arrestin-3
Bovine	Arrestin-1	X	92%	72%	69%
Human	Arrestin-1	92%	X	73%	69%
	Arrestin-2	72%	73%	X	87%
	Arrestin-3	69%	69%	87%	X

**Table 1.** Protein sequence homology of arrestins (red: strong; yellow: intermediate; green: low relative homology scores). Alignments were performed using the online Basic Local Alignment Search Tool (BLAST, US National Library of Medicine)<sup>23,24</sup>.

### C.2. Arrestin structure

In this section, the structural features of arrestins are described using the bovine arrestin-1 as an example. Bovine arrestin-1 (figure 3) is a cytosolic protein (45 kDa) composed of two large globular domains called N- and C-domains. These two semi-symmetric regions are mainly composed of antiparallel  $\beta$ -sheets connected by a flexible hinge region of 12 amino acids (from H179 to E191). Between the N- and C-domains, the so-called central crest is partially obstructed in the inactive arrestin

state by flexible loops emerging from the two globular domains. In the upper section of the central crest lie: the finger loop (Y67-F79), the C-loop (V247-D253) and the middle loop (L132-C143). On the lower side of the central crest, the gate loop (N287-T305) located in the front opposes the back loop (I311-K318). On the C-edge of the protein, the so-called 199-loop (F197-D200) and 344-loop (V335-S345) prevail. The carboxy(C)-terminus of arrestin is composed of a flexible and unstructured sequence called the “C-tail” (P360-E404) that mainly rests on the N-domain in the basal arrestin state. An extensive network of hydrogen bonds called the polar core connects the N-domain of arrestin (D30 and R175) to the gate loop (D296 and D303). Finally, the so-called three-element interaction of arrestin is composed of hydrophobic residues spanning the N-domain (V11, L103, L107, L111) and the C-tail (F375 and F377).

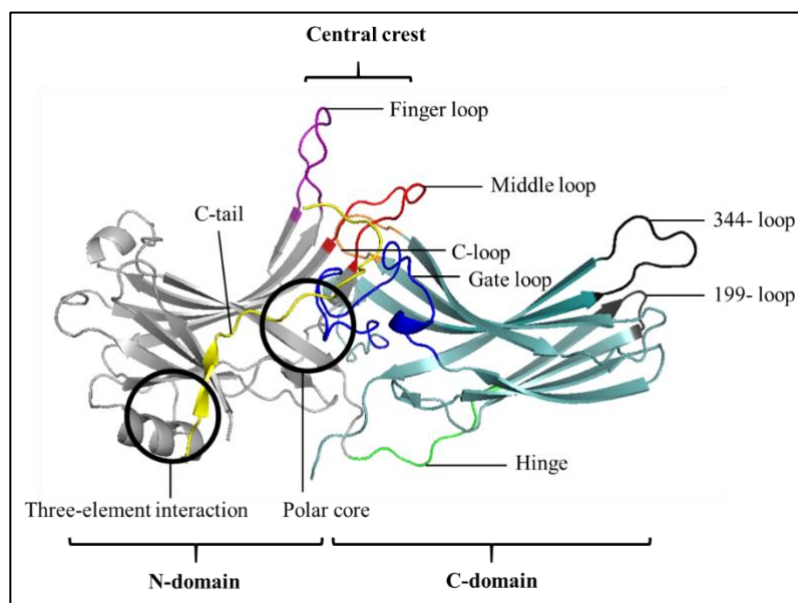


**Figure 3.** Crystallographic structure of inactive bovine arrestin-1 (PDB 1CF1). Grey: N-domain. Turquoise: C-domain. Green: hinge (H179-E191). Purple: finger loop (Y67-F79). Orange: C-loop (V247-D253). Red: middle loop (L132-C143). Dark blue: gate loop (N287-T305). Black: 199- (F197-D200) and 344- (V335-S345) loops on the C-edge. Yellow: C-tail (P360-E404). The sequence of amino acids from E394 to E404 is not resolved in this structure.

### C.3. Arrestin activation

In the basal state, arrestin is stabilized by three structural features (figures 3 and 4): the C-tail, the polar core (a conserved pocket of arginine and aspartic acid residues<sup>25-27</sup> and the three element interaction (a pocket of hydrophobic residues<sup>27-29</sup>). Before activation, the C-tail of arrestin lies on the N-domain and acts as the main inhibitor of arrestin activation<sup>18,30</sup>. In the presence of an activated GPCR, the C-tail of arrestin is replaced by the phosphorylated C-terminus of the receptor: this phenomenon is called the C-tail exchange or C-tail interaction. As a result, the C-tail release induces the disruption of

the polar core<sup>25–27</sup> and the three element interaction<sup>27–29</sup>. At this stage, arrestin is found in a so-called pre-activated state similar to p44, a splice variant of arrestin-1 which lacks the inhibitory C-tail<sup>18,30</sup>. Crystal structures of p44 and arrestin-2/V2Rpp<sup>31</sup> (V2Rpp being a peptidomimetic of the phosphorylated C-terminus of the vasopressin receptor 2) reveal that fully engaged arrestins undergo an intramolecular 20–21° rotation between the N- and C-domains. This inter-domain rotation has been used as the hallmark of complete arrestin activation ever since<sup>32</sup>. In the fully activated arrestin structure, the central crest is unveiled, resulting in the exposure of receptor binding sites. Flexible loops of the central crest are now extended in an upward conformation (finger loop), moved to the back of the central crest (C-loop), extended on the N-domain (gate loop) or simply away from the main arrestin body (middle loop and back loop)<sup>33,34</sup>. In structures where arrestin interacts with rhodopsin<sup>34</sup> or inositol hexakisphosphate (IP6)<sup>33</sup>, the finger loop is also found in a short helix conformation. However, recent molecular dynamics simulations and site-directed fluorescence quenching data<sup>35</sup> have shown that the helix rearrangement underwent finger loop is independent from the rotation event.

Interestingly, the network of hydrogen bonds governing the polar core regions of arrestin-2 and arrestin-3 are weaker than that of arrestin-1<sup>17</sup>. This observations entails that arrestin-2 and arrestin-3 are able to adopt an active conformation more frequently than arrestin-1, even in the absence of a GPCR<sup>14,17</sup>. The use of pre-activated mutants of arrestin-2 and arrestin-3 have been reported in the literature: by disruption of the polar core (R170E<sup>36,37</sup> and R393E in arrestin-3<sup>38</sup>), by truncation of the C-tail<sup>14,39</sup>, by inactivation the phosphate binding residues in arrestin-2<sup>39</sup> and other alanine mutations (R8A and K108A in arrestin-3<sup>40</sup>).

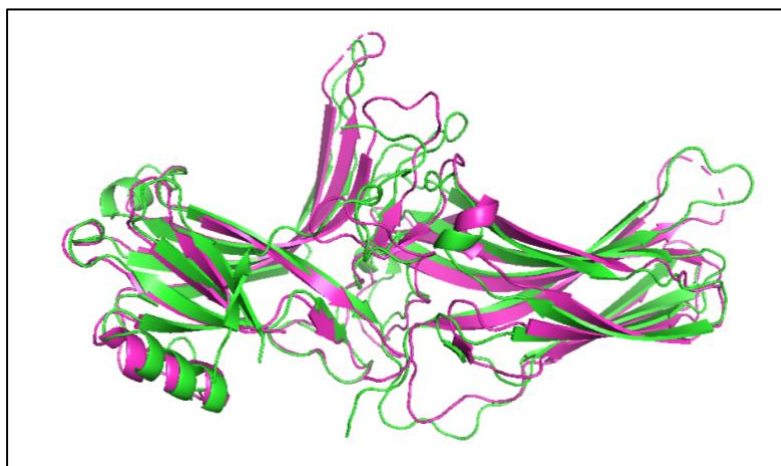


**Figure 4.** Overlap of an inactive bovine arrestin-1 (PDB 3P2D) in green and the pre-activated arrestin-1 variant p44 (PDB 4J2Q) in pink.

#### C.4. The role of arrestins in GPCR trafficking

Arrestins are recruited to ligand-activated GPCRs, following G protein activation<sup>14</sup>. According to spin label<sup>41</sup> and site-directed fluorescence quenching<sup>42</sup> data, arrestins act as direct competitors of G proteins, thereby terminating or “arresting” the GPCR induced G protein signal (hence the name “arrestin”). In fact, crystallographic data<sup>43</sup> suggests that the finger loop of arrestin interacts with activated GPCRs at the exact interface occupied by the C-terminal helix of the G $\alpha$  subunit, leading to G protein desensitization. It is worth noting that one study from *Prokop S. et al., 2017*<sup>44</sup> also suggested constitutive arrestin recruitment *in vitro* to the  $\beta$ 2AR, certain conformations of rhodopsin and the muscarinic receptor M2<sup>44</sup>.

In addition to G protein desensitization, arrestin-2 and arrestin-3 are also directly responsible for the internalization of GPCRs via the clathrin pathway<sup>45</sup>. On the C-terminus of arrestin-2 and arrestin-3, LIEFE/LIELD motifs interact with the heavy chain of clathrin<sup>46–48</sup>. The neighboring RxR motif also interacts with  $\beta$ 2-adaptins from the adaptor protein 2 (AP-2) complex<sup>49,50</sup>, an early effector of the clathrin endocytosis machinery. As such, arrestins are responsible for the aggregation of GPCRs to clathrin coated pits<sup>49</sup>. Interestingly, arrestin-1 does not bind to clathrin and AP-2, nor colocalizes with receptors to clathrin coated pits<sup>16</sup>. Inositol hexakisphosphate (IP6) was reported to be involved in clathrin coated pit formation when bound to arrestin, suggesting that the scaffold function of arrestin is crucial for GPCR internalization<sup>51</sup>. Ultimately, arrestins function as GPCR trafficking regulators by controlling the onset of internalization, degradation and recycling of the receptors<sup>52</sup>.

#### C.5. The role of arrestins in regulating GPCR signaling

Arrestins have been linked to play a role in multiple signaling pathways related to cell proliferation, cell growth, survival/apoptosis, cell migration, regulation of the immune system, embryonic development and central nervous functions<sup>52</sup>. In this section, the pivotal role of arrestin in activation and regulation of the Mitogen Activated Protein Kinases (MAPK) pathway is detailed.

In a study from *Luttrell et al., 2001*<sup>53</sup>, all three precursors of the Mitogen Activated Protein Kinase (MAPK) pathway (e.g. MAPK, MAPK kinase and MAPK kinase kinase) were shown to directly interact with the arrestin scaffold. In this study, the authors suggested that the dynamic nature of arrestin conformations regulate the activity of these enzymes, making arrestin dictate the efficiency, fidelity, and compartmentalization of the MAPK signaling cascade<sup>53</sup>. For example, the cRaf1-MEK1/2-ERK1/2 pathway (CD40 Receptor Associated Factor 1 - MAPK/ERK kinase 1/2 - ERK1/2) controls the cell cycle<sup>54</sup> and all three proteins are bound to arrestin-2 and -3<sup>53,55</sup>. Interestingly, ERK2 and c-Raf1 exhibit



the highest affinity for the pool of GPCR-activated arrestin. At the same time, ERK1/2 shows a higher affinity for microtubule-bound arrestin compared to the inactivated pool of arrestin<sup>56,57</sup>. In other words, it appears that by changing conformations, arrestin inhibits basal ERK activity, while promoting its activation upon GPCR stimulation.

Another MAPK signaling cascade modulated by arrestin is the one triggered by c-Jun kinases (JNK), which are involved in stress cellular response, cell proliferation, apoptosis, migration and differentiation<sup>58,59</sup>. Similar to the ERK signaling cascade, early kinases involved in the ASK1-MKK4/7-JNK3 pathway (apoptosis signal-regulating kinase 1 – MAPK kinase 4/7 – JNK3) all interact with the arrestin scaffold<sup>58</sup>. It is worth noting that, contrary to previously described ERK pathways, the JNK cascade is constitutively active in the absence of a stimulated GPCR<sup>60</sup>. In conclusion, it appears that through direct interaction with early effector proteins and dynamic conformational changes, arrestin is able to closely regulate GPCR related signaling pathways.

#### C.6. Arrestin scaffold function

Arrestins are scaffold molecules able to associate and dissociate with various cargo proteins<sup>52</sup>. This activity heavily depends on: arrestin conformations, the presence of an activated GPCR and arrestin subcellular localization (arrestin can be microtubule-bound, GPCR-bound, cytosolic or nucleic). More than 400 interacting partners of arrestin-2 and arrestin-3 were identified in proteomic studies<sup>61</sup>. For this reason, only a few of the most important scaffold functions of arrestins are highlighted in this section.

The amount of free arrestin in the cytosol is regulated by Ca<sup>2+</sup>-calmodulin, a protein that prevents the association of arrestins to microtubules or activated GPCRs, by sharing a mutually exclusive binding site<sup>62</sup>. In addition, arrestins are able to shuttle between the cytosol and the nucleus, with the exception of arrestin-3, which has a nuclear export signal on its C-terminus<sup>63</sup>. Nuclear c-Jun N-terminal kinase 3 (JNK3) and E3 ubiquitin ligase (Mdm2) constitute examples of cargo proteins preferably bound to the inactivated cytosolic pool of arrestin. Therefore, arrestin-3 acts as a regulator of nucleus signaling cascades by sequestration of such cargo proteins, notably JNK and ERK1/2<sup>52</sup>. Second messenger IP6 was shown to promote arrestin-2 oligomerization<sup>64</sup>, which in turns prevents nuclear translocation of arrestin-2 and the subsequent activation of the following nuclear pathways: NkκB/p65/RelA<sup>65</sup>, STAT1/TC45<sup>66</sup> and p300 histone acetyltransferase<sup>67</sup>, among others. Additionally, these nuclear signaling pathways are indirectly promoted when the high affinity GPCR-arrestin complex displaces the pool of cytosolic arrestin away from oligomerization. Microtubule-bound arrestins are found in a different conformation than GPCR-bound arrestins and ERK1/2 interacts with both complexes but is only activated through the GPCR/arrestin complex<sup>56,57</sup>. Additionally, microtubule-bound arrestins are

less prone to ubiquitination<sup>56</sup>, suggesting that this pool of arrestins may present a reserve of cargo proteins waiting to interact with activated GPCRs<sup>52</sup>.

## **D. GPCR activation**

### D.1. Core activation of a GPCR upon ligand activation

Upon stimulation by a ligand, GPCRs undergo dramatic structural rearrangements, as evidenced by the inactive and activate structures of a  $\beta$ 2AR/Gs complex by *Rasmussen et al., 2011*<sup>11</sup>. At the transmembrane level, an activated  $\beta$ 2AR undergoes a significant 14Å outward extension of the transmembrane helix 6 (TM6) and a smaller outward extension of TM5<sup>11</sup>. As a consequence, the intracellular loop 2 (ICL2) of the  $\beta$ 2AR extends downward into the cytosol and the flexibility of the ICL3 is increased<sup>11</sup>. These conformational changes operate in a dynamic equilibrium and lead to the opening of inter-helical cavity (further called “activated core”) on the cytoplasmic side of the receptor<sup>68</sup>. The opening of the receptor core in turn dramatically increases the overall affinity of the receptor for its direct signaling effectors, namely the G protein G $\alpha$  subunit (see *B. G proteins*), GPCR-related kinases and arrestins<sup>52</sup>.

### D.2. Phosphorylation of the carboxy-terminus of GPCRs by GPCR Related Kinases

Upon receptor stimulation and following G protein activation, GPCR-related kinases (GRKs) are recruited to the receptor to phosphorylate its C-terminal serine and threonine residues<sup>69</sup>. Structural data of the GRK1/rhodopsin complex<sup>70</sup> and the GRK5/ $\beta$ 2AR complex<sup>71</sup> indicate that GRKs interact with an activated GPCR core, which in turn promotes the recruitment of arrestins to the receptor<sup>72</sup>. A co-localization study by *Pan et al., 2002*<sup>73</sup> confirmed that GRK2 phosphorylation of the C-terminus of the  $\beta$ 2AR and the subsequent recruitment of arrestin-2 was essential for the internalization of the receptor. However, a ligand independent – i.e. constitutive - phosphorylation by GRK4 has been described for several receptors ( $\beta$ 2AR<sup>74</sup>, the muscarinic receptor type 2<sup>74</sup> and the dopamine receptor type 1<sup>75</sup>). In addition to GRKs, protein kinase A has also been shown to phosphorylate the ICL3 and the proximal C-terminus of  $\beta$ 2AR following ligand activation<sup>76,77</sup>.

The involvement of several GRK subtypes in the phosphorylation of the  $\beta$ 2AR led to the hypothesis of distinct phosphorylation “barcodes”, thereby driving different arrestin functions. For instance, mass spectrometry, small interfering RNA (siRNA) silencing, BRET and western blot data<sup>77</sup> have suggested that GRK2 and GRK6 induce different phosphorylation intensities on the  $\beta$ 2AR. Authors suggest that

GRK6-mediated phosphorylation of the GPCR favors arrestin-dependent activation of ERK, whereas GRK2-mediated phosphorylation of the GPCR promotes arrestin-mediated internalization of the receptor<sup>77</sup>.

Another study on the vasopressin receptor 2 by *Ren et al., 2005*<sup>78</sup> linked GRK2/3 mediated receptor phosphorylation to G protein desensitization by arrestin-2 and arrestin-3, while GRK5/6 mediated receptor phosphorylation favored the activation of the MAP-kinase/ERK signaling pathway. Similar discoveries by *Kim et al., 2005*<sup>79</sup> were made with the angiotensin receptor type II, where GRK2/3 activity led to an increase in G protein desensitization and receptor endocytosis, while GRK5/6 promoted ERK signaling. A ligand dependent differential recruitment of GRKs was shown by *Zidar et al., 2009*<sup>80</sup> for the chemokine receptor type 7 (CCR7). Here, the chemokine CCL21 triggered both GRK3 and GRK6 mediated receptor phosphorylation, resulting in receptor internalization and ERK activation, respectively. CCL19, however, only triggered GRK6 mediated receptor phosphorylation.

More recently, *Mayer et al., 2019*<sup>81</sup> investigated the functional relevance of phosphorylation patterns on the C-terminus of bovine rhodopsin for arrestin-1 recruitment and activation. This *in vitro* phosphorylation barcode screen revealed that two residues out of seven in rhodopsin (T340 and S343) must be phosphorylated for proper arrestin recruitment, much in line with another study highlighting the importance of these residues in an arrestin-1/rhodopsin structure<sup>82</sup>. Additionally, the *in vitro* screen unveiled for the first time the inhibitory (T342) and modulating roles (S334 to S338) of certain phosphorylation sites on rhodopsin for the recruitment of arrestin<sup>81</sup>. Phosphorylation of rhodopsin residue pT342 was shown to decrease arrestin-1 and arrestin-3 binding to peptides derived from the C-terminus of rhodopsin containing three phosphate groups in total. This inhibitory effect appeared compensated by higher degrees of peptide phosphorylation. Mechanistically, residue pT342 might compete with key phosphorylated residues pT340 and pS343 as the spacing between these last two amino acids must be exact to be simultaneously recognized by arrestin. *Mayer et al., 2019*<sup>81</sup> also describe the modulating role – in terms of arrestin conformational changes and arrestin activation – of rhodopsin residues D330 and D331, through their interaction with residues on the finger loop and middle loop of arrestin. For other GPCRs, this modulating role might be ensured by phosphorylated residues as shown with amino acid pS350 on a structure of arrestin-2/V2Rpp<sup>31</sup> (a peptidomimetic of the phosphorylated vasopressin receptor 2). These modulating sites probably anchor the receptor for proper phosphate group placement onto the N-domain of arrestin. Interestingly, class A GPCRs (according to *Oakley et al., 2000*<sup>16</sup>) tend to lack the proper spacing between phosphorylation sites which could explain the transient nature of the class A GPCR/arrestin complexes<sup>81</sup>. However, class B GPCRs generally contain the appropriate spacing between modulating sites and the two phosphorylation sites to support a sustained interaction with arrestin<sup>81</sup>.

### D.3. The GPCR-arrestin interface

Arrestin interacts with three components of GPCRs and the plasma membrane: i) the phosphorylated C-tail of stimulated GPCRs (C-tail interaction), ii) the open GPCR core on the cytoplasmic side (core-interaction) and iii) the surrounding bilayer membrane (membrane anchor). Unless specifically mentioned, the following amino acid nomenclature is of bovine arrestin-1.

To initiate the C-tail interaction with a GPCR, the C-tail of arrestin must be released from the N-domain where it is nestled within the protein in its basal state. Once arrestin is in the so-called pre-activated state, the phosphorylated C-terminus of an activated GPCR replaces the C-tail of arrestin on the N-domain<sup>34</sup>. Structural data of an arrestin-1/rhodopsin complex<sup>82</sup> suggest that the phosphorylated C-terminus of rhodopsin adopts a  $\beta$ strand conformation and interacts with three positively charged pockets of arrestin-1. Pocket A (K15, R18 and R171) accommodates pT340 of bovine rhodopsin, pocket B (K15, R29 and K300) stabilizes pS343 and pocket C (K14 and K110) forms ionic bonds with E341<sup>81,82</sup> (figure 5). Previous mutagenesis data corroborate the crucial role of N-terminal residues R18, K14 and K15 in phosphate sensing<sup>29</sup>. All residues from the three phosphate binding pockets are conserved in arrestin-2 and arrestin-3, with the exception of R19 which is replaced by a proline residue, as shown in figure 5<sup>81,82</sup>. Additionally, conformational changes in the N-domain of arrestin-1 were observed in the presence of a peptide mimicking the rhodopsin phosphorylated C-tail by nuclear resonance magnetism<sup>81</sup>. Nevertheless, due to the dynamic nature of ionic interactions these well-established phosphate-binding pockets are not necessarily the only ones to exist. Interestingly, a phosphorylated GPCR C-terminus appears less critical for the activation of arrestin-2 and especially arrestin-3 compared to arrestin-1, as these arrestins are reported to adopt an activated conformation in the absence of a GPCR more often<sup>15</sup>.

By comparing full-length arrestin-1 to p44, an arrestin-1 variant lacking the last 34 amino acids of the inhibitory C-tail, Schröder *et al.*, 2002<sup>30</sup> have shown that p44 and other C-tail truncated arrestin-1 variants exhibit a faster binding kinetic to light-activated phosphorhodopsin and are also able to couple with lesser activated forms of rhodopsin (not phosphorylated or not light activated). In addition, Schröder *et al.*, 2002<sup>30</sup> were among the first teams to propose a two-step mechanism for arrestin recruitment to rhodopsin by kinetic light scattering measurements of various arrestin/rhodopsin complex combinations. In fact, this theory discerns a pre-complex formed by arrestin-1 and rhodopsin via the C-tail exchange alone and a high affinity complex able to directly bind the cytoplasmic components of the receptor in addition to the C-tail exchange. More precisely, the crystal structure of the p44 variant by Kim *et al.* 2013<sup>17</sup> reveals that, in the pre-activated form, the arrestin C-tail has been displaced and that the hydrogen bond network of the polar core has been compromised by the displacement of the gate loop onto the N-domain. The most important feature revealed by the crystal

structure of p44 is that the finger loop adopts an extended upward position and that the middle loop is retracted on the N-domain, in addition to a 20° rotation of the C-domain from the N-domain creating a cleft in the central crest region. In the transition from the pre-complex to the high-affinity complex, *Beyrière et al., 2015*<sup>83</sup> have demonstrated by Fourier Transform Infrared (FTIR) on arrestin-1/rhodopsin complexes that arrestins experience a moderate loss in  $\beta$ -sheet content, indicating an increased flexibility of the protein in the high affinity complex. Finally, *Lally et al., 2017*<sup>84</sup> proved by molecular dynamics simulations and fluorescence quenching experiments that the C-edge of arrestin (figure 3) interacts with the phospholipids surrounding the receptor both in the pre-complex and the in high-affinity complex. In fact, the mode of interaction of the C-edge was found to differ in the two complexes: the 199-loop is solely engaged with the membrane in the high affinity complex and the 344-loop is more buried in the membrane in the pre-complex than in the high-affinity complex. To come in effect, the membrane anchor requires the C-tail interaction and central crest conformational rearrangements<sup>84</sup>. It is worth noting that the implication of the C-edge in arrestin binding might differ among members of the arrestin family as arrestin-3 does not contain any 344-loop and the so-called long splice variant of arrestin-2 contains an insert of 8 amino acids in its 344-loop that is also involved in clathrin binding<sup>48</sup>.

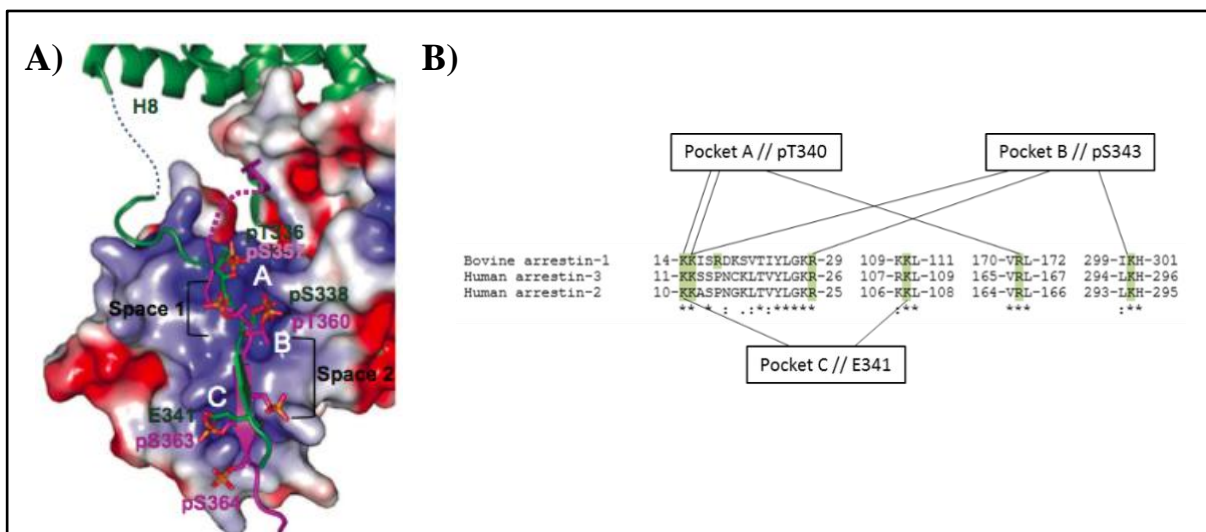


**Figure 5.** A) Placement of the phosphorylated C-terminus of human rhodopsin (green amino acids, PDB 5W0P) and V2Rpp, an analogue of the phosphorylated C-terminus of the vasopressin receptor (pink amino acids, PDB 4JQI) on arrestin-1. Blue arrestin-1 residues: positively charged amino acids. Red arrestin-1 residues: negatively charged amino acids. The picture was extracted from Zhou et al., 2017<sup>82</sup>, figure 6B. B) Alignment of phosphate binding sites in arrestin-1, -2 and -3 as proposed by Zhou et al., 2017<sup>82</sup> and Mayer et al., 2019<sup>81</sup>. Pockets A recognizes pT340 in bovine rhodopsin, pocket B stabilizes pS343 and pocket C senses negatively charged residue E341.

Upon arrestin recruitment to GPCRs, the central crest of arrestin interacts with the activated core of the receptor (figure 6)<sup>34,85</sup>. According to an arrestin-1/rhodopsin structure from *Kang et al., 2015*<sup>34</sup> and mutagenesis experiments by *Peterhans et al., 2016*<sup>86</sup>, arrestin N- and C-domains have experienced a 20° rotation from one another compared to the basal state of arrestin-1 and arrestin-1 variant p44<sup>17</sup>. As

a result, the extended finger loop (D73, M75, G76 and L77) now interacts with the cytosolic helix 8 (Q312), the intracellular loop 1 (ICL1) and transmembrane helix 7 (TM7) of rhodopsin. Additionally, the middle loop is displaced from the main body of arrestin and residues Q133 and D138 now face the intracellular loop 2 (ICL2) of rhodopsin at G149<sup>34</sup>. The C-loop is also displaced from the central crest thus exposing L249 and Y250 to residues T229 and A233 on the ICL2 of rhodopsin<sup>34,85</sup>. Back loop residue K318 interacts with Q237 of the transmembrane helix 5 (TM5) of rhodopsin<sup>34</sup>. Finally, the  $\beta$  strand of the N-domain adjacent to the finger loop is engaged from residue S78 to F85 with TM5 and TM6 as well as ICL<sup>34</sup>.

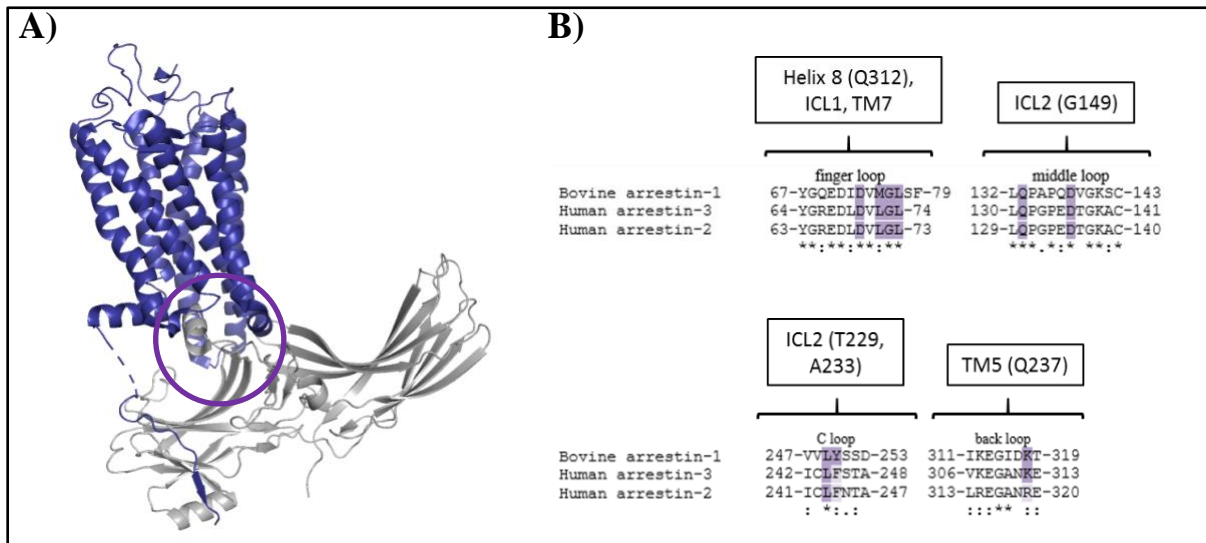


**Figure 6.** A) Rhodopsin-arrestin-1 complex resolved by X-ray crystallography (PDB 5W0P). Purple circle: core-interaction between the open transmembrane core of rhodopsin and central crest loops (finger loop, middle loop, C-loop and back loop). B) Alignment of core-interaction binding sites in arrestin-1, -2 and -3 as proposed by Kang *et al.*, 2015<sup>34</sup>. ICL: intracellular loop. TM: transmembrane domain.

As for the temporal aspect of arrestin-GPCR complexes in cells, association and dissociation constants for these complexes vary from seconds ( $\beta$ 2AR)<sup>87</sup> to minutes (vasopressin receptor type 2)<sup>88,89</sup>, depending on the GPCR and the method of detection used. In a landmark study from Oakley *et al.*, 2000<sup>16</sup>, confocal microscopy data were used to divide GPCRs in two major classes in terms of arrestin recruitment:

- Class A GPCRs recruit preferably arrestin-3 over arrestin-2 and almost no arrestin-1. Their physiological ligands are biogenic amines and peptide ligands. Class A GPCRs, as the  $\beta$ 2AR, form transient complexes with arrestins which dissociate at or near the plasma membrane. The short-lived complexes could be explained by the inadequate spacing of phosphorylated sites and arrestin-binding modulating sites on the C-terminus of class A GPCRs, thus impeding full arrestin recruitment (see D.2. Phosphorylation of the carboxy-terminus of GPCRs by GRKs)<sup>81</sup>.

- Class B GPCRs are stimulated by peptide ligands and can recruit arrestin-1, -2 and -3 to a similar extent. Class B GPCRs, as the angiotensin II receptor type 1, tend to form long-lasting complexes with arrestins that subsist in early endosomes during receptor internalization. Robust GPCR/arrestin complexes could be explained by the optimized spacing between arrestin-binding residues on the C-terminus of class B GPCRs<sup>81</sup> (see *D.2. Phosphorylation of the carboxy-terminus of GPCRs by GRKs*).

#### D.4. Biased signaling

Arrestins have a multi-faceted role in G protein desensitization, GPCR trafficking and GPCR signaling (figure 7). Over the past two decades, the theory of biased signaling or functional selectivity has emerged in the GPCR field<sup>2,76,80</sup>. It entails that different ligands activating the same receptor are able to trigger distinct pathways (or at least privilege one pathway over others). As depicted in figure 7, biased signaling can occur at two levels: either i) through a preference for G protein activation over arrestin recruitment or ii) on the level of distinct arrestin conformations elicited by distinct phosphorylation patterns on the C-terminus of a GPCR (also known as phosphorylation barcodes)<sup>37,77</sup>. Such phosphorylation barcodes were shown to transduce separate arrestin functions by adopting distinct conformations (see *D.2. Phosphorylation of the carboxy-terminus of GPCRs by GPCR Related Kinases*). It is worth noting that the G protein desensitization and the GPCR trafficking regulator roles of arrestin have reached a large consensus in the GPCR community. However, in the advent of novel experimental tools (e.g. CRISPR/CAS9 technology by *Grundmann et al., 2018*<sup>90</sup>), the exclusive signaling function of arrestin – i.e. independent from prior G protein activation - has recently been challenged<sup>80,90</sup>. In any case, the biased signaling paradigm remains valid, as arrestin influences the G protein pathways by G protein desensitization and its scaffold function. In the end, the aim of biased signaling is that clinically favorable signaling events can be obtained by designing signaling-selective drugs. Thus, the understanding of the intricacies of arrestin mechanisms and activation modes remains a subject of intense research.

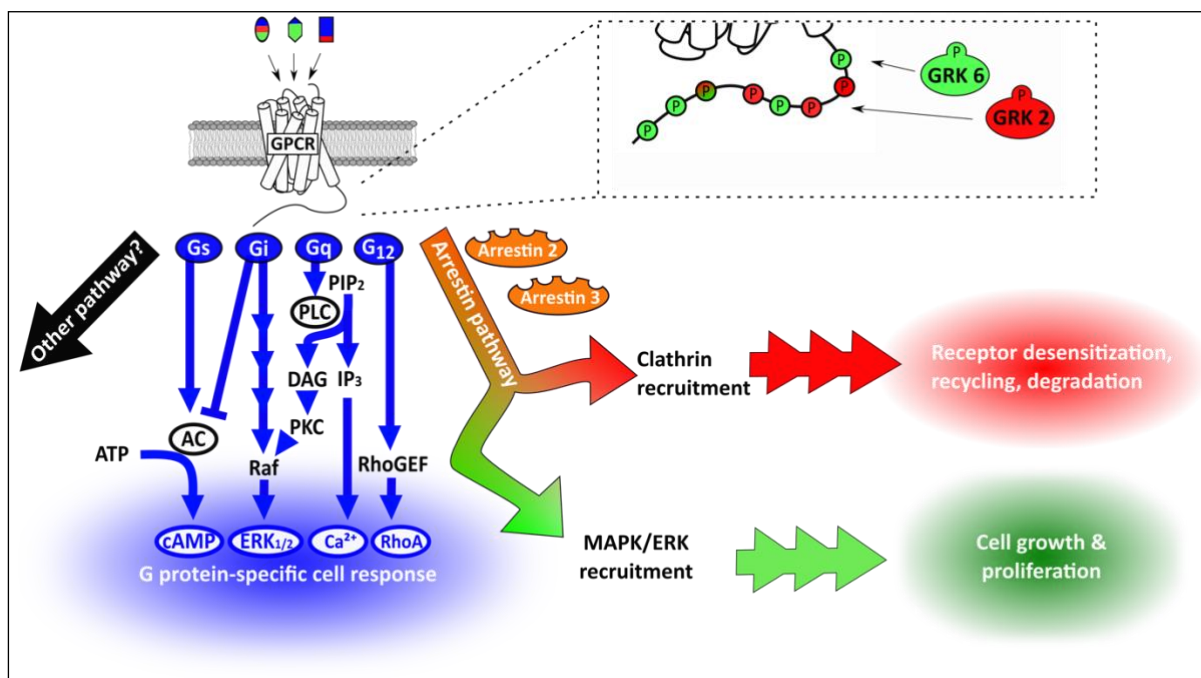


**Figure 7.** Overview of early GPCR signaling cascades with the canonical G protein (blue) and arrestin pathways (orange). The color code in ligands and pathways illustrate the principle of biased signaling: distinct ligands activate preferred downstream signaling cascades. *Gas*, *Gai*, *Gaq*, *Ga12*: *Ga* subtypes. AC: adenylyl cyclase. ATP: adenosine triphosphate. cAMP: cyclic adenosine monophosphate. Raf: rapidly accelerated fibrosarcoma kinase. PIP<sub>2</sub>: phosphatidylinositol 4,5-bisphosphate. PLC: phospholipase C. DAG: diacylglycerol. IP<sub>3</sub>: inositol triphosphate. PKC: protein kinase C. ERK1/2: extracellular signal-regulated kinases type 1 and 2. RhoGEF/A: Ras homologous proteins. MAPK: mitogen-activated protein kinase. GRK2/6: G protein coupled receptor related kinases.

## E. Aim of thesis

Arrestins are multi-functional proteins with a significant but complex influence on GPCR signaling. As such, they stimulate a great interest for the development of signaling-biased drugs targeting GPCRs, provided their role in pathway activation is better understood. Major advancements have been made in understanding the molecular mechanisms behind arrestin recruitment and activation by GPCRs. Nevertheless, the current paradigm is primarily based on crystal structures and limited mutagenesis experiments, mostly performed on arrestin-1. In order to secure a single static snapshot of the relevant complex, structural approaches have the technical disadvantages to use heavily modified proteins<sup>91</sup>, unnatural partners for complex stabilization<sup>31</sup> (lysozyme, antibodies) and extreme experimental conditions<sup>31,91</sup>. Mutagenesis studies performed in cells depend on large chromophores for functional studies<sup>60</sup>, which almost certainly affects arrestin scaffold and signaling functions. This thesis focuses on alternative experimental strategies to investigate the molecular mechanism governing human arrestin-3 recruitment to two categories of GPCRs: receptors of the adrenergic family ( $\beta$ 2AR and  $\beta$ 1AR) and rhodopsin.



Objectives were:

1. To map the human arrestin-3 sequence for residues involved in the recruitment to the  $\beta$ 2AR
2. To engineer arrestin-3 mutants that are strongly recruited to the  $\beta$ 2AR and to variants of the  $\beta$ 1-adrenergic receptor
3. To compare the recruitment of WT arrestin 1/2/3 and arrestin-3 constrained mutants to rhodopsin *in vitro*

In the first part of this study, I used a large-scale and unbiased approach to study human arrestin-3 recruitment to the human  $\beta$ 2-adrenergic receptor in cells. For this, I generated an alanine library of 383 arrestin-3 single point mutants that were screened by a novel technique called split nanoluc (Promega)<sup>92</sup>. The split nanoluc technology is a protein-fragment complementation assay involving a brighter, smaller and more sensitive reporter enzyme than the commonly used renilla or firefly luciferase<sup>89,93</sup>. The two components of the nanoluciferase enzyme were fused to wild-type (WT) arrestin-3 and the plasma membrane (using a membrane motif for protein prenylation: CAAX) and stably expressed in HEK293 cells together with the  $\beta$ 2AR. The ability of the arrestin-3 mutants to compete with the endogenous arrestin-3 proteins expressed in the cells was used to determine the respective affinities of the arrestin-3 mutants for the  $\beta$ 2AR. Objectives were to i) validate the new split nanoluc approach and ii) discover new arrestin-3 binding modes to the  $\beta$ 2AR. The principle advantage of this split nanoluc approach was to refrain from using bulky fluorescent tags on the  $\beta$ 2AR. This project was developed in collaboration with Dr. Martin Ostermaier (InterAx Biotech AG), Martin Spillmann (Paul Scherrer Institute), Dr. Philipp Berger (Paul Scherrer Institute) and supported by the Swiss Commission for Technology and Innovation (CTI, now Innosuisse, project #18540.1 IP-LPS).

In the second part of the study, several arrestin-3 mutants were designed based on results from *Haider et al., 2019*<sup>94</sup>, who discovered several arrestin-1 mutants that displayed a high affinity to rhodopsin. Here, the recruitment of double and triple alanine mutants of arrestin-3 towards i) the  $\beta$ 2-adrenergic receptor and ii) variants of the  $\beta$ 1-adrenergic receptor was analyzed using the Bioluminescence Resonance Energy Transfer (BRET) assay. The truncated  $\beta$ 1-adrenergic receptors were provided by Prof. Christopher Tate (Medical Research Council, Cambridge, UK). The objective was to identify arrestin-3 mutants that bound strongly to the  $\beta$ 1-adrenergic receptor ( $\beta$ 1AR) in order to enable the generation of a stable crystal structure of the  $\beta$ 1AR bound to arrestin-3. This project was developed in collaboration with Prof. Christopher Tate (MRC, Cambridge, UK) and Dr. Maria Waldhoer (InterAx Biotech AG), Dr. Philipp Berger (Paul Scherrer Institute).

Finally, I focused on purified proteins to study the recruitment of human arrestin-3 to rhodopsin *in vitro*. Objectives were i) to compare the recruitment of different arrestins to rhodopsin (provided by Dr. Martha Sommer from Universitätsmedizin Charité Berlin, Germany) or ii) to use structurally constrained arrestin-3 mutants. The rhodopsin *in vitro* system has the advantage to straightforwardly assess the arrestin-GPCR interactions, exempt from cellular background (receptor internalization, G protein competition). Rhodopsin activated states (and arrestin binding modes to rhodopsin) can be experimentally separated in centrifugal pull-downs. The so-called pre-complex with dark-state phosphorhodopsin solely involves the C-tail exchange and the membrane anchor whereas the high-affinity complex with light activated phosphorhodopsin involves the core-interaction in addition to the C-tail interaction and the membrane anchor. Arrestin-3 mutants were constrained by cysteine crosslinking, conveniently designed from structural data, and span all functionally relevant regions for arrestin recruitment or activation: loops of the central crest, the polar core, the three-element interaction, the C-tail and the membrane anchor. This project was developed in collaboration with Dr. Martha Sommer (Universitätsmedizin Charité Berlin, Germany), Jonas Mühle (Paul Scherrer Institute), Alain Blanc (Paul Scherrer Institute) and Dr. Maria Waldhoer (InterAx Biotech AG), Prof. Gebhard Schertler (Paul Scherrer Institute).

## **CHAPTER 1 – An alanine scan on arrestin-3 for assessing the requirements of arrestin-3 recruitment to the $\beta$ 2-adrenergic receptor**

In 2014, *Ostermaier et al.*<sup>40</sup> used an alanine scan approach to investigate the recruitment of bovine arrestin-1 to rhodopsin *in vitro*. In this unbiased and large scale approach, each amino acid of arrestin-1 was mutated to an alanine in order to identify critical residues for the recruitment of arrestin to various states of rhodopsin. Here, the same approach was used to identify arrestin-3 residues involved in the recruitment to the  $\beta$ 2AR using a novel protein-fragment complementation assay called split nanoluc. In this competitive assay, the recruitment of arrestin-3 mutants to the  $\beta$ 2AR was assessed by their ability to compete with endogenous, wild-type (WT) arrestin-3 for the  $\beta$ 2AR. A total of 383 single point alanine mutants of human arrestin-3 were screened against the  $\beta$ 2AR using the split nanoluciferase technology. This project was developed in collaboration with Dr. Martin Ostermaier (InterAx Biotech AG), Martin Spillmann (Paul Scherrer Institute), Dr. Philipp Berger (Paul Scherrer Institute) and supported by the Swiss Commission for Technology and Innovation (CTI, now Innosuisse, project #18540.1 IP-LPS).

### **Material and methods**

#### **1.1. PCR-driven mutagenesis**

In an alanine scan approach, each amino acid of a protein is mutated to an alanine in order to evaluate the importance of each residue for a given function. Alanine is a non-bulky and electrically neutral amino acid that does not influence protein secondary structures. In this case, 383 single point alanine mutants, covering 96.3% of the arrestin-3 sequence, were generated to explore the mechanism of arrestin-3 recruitment to the  $\beta$ 2-adrenergic receptor ( $\beta$ 2AR).

The alanine scan library was generated by site-directed mutagenesis from a single multi-gene expression<sup>95</sup> template plasmid (AG10-B2AR-DS2-bArr2-EGFP, plasmid #589, PSI) described in figure 8. The plasmid #589 contained two coding sequences: the fusion protein EGFP (Enhanced Green Fluorescent Protein)-arrestin-3 and the wild-type (WT-)  $\beta$ 2AR. The plasmid #589 uses a CMV-promotor for maximal expression in mammalian cells (DNA sequences in appendix 1).

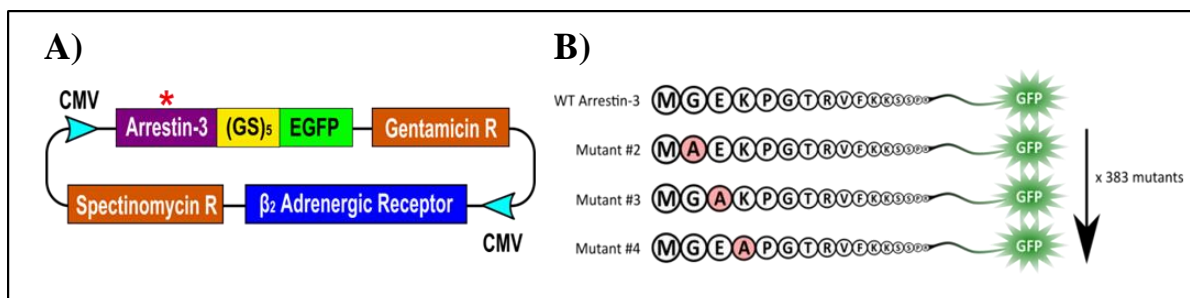


**Figure 8.** A) Plasmid map of the template plasmid #589. R: resistance. EGFP: engineered green fluorescent protein. Red asterisk: cloning region. B) Alanine scan strategy where each amino acid is replaced one by one by an alanine residue.

Polymerase Chain Reaction (PCR) primers for the entire protein were generated using the freeware Mutantchecker<sup>96</sup>. PCR-driven mutagenesis was performed in large batches of 24 to 48 reactions with the following amounts per reaction: 50 ng template DNA (#589), 8% DMSO (99.9%, Sigma-Aldrich, #472301), 53% Phusion GC PCR mix (New England Biolabs, #M0532S) and 75 nM of each PCR primers (Microsynth) in a total volume of 20  $\mu$ L in Triple-Q water (PSI). PCR tubes were placed on the thermal cycler according to their calculated annealing temperature ( $T_m$ ) as shown in figure 9.

Primer	Primer sequence	Annealing temperature ( $T_m$ )	Averaged $T_m$	Adjusted $T_m$ to 8% DMSO content ( $T_m - 4.6^\circ\text{C}$ )
G2A_Forward	ccatgGCGgagaaccgggac	62.3	61.95	57.35
G2A_Reverse	tttctcCGCcatggtatctcttggagc	61.6		
E3A_Forward	ggggGCGaaaccgggaccag	64.1	63.4	58.8
E3A_Reverse	gggtttCGCccccatggtatctcc	62.7		
K4A_Forward	ggagGCAccgggaccagggtc	66	65.9	61.3
K4A_Reverse	cccgggTGCctccccatggtatctc	65.8		
P5A_Forward	ggagaaaGCGgggaccagggtcttc	64.2	64.25	59.65
P5A_Reverse	cccCGCtttcccccatggtatctc	64.3		

PCR reactions layout												
Temperature gradient ( $^\circ\text{C}$ )	57.35	57.71	58.07	58.43	58.79	59.15	59.50	59.86	60.22	60.58	60.94	61.30
	1	2	3	4	5	6	7	8	9	10	11	12
A	G2A				E3A		P5A					K4A
B												
C												
D												
E												
F												
G												
H												

**Figure 9.** Primer annealing temperatures ( $T_m$ ) were averaged from each oligonucleotide  $T_m$  values. DMSO content was taken into account in  $T_m$  calculations according to the manufacturer's recommendations. As shown in the PCR reaction layout, the samples were placed in the PCR thermal cycler at their optimal temperature for maximal DNA amplification.

The thermal cycler was programmed as follows for the PCR reaction:

Number of cycles	Temperature	Time
1x	98°C	2 min
30x	1) 98°C 2) Temperature gradient (from 57.35 to 61.3°C in the case of K4A in figure 9) 3) 72°C	1) 20 s 2) 30 s 3) 5 min
1x	72°C	3 min
END	10°C	Until sample pickup

After amplification, each reaction was subjected to two DpnI digestions (New England Biolabs, #R0176S) at 37°C in order to eliminate the template DNA: one overnight and one for 4h. Then, 0.5 µL of each PCR reaction was used to transform 50 µL of XL1 Blue cell suspension (PSI) by heat shock for 45 seconds at 42°C. After a 2h30 incubation at 37°C on a thermal cycler, cell suspensions were dispersed onto agar plates (Gerbu, #1416.2500) that were infused with 5 µg/mL gentamicin (Sigma-Aldrich, #472301) and 10 µg/mL spectinomycin (Sigma, #S4014-5G). Finally, agar plates were incubated overnight at 37°C.

The next day, four colonies per mutant were marked, picked up and inoculated onto GATC 96-well sequencing agar plates (GATC-Biotech, #S0317). GATC agar plates were sent to be sequenced with the following primers: 5'-GTTGAGCCACAGGACACTTG-3' (custom-made primer, "arr3-AA256-rev", GATC) and 5'-GCTTGCCGTAGGTGGCATC-3' (standard primer "EGFP-N-rev", GATC). Upon reception of results, positive colonies were picked from the original agar plates and inoculated to 10 mL of LB-medium (Gerbu, #1416.2500) in the presence of gentamicin and spectinomycin.

Finally, cell suspensions were harvested and DNA constructs were purified using a miniprep kit (Thermo Fisher Scientific, #K0503). To insure plasmid integrity, three analytical digests were performed on each purified construct as follows:

<b>Mastermix components</b>	<b>Per reaction</b>
DNA construct	0.5 µg
Restriction enzyme	0.3 µL
CS buffer	10% total volume
Water	to 20 µL

The restriction enzymes (New England Biolabs) consisted of:

- 1) PvuI-HF (#R3150S) and PvuII-HF (#R3151S)
- 2) NcoI-HF (#R3193S)
- 3) HindIII-HF (#R3104S)

Digestion of DNA constructs occurred for 3h minimum at 37°C and 7 µL of reaction was loaded on a 1.1% agarose gel (Gerbu, #1036.0500) infused with ethidium bromide (Sigma, #E1385). After a 30-minute run at 100 V, positive constructs were expected to match the digestion profile displayed in figure 10. Finally, positive plasmids were stored at -20°C.

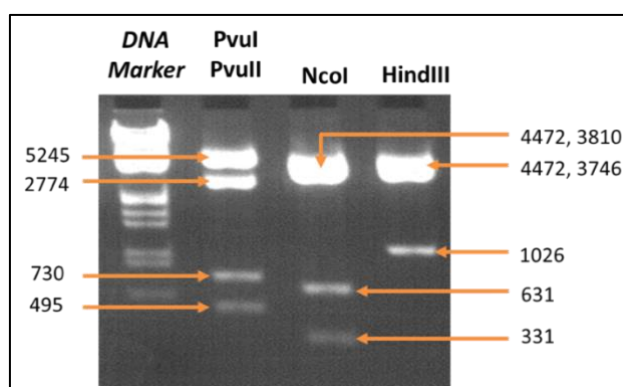


**Figure 10.** Expected digestion profile of intact plasmids. Band size are expressed in base pairs.

## **1.2. Alanine arrestin-3 mutant screening by split nanoluciferase**

The split nanoluc assay<sup>97,98</sup> (Promega) was used to investigate the recruitment capability of the previously generated alanine arrestin-3 mutants to the  $\beta$ 2AR in HEK293 cells. The nanoluciferase used here has been reported to be smaller, brighter, ATP-independent, and 100-fold more sensitive than renilla or firefly luciferase<sup>98</sup>. For this assay, a HEK293-based cell line called Split Nanoluc Competition assay of Arrestin-3 or SCAR3 was used. The SCAR3 cell line was engineered by Martin Spillmann (Paul Scherrer Institute) and kindly provided for the present study. The SCAR3 cells stably express the

two components of the nanoluciferase enzyme: subunit 11S (18 kDa) was fused to the plasma membrane anchor CAAX (a physiological motif for protein prenylation, thereby decorating the plasma membrane) while subunit 114 (1.3 kDa) was fused to the wild-type version of arrestin-3 (WT arrestin-3).

In this competition assay (figure 11), SCAR3 cells were transiently transfected with plasmids, derived from plasmid #589 by site-directed mutagenesis, encoding CMV-promoted EGFP-arrestin-3 alanine mutants and the WT- $\beta$ 2AR (see figure 8.A for the plasmid map and appendix 1 for DNA sequences). The functionality of alanine mutants was assessed by their ability to compete off the signal induced by the tri-complex formed by 114-arrestin-3, a ligand-activated  $\beta$ 2AR and 11S-CAAX.

In addition to the split nanoluc assay, the expression level of each mutant in cells was measured by GFP fluorescence at 520 nm.

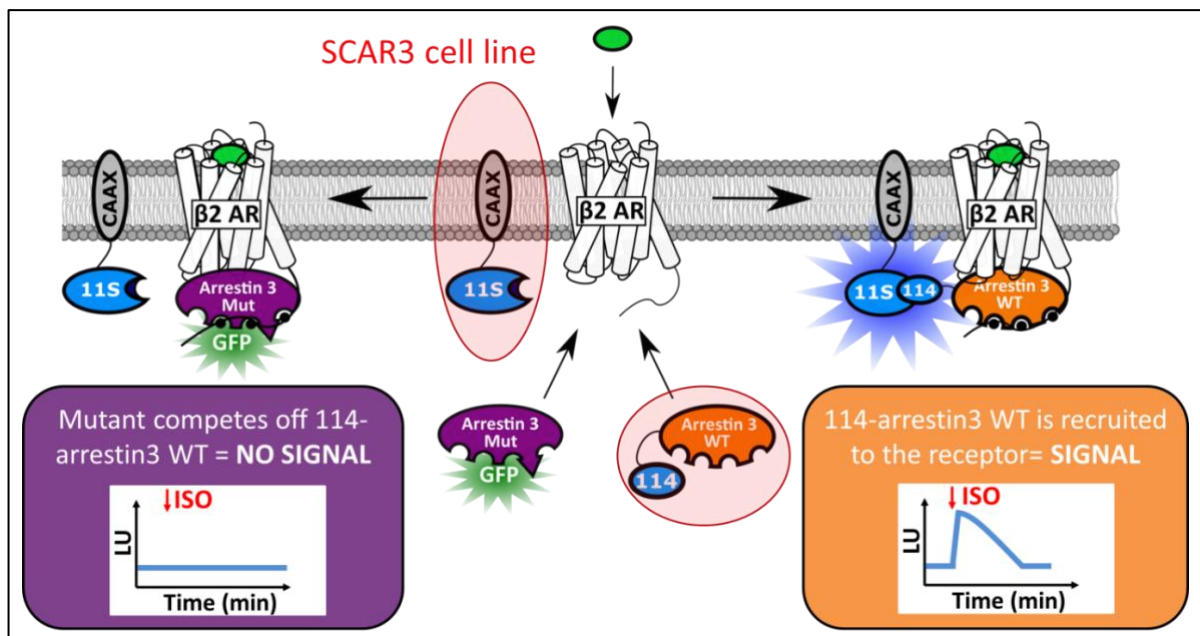


**Figure 11.** Principle of the split nanoluc assay in SCAR3 cells. SCAR3 cells stably express the two components of the split nanoluciferase, either fused to WT arrestin-3 (114) or to the prenylation motif CAAX (11S), which decorates the plasma membrane. Upon recruitment of 114-WT-arrestin-3 to the plasma membrane, the nanoluciferase subunits (114 and 11S) are reunited and the luminescence signal produced is detected in a plate reader (right half of the panel). Upon transient transfection of  $\beta$ 2AR and an arrestin-3 mutant (in purple), SCAR3 cells undergo a reduction in luminescence signal reflecting the capability of the said arrestin-3 mutant to compete off the signal produced by 114-WT arrestin-3 (left half of the panel). Green circle or ISO: 10  $\mu$ M isoproterenol (Tocris, #1747).

### 1.2.1. Cell transfection

The SCAR3 cell line was maintained at all times in Dulbecco's Modified Eagle's Medium (DMEM, Bioconcept, #1-26-F03-I) + 10% fetal calf serum (FCS, Seralog, #S4500) + Penicillin/Streptomycin (PS, Lonza, #DE17-602E) + Zeocin (InvivoGen, #ant-zn) + Geneticin (PSI, #GLN-38-05A) in order to

conserve the expression of the split nanoluc elements 114 and 11S. This cell culture medium will be further referred to as DMEM-PS-ZG.

On the first day, DMEM-PS-ZG was removed out of four 10-cm plates (SPL Life Sciences, #20101) containing SCAR3 cells at near confluence. Cells were washed with 6 mL of Phosphate Buffer Saline (PBS, Gerbu, #1680,7010) and treated with 1 mL trypsin-ethylenediaminetetraacetic acid (Trypsin-EDTA, BioConcept, #5-51F00-H) for 2 to 8 minutes at 37°C, 5% CO<sub>2</sub>, until Trypsin-EDTA was inactivated by adding 6 mL DMEM-PS-ZG. Collected cells were then counted in a Neubauer chamber (Celeromics) and 0.5x10<sup>6</sup> cells were seeded in 15x 6-well plates (SPL Life Sciences, #13485). On the next day, cells were expected to be at 30-40% confluency, the ideal condition for polyethylenimine (PEI, Sigma, #408727) transfections. Transfection reagents were prepared per reaction as such:

<b>Tube A</b>	<b>Tube B</b>
1.5 µg of carrier plasmid (empty pcDNA3 vector, PSI)	6 µg PEI (1µg/ µL)
0.5 µg of arrestin-3 mutants/β2AR plasmid (#589)	
150 µL of Opti-MEM (Life Technologies, #31985-047)	150 µL of Opti-MEM (Life Technologies, #31985-047)

- For tube A :

A mastermix of carrier plasmid + Opti-MEM was prepared. For 88 transfections, 148.2 µL of carrier plasmid (0.96 µg/µL) was diluted in 14.5 mL Opti-MEM in a 50 mL falcon tube. After a 5-minute incubation, 151.5 µL of this mastermix was aliquoted in individual Eppendorf tubes. Finally, the calculated volumes of arr3 mutants-β2AR constructs equivalent to 0.5 µg was added in each Eppendorf tube. To insure homogeneity of the solutions, the tube rack was shaken and incubated for at least 5 minutes at room temperature.

- For tube B :

A mastermix of PEI + Opti-MEM medium was prepared. For 88 transfections, 570 µL of PEI was diluted in 14.5 mL Opti-MEM in another 50 mL falcon tube.

A total of 156 µL of mastermix B was added in each Eppendorf tube containing DNA constructs in Opti-MEM. Transfection mixtures were incubated for 30 minutes at room temperature before 260 µL was added per well and cells were brought back to the incubator for 48h.



After 24h, the transfection efficiency could be visually estimated by the GFP signal emitted by the EGFP-arrestin-3 mutants, although a 48h incubation period was necessary to reach maximal arrestin-3 mutant expression.

### 1.2.2. EGFP fluorescence and split nanoluc assay

On the day of analysis, cell suspensions were carefully prepared in a standardized fashion. First, cells were collected from 6-well plates in Eppendorf tubes with PBS/20 mM EDTA (PSI) for 5 minutes at 37°C. Then, cells were centrifuged at 500g for 12 minutes and the Opti-MEM buffer was replaced by clear DMEM-HEPES buffer (PSI). Finally, 64  $\mu$ L of cell suspension was pipetted into 96-well plates in duplicates as shown in figure 12. Two sets of 96-well plates were required: one clear bottom black plate to measure the expression of arrestin-3 mutants via GFP fluorescence and one white plate with an opaque bottom for the split nanoluc assay. Plates were stored 2h at 37°C, 5% CO<sub>2</sub> to prepare assay reagents and let cells recover.

	1	2	3	4	5	6	7	8	9	10	11	12
A												
B		349	349	$\beta$ 2AR	$\beta$ 2AR	137	137	229	229	$\beta$ 2AR + M	$\beta$ 2AR + M	
C		263	263	Arr3 WT	Arr3 WT	82	82	167	167	$\beta$ 2AR + A	$\beta$ 2AR + A	
D		392	392	298	298	121	121	261	261	291	291	
E		329	329	150	150	85	85	224	224	42	42	
F		306	306	272	272	254	254	304	304	243	243	
G		307	307	138	138	393	393	183	183	187	187	
H												

**Figure 12.** Standard split nanoluc plate layout. Mutants were identified by the location of the introduced mutations on the arrestin-3 sequence (e.g. mutant 349 refers to arrestin-3 mutant P349A). Mutants were screened in horizontal duplicates.  $\beta$ 2AR was the condition where only the receptor was transfected and maximum signal was expected (positive control). Arr3 WT was the condition where WT arrestin-3 competed with light producing 114-Arr3 WT (negative control).  $\beta$ 2AR+M was the condition where only medium was added to the well after the substrate (negative control).  $\beta$ 2AR+A was the condition where 100  $\mu$ M of antagonist ICI 118,551 + 10  $\mu$ M of agonist isoproterenol were added in the same mixture (specificity control). Bordering wells in grey were avoided.

The following split nanoluc reagents were prepared in a timely manner:

- 1) **Substrate** – Fumirazine 20X + LCS buffer (NanoGlo Live Assay System)
- 2) **Ligand** – 10  $\mu$ M isoproterenol (ISO, Tocris, #1747)
- 3) **Medium** – Clear DMEM-HEPES (Bioconcept, #1-26-F03-I)
- 4) **Antagonist + Ligand** – 100  $\mu$ M ICI 118,551 (Tocris, #0821) + 10  $\mu$ M isoproterenol (Tocris, #1747)

For a total of 180 wells (3x 96-well plates with 60 wells actually being used), reagents were prepared as follows:

	TOTAL	Fumirazine ( $\mu\text{L}$ )	LCS ( $\mu\text{L}$ )	(1) ( $\mu\text{L}$ )	1M ISO ( $\mu\text{L}$ )	ICI 118,551 ( $\mu\text{L}$ )	DMEM- HEPES ( $\mu\text{L}$ )
(1) SUBSTRATE	4.6 mL	230	4370	/	/	/	/
(2) LIGAND	4 mL	/	/	800	200	/	3000
(3) MEDIUM	50 $\mu\text{L}$	/	/	10	/	/	40
(4) ANTAGONIST + LIGAND	50 $\mu\text{L}$	/	/	10	2.5	25	12.5

Measurements of GFP fluorescence and luminescence for the split nanoluc assay were performed on a PheraStar FSX microplate reader (BMG Biotech) according to settings detailed in appendix 2 and 3. For the split nanoluc assay, 16  $\mu\text{L}$  of nanoluciferase substrate were added via a pipetting automat (ViaFlow, Integra) to 64  $\mu\text{L}$  of cell suspension. Then, the 96-well plate was introduced to the plate reader for baseline measurement. After 10 minutes, the 96-well plate was withdrawn and 20  $\mu\text{L}$  of ligand was added in each well via the pipetting automat before the plate was quickly re-introduced into the plate reader for 20 minutes.

For the large scale mutant screen, strong  $\beta 2\text{AR}$  agonist isoproterenol was chosen as a reference ligand. For a selected number of mutants, other well-established partial agonists were used: carvedilol (Tocris, #2685), salmeterol (Tocris, #4712), formoterol (Sigma, #F9552) and salbutamol (Tocris, #0634).

### 1.2.3. Data analysis

Measurements of GFP fluorescence at 515 nm were calculated to reflect the expression level of each mutant compared to WT arrestin-3, as follows:

$$Exp (\%) = \left[ \frac{GFP_{mutant}}{GFP_{WT}} \right] - GFP_{empty\ well}$$

For the split nanoluc assay, kinetic traces were measured for at least 30 minutes, with the first 10 minutes dedicated to reach a stable baseline after adding the luciferase reagent. In this portion of the graph, the baseline was modeled as a simple linear function for each mutant. Then, the ligand was added and the area under curve over 20 minutes was calculated as the increase of luciferase signal minus the previously defined baseline. For clarity, results were expressed by the following ratio:

$$R_{AUC} = \frac{(AUC_{WT} / \textit{Average baseline}_{WT})}{(AUC_{mut} / \textit{Average baseline}_{mut})}$$

where  $R_{AUC}$  a strongly recruited mutant, therefore strong competitor of 114-WT arrestin-3, is reflected by a high  $R_{AUC}$  value. In kinetic traces, the baseline is defined as the average of values in the first 10 minutes of measurement prior addition of ligand.

### **1.3. Bioluminescence Resonance Energy Transfer (BRET) assay**

Similar to the split nanoluc assay, the BRET assay is a technique used to study protein-protein interactions in living cells<sup>99,100</sup> (figure 13.A). Here, the  $\beta$ 2-adrenergic receptor ( $\beta$ 2AR) is tagged to a full-length renilla luciferase (Rluc8) facing the cytoplasmic matrix (see figure 13.B for plasmid maps and appendix 1 for DNA sequences). Upon activation of the receptor, a GFP-tagged arrestin is recruited to the receptor and to the plasma membrane. In this complex, the fluorophore donor probe (Rluc8, peak emission at 410 nm) is now in close proximity to the acceptor probe (GFP tag, peak emission at 515 nm) allowing for photon transfer. Hence, the GFP fluorescence detected in cells is used as a reporter of arrestin- $\beta$ 2AR interactions over time. In chapter 2, arrestin-3 variants suitable for crystallography were screened against variants of the turkey  $\beta$ 1-adrenergic receptor (see appendix 1 for DNA sequences of receptors B6-Rluc8 and B44-Rluc8) in a collaboration with Prof. Christopher Tate (Medical Research Council, Cambridge, UK).

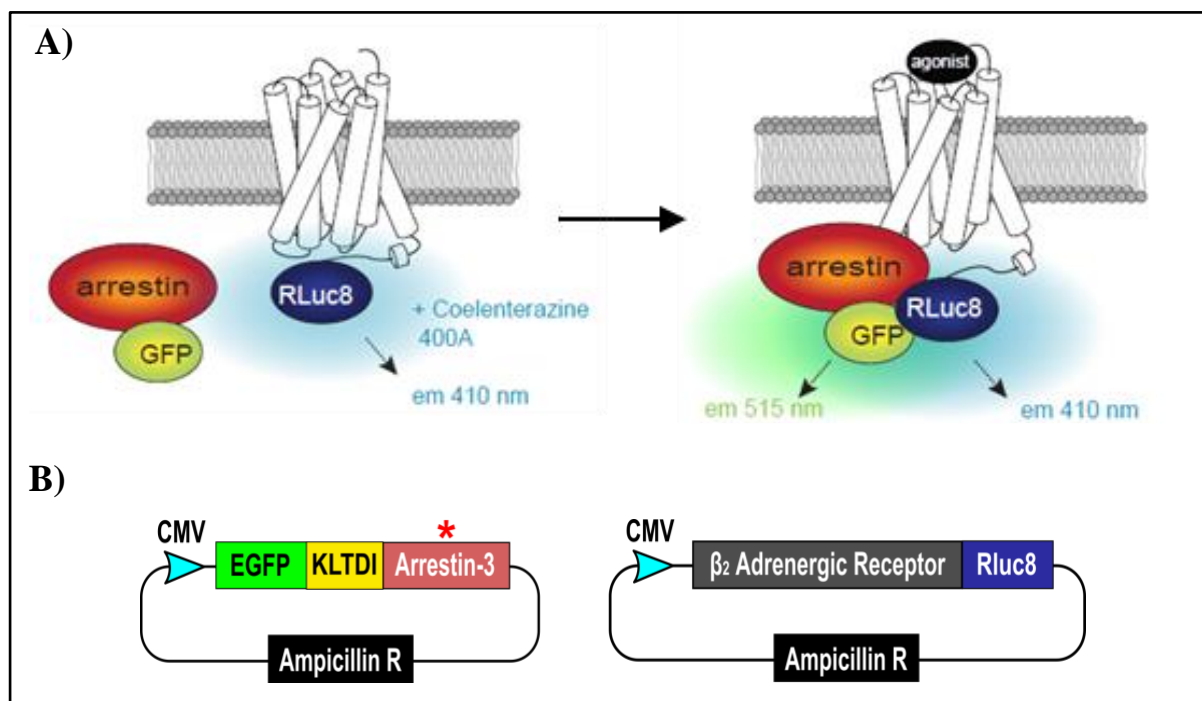


**Figure 13.** A) Schematic representation of the BRET assay. Upon recruitment of arrestin to an activated GPCR, acceptor probe GFP is stimulated by donor probe RLuc8 and light emission at 515 nm (GFP fluorescence) is measured in a plate reader over time as a reporter for arrestin/GPCR interactions. GFP: Green Fluorescent Protein. RLuc8: Renilla luciferase. Image provided by InterAx Biotech. B) Plasmid maps of pcDNA3 constructs encoding EGFP-(WT)arrestin-3 and  $\beta_2$ AR-RLuc8. R: resistance.

### 1.3.1. Cell transfection

In this assay, HEK293 cells were maintained with DMEM (Bioconcept, #1-26-F03-I) + 10% fetal calf serum (FCS, Seralog, #S4500) in 10 cm plates (SPL Life Sciences, #20101). Cells were washed with 6 mL of PBS (Gerbu, #1680,7010) and detached from the plate with 1 mL of PBS/20 mM EDTA (PSI). Collected cells were then counted with a Neubauer chamber (Celeromics) and 15,000 to 25,000 cells per well were seeded in a white cleared-bottom 96-well plate. On the next day, cells reached 40 to 60% confluency and were transfected with lipofectamine 2000 (Thermo, #11668-019) as follows:

Tube A	Tube B
90 ng of a EGFP-arrestin-3 plasmid (#444, see appendix 1)	0.6 $\mu$ L of lipofectamine 2000 transfection reagent (Thermo, #11668-019)
10 ng of a GPCR-RLuc8 plasmid (#448, 523 or 524, see appendix 1)	
50 $\mu$ L of Opti-MEM (Life Technologies, #31985-047)	50 $\mu$ L of Opti-MEM (Life Technologies, #31985-047)

After 5 minutes, tubes A and B were mixed and incubated 20 minutes at room temperature. Finally, 50  $\mu$ L of the resulting transfection mix was added per well on top of cells and the 96-well plate incubated overnight at 37°C, 5% CO<sub>2</sub>. The next day, the transfection mix was replaced by DMEM-10%FCS and cells were let to recover for another 24h.

### 1.3.2. BRET measurement

On the day of the BRET assay, 2x 96-well plates of reagents were prepared. One 96-well plate contained the Rluc8 substrate (coelentrazine 400a, Cayman chemicals, #16157) at a concentration of 5  $\mu$ M in Hanks' Balanced Salt Solution (HBSS, Life technologies, #14025050). The other 96-well plate contained isoproterenol (Tocris, #1747) at concentrations ranging from 0 to 100  $\mu$ M, which corresponded to 10-fold more concentrated stocks compared to final concentrations. The ligand plate layout below mimics the standard 96-well plate display for concentration-response experiments (figure 14).

	GPCR-Rluc8 + eGFP-Mutant A		GPCR-Rluc8 + eGFP-Mutant B		GPCR-Rluc8 + eGFP-Mutant C		GPCR-Rluc8 + eGFP-Mutant D		GPCR-Rluc8 + eGFP-Mutant R170E		GPCR-Rluc8 + eGFP-WT Arrestin-3	
	Rep 1	Rep 2	Rep 1	Rep 2	Rep 1	Rep 2	Rep 1	Rep 2	Rep 1	Rep 2	Rep 1	Rep 2
1 $\mu$ M ISO												
100 nM ISO												
10 nM ISO												
1 nM ISO												
100 pM ISO												
10 pM ISO												
1 pM ISO												
buffer												

**Figure 14.** Standard plate layout for concentration-response BRET experiments. Background colors in cells represent the ranging concentrations of isoproterenol (first column). Rep: technical replicate. Red: negative control R170E. Blue: positive control: WT arrestin-3.

For GFP fluorescence, DMEM+10%FCS was replaced by 100  $\mu$ L of clear HBSS buffer and measurements were carried out according to settings in appendix 2. For the BRET assay (settings in appendix 5), the previously clear bottom of the 96-well plate was sealed at the bottom with an opaque sticker provided by the plate manufacturer. The HBSS medium was replaced by 90  $\mu$ L of coelentrazine using the ViaFlow pipetting automat (Integra). The baseline was measured for 3 data points and 10  $\mu$ L of 10X isoproterenol were added per well with the ViaFlow. Finally, the plate was quickly re-introduced in the plate reader and the assay ran for 30 minutes.

### 1.3.3. Data analysis

Kinetic traces were measured for at least 25 minutes. The first three data points were dedicated to baseline stabilization after adding the luciferase reagent. Then, the ligand was added and the area under

curve over 20 minutes was calculated as the increase of luciferase signal induced by the ligand minus the area under curve of the respective “buffer” condition. Areas under curve (AUC) were plotted against isoproterenol concentrations and concentration-response curves were generated by the following non-linear regression formula:

$$y = Xmin + \frac{Xmax - Xmin}{1 + 10^{(\log EC_{50} - X)}}$$

where  $EC_{50}$  corresponds to the half maximal effective response (in this case, the concentration of isoproterenol required to stimulate half the maximal BRET signal). For clarity,  $EC_{50}$  are often expressed as  $pEC_{50}$ :

$$pEC_{50} = -\log (EC_{50})$$

## Results

### 1.4. Alanine scan approach for the recruitment of arrestin-3 to $\beta$ 2AR

#### 1.4.1. Large-scale screening of single point alanine mutants of arrestin-3

The objective of this study was to map the human arrestin-3 sequence for residues involved in the recruitment to the  $\beta$ 2AR. Here, the recruitment capability of 383 single point alanine mutants of arrestin-3 to the  $\beta$ 2AR was measured in SCAR3 cells using the split nanoluc assay (see complete dataset in appendix 5 and 6).

The expression levels of the arrestin-3 alanine mutants in SCAR3 cells were generally lower compared to WT arrestin-3, with 69% of the mutants expressed between 50% and 100% of WT arrestin-3 levels in cells (figure 15). Interestingly, four mutants were expressed at significantly higher levels than WT arrestin-3 (right side of the graph in figure 15): P98A ( $R_{AUC}$ = 0.84,  $Exp_{GFP}$ = 122%), E177A ( $R_{AUC}$ = 8.70,  $Exp_{GFP}$ = 203%), S303A ( $R_{AUC}$ = 0.28,  $Exp_{GFP}$ = 141%) and R323A ( $R_{AUC}$ = 0.44,  $Exp_{GFP}$ = 132%). Alanine mutations inducing a high expression of arrestin-3 seem randomly distributed over the protein with no particular common feature: P98 is near the three-element interaction, R323 lies on the C-terminal  $\beta$ -sheets, S303 is in the inter-domain region and E177 located near the polar core.

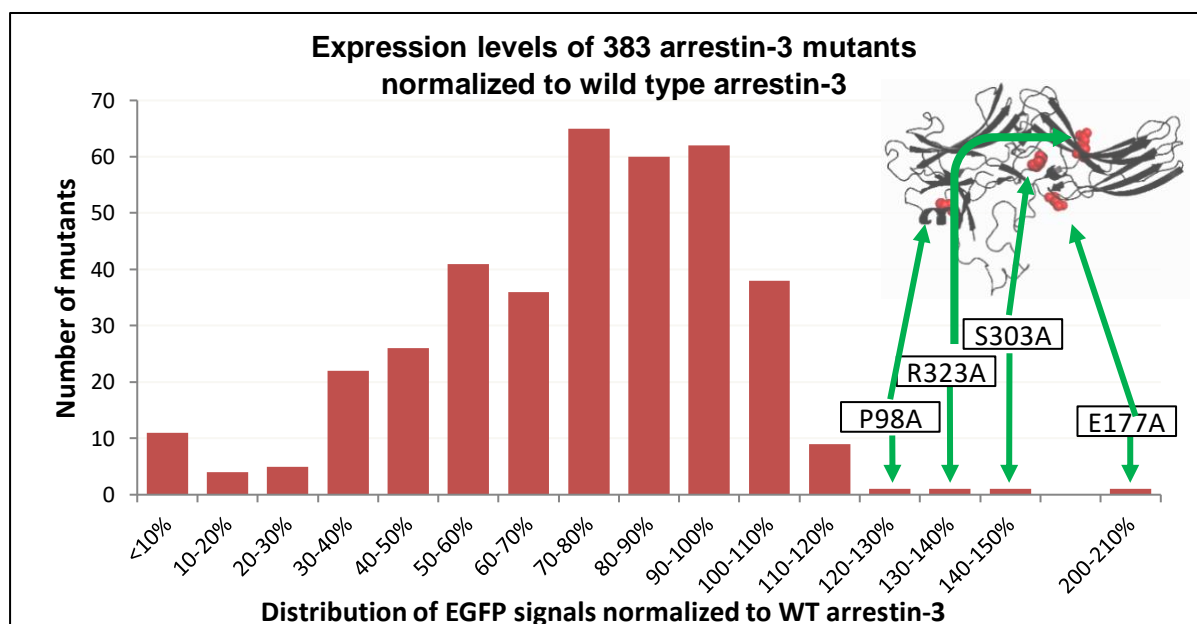


**Figure 15.** Distribution of GFP-tagged single alanine arrestin-3 mutants in SCAR3 cells. Expression levels are normalized to WT arrestin-3, which was present in each measurement round. Mutations inducing high expression of arrestin are indicated on a structure of inactive arrestin-3 (PDB 3P2D).

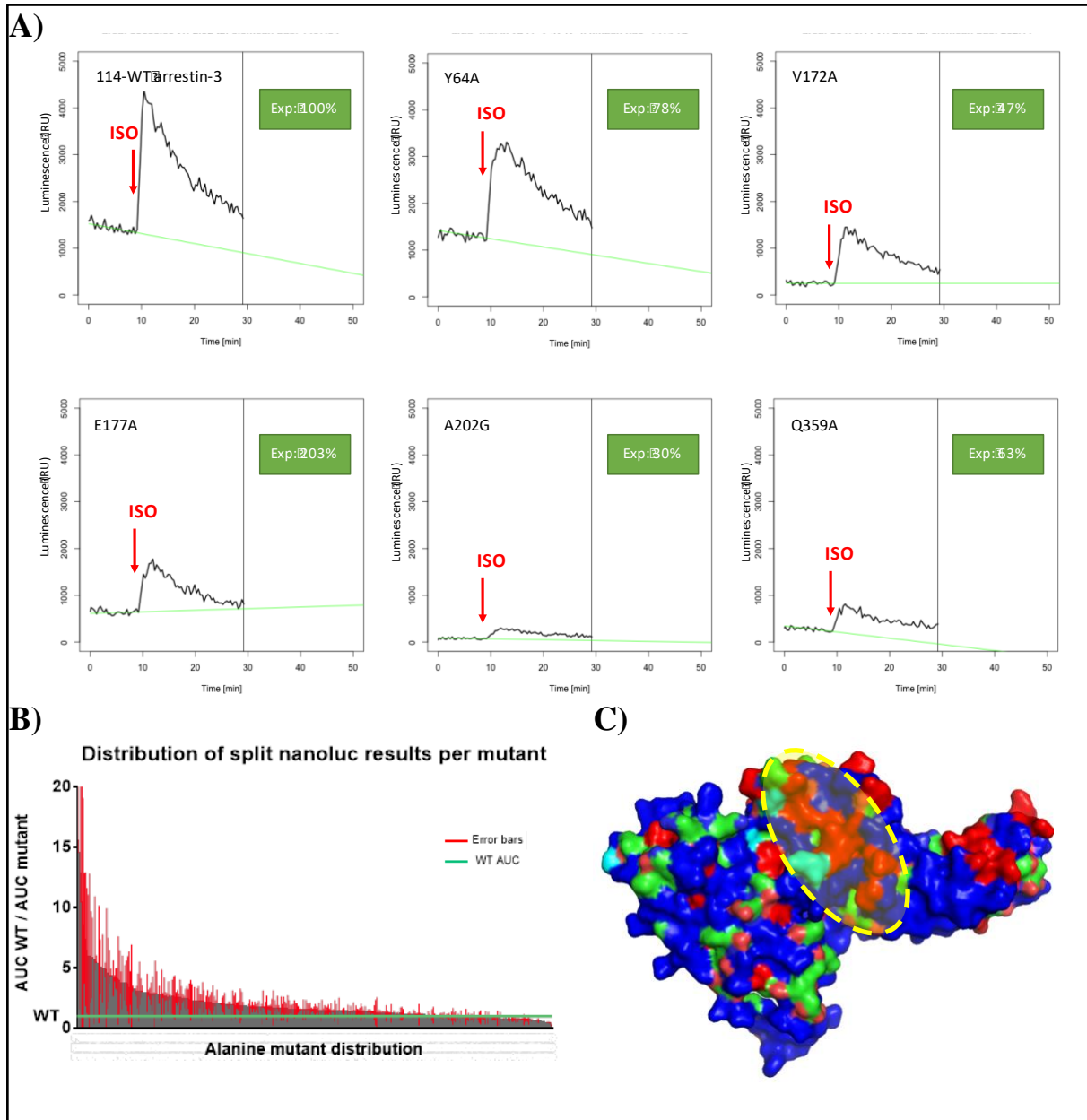


**Figure 16.** Recruitment of arrestin-3 alanine single point mutants to the  $\beta$ 2AR upon stimulation with 10  $\mu$ M isoproterenol using the split nanoluc assay. A) Kinetic traces of 6 arrestin-3 mutants (black curves). Baselines (green) were calculated from the first 10 minutes of measurement. After addition of 10  $\mu$ M isoproterenol (ISO), AUCs were calculated for 20 minutes. Exp: GFP fluorescence of arrestin-3 mutants normalized to transfected WT arrestin-3. B) Distribution of alanine mutants (grey) according to their  $RAUC$  score (see 1.2.3. Data analysis) and compared to WT arrestin-3 (green line). C) Protein mapping of arrestin-3 (PDB 3P2D). Blue: strongly recruited mutants ( $RAUC \geq 1.5$ ). Red: poorly recruited mutants ( $RAUC < 1.5$ ). Cyan: unexpressed mutants. Green: mutants not acquired. Yellow circle: poorly recruited mutants further-called “red-line” mutants.

*Marion et al., 2005*<sup>85</sup> and *Kang et al., 2015*<sup>34</sup> have shown in arrestin/GPCR structures that loops of the central crest of arrestin are critical for the recognition of an activated GPCR core (see D.3. GPCR-arrestin interface). In this region (yellow circle in figure 16.C), a patch of weak arrestin-3 recruiters to the  $\beta$ 2AR following receptor stimulation with 10  $\mu$ M of the agonist isoproterenol were identified using



the split nanoluc assay. The  $R_{AUC}$  scores (see 1.2.3. *Data analysis*) of these mutants ranged from 0.68 (L290A) to 1.42 (L288A) and consisted E67A ( $R_{AUC}= 1.36$ ), V71A (0.69), G73A (0.70), L74A (0.50), S75A (0.77), Q131A (0.88), N282A (0.76), R283A (1.30), K285A (0.87), G287A (0.84), L288A (1.42), L290A (0.68) and L294A (0.80). In addition to the neighboring low-recruiting mutants R66A ( $R_{AUC}= 1.51$ ), H211A (0.47), G212A (1.17), V254A (0.68) and S380A (1.12), this set of mutants will be further referenced as “red-line” mutants.

Baseline measurements (green lines in figure 16.A) were found to be highly variable in terms of luminescence intensity (Y64A signal starts at 1274 relative luminescence units (RLU) whereas mutant A202G starts at 48 RLU). This observation is probably due to a different number of cells per well (different starting points), which in itself induces a different consumption rate of luciferase reagent (different slopes). Secondly, the inter-assay variability was generally very high (red bars on left side of the graph in figure 16.B), particularly for mutants well recruited to the  $\beta$ 2AR.

At this point, two subsets of mutants were defined:

- The “red-line” mutants located in the central crest of arrestin-3, at the intersection of the N- and C-domains, and involved in the core interaction. These low-recruited arrestin mutants are located on the finger loop (R66A, E67A, V71A, G73A, L74A, S75A), the middle loop (Q131A) and the gate loop, (N282A, R283A, K285A, G287A, L288A, L290A, L294A) or near the central crest (H211A, G212A, V254A, S280A). The “red-line” mutants were further tested in a small-scale ligand screen, as I hypothesized that these mutants might behave differently when the  $\beta$ 2AR adopts distinct ligand-induced conformations.
- Strong arrestin recruiters to  $\beta$ 2AR: K172A ( $R_{AUC}= 8.76$ ), L373A (4.79), Q359A (14.53), P368A (9.11), R357A (20.88), R376A (4.97), L278A (5.48) and V242A (4.76). Strong recruiters were analyzed in the well-established BRET assay<sup>89,93</sup> in order to verify their high-recruitability in an independent standardized arrestin recruitment assay (see 1.3. *Bioluminescence Resonance Energy Transfer (BRET) assay* and 1.5. *Validation of split nanoluc results by BRET*).

#### 1.4.2. Ligand screen of “red-line” mutants by split nanoluc

In the split nanoluc screen in 1.4.1. *Large-scale screening of single point alanine mutants of arrestin-3*, the  $\beta$ 2AR agonist isoproterenol was used to initiate the recruitment of 383 single point alanine mutants of arrestin-3 to the  $\beta$ 2AR in HEK293 cells. As a result, a subset of arrestin mutants with weak/reduced recruitment to the  $\beta$ 2AR were identified and named “red-line” mutants. The position of the alanines in these red-line arrestin mutants suggested that the corresponding native residues of arrestin-3 – namely mutations in the finger loop, the middle loop and gate loop – were important for the

recruitment of arrestin-3 to  $\beta$ 2AR. Here, the recruitment of the “red-line” arrestin mutants to the  $\beta$ 2AR were tested using additional four known agonists of the  $\beta$ 2AR with varying potencies and efficacies: carvedilol, formoterol, salbutamol and salmeterol<sup>101</sup>. The aim of this study was to identify potential differences in arrestin-3 mutant sensitivity towards distinct ligand-activated receptor states. In addition to the “red-line” mutants, alanine mutants replacing positively charged residues near the central crest of arrestin-3 (K25A, R26A, H31A, R63A, R170A and K171A) were also investigated. The selection of these mutants was based on the assumption that the phosphorylated and typically negatively charged C-terminus of the  $\beta$ 2AR would engage with positively charged residues of arrestin-3.

Figure 17.A) displays the recruitment alanine mutants replacing positively charged residues near the central crest of arrestin-3 (K25A, R26A, H31A, R63A, R170A and K171A) to the  $\beta$ 2AR stimulated by 1  $\mu$ M of either ligand: isoproterenol (blue), formoterol (green), carvedilol (red), salbutamol (purple) and salmeterol (orange). Four arrestin-3 mutants (K25A, R26A, H31A and R63A) showed no response to the stimulation of  $\beta$ 2AR by any ligand. The mutants R170A and K171A showed a mild recruitment to  $\beta$ 2AR (10% increase in luminescence signal) upon stimulation of the receptor by 1  $\mu$ M isoproterenol or 1  $\mu$ M formoterol.

All “red-line” mutants were recruited to the  $\beta$ 2AR upon receptor stimulation with 1  $\mu$ M isoproterenol (figure 17.B). However, the isoproterenol-induced recruitment efficacy of these arrestin-3 mutants varied from a 6% increase (mutant S75A) to 50% increase (mutant R66A) in luminescence signal. Formoterol promoted low (R66A: 19% increase in luminescence signal) to isoproterenol-like (G212A: 16% increase in luminescence signal) recruitment of “red-line” mutants to  $\beta$ 2AR. Salbutamol, carvedilol and salmeterol were not able to induce a detectable level of arrestin-3 recruitment.

However, similar to the previous large-scale split nanoluc screen (figure 16.A.), profound variations in the overall luminescence signal were detected in this ligand screen (figure 17): for instance, the arrestin-3 mutant L290A reached a maximum of 290 RLU after adding the split nanoluc reagent, while the H211A mutant reached 1250 RLU. These fluctuations of luminescence intensity were most likely due to variations in expression levels of the respective arrestin-3 mutants, since all constructs were transiently transfected into the SCAR3 cells. Despite variations of luminescence signals across mutants, luminescence maxima and slopes per mutant were nearly identical regardless of the ligand used. This observation indicates that cell count is highly homogenous across the 96 well plate and that variations of luminescence signal are likely caused by different transfection efficiencies and expression levels when comparing mutants.

In conclusion, the agonists isoproterenol and formoterol were the only ligands able to induce the recruitment of the arrestin-3 mutants out of the five ligands tested (isoproterenol, formoterol, carvedilol,

salbutamol and salmeterol). In addition, the narrow assay window did not allow for the identification of differential arrestin-3 mutant recruitment to the  $\beta$ 2AR between isoproterenol and formoterol stimulations. Therefore, none of the tested “red-line” and positively charged arrestin-3 mutants displayed a preference for a ligand-specific  $\beta$ 2AR activation state.

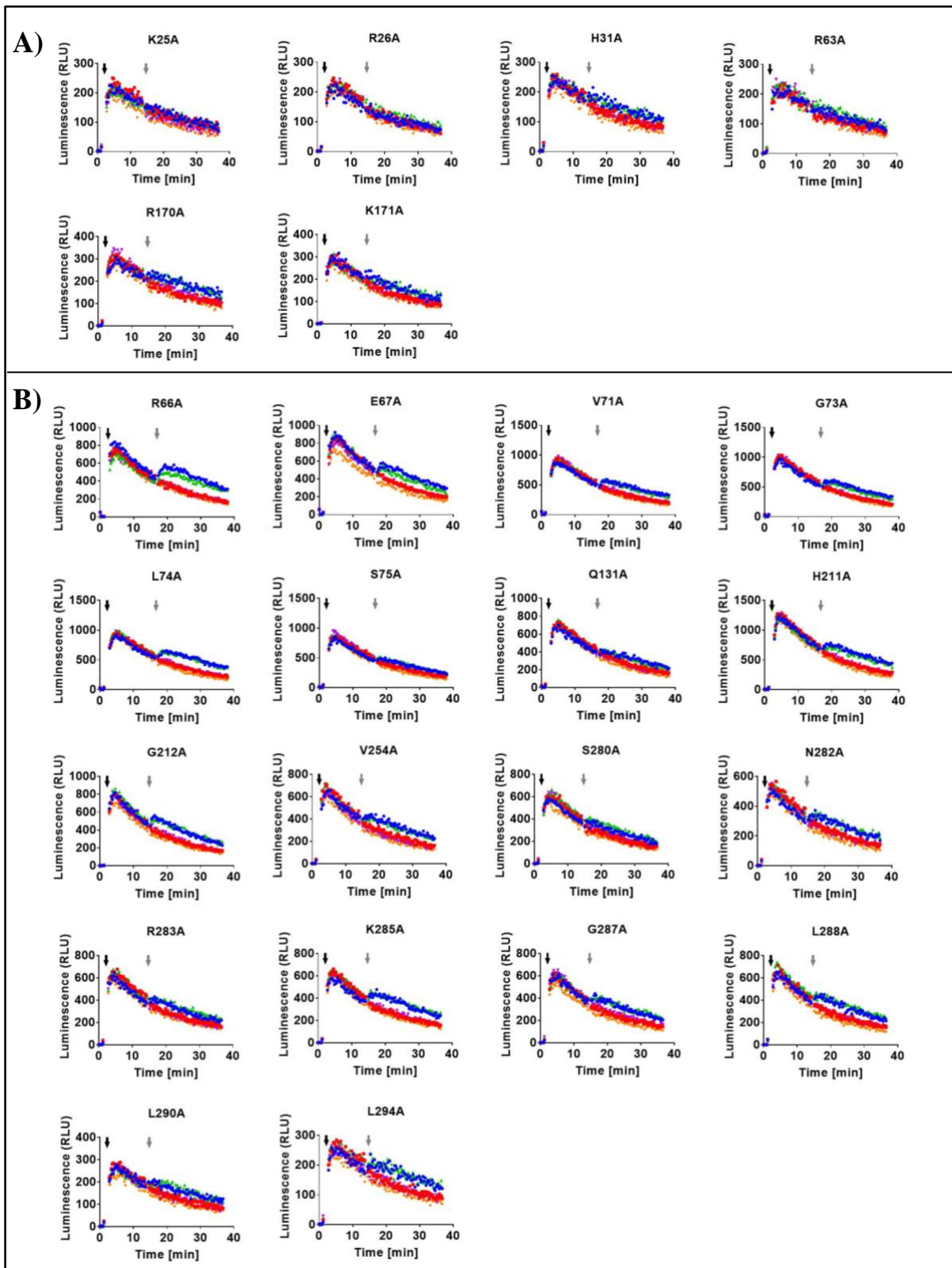


**Figure 17.** Recruitment of arrestin-3 mutants to the  $\beta_2$ AR in SCAR3 cells, using five different  $\beta_2$ AR agonists in the split nanoluc assay. The arrestin-3 mutants tested were A) the mutants replacing the positively charged residues K25A, R26A, H31A, R63A, R170A and K171A and B) “red-line” mutants described in the paragraph above. A black arrow indicates the addition of the split nanoluc reagent (fumarazine) and ligand (grey arrow) was added after 10 minutes of baseline stabilization. The  $\beta_2$ AR agonists were: Blue symbols: 1  $\mu$ M isoproterenol. Green symbols: 1  $\mu$ M formoterol. Red symbols: 1  $\mu$ M carvedilol. Purple symbols: 1  $\mu$ M salbutamol. Orange symbols: 1  $\mu$ M salmeterol.

### **1.5. Validation of arrestin-3 alanine mutant split nanoluc results by a BRET assay**

The recruitment of 383 alanine mutants of arrestin-3 to the  $\beta$ 2AR was investigated by the implementation of the novel split nanoluc assay (see *1.4.1. Large-scale screening of single point alanine mutants of arrestin-3*). To validate this split nanoluc approach, a subset of high arrestin-3 recruiters (K172A, L373A, Q359A, P368A, R357A, R376A, L278A and V343A) was selected (table 2) and their respective recruitment to the  $\beta$ 2AR was assessed in the well-established BRET assay<sup>93</sup>. For this, the arrestin-3 mutants were generated by site-driven mutagenesis (see *1.1. PCR-driven mutagenesis*) using an EGFP-(WT)arrestin-3 pcDNA3 plasmid (see plasmid map in figure 13.B and DNA sequences in appendix 1) and the arrestin-3-EGFP mutants were screened against the  $\beta$ 2AR. In this assay, the C-terminus of the  $\beta$ 2AR was fused to renilla luciferase 8 (see appendix 1 for DNA sequences). In the BRET assay, EGFP-arrestin-3 mutants and  $\beta$ 2AR-Rluc8 were transiently co-transfected into HEK293 cells. Three days post-transfection, the recruitment of arrestin-3 mutants was measured over time upon stimulation of the receptor by increasing concentrations of isoproterenol.

Mutants	R <sub>AUC</sub> score
WT arrestin-3	1.00
K172A	8.76
L373A	4.79
Q359A	14.53
P368A	9.11
R357A	20.88
R376A	4.97
L278A	5.48
V343A	4.76

**Table 2.** Split nanoluc results of highly recruitment arrestin-3 mutants to the  $\beta$ 2AR. High R<sub>AUC</sub> scores represent a high recruitment capability of arrestin-3 mutants to the  $\beta$ 2AR (see *1.3.3. Data analysis* for calculations). Full dataset of the split nanoluc assay can be found in appendix 6 and 7.

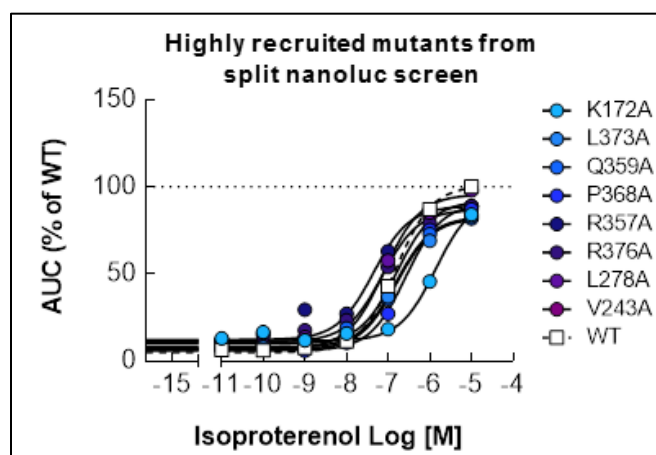


**Figure 18.** Concentration-response curves on the recruitment of strong arrestin-3 recruiters (K172A, L373A, Q359A, P368A, R357A, R376A, L278A and V343A). HEK293 cells were co-transfected with EGFP-arrestin-3 mutants and  $\beta$ 2AR-Rluc8. Receptors were stimulated by increasing concentrations of isoproterenol (0-10  $\mu$ M). Areas under curve (AUC) of 20 minutes post-stimulation were normalized to WT arrestin-3 and plotted against isoproterenol concentrations. A three parameter non-linear regression analysis to derive the efficacy and potency of arrestin-3 recruitment was performed (see equation in 1.3.3. Data analysis). AUC: area under curve.

Efficacy is defined as the maximal response intensity attainable upon ligand stimulation (here, the recruitment of an arrestin-3 mutant to  $\beta$ 2AR upon 10  $\mu$ M isoproterenol stimulation) and the potency corresponds to the half maximal effective response (here, the isoproterenol concentration required to obtain 50% of the maximal recruitment of an arrestin-3 mutant). Efficacy and potency values do not represent the affinity of arrestin for the  $\beta$ 2AR but allow for the comparison of the sensitivity of arrestin-3 mutants to the activated  $\beta$ 2AR.

In contrast to the data derived from the split-nanoluc assay (see table 2), the arrestin-3 mutants tested in the BRET assay (figure 18) showed a lower or WT-like recruitment efficacy compared to WT arrestin-3 (white squares, dotted line in figure 18). In fact, the efficacy of mutants R357A, P368A, Q359A, L373A, V343A, L278A and R376A ranged from  $82.2 \pm 5.3\%$  (L373A) to  $93.8 \pm 8.0\%$  (R376A). In comparison,  $R_{AUC}$  scores (which are also a ratio of the recruitment efficacy of a given arrestin-3 mutant to WT arrestin-3) found in the split nanoluc assay ranged from 4.76 (V343A) to 20.88 (R357A).

Discrepancies of recruitment results of arrestin-3 mutants to  $\beta$ 2AR between the split nanoluc and the BRET assays could be explained by the detection method of the two techniques. In the BRET assay, fluorophores are directly fused to the proteins of interest (namely arrestin-3 and the  $\beta$ 2AR). In the split nanoluc assay, the two subunits of the split nanoluciferase are fused to arrestin-3 mutants and the prenylation motif CAAX, that decorates the plasma membrane. As a result, noise is reduced in the BRET assay compared to the split nanoluc assay, where random interactions between arrestin-3 mutants and the plasma membrane are more frequent. In addition, in the BRET assay, the proteins of interest

are co-transfected in HEK293 cells which entails that variations in transfection efficiencies are likely to affect both plasmids at the same time. In the split nanoluc assay, however, the two components of the nanoluciferase were stably expressed in SCAR3 cells, on top of which arrestin-3 mutants and the  $\beta$ 2AR were transfected via a single plasmid. Therefore, variations in transfection efficiency in the split nanoluc assay will only affect the expression of arrestin-3 mutants and the  $\beta$ 2AR, but not the endogenous WT-arrestin-3 levels. In comparison, the BRET detection method relies on the measurement of a fluorescence ratio (515/410 nm) that accounts for variations in expression of the donor probe (Rluc8) or the acceptor probe (EGFP).

## Discussion, chapter 1

In this study, I generated 383 single point alanine mutants of human arrestin-3 and analyzed their recruitment ability to the  $\beta$ 2AR using a novel detection method called split nanoluc. In the literature, three categories of arrestin mutants have been reported in recruitment studies to GPCRs: truncated or chimeric arrestins<sup>14,17</sup>, single point mutations aimed to reverse native residue charges<sup>25,26,39</sup> and alanine single point mutants used to neutralize a particular residue function<sup>39,40</sup>. In addition, most studies<sup>14,25,40,94</sup> focused on the recruitment of arrestin-1 mutants to rhodopsin. Therefore, to compare arrestin-3 recruitment results to  $\beta$ 2AR, I choose to refer to single point alanine mutants of arrestin-1. One study in particular from *Ostermaier et al., 2014*<sup>40</sup> used an alanine scan approach where the recruitment of single point alanine mutants spanning the entire arrestin-1 sequence was investigated to various activated states of rhodopsin by pull-down assays.

Although a small scale BRET-assay screen of selected arrestin-3 mutants (see section 1.5) failed to confirm the results of the split nanoluc results (see section 1.4), I will nevertheless highlight a series of interesting mutants found in this alanine scan of arrestin-3 and speculate on their respective properties in relation to data derived with arrestin-1<sup>40</sup>. However, throughout the following discussion, differences in the experimental setups must be taken into consideration. *Ostermaier et al., 2014*<sup>40</sup> analyzed the recruitment of purified arrestin-1 mutants to rhodopsin in nanodiscs (phospholipid bilayer encasing the receptor) by pull-down assays. In contrast, the split nanoluc study (see section 1.4) explored the recruitment of arrestin-3 to the  $\beta$ 2AR in mammalian cells. The comparison of the two studies will focus on alanine mutants of residues involved in arrestin pre-activation (i.e. polar core<sup>26</sup>, three element interaction<sup>39</sup>) or direct interaction with GPCRs (central crest residues interacting with the GPCR core<sup>102</sup>, residues recognizing the phosphorylated C-terminus of GPCRs). To assess the apparent stability of the arrestin/rhodopsin complex, *Ostermaier et al., 2014*<sup>40</sup> quantified the amount of bound arrestin to rhodopsin in sodium chloride titrations. Salt sensitivity of a protein-protein complex is not a strict

measurement of affinity. Sodium chloride acts as an inhibitor of the ionic bonds formed by rhodopsin and arrestin-1 mutants. In practice, the stability of arrestin-1/rhodopsin complexes can be evaluated by their IC<sub>50</sub> values, or the concentration of NaCl required to dissociate half of the arrestin-1/rhodopsin complexes. Therefore, the recruitment of arrestin-1 mutants will be expressed in fold-change of IC<sub>50</sub> values to WT arrestin-1 (IC<sub>50, WT</sub> = 0.41 M NaCl) in order to be compared to RAUC scores of arrestin-3 mutants from the split nanoluc assay. As defined in 1.2.3. *Data analysis*, RAUC scores directly compare the ability of one mutant to form a stable complex with β2AR to WT-arrestin-3 (which has a RAUC score of 1).

### **A comparison of arrestin-1 versus arrestin-3 mutants of the polar core and the three element interaction site**

In all arrestins, it has been shown<sup>25,103</sup> that the disruption of the so-called polar core – a pocket of hydrophilic residues – results in arrestin activation. This polar core disruption is typically initiated by the binding of the phosphorylated C-terminus of a given GPCR to the arrestin protein.

In *Ostermaier et al., 2014*<sup>40</sup>, alanine substitution of polar core residues induced a 1.5- (D30A) to 2.3- (R382A) fold increase in IC<sub>50</sub> values of the arrestin-1/rhodopsin complexes (table 3). In comparison, cognate mutations of the polar core in the arrestin-3/β2AR screen yielded to RAUC scores ranging from 0.9 (R170A and R393A) to 2.8 (D28A). Surprisingly, the alanine substitution leading to the lowest stability increase of the arrestin-1/rhodopsin (D30A, 1.5 fold-change compared to WT arrestin-1) appears to be the highest stabilizer of the arrestin-3/β2AR complex (D28A, 2.8 fold-change compared to WT arrestin-3). In arrestin-1, mutations R175A and R382A engendered the highest polar core disruption and subsequent recruitment to rhodopsin with a 2.2 and 2.3 fold-changes in IC<sub>50</sub> values compared to WT arrestin-1, respectively. Additionally, glutamate substitution on arrestin-1 residue R175 and R382 were also reported by *Granzin et al., 2015*<sup>26</sup> and *Vishnivetskiy et al., 1999*<sup>25</sup> respectively to enhance arrestin pre-activation and coupling to all forms of rhodopsin (including inactive and/or non-phosphorylated states of rhodopsin). However, in the split nanoluc assay, cognate mutants R170A and R393E led to a WT-like recruitment of arrestin-3 with RAUC scores of 0.9.

In all arrestins, it has been shown<sup>103</sup> that the perturbation of a hydrophobic pocket called the three element interaction also participates in the activation of arrestin. In *Ostermaier et al., 2014*<sup>40</sup>, the mutation of F375 to alanine in arrestin-1 led to the highest IC<sub>50</sub> increase, with a fold-change in IC<sub>50</sub> of 3.1 compared to WT arrestin-1. The mutant F375A was confirmed by *Haider et al., 2019*<sup>94</sup> to be a highly recruited arrestin-1 to rhodopsin. In the split nanoluc screen, a likewise highly recruiting behavior of the cognate mutant I386A in arrestin-3 was detected. In fact, both F375A in arrestin-1 and cognate mutant I386A in arrestin-3 were the strongest recruiters in their respective group of mutants



that inactivate the three-element interaction (which include L101A and L105A for arrestin-3; L103A and L107A for arrestin-1).

	Arrestin-3 mutants from the split nanoluc assay ( $R_{AUC}$ values, corresponding to fold-changes in recruitment to $\beta$ 2AR compared to WT arrestin-3)	Arrestin-1 mutants from pulldown assays by <i>Ostermaier et al., 2014</i> <sup>28</sup> (fold-changes in $IC_{50}$ values of the arrestin-1 mutant/rhodopsin complexes compared to WT arrestin-1)
Polar core	D28A (2.8)	D30A (1.5)
	D291A (2.3)	D296A (2.2)
	D298A (2.1)	D303A (2.1)
	R170A (0.9)	R175A (2.2)
	R393A (0.9)	R382A (2.3)
Three-element interaction	L101A (2.1)	L103A (1.2)
	L105A (2.7)	L107A (1.0)
	I386A (3.1)	F375A (3.1)

**Table 3.** Polar core and three element interaction mutants: recruitment capability of i) arrestin-3 mutants to the  $\beta$ 2AR ( $R_{AUC}$  scores) and ii) arrestin-1 mutants to rhodopsin (fold-change in  $IC_{50}$  values).  $R_{AUC}$  scores correspond to the ratio of area under curve between an arrestin-3 mutant and WT arrestin-3. Fold-change in  $IC_{50}$  values compare the stability of an arrestin-1 mutant/rhodopsin complex to that of WT arrestin-1, as reported by *Ostermaier et al., 2014*<sup>40</sup>.

### A comparison of arrestin-1 and arrestin-3 phosphate-sensing mutants

*Zhou et al., 2017*<sup>84,85</sup> and *Mayer et al., 2019*<sup>81</sup> have demonstrated that three conserved regions of arrestin-1 interact directly with the phosphate groups located at the C-terminus of rhodopsin (see *D.3. GPCR-arrestin interface*, figure 6).

For arrestin-1 and arrestin-3, phosphate-sensing mutants (table 4) refer to arrestin mutants that substitute any of these amino acids involved in this interaction to an alanine (K14, K15, R18, R29, R171 and K300 in arrestin-1; K11, K12, R26, R107, R166 and K293 in arrestin-3). In pull-down assays by *Ostermaier et al., 2014*<sup>40</sup>, fold-change in  $IC_{50}$  values of arrestin-1/rhodopsin complexes ranged from 0.6 (R66A) to 1.3 (R171A). With the exception of R171A (1.3), the reported fold-changes of  $IC_{50}$  values are lower than 1 for the mutants K14A, K15A, R18A, R29A and K300A of arrestin-1, which indicates a reduction in complex stability with rhodopsin. However, for arrestin-3,  $R_{AUC}$  values ranged between 1.1 (K293) and K12A (3.9), which indicates a higher recruiting behavior for the mutants K11A, K12A, R26A, R107A, R166A and K293A. Therefore,  $R_{AUC}$  values of arrestin-3 mutants indicate that, by disturbing the ionic bonds tethering the C-tail of arrestin-3 on the N-domain, alanine mutations in these positions might indirectly promote a fully activated conformation of arrestin-3.

	Arrestin-3 mutants from the split nanoluc assay ( $R_{AUC}$ values, corresponding to fold-changes in recruitment to $\beta 2AR$ compared to WT arrestin-3)	Arrestin-1 mutants from pulldown assays by <i>Ostermaier et al., 2014</i> <sup>28</sup> (fold-changes in $IC_{50}$ values of the arrestin-1 mutant/rhodopsin complexes compared to WT arrestin-1)
Pocket A	n. a.	R18A (0.8)
	R166A (2.1)	R171A (1.3)
Pocket A & B	K12A (3.9)	K15A (0.8)
Pocket B	R26A (3.6)	R29A (0.6)
	K293A (1.1)	K300A (0.8)
Pocket C	K11A (1.5)	K14A (0.7)
	R107A (2.3)	L110A (0.9)

**Table 4.** Phosphate sensing mutants: recruitment capability of i) arrestin-3 mutants to the  $\beta 2AR$  ( $R_{AUC}$  scores) and ii) arrestin-1 mutants to rhodopsin (fold-change in  $IC_{50}$  values). Pockets A, B and C are residues that interact with phosphate groups of rhodopsin according to *Zhou et al., 2017*<sup>82</sup> and *Mayer et al., 2019*<sup>81</sup>.  $R_{AUC}$  scores correspond to the ratio of area under curve between an arrestin-3 mutant and WT arrestin-3. Fold-change in  $IC_{50}$  values compare the stability of an arrestin-1 mutant/rhodopsin complex to that of WT arrestin-1, as reported by *Ostermaier et al., 2014*<sup>40</sup>.

### A comparison of arrestin-1 and arrestin-3 mutants of the core-interacting residues

Arrestin/rhodopsin structures from *Kang et al., 2015*<sup>34</sup> and *Marion et al., 2006*<sup>85</sup> indicate that arrestin-1 residues located at the so-called central crest – a protein region rich in flexible loops – recognize the activated core of a GPCR (see *D.3. GPCR-arrestin interface*, figure 7). In the central crest, amino acids of the finger loop, the middle loop, the C-loop and the back loop interact with intracellular components of rhodopsin.

For arrestin-1, inactivation of the finger loop residues G76 and L77A led to a WT-like recruitment to rhodopsin with a reported fold-change in  $IC_{50}$  values of 1.0 and 0.8, respectively. In comparison (table 5), cognate mutants G76A and L77A of arrestin-3 appeared to be less recruited than WT arrestin-3 with  $R_{AUC}$  values of 0.7 and 0.5, respectively. In the middle loop, mutation Q131A did not impact the recruitment of arrestin-3 to the  $\beta 2AR$  ( $R_{AUC}$  value of 0.9), while mutant D136A induced a significant increase in arrestin-3 recruitment to the  $\beta 2AR$  ( $R_{AUC}$  value of 1.6). In arrestin-1, both cognate mutants Q133A and D138A led to a WT-like recruitment to rhodopsin (fold changes in  $IC_{50}$  values of 0.9 and 1.0 respectively). In addition, mutation L244A in the C-loop of arrestin-3 appears improve arrestin-3 binding with an  $R_{AUC}$  value of 1.5. However, the arrestin-1/rhodopsin structure of *Kang et al., 2015*<sup>34</sup> shows that residues Q133 and D138 of the middle loop and residue L249 of the C-loop form tight

interactions with the intracellular loop 2 of rhodopsin. Therefore, the increased recruitment of cognate arrestin-3 mutants Q131A, D136A and L244A to the  $\beta$ 2AR is in reality very unlikely, unless the core-interaction of the arrestin-3/ $\beta$ 2AR complex is fundamentally different than arrestin-1/rhodopsin complex.

	Arrestin-3 mutants from the split nanoluc assay ( $R_{AUC}$ values, corresponding to fold-changes in recruitment to $\beta$ 2AR compared to WT arrestin-3)	Arrestin-1 mutants from pulldown assays by <i>Ostermaier et al., 2014</i> <sup>28</sup> (fold-changes in $IC_{50}$ values of the arrestin-1 mutant/rhodopsin complexes compared to WT arrestin-1)
Finger loop	G73A (0.7)	G76A (1.0)
	L74A (0.5)	L77A (0.8)
Middle loop	Q131A (0.9)	Q133A (0.9)
	D136A (1.6)	D138A (1.0)
C-loop	L244A (1.5)	L249A (1.0)
Back loop	K313A (1.0)	K318A (0.9)

**Table 5.** Core-interacting mutants: recruitment capability of i) arrestin-3 mutants to the  $\beta$ 2AR ( $R_{AUC}$  scores) and ii) arrestin-1 mutants to rhodopsin (fold-change in  $IC_{50}$  values). Residues on the finger loop, the middle loop, the C-loop and the back loop are involved in the core-interaction with rhodopsin as described by *Kang et al., 2015*<sup>34</sup> and *Marion et al., 2006*<sup>85</sup> (see D.3. *GPCR-arrestin interface*).  $R_{AUC}$  scores correspond to the ratio of area under curve between an arrestin-3 mutant and WT arrestin-3. Fold-change in  $IC_{50}$  values compare the stability of an arrestin-1 mutant/rhodopsin complex to that of WT arrestin-1, as reported by *Ostermaier et al., 2014*<sup>40</sup>.

The analysis of arrestin-3 mutants generated in section 1.4, focusing on the membrane anchor residues of the C-edge of arrestin-3 (*Lally et al., 2017*<sup>84</sup>), are hampered by the fact that this protein-membrane interface is governed by hydrophobic interactions. Since the alanine residues of the arrestin-3 mutants (see section 1.4) might still be able to partially assume hydrophobic interactions with the plasma membrane through their methyl group, a clear-cut analysis of these mutants is not possible.

In conclusion, the development of the split nanoluc assay (see section 1.4) as a novel, flexible and reliable analysis tool for arrestin-3 recruitment to GPCRs was met with significant technical limitations. Nevertheless, the data allowed for a basic analysis of the importance of several corresponding key residues in both arrestin-1 and arrestin-3. Out of twenty residues involved in arrestin pre-activation (polar core, three-element interaction) or direct GPCR interactions (phosphate-sensing residues, central crest residues), only eight alanine mutants of arrestin-3 matched the recruitment profile of arrestin-1 alanine mutants to rhodopsin. In fact, the mutants D291A/D296A (polar core), D298A/D303 (polar core), D28A/D30A (polar core), I386A/F375A (three element interaction), L101A/L103A (three element interaction), and R166A/R171A (phosphate sensing residue) exhibited a higher recruitment

behavior compared to WT arrestin-3/WT arrestin-1. In comparison, mutants Q131A/G133A (middle loop) and L74A/L77A (finger loop) showed a reduced recruitment compared to WT arrestin-3/WT arrestin-1.

## **CHAPTER 2 – Engineered arrestins for the stabilization of $\beta$ 1-adrenergic receptor variants**

*Haider et al., 2019*<sup>94</sup> have generated 403 single point alanine mutants of bovine arrestin-1 in order to design strong recruiters to rhodopsin. Their objective was to increase the affinity of arrestin-1 to phosphorylated and light activated rhodopsin by combining mutations, while conserving the thermostability and the expression level of arrestin-1 in mammalian cells. Here, four arrestin-3 cognates of the best arrestin-1 recruiters identified<sup>94</sup> were generated in order to test their recruitment capability to the  $\beta$ 2AR and variants of the  $\beta$ 1AR in a BRET assay. In addition, the recruitment of combined arrestin-3 mutants were compared to nine single point pre-activated mutants (R393E<sub>25</sub>, R170E<sub>26</sub>, I386A<sub>94</sub>, R8A<sub>104</sub>, R26A<sub>81,82</sub>, K108A<sub>81,82</sub>, K78A<sub>102</sub>, R66A<sub>102</sub> and A248V<sub>33</sub> in arrestin-3) described in the literature, as these pre-activated arrestin mutants exhibited a high recruiting behavior to GPCRs. The single point mutations were designed to either disturb the stabilizing pockets of arrestin-3 (polar core with R393E<sub>25</sub>, R170E<sub>26</sub> or the three element interaction with I386A<sub>94</sub>), inactivate residues involved in the interaction with GPCR phosphate groups (R8A<sub>104</sub>, R26A<sub>81,82</sub>, K108A<sub>81,82</sub>) or the pre-activating loops that are engaged with an activated GPCR core (K78A<sub>102</sub>, R66A<sub>102</sub> and A248V<sub>33</sub>). The objective of this study was to develop strong arrestin-3 recruiters to truncated variants of  $\beta$ 1AR. This was a joint project with Prof. Christopher Tate, Medical Research Council, Cambridge, UK, who would further test the utilization of such strong arrestin-3 binders to the  $\beta$ 1AR for crystallization purposes. This project was also developed in collaboration with Dr. Maria Waldhoer (InterAx Biotech AG).

### **Material and methods**

#### **2.1. Combined alanine mutants of arrestin-3**

In a pull-down assay involving purified arrestin-1 and rhodopsin in nanodiscs (phospholipid bilayer encasing the receptor), *Haider et al., 2019*<sup>94</sup> assessed the stability of complexes formed by rhodopsin and arrestin-1 mutants by sodium chloride titrations. Their main finding was that the mutant F375A was the most complex-stabilizing mutation among single point alanine mutants with an IC<sub>50</sub> value of 1.31 M compared to 0.41 M for WT arrestin-1. From there, additional point mutations were combined until a 5- (mutant T304A+F375A), 7.1- (mutant D303A+T304A+E341A+F375A) and 7.2- (mutant R171A+T304A+E341A+F375A) fold increase in binding capability of such multiple-mutant arrestin-1 to activated rhodopsin was reached. The three aforementioned multiple-mutants of arrestin-1 were transferred to arrestin-3 as: double mutant A (T299A+I386A), triple mutant B (T299A+I386A+R166A)

and triple mutant C (T299A+I386A+D298A). Because of its shorter 344-loop, no amino acid in arrestin-3 corresponds to E341 in arrestin-1.

Moreover, mutation R382A in the polar core of arrestin-1 was reported by *Vishnivetskiy et al., 1999*<sup>25</sup> to pre-activate arrestin-1 and promote its recruitment to dark- and/or non phosphorylated forms of rhodopsin. Therefore, a fourth arrestin-3 multiple-mutant was investigated: triple mutant D (T299A+I386A+R393A). Arrestin-3 mutants were generated by site-directed mutagenesis (see 1.1. *PCR-driven mutagenesis*).

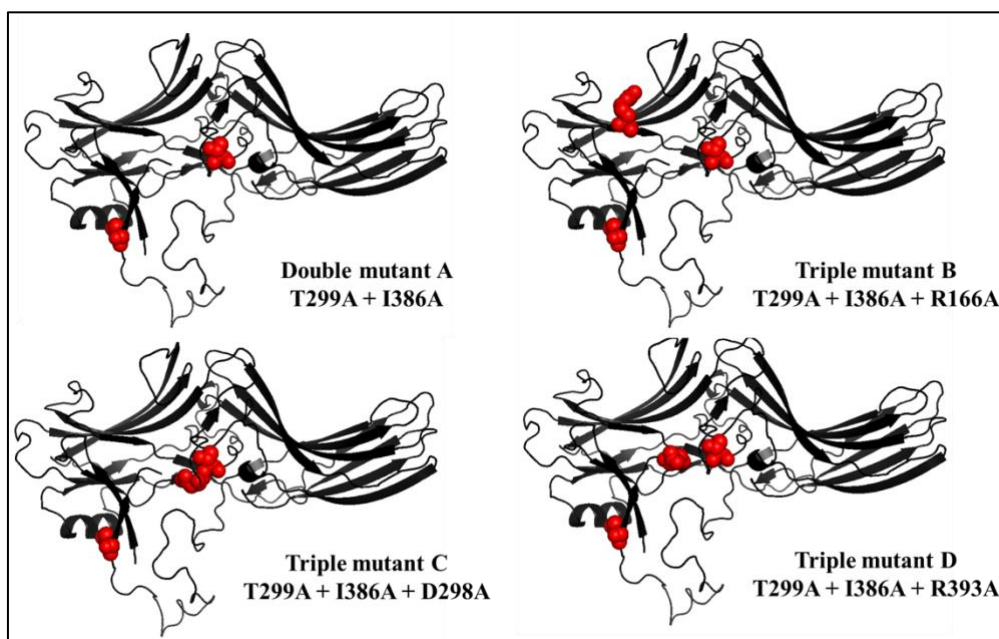


**Figure 19.** Strong recruiters (double and triple alanine mutants) transferred from an arrestin-1/rhodopsin screen performed by *Haider et al., 2019*<sup>94</sup>. Mutations are projected on an inactive arrestin-3 structure (PDB 3P2D) Mutations are located near or at the polar core (T299A, D298A and R393A) and at the three-element interaction (I386A).

## 2.2. Variants of the turkey $\beta$ 1-adrenergic receptor

The arrestin-3 pre-activated mutants (R393E<sub>25</sub>, R170E<sub>26</sub>, I386A<sub>94</sub>, R8A<sub>104</sub>, R26A<sub>81,82</sub>, K108A<sub>81,82</sub>, K78A<sub>102</sub>, R66A<sub>102</sub> and A248V<sub>33</sub>) and combined mutants transferred from arrestin-1 were first tested for their respective binding affinities towards the  $\beta$ 2AR in HEK293 cells (see protocol in 1.3. *Bioluminescence Resonance Energy Transfer (BRET) assay*). Subsequently, the arrestin-3 mutants were tested for their binding patterns on receptor variants of the turkey  $\beta$ 1-adrenergic receptor ( $\beta$ 1AR), described in *Warne et al., 2001*<sup>105</sup>. The  $\beta$ 1AR mutants were designed for crystallography and therefore contain major modifications from WT  $\beta$ 1AR (figure 20 and appendix 4 for detailed sequences):

- **Receptor B6** contains a cellular expression-enhancing mutation C116L, a 33 amino-acid truncation on the amino(N)-terminus and a reduced C-tail by 59 amino acids.

- **Receptor B44** presents the same modifications as B6. In addition, the mutation C358A (further enhancing the expression of the receptor in cells) was introduced, a C-tail truncation of 115 amino acids and a reduced intracellular loop 3 from 30 amino acids to 2.

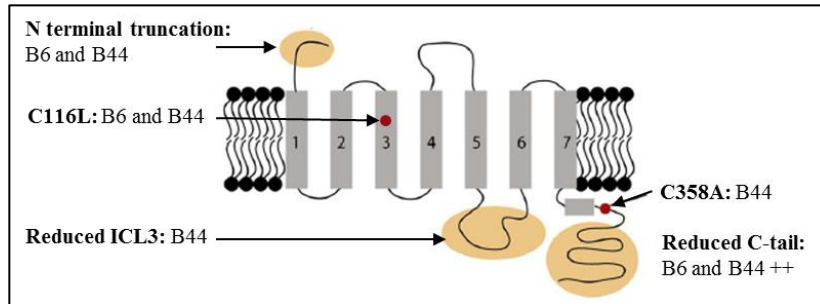


**Figure 20.** Schematic view of receptor mutants B6 and B44 of the turkey  $\beta 1$ AR.

Image adapted from *Warne et al., 2009*<sup>105</sup>.

## Results

The recruitment of arrestin-3 single point mutants and combined mutants derived from *Haider et al., 2019*<sup>94</sup> to the  $\beta 2$ AR were compared based on their efficacy (maximal response intensity attainable after ligand stimulation) and potency levels (half maximal effective response). Here, efficacy values correspond to the maximal recruitment of arrestin-3 mutants to  $\beta 2$ AR upon 10  $\mu$ M isoproterenol stimulation and potency reflects the isoproterenol concentration required to obtain 50% of the maximal recruitment.

### **2.4. Recruitment of single point pre-activated mutants to the $\beta 2$ -adrenergic receptor**

The single point pre-activated mutants of arrestin-3 – which were previously suggested to be strongly recruited to GPCRS<sub>25,26,34,81,82,94,102,104</sub> – were tested for their respective binding properties to the  $\beta 2$ AR (figure 21). The objective was to reproduce the recruitment behavior of such mutants towards the  $\beta 2$ AR in the BRET assay, and to obtain reference data for the comparison of combined mutants. The selected pre-activated single point arrestin-3 mutants are:

- R393E<sub>25</sub> and R170E<sub>26</sub>, that disrupt the arrestin polar core by charge reversal
- I386A that disturb the hydrophobic interactions in the three-element interaction<sup>94</sup>
- R8A, R26A and K108A that inactivate residues involved in the recognition of phosphates on the C-terminus of an activated GPCR<sub>81,82,104</sub>
- K78A and R66A that pre-activate the finger loop, necessary for the so-called core interaction with GPCRS<sub>102</sub>

- A248V, located on the C-loop which is involved in the core-interaction with GPCR<sub>S33</sub>

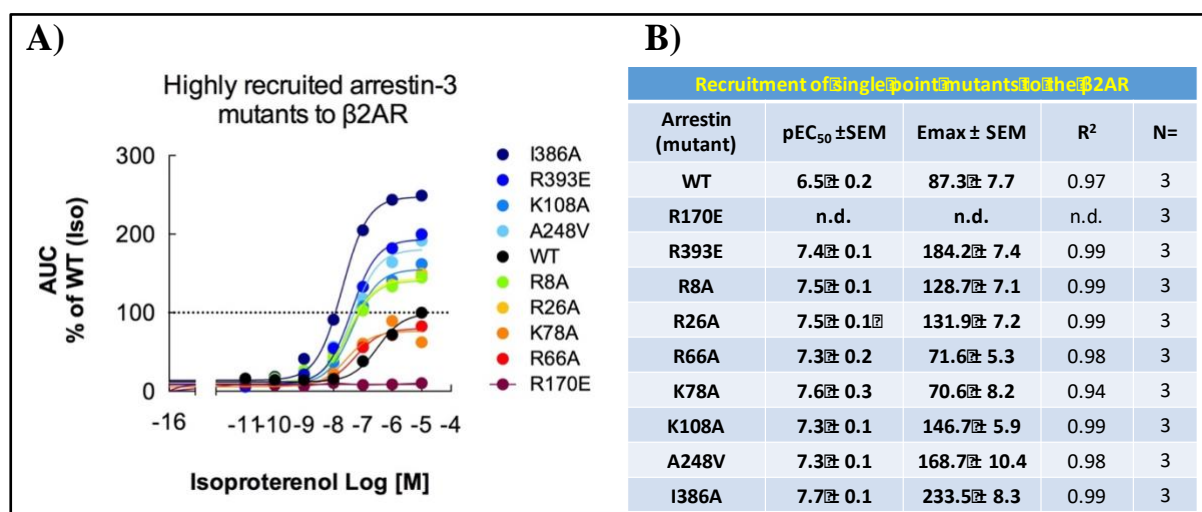


**Figure 21.** A) Concentration-response curves showing the recruitment of pre-activated arrestin-3 mutants against the  $\beta$ 2AR. HEK293 cells were transiently co-transfected with EGFP-arrestin-3 mutants and  $\beta$ 2AR-Rluc8 containing plasmids. Receptors were stimulated by increasing concentrations of isoproterenol (0-10  $\mu$ M). Areas under curve (AUC) of BRET kinetic traces were measured for 20 minutes, then normalized to WT arrestin-3 and plotted against isoproterenol concentrations. A three parameter non-linear regression analysis to derive the efficacy and potency of arrestin-3 recruitment was performed (see equation in 1.3.3. Data analysis). AUC: area under curve. B) Non-linear regression parameters. pEC<sub>50</sub>: -log(EC<sub>50</sub>); E<sub>max</sub>: efficacy. SEM: standard error of the mean. R<sup>2</sup>: coefficient of determination. N: number of replicates.

As shown in figure 21.A), the arrestin-3 mutants K78A (orange circles) and R66A (in red) exhibited lower efficacies –  $70.6 \pm 8.2\%$  and  $71.6 \pm 5.3\%$ , respectively – compared to WT arrestin-3 (black). Despite a charge reversal in the polar core, the arrestin-3 mutant R170E (dark red) appeared non-functional in the BRET assay. For this reason, mutant R170E was later used as a negative control. All other single point mutants (R393E, I386A, R8A, R26A, K108A and A248V) showed a higher recruitment capability to the  $\beta$ 2AR with efficacies ranging from 129% (R8A in green) to 233% (I386A in dark blue) of WT arrestin-3. Therefore, efficacy values suggest that one mutation in the polar core (R393E), one mutation of the three element interaction (I386A), two inactivation of phosphate sensing residues (R8A, R26A) and one mutation of the C-loop (A248V) were successful in pre-activating arrestin-3, therefore increasing its affinity to  $\beta$ 2AR.

Potencies also shifted among pre-activated mutants from  $316.5 \pm 184.7$  nM (WT arrestin-3) to  $19.9 \pm 5.2$  nM (mutant I386A). Surprisingly, recruitment of WT arrestin-3 to the  $\beta$ 2AR did not reach saturation at 10  $\mu$ M isoproterenol stimulation, as indicated by the E<sub>max</sub> value of  $87.3 \pm 7.7\%$  in figure 21.B).



## **2.5. Recruitment of combined arrestin-3 mutants to the $\beta$ 2-adrenergic receptor and variants of the $\beta$ 1-adrenergic receptor**

The recruitment capability of combined arrestin-3 mutants to  $\beta$ 2AR, receptor B6 and receptor B44 (abovementioned variants of the  $\beta$ 1AR) were assessed in the BRET assay. Arrestin-3 combined mutants were designed in order to achieve a high recruitment capability of such arrestins for a given GPCR. Arrestin-3 combined mutants were generated based on previous studies performed in arrestin-1 mutants and their respective recruitment patterns to rhodopsin by *Haider et al., 2019*<sup>94</sup>. Combined arrestin-3 mutants consisting of a double mutant A (T299A+I386A), a triple mutant B (T299A+I386A+R166A), a triple mutant C (T299A+I386A+D298A) and a triple mutant D (T299A+I386A+R393A) were designed. In addition, four single point pre-activated mutants were selected from the BRET assay described in 2.4. *Recruitment of single point pre-activated mutants to the  $\beta$ 2-adrenergic receptor: I386A, R393E, K108A and R8A*. The objective was to compare the recruitment capability of combined mutants and single point pre-activated mutants of arrestin-3 to the three GPCRs:  $\beta$ 2AR, receptor B6 and in particular receptor B44.

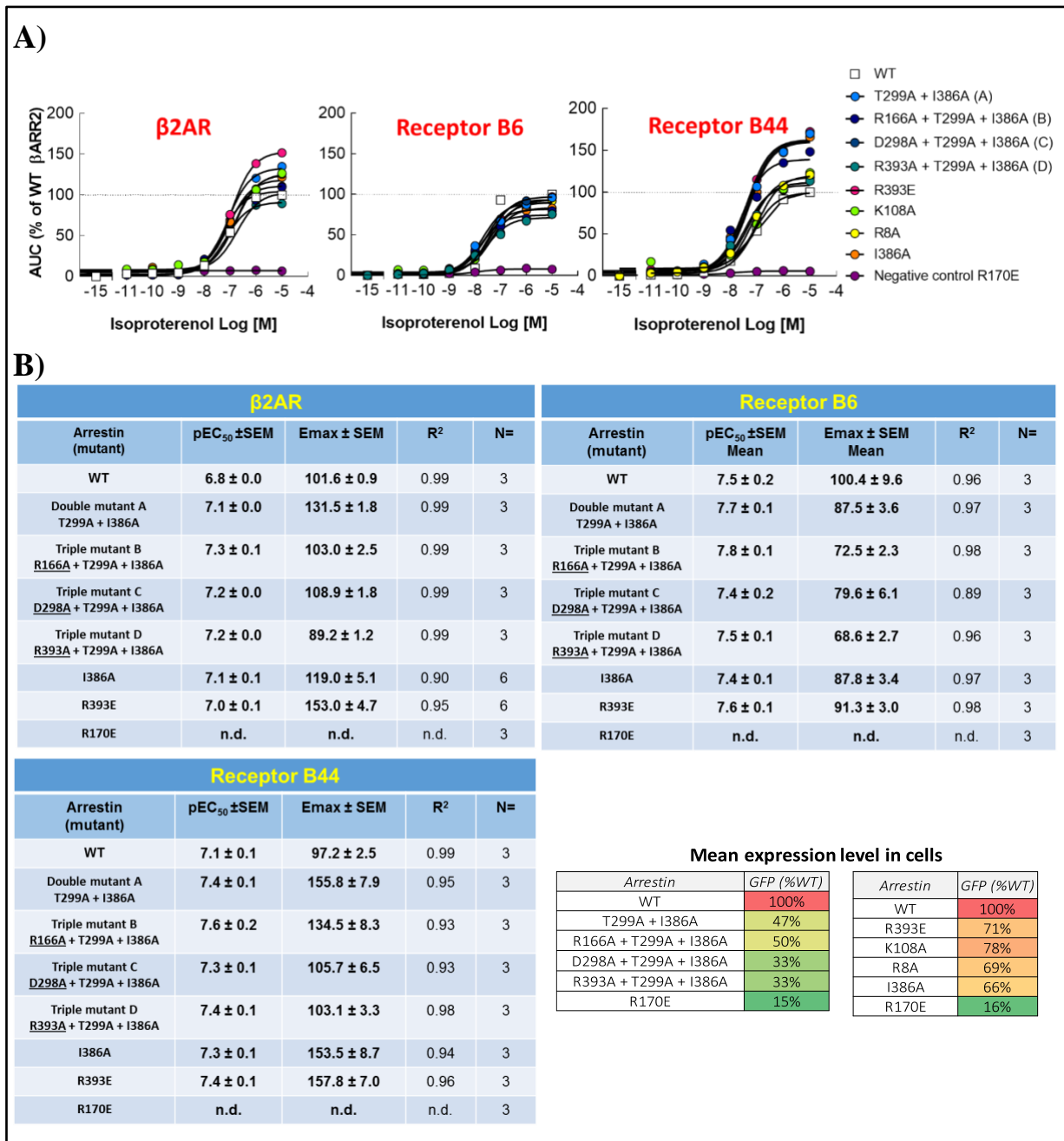


**Figure 22.** A) Concentration-response curves showing the recruitment of single, double and triple arrestin-3 mutants against the  $\beta$ 2AR. HEK293 cells were transiently co-transfected with EGFP-arrestin-3 mutants and either  $\beta$ 2AR-Rluc8, B6-Rluc8 or B44-Rluc8 containing plasmids. Receptors were stimulated by increasing concentrations of isoproterenol (0-10  $\mu$ M). Areas under curve (AUC) for 20 minutes post-stimulation were normalized to WT arrestin-3 and plotted against isoproterenol concentrations. A three parameter non-linear regression analysis to derive the efficacy and potency of arrestin-3 recruitment was performed (see equation in 1.3.3. *Data analysis*). AUC: area under curve. B) Non-linear regression parameters and expression level of combined arrestin-3 mutants in cells. pEC<sub>50</sub>: -log(EC<sub>50</sub>); E<sub>max</sub>: efficacy. SEM: standard error of the mean. R<sub>2</sub>: coefficient of determination. N: number of replicates. GFP signals are normalized to WT arrestin-3.

Figure 22 depicts in A) concentration-response curves of the recruitment of single point and combined arrestin-3 mutants to the  $\beta$ 2AR, receptor B6 and B44 and in B) the corresponding non-linear regression

parameters. Firstly, the non-linear regression parameters of  $\beta$ 2AR recruitment results (1<sup>st</sup> graph in figure 22A) and 1<sup>st</sup> table in figure 22.B) reports higher efficacies (maximal responses) for the double mutant A ( $131.5 \pm 1.8\%$ , light blue circles) and triple mutant C ( $108.9 \pm 1.8\%$ , dark blue circles) compared to WT arrestin-3 ( $101.6 \pm 0.9\%$ , white squares). However, the reported efficacy for R393E ( $153.0 \pm 4.7\%$ , pink circles) exceeds that of the double mutant A and triple mutant C. In the case of arrestin-3 mutants recruited to receptor B6 (2<sup>nd</sup> panel in figure 22.A and 2<sup>nd</sup> table in figure 22.B), no mutant surpassed WT arrestin-3 (white squares) in terms of efficacy ( $100.4 \pm 9.6\%$ ): the second-best candidate for B6-recruitment was the mutant I386A with an efficacy of  $87.8 \pm 3.4\%$  (orange circles). For the recruitment of arrestin-3 mutants against the receptor B44 (3<sup>rd</sup> panel in figure 22.A and 3<sup>rd</sup> table in figure 22.B), the high-recruiting behavior of every mutant (R393E, K108A, R8A, I386A, double mutant and triple mutants B, C and D) was restored. Compared to WT arrestin-3 ( $97.2 \pm 2.5\%$ , white squares), double mutant A (light blue), R393E (pink) and I386A (orange) were the arrestin-3 mutants forming the most stable complexes to receptor B44 with efficacies of  $155.8 \pm 7.9\%$ ,  $157.8 \pm 7.0\%$  and  $153.5 \pm 8.7\%$ , respectively.

In conclusion, the efficacy values derived in this analysis suggest that combined arrestin-3 mutants A and B are not recruited to the activated  $\beta$ 2AR as well as the single point arrestin-3 mutant R393E. In addition, the arrestin-3 mutants A and B are not recruited to receptor B6 as well as WT arrestin-3 but are match the recruitment efficacy of single point mutants R393E and I386A to receptor B44.

In tables of figure 22.B), potencies of the recruitment of single and combine mutants of arrestin-3 to  $\beta$ 2AR are displayed. Interestingly, the double mutant A and triple mutant B are recruited to the respective GPCRs with higher potencies than the WT arrestin-3, meaning that mutants A and B require less isoproterenol stimulation than WT arrestin-3 to form the same amount of arrestin-3/receptor complexes. For example, in the recruitment to  $\beta$ 2AR, pEC50 values of double mutant A, triple mutant B and WT arrestin-3 are:  $7.1 \pm 0.0$ ,  $7.3 \pm 0.0$  and  $6.8 \pm 0.0$ , respectively. For receptor B6, pEC50 values of double mutant A, triple mutant B and WT arrestin-3 are:  $7.7 \pm 0.1$ ,  $7.8 \pm 0.1$  and  $7.5 \pm 0.2$ , respectively. Finally, for receptor B44, pEC50 values of double mutant A, triple mutant B and WT arrestin-3 are:  $7.4 \pm 0.1$ ,  $7.6 \pm 0.2$  and  $7.1 \pm 0.1$ , respectively.

The expression levels in HEK293 cells of arrestin-3 mutants are displayed in the lower left table of figure 22. B). Single point mutants were expressed between 66% (I386A) and 78% (R393E) compared to WT arrestin-3 levels, whereas combined mutants were expressed between 33% (triple mutants C and D) and 50% (triple mutant B) of WT arrestin-3 levels. The significant lower expression levels of the combined arrestin-3 mutants could be explained by the multi-site modifications that were introduced into the arrestin structure, which may be more disturbing than single point mutations in the protein.

## **2.6. Patent filing: EP19153159 “β-arrestin mutants”**

The arrestin-3 double mutant A (T299A+I386A), triple mutant B (T299A+I386A+R166A) and triple mutant C (T299A+I386A+D298A) exhibited recruitment efficacies to the β2AR of  $131.5 \pm 1.8\%$ ,  $103.0 \pm 2.5\%$  and  $108.9 \pm 1.8\%$ , respectively, compared to WT arrestin-3 (figure 22.B, 1<sup>st</sup> table). The increase in recruitment efficacy to β2AR by double mutant A, triple mutant B and triple mutant C are caused by the pre-activation – therefore increased sensibility towards activated GPCRs – induced by alanine mutations, as evidenced by the shift in potency ( $7.1 \pm 0.0$  for double mutant A,  $7.3 \pm 0.0$  for triple mutant B,  $7.2 \pm 0.0$  for triple mutant C and  $6.8 \pm 0.0$  for WT arrestin-3). Mechanistically, alanine mutations are located at or near stabilizing pockets of the protein, and their combination pushes arrestin-3 to the activated state: the polar core is disturbed by R166A, R393A, T299A, D398A and the three-element interaction by I386A (as shown in figure 19). As a result, pre-activated mutants require less energy than WT arrestin-3 to bind to an activated GPCR. Another consequence of combining multiple mutations at different locations on arrestin-3 was the lower expression level in cells of double and triple alanine mutants (33% to 50% of WT arrestin-3 levels) compared to single point mutant (66% to 71% of WT arrestin-3 levels), as shown in figure 22.B. However, in structural studies as intended by Prof. Christopher Tate (Medical Research Council, Cambridge UK) on the turkey β1AR receptor mutant B44, the described arrestin-3 mutants will not be tested in mammalian cells. Instead, the relevant arrestin-3 mutants will be expressed in recombinant form as purified proteins and further used in crystallography studies.

Summarized, the use of double and triple arrestin-3 mutants described above will be of great interest for the stabilization of GPCRs in structural studies. In addition, the fact that I succeeded to design arrestin-3 mutants with higher efficacies and affinities for these two adrenergic receptors, suggest that such arrestin-3 mutants could be applicable for arrestin-recruitment studies with other GPCRs. In particular, the use of the double mutant A (T299A+I386A), triple mutant B (T299A+I386A+R166A) and triple mutant C (T299A+I386A+D298A) and D (T299A+I386A+D393A) could result in much improved assay windows for GPCRs that have a per se lower propensity of arrestin-3 recruitment capabilities. The work described in this chapter has been filed as a European Patent application EP5657EP00 “β arrestin mutants” in January 2019<sup>106</sup>

## Discussion, chapter 2

In this study, the recruitment ability of the combined mutants (mutant A, B, C and D) and the single point mutants (R393E<sub>25</sub>, R170E<sub>26</sub>, I386A<sub>94</sub>, R8A<sub>104</sub>, R26A<sub>81,82</sub>, K108A<sub>81,82</sub>, K78A<sub>102</sub>, R66A<sub>102</sub> and A248V<sub>33</sub>) of arrestin-3 was investigated against the  $\beta$ 2AR and variants of the  $\beta$ 1AR (figure 22). The combined mutant A (T299A+I386A), mutant B (T299A+I386A+R166A) and mutant C (T299A+I386A+D298A) and mutant D (T299A+I386A+D393A) were derived from strong recruiters of arrestin-1 to rhodopsin (from *Haider et al., 2019*<sub>94</sub>) that contained pre-activating mutations (by disruption of the polar core with D303A, T304A and the three element interaction with F375A). Similar to arrestin-1 mutants, arrestin-3 mutations in the combined mutants are predicted to pre-activate arrestin-3 through perturbation of the polar core (via T299A, D298A and R393A) and the three-element interaction (I386A). Indeed, the shift in potency values (i.e. a higher recruitment potency of mutants A, B, C and D as compared to WT arrestin-3 for each receptor, reported in figure 22.B) supports the assumption that the combined arrestin-3 mutants display a higher pre-activation level than WT arrestin-3. For example, in the recruitment to  $\beta$ 2AR, the double mutant A and triple mutant B exhibited higher potencies (with pEC<sub>50</sub> values of  $7.1 \pm 0.0$  and  $7.3 \pm 0.0$ , respectively), compared to WT arrestin-3 ( $6.8 \pm 0.0$ ), see figure 22.B.

*Vishnivetskiy et al., 1999*<sub>25</sub> have shown that charge neutralization by alanine substitution of a polar core residue (D296A) in arrestin-1 was not as efficacious to pre-activate arrestin and improve its recruitment to rhodopsin as a full charge reversal of the same residue (D296R). In the BRET assay reported in section 2.5, the recruitment efficacy of the arrestin-3 mutant R393E ( $153.0 \pm 4.7\%$ , pink circles in figure 22. A) to the  $\beta$ 2AR receptor is highly increased compared to WT arrestin-3 ( $101.6 \pm 0.9\%$ , white squares). Similar to the mutant D296R in arrestin-1 from *Vishnivetskiy et al., 1999*<sub>25</sub>, the charge reversal of arginine 393 in arrestin-3 by a glutamate residue seems to induce a high disturbance of the polar core and improve its recruitment to  $\beta$ 2AR. In comparison, alanine mutations in the double mutant A (light blue circles, figure 22. A) and the triple mutant B (dark blue circles, figure 22. A) do not reach the recruitment efficacy of single point mutant R393E (E<sub>max</sub> values:  $131.5 \pm 1.8\%$  and  $103.0 \pm 2.5\%$ , respectively from figure 22. B, 1<sup>st</sup> table).

Due to its C-terminus truncation, the turkey  $\beta$ 1AR receptor variant B6 lacks seven threonine residues out of the eleven found in WT  $\beta$ 1AR. However, all eleven serine residues are still conserved in the B6 receptor variant (see appendix 4 for protein sequences). BRET data on the recruitment of arrestin-3 to variants of the  $\beta$ 2AR in HEK293 cells (*Krasel et al., 2008*<sub>107</sub>) showed that arrestin-3 binding to  $\beta$ 2AR was not impaired by a truncation of 32 amino acids on the C-terminus of the receptor (thus removing seven/conserving four possible phosphorylation sites). In fact, phosphorylation motifs  $Px(x)PxxP/E/D$

(where P represent phosphorylated residues and E/D, glutamate/aspartate moities) required for arrestin binding as suggested by Zhou *et al.*, 2017<sup>82</sup> (see D.2. *Phosphorylation of the carboxy-termini of GPCRs by GPCR Related Kinases*) are conserved on receptor B6: at positions 406-SESSLE-411, 406-SESSLEE-412, 415-SKTSRS-420 and 415-SKTSRSE-421. In conclusion, the  $\beta$ 1AR receptor B6 is able to recruit WT arrestin-3 (figure 22.A, 2<sup>nd</sup> panel, white squares) via the phosphorylation motifs that remained on its truncated C-terminus and the core-interaction. Interestingly, all arrestin-3 mutants tested (combined mutants A, B, C, D and single point mutants R393E, I386A, R8A and K108A) – that are phosphorylation independent by their pre-activated nature – exhibit lower recruitment efficacy than WT arrestin-3 to receptor B6 as opposed to  $\beta$ 2AR or receptor B44. Therefore, one possible explanation for this observation is that the modifications in receptor B6 (truncated N- and C-termini) have altered the integrity of the activated GPCR core, thus hampering arrestin-3 recruitment through this interface.

In conclusion, the use of double and triple arrestin-3 mutants described above will be of great interest for the stabilization of GPCRs in structural studies. In addition, the fact that I succeeded to design arrestin-3 mutants with higher efficacies and affinities for these two adrenergic receptors, suggest that such arrestin-3 mutants could be applicable for arrestin-recruitment studies with other GPCRs. In particular, the use of the double mutant A (T299A+I386A), triple mutant B (T299A+I386A+R166A) and triple mutant C (T299A+I386A+D298A) and D (T299A+I386A+D393A) could result in much improved assay windows for GPCRs that have a per se lower propensity of arrestin-3 recruitment capabilities. The work described in this chapter has been filed as a European Patent application EP5657EP00 “ $\beta$  arrestin mutants” in January 2019<sup>106</sup>

## **CHAPTER 3 – Recruitment of arrestin 1/2/3 and constrained arrestin-3 mutants to rhodopsin by centrifugal pull-downs**

In this section, the recruitment of different arrestins (-1, -2 and -3) and constrained arrestin-3 mutants was investigated against rhodopsin by centrifugal pull-downs, as performed by *Kuhn et al., 1984*<sup>108</sup> and *Sommer et al., 2005*<sup>109</sup>. The objective of the study was to explore the different mechanisms involved in the recruitment of arrestins to four activated states of rhodopsin (dark-state, light activated rhodopsin and their phosphorylated counterparts). In arrestin-3 mutants, constraints in the form of disulfide bridges were introduced to restrict movement of key structural features for the C-tail or the core interaction with GPCRs. Guided by inactive arrestin-3 (PDB 3P2D) and pre-activated arrestin-1 (PDB 4J2Q) crystal structures, cysteine residues were optimally inserted for spontaneous crosslinking. In addition to functional pull-down assays, the structural integrity of arrestin-3 mutants was thoroughly characterized by mass spectrometry, circular dichroism and limited trypsinization. This project was carried out in collaboration with Dr. Martha Sommer (Universitätsmedizin Charité Berlin, Germany) who kindly provided arrestin-1, arrestin-2 and rhodopsin membrane samples. This project was also developed in collaboration with Jonas Mühle (Paul Scherrer Institute), Alain Blanc (Paul Scherrer Institute) and Dr. Maria Waldhoer (InterAx Biotech AG).

### **Material and methods**

#### **3.1. Design of di-cysteine and glycine mutants of arrestin-3**

Arrestin-1 has been reported to interact with rhodopsin and the plasma membrane via three interfaces: the core-interaction<sup>14,34,47</sup> (between the so-called central crest of arrestin and the cytoplasmic components of rhodopsin), the C-tail interaction<sup>19,82,110</sup> (between residues on the N-domain of arrestin and the phosphorylated C-terminus of rhodopsin) and the membrane anchor<sup>84</sup> (between C-edge of arrestin and the phospholipids surrounding the receptor). In order to selectively restrict one binding interface between arrestin and rhodopsin (see sections *C.3. Arrestin activation* and *D.3. The GPCR-arrestin interface*), constraints in the form of disulfide bridges or point glycine mutations were introduced in human arrestin-3. Disulfide bridges have the advantage over mutagenesis studies to be reversible by addition of reducing agents (e. g. 1,4-DiThioThreitol, DTT). Four sets of arrestin-3 mutants were designed based on available inactive (PDB 3P2D) and active (PDB 4J2Q) crystal structures:

- Mutants interfering with the core-interaction. Disulfide bridges were introduced to i) restrict superficial loop movements in the central crest (finger loop, middle loop, C loop) or ii) covalently lock basal state stabilizing pockets of arrestin (the polar core and the three-element interaction).
- Mutants preventing the C-tail interaction. The C-terminus of arrestin is tethered to the N-domain, either proximally (at the polar core) or distally (at the tip of the C-terminus). Only the distally anchored mutant was designed by molecular dynamics simulations instead of structural data.
- Mutants locked in an activated conformation. For these mutants, the activated state of arrestin is maintained by anchoring the gate loop to the N-domain, which retains the 20-21° rotation between the N-domain and the C-domain, necessary for GPCR core engagement (see *C.3. Arrestin activation*).
- Mutants inactivating the membrane anchor by glycine mutations. Residues F197, M198 and S199, located at the C-edge of arrestin, were showed to interact via hydrophobic interactions with the phospholipids of the plasma membrane upon recruitment to rhodopsin<sup>84</sup>.

#### 3.1.1. Constrained arrestin-3 mutants and cloning

Guided by inactive arrestin-3 (PDB 3P2D) and pre-activated arrestin-1 (PDB 4J2Q) crystal structures, disulfide bridges were inserted in selected regions of the protein that are known to be involved in arrestin-3 activation or recruitment to GPCRs. As summarized in table 5, cysteine residues were introduced to enable spontaneous disulfide bond formation. For this, cysteine residues were designed by collaborator Martha Sommer (Universitätsmedizin, Charité Berlin, Germany) to be within 5 to 13Å from each other and present a favorable geometry for disulfide bond formation.

- **Mutants L69C/E146C (B16) and L69C/E293C (B19)**. One example of constrained bovine arrestin-1 by intramolecular cysteine crosslinking was reported by *Sommer et al., 2007*<sup>111</sup> in a recruitment study to rhodopsin by centrifugal pull-downs. In this study<sup>111</sup>, the finger loop was tethered from I72 to either the cup of the N-domain (E148) or the gate loop (K298). Both mutants were proven to prevent association with light activated rhodopsin (P-Rho\*) by restricting loop movements of the finger loop. Nevertheless, assays were performed at 130mM NaCl which severely limits pre-complex formation to dark state phosphorylated rhodopsin (P-Rho). Here, arrestin-3 mutant cognates were designed to recreate and explore their recruitment behavior towards both rhodopsin states.



- **Mutant R66C/K139C (B20).** Disruption of the conserved middle loop in mouse arrestin-1 (L133 to S143), particularly residue K142 and on adjacent finger loop D72 was proven to increase binding to non-phosphorylated and light activated rhodopsin (Rho\*), P-Rho and P-Rho\* when measured by gel filtration<sup>112</sup>. In other words, arrestin-1 lost its functional selectivity towards P-Rho\*, accompanied by a lower thermal stability profile. Here, one mutant was designed to tether the finger loop and middle loop together from residue R66 and K139, respectively.
- **Mutant D136C/Y250C (B21).** To this day, no studies have investigated interactions between the previously described middle loop and the C-loop. Upon arrestin activation, the C-loop has to move away from the central crest in order to accommodate intracellular loops 2 and 3 of rhodopsin<sup>17</sup>. Here, the arrestin-3 mutant B21 aims to restrict this rearrangement by maintaining the C-loop (from residue Y250) above the central crest (to residue D136 of the middle loop).
- **Mutants L294C/Q131C (B26) and L294C/K285C (B28).** According to molecular dynamics simulations and site-directed fluorescence quenching data<sup>35</sup>, the gate loop appears as a mediator between the disruption of the polar core and the 20-21° rotation of the N- and C-domains, a hallmark of arrestin activation. These two mutants aim to stabilize arrestin in its inactive state by stitching the gate loop (from residue L294) to the middle loop (Q131 in mutant B26) or to adjacent residue K285 (B28).
- **Mutants S246C/Y64C (B29), F245C/F76C (B33) and F245C/Y64C (B34).** Based on site-directed fluorescence quenching studies<sup>109</sup>, residues S246/F245 (on the C-loop) and Y64 (on the finger loop) in arrestin-3 are known to be in close proximity in the basal state. By tethering the C-loop to either end of the finger loop, these three mutants aim to connect the N- and C- domains and close the central crest.
- **Mutants D298C/L167C (B15) and L293C/V168C (B17).** According to structural data<sup>17</sup>, the gate loop appears as a mediator between the disruption of the polar core and the 20-21° rotation of the N- and C-domains, a hallmark of arrestin activation. Arrestin-3 mutants B15 and B17 aim to stabilize arrestin in an active state by attaching the gate loop (from residue D298 or L293) to the N-domain (V168 for mutant B17 or L167 for mutant B15).
- **Mutants R170C/D291C (B14), R170C/D27C (B18), F391C/R26C (B25) and V9C/L105C (B31).** The so-called polar core and 3-element interaction are well-known stabilizers of the basal state of arrestin<sup>40,86</sup>, governed by hydrogen and hydrophobic interactions, respectively. If previously described mutants targeted superficial loops, this series of mutations are deeply buried

in the protein core and aim to strengthen the functional role of the two pockets. In fact, arrestin-3 mutants B14 and B18 are anticipated to strengthen the polar core whereas mutants B25 and B31 should reinforce the three-element interaction.

- **Mutants R393C/R26C (B27), R393C/H296C (B35) and K295C/Y404C (B30).** The C-tail truncated variant of arrestin-1 also called p44, exhibits a pre-activated behavior, suggesting an inhibitory role of the C-tail in arrestin activation<sup>17,19</sup>. Structurally, the proximal region of the arrestin C-tail interacts with the polar core (at residue R393) while the location of the distal C-tail of arrestin (after R393) is unknown, since it had never been resolved in any crystal structure. Arrestin-3 mutants B27 and B35 aim to lock the proximal portion of the C-tail (at residue R393) to the arrestin N-domain (at residue 26 or 296), whereas mutant B30 aims to anchor the distal portion of C-tail (at Y404) to the N-domain (at residue 295) in order to completely hamper C-tail release.
- **Mutants L192G (B22), M193G (B23) and S194G (B24).** According to molecular dynamics simulations and site-directed fluorescence quenching<sup>84</sup> and mutagenesis<sup>40</sup> experiments, two unstructured loops located at the C-edge of arrestin are forming hydrophobic interactions with the membrane bilayer. Here, we chose to focus on three amino acids (L192, M193 and S194) on the 192-loop and mutate them to glycine residue to neutralize hydrophobic interaction with the plasma membrane.
- **Mutants L192G/M193G (B36), L192G/S194G (B37) and L192G/M193G/S194G (B38).** These are simple combinations of the last set.

R170C-D291C (B14)	D298C-L167C (B15)	L69C-K293C (B16)	L293C-V168C (B17)	R170C-D27C (B18)	L69C-E146C (B19)
Polar core to gate loop	Gate loop to N-dom	Finger loop to gate loop	Gate loop to N-dom	Polar core to N-domain	Finger loop to N domain
R66C-K139C (B20)	D136C-Y250C (B21)	L192G (B22)	M193G (B23)	S194G (B24)	F391C-R26C (B25)
Finger loop to middle loop	Middle loop to C-loop	Inactivating membrane anchor <b>sequentially</b>			3-element interaction
L294C-Q131C (B26)	R393-D27C (B27)	L294C-K285C (B28)	S246C-Y64C (B29)	K295C-Y404C (B30)	V9C-L105C (B31)
Gate loop to middle loop	Polar core to C-tail	Gate loop to loop 14-18	C loop to back of finger loop	Distal C-tail to N-dom	3-element interaction
F245C-F76C (B33)	F245C-Y64C (B34)	R393C-H296C (B35)	L192G + M193G (B36)	L192G + S194G (B37)	L192G + M193G + S194G (B38)
C loop to back of finger loop	C loop to back of finger loop	Polar core to C-tail	Inactivating membrane anchor <b>incrementally</b>		

Blocking core-interaction	20° rotation	C-tail anchoring	Membrane anchor deficient
at loop level	at proximal position	at distal position	Locked in activated conformation
at core level			

**Table 5.** Di-cysteine and glycine arrestin-3 mutants highlighted on an inactive arrestin-3 structure (PDB 3P2D).

Arrestin-3 mutant DNA sequences were generated by site-directed mutagenesis (see section 1.1. *PCR-driven mutagenesis* for the cloning strategy) on a pET15 vector (PSI). The gene sequence was optimized for *E. coli* expression and all arrestin-3 mutants contained an N-terminal His(6)-Tag followed by a TEV protease cleaving site (see appendix 1 for DNA sequence).

### 3.2.2. Expression of arrestin-3 mutants in *Escherichia Coli*

Once the DNA constructs were verified, *E. Coli* cells (NiCo21 DE3, New England Biolabs) were transformed by heat shock (see 1.1. *PCR-driven mutagenesis*) and plated on ampicillin (Gerbu, #1046.0250) infused agar plates (Gerbu, #1416.2500) before an overnight incubation at 37°C. The next

day, agar plates were either stored at 4°C or directly used. A total of 5 colonies were selected and inoculated in a pre-culture of 500 mL of Terrific Broth medium (TB, Gerbu #1425.5000) + 1% carbenicillin (Gerbu, #1039.0100) in a baffled 2L flask before an overnight incubation at 30°C, shaking at 160 rpm. In the following morning, 50 mL of pre-culture were inoculated to 500 mL of TB + 1% carbenicillin in baffled flasks for a total volume of 3 or 6 L per protein and incubated at 37°C, 160 rpm until the optical density at 600 nm of cell suspensions reached a value superior to 2. Only then, the incubation temperature was decreased to 20°C for one hour until 32.4 µL of 0.5 M isopropyl β-D-1-thiogalactopyranoside (IPTG, Gerbu, #1043.0250) were added per flask to induce protein expression. Finally, cells were centrifuged 24h post-induction at 3000g for 20 minutes and pellets were stored at -20°C until use.

### 3.2.3. Purification of arrestin-3 mutants

Arrestin-3 mutants were purified in a two-step chromatography approach for which the following buffers were used (table 6):

	Final concentration (mM)	Stock solution (mM)	Volume to add (mL)	Water (mL)
<b>LYSIS BUFFER</b>			<b>200</b>	
Bis-Tris-Propane pH 7.0 (Gerbu, #1305.0250)	50	1000	10	
NaCl (Fischer Scientific, #S271-500)	500	5000	20	
MgCl <sub>2</sub> (Gerbu, #20908)	2	2000	0.200	
Roche protease inhibitor cocktail (cOmplete, Roche)	10mg/mL		3 tabs	
β-mercaptoethanol (Sigma, #516732)	8	14300		170
<b>Ni-NTA BUFFER A</b>			<b>500</b>	
Bis-Tris-Propane pH 7.0	20	1000	10	
NaCl	500	5000	50	
Glycerol (Fischer Scientific, #G33-500)	10%	99.50%	50	
β-mercaptoethanol	8	14300	0.280	389
<b>Ni-NTA BUFFER B</b>			<b>200</b>	
Bis-Tris-Propane pH 7.0	20	1000	4	
NaCl	500	5000	20	
Imidazole pH 7.0 (Fisher Chemicals, #O3196-500)	500	2000	50	
Glycerol (Merck, #G9012)	10%	99.50%	20	
β-mercaptoethanol	8	14300	0.112	106
<b>DIALYSIS BUFFER</b>			<b>1000</b>	
Bis-Tris-Propane pH 7.0	20	1000	20	
NaCl	120	5000	24	
Glycerol	10%	99.50%	101	
β-mercaptoethanol	14.3	14300	1	854
<b>DILUTION BUFFER</b>			<b>100</b>	
Bis-Tris-Propane pH 7.0	20	1000	2	
Glycerol	10%	99.50%	10	
β-mercaptoethanol	14.3	14300	0.100	88
<b>HEP-A BUFFER</b>			<b>500</b>	
Bis-Tris-Propane pH 7.0	20	1000	10	
NaCl	50	5000	50	
Glycerol	10%	99.50%	50	
β-mercaptoethanol	14.3	14300	0.500	385
<b>HEP-B BUFFER</b>			<b>200</b>	
Bis-Tris-Propane pH 7.0	20	1000	4	
NaCl	1000	5000	40	
Glycerol	10%	99.50%	20	
β-mercaptoethanol	14.3	14300	0.200	136
<b>COLUMN FLUSHING BUFFER</b>			<b>100</b>	
Bis-Tris-Propane pH 7.0	20	1000	2	
NaCl	2000	5000	40	58

**Table 6.** List of purification buffers.

#### 3.2.3.1. Cell lysis

Cell pellets containing the expressed protein were carefully thawed in cold water and kept on ice. Then, cell suspensions were homogenized using a loose Dounce homogenizer and collected in a 400 mL becher. Cells were diluted up to 120 mL in lysis buffer before sonication (Vibra Cell VCX 400, Sonics). A sonication cycle was set with the following parameters: 1s on/ 0.5s off pulses for 7.5 minutes

while stirring. Each preparation underwent 3 cycles separated by a 10-minute rest on ice. Cells were quickly subjected to ultra-centrifugation (Ti45 rotor, Beckman, #339160) at 40,000 rpm for 1h at 4°C. Finally, the supernatant was manually filtered through a 0.45 µm porous membrane (Whatman, #Z746266) and imidazole was added to a final concentration of 30 mM.

### 3.2.3.2. Immobilized Metal Affinity Chromatography (IMAC)

Samples were loaded on a pre-equilibrated nickel column (HisTrap Ni-NTA FF 5mL, GE Healthcare, #17525501) using buffers Ni-NTA buffer A and B (table 6). As shown in figure 23, a step gradient was applied (black curve) at a flowrate of 4 mL/min. Proteins were tracked by their absorption at 215 nm (green curve) and 280 nm (blue curve).

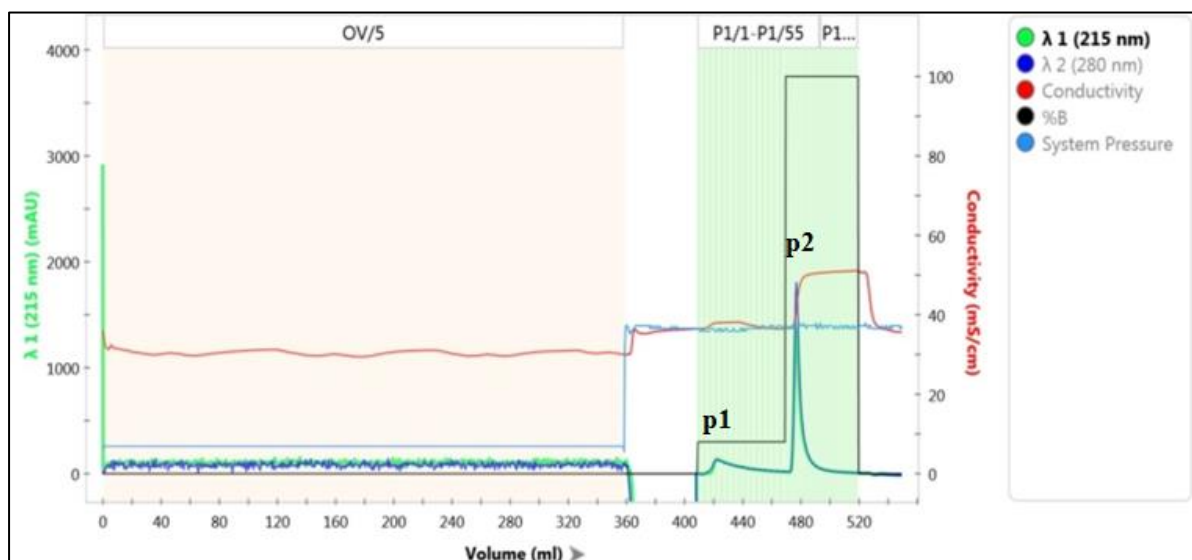


**Figure 23.** Immobilized metal ion affinity chromatography (IMAC) of His-tagged WT arrestin-3. Unretained proteins were discarded (red portion) in the flow-through for 72 column volumes (CV). Then, a step increase to 8% Ni-NTA buffer B or 40 mM imidazole was applied to discard undesired histidine-rich proteins (p1). Finally, the His-tagged arrestin was eluted at 100% buffer B or 500 mM imidazole (p2). Green bars represent eluted fractions.

After the first chromatography, relevant fractions were run on a SDS-PAGE gel (4-20% TGX MiniProtean, Bio-Rad, #456-8095) as shown in figure 25. After being pooled, protein samples were subjected to dialysis overnight (6-8kDa MWCO tubing, Repligen, #132645) in the presence of 0.5 mg TEV protease (PSI) in order to remove the His-tag and dilute the imidazole.

### 3.2.3.3. Optimization of the second chromatography

The protocols described in 3.3.2. *Expression of arrestin-3 mutants* and 3.3.3. *Purification of arrestin-3 mutants* were originally optimized for human arrestin-1. In the arrestin-1 purification protocol, a strong anion exchange chromatography (SAX) was preconized after the IMAC run. In order to adapt the purification protocol to arrestin-3, different post-IMAC purification strategies were explored. In this section are several purification techniques that ultimately led to the replacement of the SAX by a heparin chromatography.

For this study, arrestin-3 mutant B15 was expressed in 6 L of *E. coli* suspension and purified by IMAC, as detailed in 3.2.3.2. *Immobilized Metal Affinity Chromatography (IMAC)*. After dialysis, arrestin-3 mutant B15 was split into four portions and the following chromatographic techniques were applied (figure 24):

- A) **Strong anion exchange chromatography** (Q Fast Flow column 1 mL, GE Healthcare, #17505301) which was the reference protocol.
  
- B) **A combination of a strong cation exchange chromatography** (SP column 1 mL, GE Healthcare, #17505401) **followed by a strong anion chromatography** (Q Fast Flow column 1 mL, GE Healthcare, #17505301). In this approach, the SP chromatography was anticipated to retain impurities whereas the Q chromatography was supposed to trap arestin mutant B15.
  
- C) The **elution strong cation exchange** carried out in B), as shown in figure 26.
  
- D) **Heparin chromatography** (HP-Hep, High Performance heparin column 5 mL, GE Healthcare, #17040701)

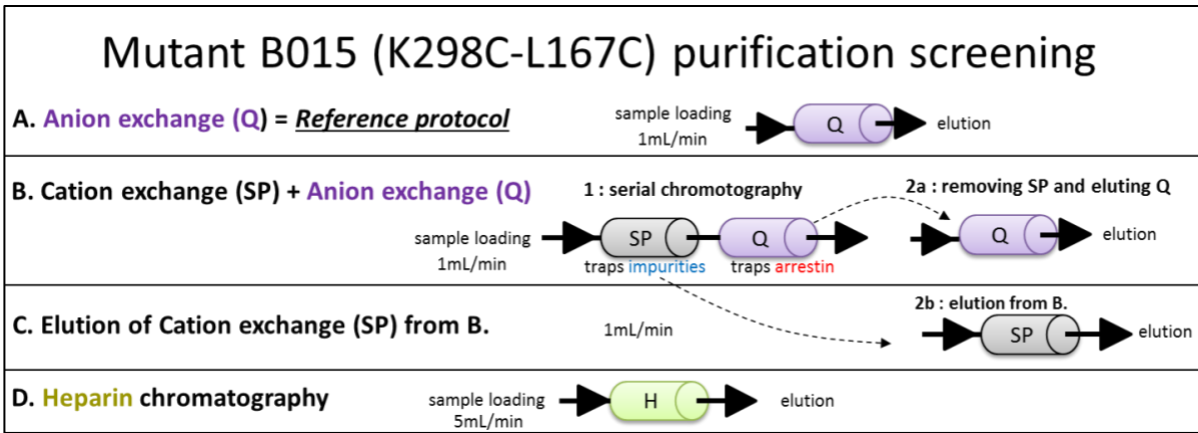


**Figure 24.** Optimization of the second purification step of arrestin-3 mutants. Arrestin mutant B15 (D298C/L167C) was expressed in *E. coli* and purified by immobilized metal affinity chromatography (see sections 3.2.2 and 3.2.3). Four strategies were explored for the second step chromatography. Q: anion exchange chromatography. SP: cation exchange chromatography. H: heparin chromatography.

### 3.2.3.4. Heparin chromatography

If protein solutions appeared turbid after dialysis, samples were subjected to centrifugation at 4,000g for 10min to remove the precipitate. Then, samples were subjected to a heparin chromatography (figure 25) using Hep buffer A and B set to 500 mM and 1 M NaCl, respectively (table 6). Samples were run through a step gradient at 4 mL/min on a pre-equilibrated heparin column (Heparin HP 5 mL, GE Healthcare, #17040701).

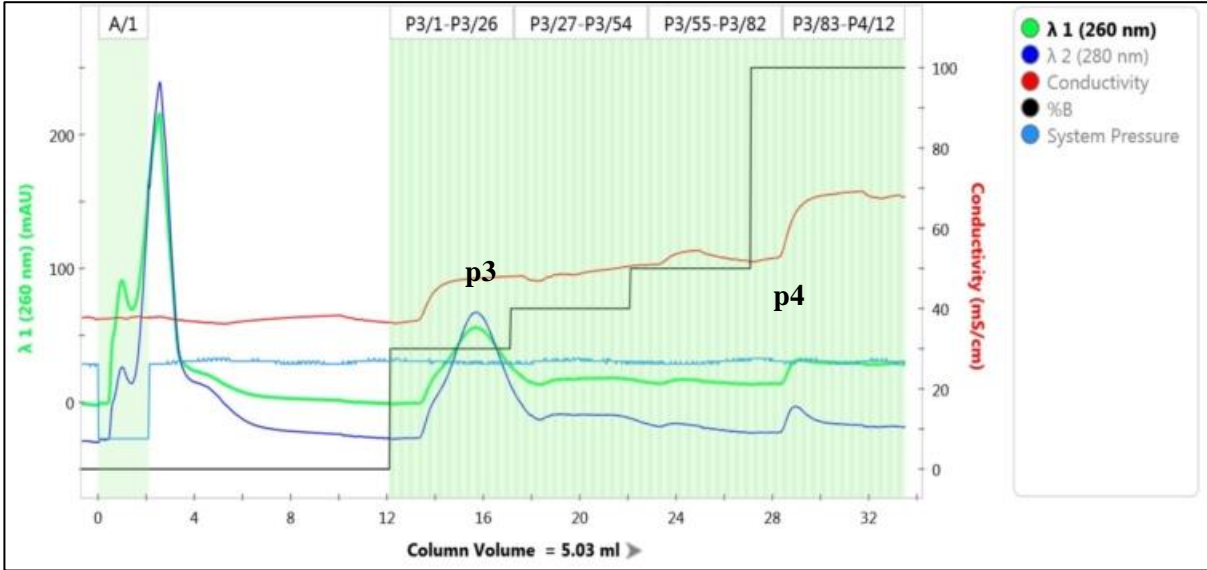


**Figure 25.** Heparin chromatography of untagged WT arrestin-3. Co-eluted proteins during the IMAC run were discarded in the flow-through (A/1 portion) for 2 column volumes (CV). For elution of arrestin-3, a step increase gradient was applied (0%, 30%, 40%, 50% and 100% buffer B). WT arrestin-3 mainly eluted in at 30% buffer B or 650 mM NaCl. Green bars represent eluted fractions.



The relevant fractions were pooled and run on a SDS-PAGE gel (figure 26). Finally, samples were aliquoted, flash-frozen and stored at -80°C.

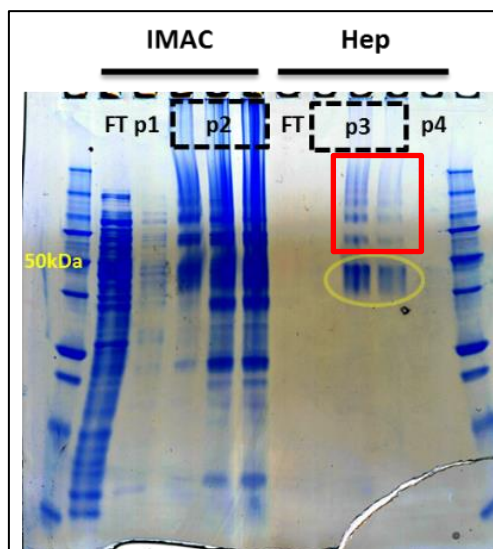


**Figure 26.** Relevant fractions of WT arrestin-3 for the IMAC and heparin purifications ran on a TruPAGE Precast gel 12% (Sigma). A strong ladder effect was detected on this type of gels (red rectangle). Hep: heparin. FT: flow-through (red portion in chromatograms). p1, p2, p3, p4: reported peaks on the respective chromatograms. Yellow circle: eluted arrestin-3.

### **3.2. Limited trypsin digestion of arrestin-3 mutants**

To investigate the conformational and structural stability of arrestin-3 mutants (see section 3.1. *Design of di-cysteine and glycine mutants of arrestin-3*), purified proteins were subjected to limited trypsin digestion. The objective was to compare digestion profiles of arrestin-3 mutants to that of WT arrestin-3. In addition, arrestin-3 mutants were compared between their constrained (in oxidizing condition, buffer A alone) and their relaxed state (in reducing condition, buffer A + 2 mM DTT).

Firstly, microconcentrators (Amicon 10k MWCO, #UFC501096) were used to set protein samples in buffer A (50 mM HEPES pH 7.0 (Gerbü, #1009), 150 mM NaCl (Fischer Scientific, #S271-500)). A total of 60 µg of protein were incubated at room temperature for 2h in buffer A alone or buffer A + 2 mM DTT (Gerbü, #14130). Then, samples were incubated at 35°C and 2 µg were taken as a “t=0 min” condition and diluted in a 2X gel loading dye. To initiate the reaction, 3 ng of trypsin (Sigma, #85450C) freshly dissolved in buffer A was added per reaction for a final weight to weight ratio of 1:75 for arrestin-1 or 1:200 for arrestin-3. For each indicated time point, 2 µg of digested protein were taken from the same tube and directly diluted in a 2X gel loading dye to stop the reaction. In the end, digested samples were run on an SDS-PAGE gel (4-20% TGX MiniProtean, Bio-Rad, #456-8095).

### 3.3. Circular dichroism

Arrestin-3 is a cytosolic protein, rich in antiparallel  $\beta$ -sheets. To compare the conformational and structural integrity of arrestin-3 mutants, samples were subjected to thermal decay while their  $\beta$ -sheet content was monitored by circular dichroism (CD). Antiparallel  $\beta$ -sheets are secondary structures that have the intrinsic characteristic to deviate polarized photons with a maximum absorption at 215nm, as shown in figure 27.

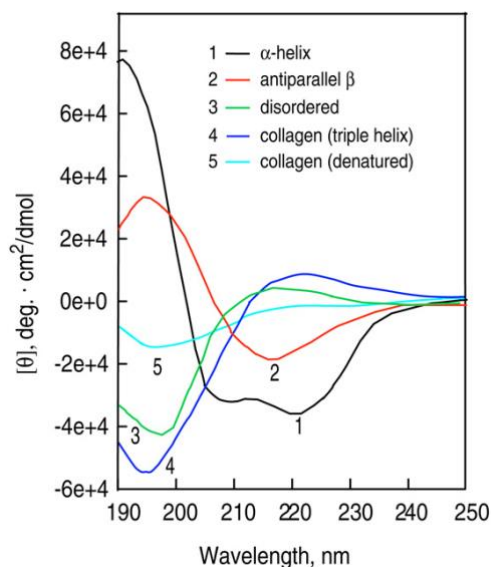


**Figure 27.** CD spectra of a poly-L-lysine polypeptide at pH 11.1 in the 1 (black)  $\alpha$ -helical and 2 (red) antiparallel  $\beta$ -sheet conformations and at pH 5.7 in the 3 (green) extended conformations and placental collagen in its 4 (blue) native triple-helical and 5 (cyan) denatured forms. Figure and legend were obtained from *Greenfield et al., 2006*<sup>113</sup>.

Firstly, microconcentrators (Amicon 10k MWCO, #UFC501096) were used to set protein samples in buffer B (50 mM HEPES pH 7.0 (Gerbü, #1009), 130 mM NaCl (Fischer Scientific, #S271-500). Proteins samples were measured at a final concentration of 15  $\mu$ M in buffer B alone or in buffer B + 2 mM DTT (Gerbü, #14130). CD spectra were acquired on a Chirascan (AppliedPhotophysics) spectrometer and a temperature gradient was applied from 25 to 83°C with a 1°C increment. The area under curve from 215 to 280 nm of each spectrum was plotted against the increasing temperature and a non-linear regression analysis was applied to determine the melting temperature ( $T_m$ ), according to this formula:

$$y = X_{min} + \frac{X_{max} - X_{min}}{1 + \frac{x^h}{IC_{50}^h}}$$

where  $X_{min}$  and  $X_{max}$  are the minimal and maximal values of the dataset,  $IC_{50}$  is the half maximal inhibitory response and  $h$  the hill factor.

### **3.4. Mass spectrometry**

#### 3.4.1. Crosslinking efficiency of constrained arrestin-3 mutants

In order to validate the integrity, purity and crosslinking ability of arrestin-3 mutants, samples were subjected to an HPLC-MS analysis. Here, samples were buffer-exchanged to 50 mM ammonium bicarbonate pH 7.0 (Sigma, #09830) and adjusted to a final concentration of 3 mg/mL. Then, proteins were let to crosslink at room temperature for 2h and three equal portions of each sample were denatured in the following buffer: 7.5 M guanidine (Pierce, #24115), 0.1 M Tris-HCl (Sigma, #T6666) and 1 mM EDTA (Fisher, #BP2482). The three experimental conditions were (figure 28):

- The **protein alone**, where the experimental molecular weight (MW) of the protein was compared to its theoretical MW. The identity and integrity of the protein was validated if the experimental MW was within 6 Da of the theoretical MW, that is with an accuracy of 99.9998%.
- **Protein + iodoacetamide** (IAA, Sigma, #I6125), where IAA alkylates free cysteines<sub>114</sub>, thus adding an exact mass of 57 Da per residue. Here, only free cysteines are reactive towards IAA and not the ones involved in a disulfide bond. For example, there are 9 native cysteines in WT arrestin-3 and no native disulfide bond. Therefore, the alkylation of 9 free cysteines by IAA adds a mass of  $9 \times 57 \text{ Da} = 513 \text{ Da}$  to WT arrestin-3 ( $MW_{\text{theo}} = 46,177 \text{ Da}$ ) resulting in an expected mass of 46,690 Da ( $46,177 + 513 \text{ Da}$ ).
- **Protein + IAA + TCEP** (tris(2-carboxyethyl)phosphine, Sigma, #C4706), wherein IAA alkylates all cysteines since reducing agent TCEP hydrolyses disulfide bonds. DTT was not retained to reduce disulfide bridges in arrestin-3 mutants because of its IAA-reactive sulfhydryl groups. For example, a successfully crosslinked mutant should appear at a MW of  $(MW_{\text{theo}} + 9 \times 57) \text{ Da}$  in the IAA condition and  $(MW_{\text{theo}} + 11 \times 57) \text{ Da}$  in the IAA + TCEP condition.

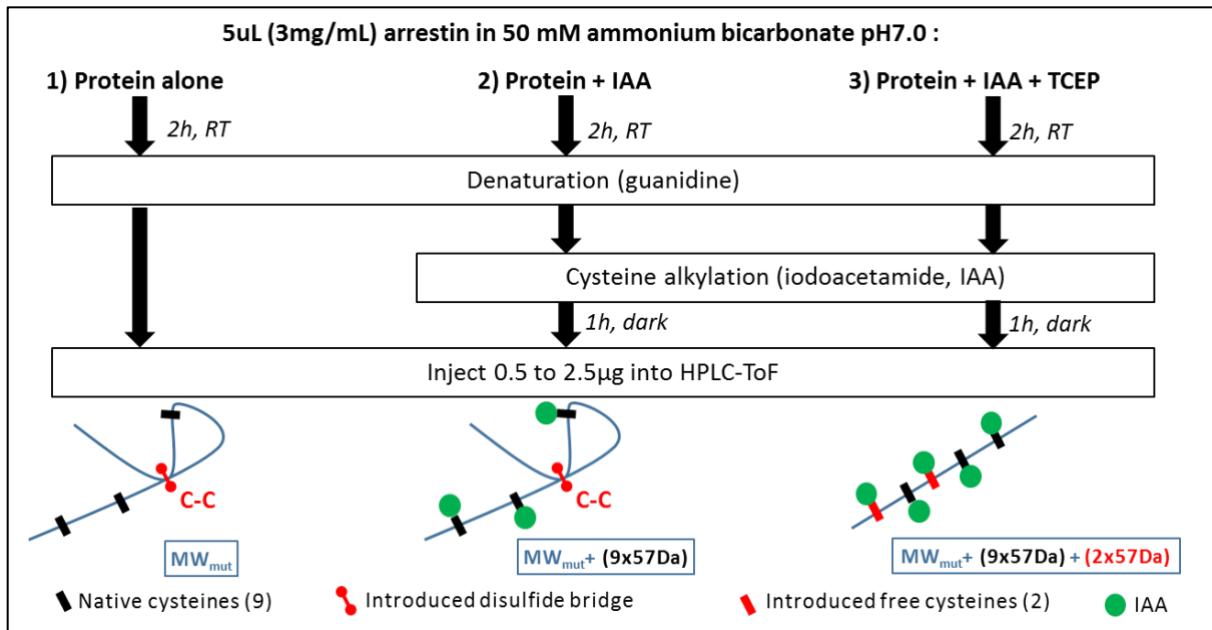


**Figure 28.** Arrestin-3 mutant characterization by mass spectrometry. Arrestin-3 samples in 5 mM ammonium bicarbonate pH 7.0; 7.5 M guanidine; 0.1 M Tris-HCl; 1 mM EDTA were either 1) analyzed alone, 2) with iodoacetamide (IAA) or 3) with IAA + tris(2-carboxyethyl)phosphine (TCEP). RT: room temperature. HPLC-ToF: High performance liquid chromatography-time of flight mass spectrometry. MW<sub>mut</sub>: molecular weight of an arrestin-3 mutant.

After cysteine alkylation, samples were systematically desalted using a C18 column (Reprosil-C18-AQ, #R15-AQ, Dr. Maisch GmbH) in a steady 0-100% acetonitrile/water gradient. After desalting, protein samples were directly injected into the mass spectrometer (ESI-ToF LCT Premier, Waters AG).

In case of successful crosslinking, a mass shift of +114 Da can be detected between conditions 2) and 3), corresponding to the mass of two cysteine adducts (2x57 Da). However, cysteine alkylation by IAA is not always complete, probably because of partial denaturation and inaccessibility of certain residues. In addition, methionine residues are the second-best reacting amino acid to IAA alkylation, although methionine alkylation is significantly slower. As a result, crosslinking efficiencies were estimated in the “Protein + IAA” condition alone by comparing the percentage of the 9- and 10-alkylated arrestins<sub>mut</sub> over all adducted arrestin products.

### 3.4.2. Phosphorylation state of PROS membrane preparations

The recruitment of arrestin 1/2/3 and arrestin-3 mutants were tested in centrifugal pull-downs to rhodopsin, a GPCR embedded in rod outer segment membranes from bovine retinas (provided by Dr. Martha Sommer, Universitätsmedizin, Charité Berlin, Germany). In fact, three membrane preparations were used in pull-down assays: non-phosphorylated rod outer segment membranes (ROS) and two independently prepared batches of phosphorylated ROS (PROS batch #1 and batch #2). To compare the phosphorylation state of membrane preparations (number of phosphate groups per rhodopsin and

overall phosphorylation level per sample), the analytical method described by *Lee et al., 2002*<sup>115</sup> was used. Briefly, the last 19 amino acids on the C-terminus of rhodopsin (DDEASTTVSKTETSQVAPA) were cleaved off by an endoprotease (AspN, Roche, #11420488001) and analyzed by LC-MS. This assay was carried out with the help of Jonas Mühle (PSI, Laboratory of Nanoscale Biology) and Alain Blanc (PSI, Center for Radiopharmaceutical Sciences).

For the assay, a total of 150 µg of ROS, PROS batch #1 and PROS batch #2 were centrifuged for 20 minutes at 21,000g, 20°C. Then, pellets were washed twice with 200 µL of 20 mM HEPES pH 7.5 between two additional centrifugation rounds. Finally, pellets were reconstituted in 20 mM HEPES pH 7.5 and 32.5 µg/mL of endoprotease Asp-N (Roche, #11420488001) and reactions were let for 18h in the dark at 22°C on a rolling platform. The next day, samples were subjected to ultracentrifugation at 195,000g for 15 minutes at 20°C. The resulting supernatants containing peptide DDEASTTVSKTETSQVAPA were analyzed by mass spectrometry whereas the reconstituted pellets containing C-terminal truncated rhodopsin in membranes were run on a 15% SDS-PAGE gel.

Peptide solutions were desalted on a HPLC peptide column (Stability, 120 BS-C23, #st10.17, Dr. Maisch GmbH) using a steady 0-100% water/acetonitrile gradient. After desalting, protein samples were then directly injected into the mass spectrometer (ESI-ToF LCT Premier, Waters AG).

The number of phosphate group per peptide was directly compared by their corresponding peak intensity. The overall phosphorylation state of a rhodopsin batch was estimated by the following equation:

$$AvPhos = \frac{0(I_0) + 1(I_1) + 2(I_2) + 3(I_3)}{I_0 + I_1 + I_2 + I_3}$$

where  $I_0$ ,  $I_1$ ,  $I_2$  and  $I_3$  represent the peak intensity of the unphosphorylated, mono-, di- and tri- phosphate peptide derived from a single spectrum.

### **3.5. Centrifugal pull-down assays**

In this functional assay, the recruitment of arrestin 1/2/3 or arrestin-3 mutants to rhodopsin is straightforwardly assessed by mixing known quantities of arrestin and rhodopsin and measuring the proportion of bound arrestin on a SDS-PAGE gel. Four activated states of rhodopsin were investigated: dark state rhodopsin (ROS), light activated rhodopsin (ROS\*) and their phosphorylated counterparts

(PROS and PROS\*). Several experimental setups were used to investigate the salt sensitivity (salt titrations) and the stoichiometry (receptor titrations) of the arrestin/rhodopsin complexes.

### 3.5.1. Preparation of Rod Outer Segment (ROS) membranes

Rhodopsin-containing rod outer segment membranes were prepared by Dr. Martha Sommer (Universitätsmedizin, Charité Berlin, Germany) according to the protocol in *Sommer et al., 2012*<sup>116</sup>, which is summarized briefly. Both unphosphorylated (ROS) and phosphorylated (PROS) membranes were investigated in centrifugal pull-downs. A total of three independently prepared membrane batches were used: ROS membranes, PROS membrane batch #1 and PROS membrane batch #2.

Briefly, rhodopsin was extracted from bovine retina using a multistep centrifugation employing different sucrose solutions. Receptors were phosphorylated by the associated rhodopsin kinase while applying light and adenosine tri-phosphate (ATP). Phosphorylation was stopped by adding hydroxylamine (HA) which converts all rhodopsin photoproducts to phosphorylated opsin (OpsP) and retinal oxime. Membranes were thoroughly washed, flash-frozen and stored at -80°C. Rhodopsin was regenerated from opsins by applying a three-fold molar excess of 11-cis-retinal for 1h at room temperature in the dark. Rhodopsin concentrations were determined using the absorbance difference spectrum of a 1:20 diluted sample in 100 mM HA. More precisely, the loss of 500 nm absorbance after a 10s illumination (>495 nm) was used in combination with the extinction coefficient ( $\epsilon$ ) of 0.0408  $\mu\text{M}^{-1}\cdot\text{cm}^{-1}$  to calculate the concentration of rhodopsin.

### 3.5.2. Centrifugal pull-downs

Four states of rhodopsin were investigated in centrifugal pull-downs: unphosphorylated dark rhodopsin (ROS), unphosphorylated light-activated rhodopsin (ROS\*) and their phosphorylated counterparts (PROS and PROS\*). Membrane preparations, arrestin-1 and arrestin-2 samples were kindly provided by Dr. Martha Sommer (Universitätsmedizin, Charité Berlin, Germany).

Two variations of this assay were run: salt titrations with a fixed arrestin:receptor ratio (1  $\mu\text{M}$  to 4  $\mu\text{M}$  respectively) and rhodopsin titrations to a fixed salt and arrestin (1  $\mu\text{M}$ ) concentration. Before the assay, arrestin-3 mutants were incubated at 4°C overnight for maximal crosslinking and, for the indicated conditions, DTT was added 30 minutes before the assay to hydrolyze the disulfide bridge. After adding rhodopsin to arrestin under dim-light conditions, samples were illuminated for 10 seconds (>495nm) through an optic fiber, and centrifuged at 16,000g for 10 min at 20°C. The resulting supernatant was discarded and membrane pellets containing the fraction of arrestin bound to the

receptor were run on a 15% SDS-PAGE gel. Arrestin bands were quantified by densitometry analysis using the freeware GelquantNET (BioChemLabSolutions).

In addition, a peptide mimicking the phosphorylated C-terminus of rhodopsin was used in competition experiments with PROS\*: **Phosphorylated peptide 7P** (CDDEA-**pS-pT-pT**-V-**pS-K-pT-E-pT-pS-QVAPA**) is derived from the C-terminus of rhodopsin and contains three additional phosphorylated residues compared to 4P<sub>81</sub>.

### 3.5.3. Data analysis

Pull-down data were fitted according to the following equations:

- (1) Four parameter nonlinear regression (salt titrations)

$$y = X_{min} + \frac{X_{max} - X_{min}}{1 + \frac{x^h}{IC_{50}^h}}$$

where X<sub>min</sub> and X<sub>max</sub> are the minimal and maximal values of the dataset, IC<sub>50</sub> is the half maximal inhibitory response and h the hill factor.

- (2) Stoichiometric saturation nonlinear regression (receptor titrations)

$$y = \frac{j + \left[ \left\{ (Kd + C + x) - \sqrt{[(Kd + C + X)^2 - 4(C * x)]} \right\} \right]}{2}$$

where K<sub>d</sub> is the dissociation constant, C is the concentration of rhodopsin at which saturation is reached and factor j allow the expression to be appropriately scaled to the experimental data. The stoichiometry is determined by comparing the value for C and the actual concentration of arrestin, according to *Lally et al., 2015*<sup>117</sup>.

## Results

In this chapter, the molecular mechanisms governing the recruitment of arrestin 1/2/3 as well as arrestin-3 mutants to rhodopsin was investigated by centrifugal pull-downs. Arrestin-3 mutants were

anticipated to hamper the recruitment of arrestin-3 to rhodopsin, either by constraining the protein by intramolecular cysteine crosslinking or by inactivation of membrane anchor residues (see 3.1. *Design of di-cysteine and glycine mutants of arrestin-3*).

### **3.6. Purification of arrestin-3 di-cysteine and glycine mutants**

#### **3.6.1. Optimization of arrestin-3 purification**

The expression and purification protocols used for arrestin-3 mutants (see 3.1. *Design of di-cysteine and glycine mutants of arrestin-3*) were initially developed for arrestin-1 and the optimization of the second purification step was considered for arrestin-3. Briefly, His-tagged arrestin-3 mutants were expressed in *E. coli*. After cell sonication, samples were subjected to ultracentrifugation and the arrestin-3 mutants were purified by immobilized nickel affinity chromatography. After an overnight dialysis and removal of the His-tag by a TEV protease, arrestin-3 samples were set for a second purification step.

For this study, arrestin-3 mutant B15 (see 3.1.1. *Constrained arrestin-3 mutant selection and cloning*) was expressed in 6 L of *E. coli* suspension and purified by IMAC, as detailed in 3.2.3.2. *Immobilized Metal Affinity Chromatography (IMAC)*. After dialysis, arrestin-3 mutant B15 was split into four portions and the following chromatographic techniques were applied (figure 29 and 30):

- A) **Strong anion exchange chromatography** (Q Fast Flow column 1 mL, GE Healthcare, #17505301) which was the reference protocol.
  
- B) **A combination of a strong cation exchange chromatography** (SP column 1 mL, GE Healthcare, #17505401) **followed by a strong anion chromatography** (Q Fast Flow column 1 mL, GE Healthcare, #17505301). In this approach, the SP chromatography was anticipated to retain impurities whereas the Q chromatography was supposed to trap arrestin mutant B15.
  
- C) The **elution strong cation exchange** carried out in B), as shown in figure 26.
  
- D) **Heparin chromatography** (HP-Hep, High Performance heparin column 5 mL, GE Healthcare, #17040701)



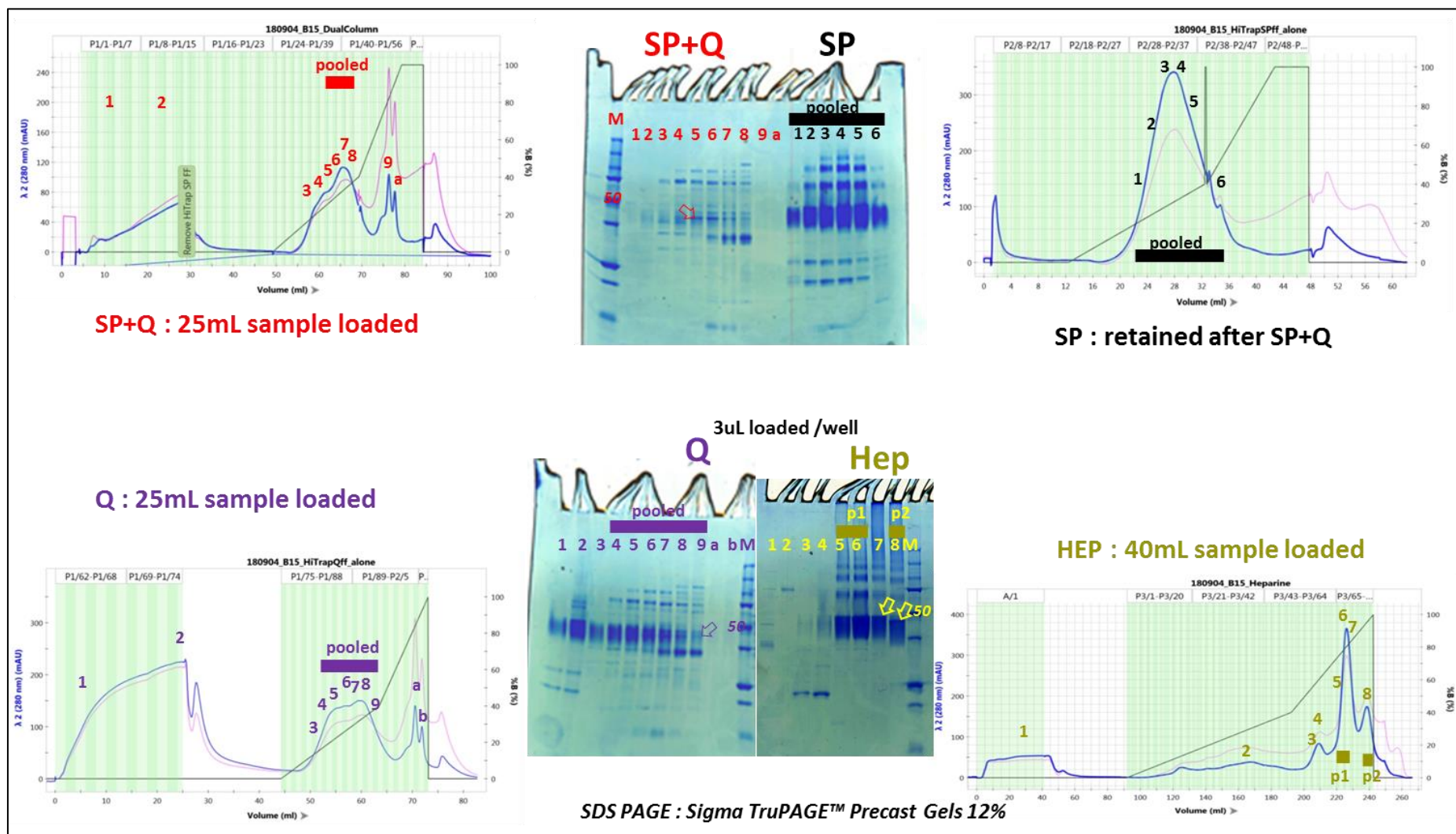


**Figure 29.** Comparison of cation exchange (SP), anion exchange (Q) and heparin (HEP) chromatographic methods on mutant B15. Lane numbers in gels represent the respective fractions on the chromatograms. Arrows highlight the expected band for mutant B15. Two distinct peaks were pooled in the heparin chromatography (p1 and p2). 50: 50 kDa.

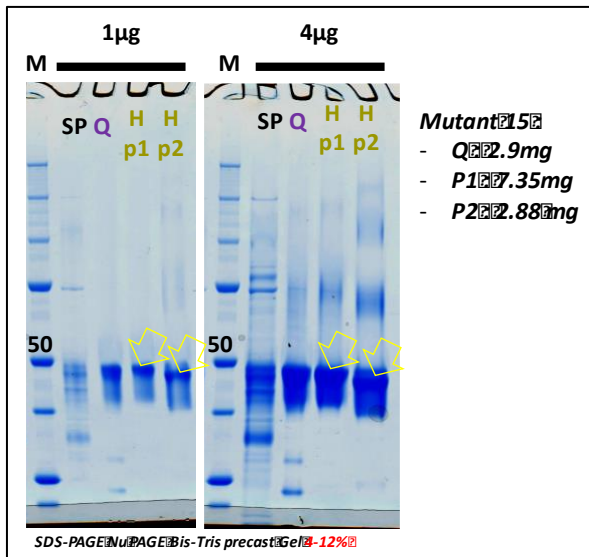


**Figure 30.** Pooled fractions the SP, G and Hep runs on a SDS-PAGE Nu PAGE gel, Bis Tris 4-20% as defined in figure 29. Arrows indicate arrestin bands. M: marker in kDa.

As indicated by figure 30, the heparin run led to higher yields of arrestin-3 mutant B15 (10.33 mg vs. 2.9 mg for the anion exchange chromatography) and had the unique advantage to separate a “second species” of the protein (two eluting peaks in the lower right chromatogram of figure 29). In fact, this distinction was only found with mutant B15 and the purification of other arrestin-3 mutants appeared more similar to WT arrestin-3 (see chromatogram in figure 24). Impurities found at a lower mass than arrestin in the cation and anion exchange chromatography runs were not detectable in the heparin run (figure 30). In addition, the ladder effect previously detected with Sigma TruPAGE gels (figure 29) was greatly diminished with NuPage gels from Invitrogen (figure 30) thus suggesting a gel artifact rather than co-eluting proteins. For all other purified arrestin-3 mutants, the heparin chromatography was chosen as a second separation method.

### 3.6.2. Expression of arrestin-3 mutants

In this section, the expression yields of arrestin-3 di-cysteine and glycine mutants are displayed (figure 31).

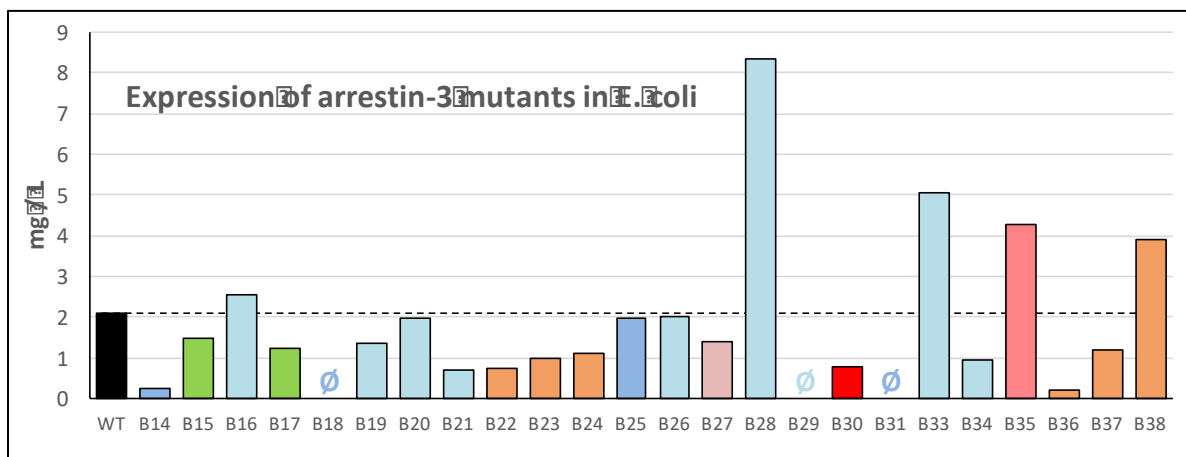


**Figure 31.** Expression of arrestin-3 mutants in *E. coli*. Black: WT arrestin-3. Light blue: di-cysteine mutants of peripheral loops. Dark blue: di-cysteine mutant targeting the protein core. Green: arrestin-3 di-cysteine mutants locked in an activated state. Pink: arrestin-3 di-cysteine mutants tethering the proximal C-tail to the N-domain. Orange: arrestin-3 glycine mutants of the membrane anchor.

### **3.7. Protein characterization of di-cysteine and glycine mutants**

#### **3.7.1. Limited trypsinization of arrestin-3 mutants**

To investigate the conformational and structural stability of arrestin-3 mutants (see section 3.1. *Design of di-cysteine and glycine mutants of arrestin-3*), purified proteins were subjected to limited trypsin digestion. The objective was to compare digestion profiles of arrestin-3 mutants to that of WT arrestin-3. In addition, arrestin-3 mutants were compared between their constrained (in oxidizing condition, buffer A alone) and their relaxed state (in reducing condition, buffer A + 2 mM DTT).

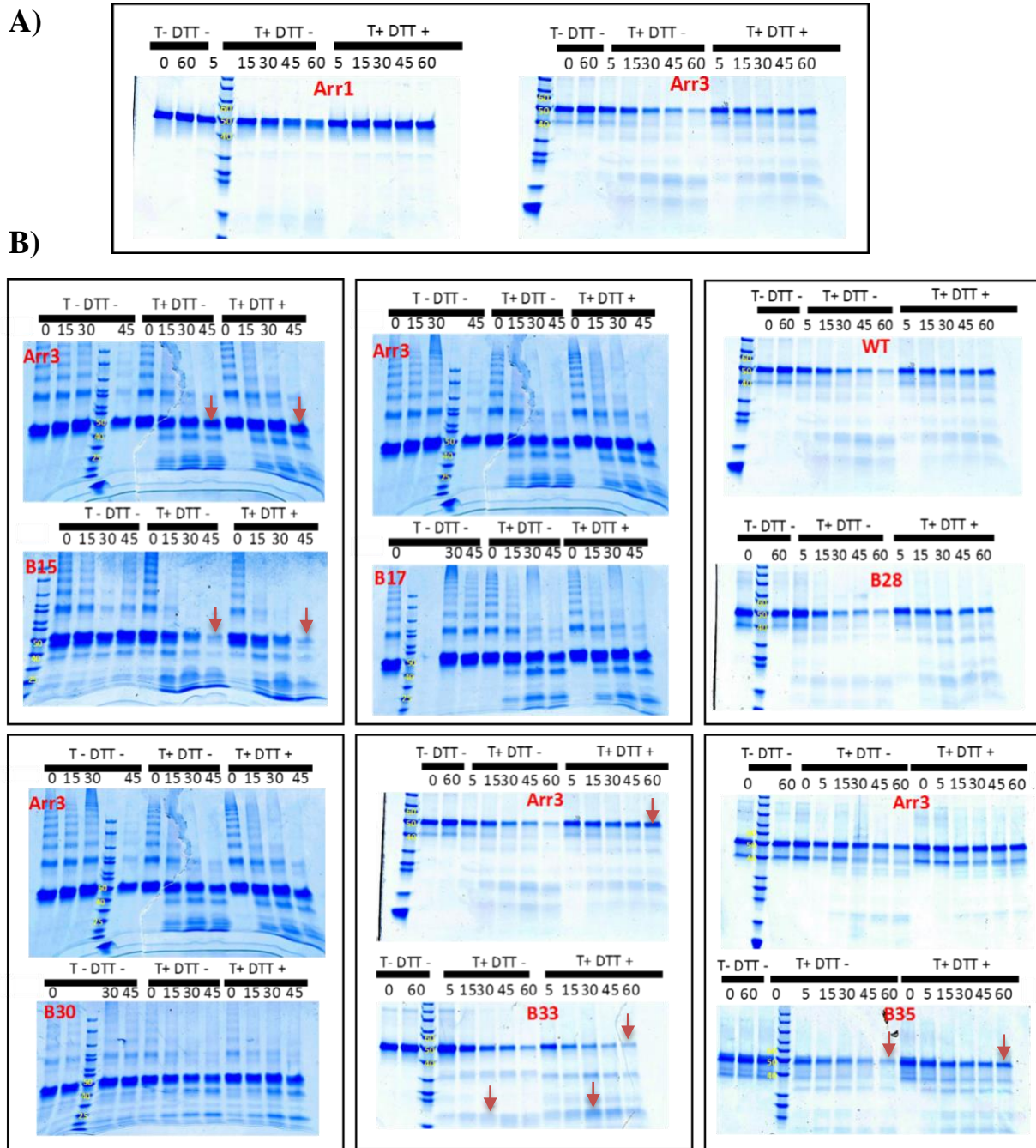


**Figure 32.** Limited trypsinization of A) arrestin -1 and -3 and B) arrestin-3 di-cysteine mutants. Arrestin samples were mixed with trypsin at a 1:75 (arrestin-1) or 1:200 (arrestin-3) ratio. After 0, 25, 30, 45 and 60 minutes, 2  $\mu$ g of proteins was mixed with 2X gel loading dye to stop the reaction, to be later run on an SDS-PAGE gel. T: trypsin. DTT: dithiothreitol. Value in black: reaction time in minutes. Yellow values: band size in kDa.

In figure 32.A), arrestin-3 appeared to be more sensitive to trypsinization than WT arrestin-1. In fact, partial trypsinization had to be run at a 1:200 ratio for arrestin-3 and 1:75 for arrestin-3. Additionally, the presence of DTT seemed to inhibit trypsinization of both proteins, particularly visible at 60 minutes for both proteins (figure 32.A).

Trypsinization profile of mutants B17, B28 and B30 in figure 32.B) did not differ from that of WT arrestin-3, suggesting that the introduced cysteines did not dramatically destabilize the overall three-dimensional conformation of arrestin. However, mutants B15 (first panel, figure 32.B) and B33 (lower middle panel, figure 32.B) appeared to be more sensitive to trypsinization compared to WT arrestin-3 regardless of DTT. In mutant B33, the higher sensitivity to trypsinization appears exaggerated by DTT (at 45 and 60 minutes time points) which might indicate successful crosslinking. Only mutant B35 (lower right panel, figure 32.B) showed an increased sensitivity towards trypsin in the oxidizing condition (45 and 60 minutes time points) which is less pronounced in the presence of DTT.

In conclusion, trypsin digests indicate that mutants B15 and B33 and B35 may have a different conformation than WT arrestin-3.

### 3.7.2. Thermal stability of arrestin-3 mutants by circular dichroism

Arrestin-3 is a cytosolic protein, rich in antiparallel  $\beta$ -sheets. To compare the conformational and structural integrity of arrestin-3 mutants, samples were subjected to thermal decay while their  $\beta$ -sheet content was monitored by circular dichroism (CD). Antiparallel  $\beta$ -sheets are secondary structures that have the intrinsic characteristic to deviate polarized photons with a maximum absorption at 215nm, as shown in figure 27.

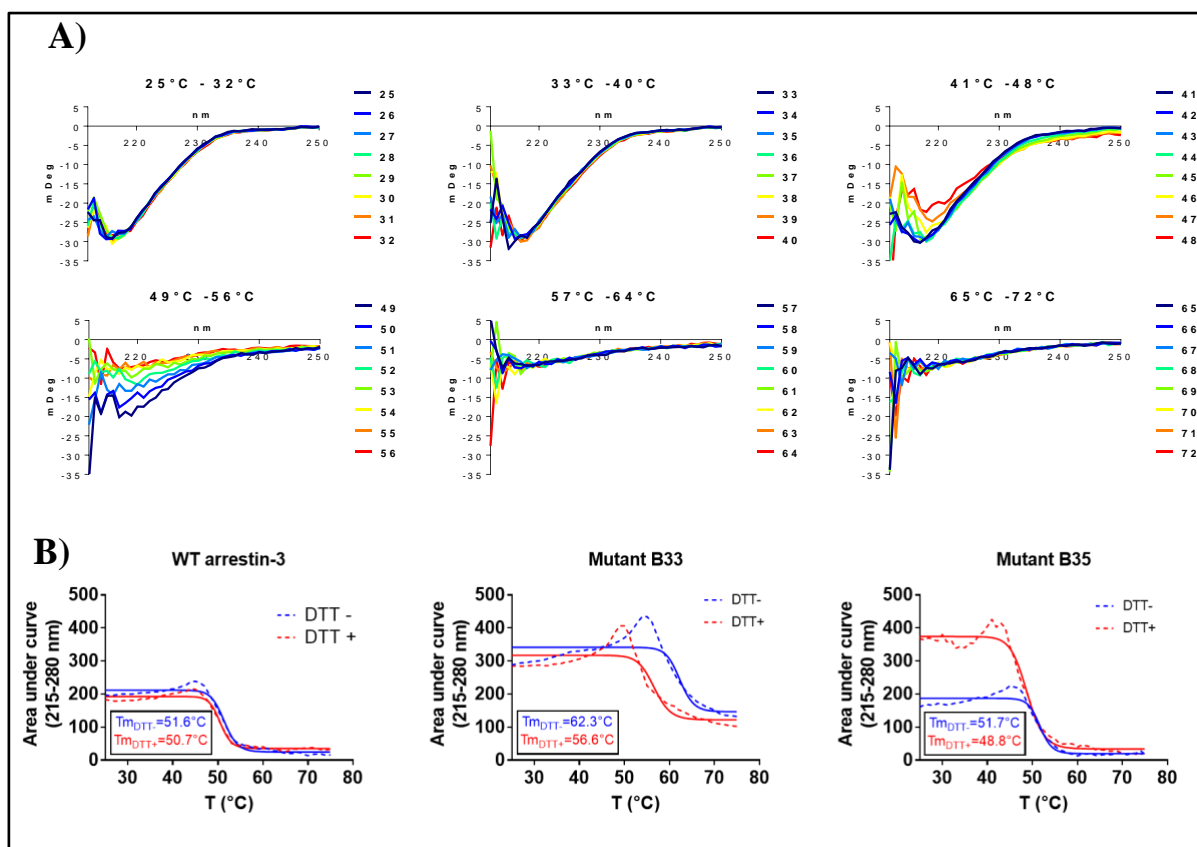


**Figure 33.** A) Thermal decay of WT arrestin-3 (single run) from 25 to 72°C monitored by circular dichroism in 50 mM HEPES. B) Area under curve measured on each CD spectrum from 215 to 280 nm and plotted against the temperature for WT arrestin-3, B33 and B35 (dotted lines). Buffers: 50 mM HEPES for WT arrestin-3 and B35; 100 mM ammonium phosphate for B33. A three-parameter non-linear regression analysis (continuous lines, see equation in 3.3. *Thermal stability of arrestin-3 by circular dichroism*) was applied to derive the indicated melting temperatures ( $T_m$ ).

Figure 33.A) displays all spectra (one per temperature) measured during the thermal decay of WT arrestin-3 in 50 mM HEPES in the absence of DTT. The expected CD signature with a maximal absorption at 215 nm was typical of anti-parallel  $\beta$ -sheets (see figure 27 for reference spectrum). Upon temperature increase, the  $\beta$ -sheet signature started to disappear above 42°C (third graph in figure 33.A). It is worth noting that HEPES also absorbed in the 200 to 210 nm range, as reported by *Greenfield et al., 2006*<sup>113</sup>. Interestingly, a residual absorption of approximately 25% at 215 nm compared to initial values was detected at high temperatures (above 57°C, last two graphs in figure 33.A), suggesting that even when aggregating under extreme conditions, arrestin is not fully denatured and maintains a certain amount of  $\beta$ -sheets.

In figure 33.B), dashed curves represent experimental area under curves (AUC) of spectra ranging from 215 to 280 nm and are plotted against the temperature. All experimental curves started with a plateau until approximately 40°C where the AUC slightly increased before plummeting into a lower plateau. The temporary increase around 45°C (in all three graphs of figure 33.B) was probably due to a partial denaturation or at least increased molecular agitation of flexible regions of arrestin, leading to a



greater exposure of  $\beta$ -sheets. The following decrease represented the disruption of the protein secondary structure and ended with a residual  $\beta$ -sheet signature despite aggregation at high temperatures, as shown in the 57-72°C spectra from figure 33.A.

The addition of DTT had no effect on the  $T_m$  of WT arrestin-3 (51.6 and 50.7°C respectively, second graph in figure 33.B). When measuring mutant B33 (which aimed to block to 20° inter-domain rotation) in 100 mM ammonium phosphate, the  $T_m$  in the absence of DTT increased by 10.7°C. The plateau of residual  $\beta$ -sheet signature at high temperature with mutant B33 also rose in intensity by approximately 150 units, compared to WT arrestin-3. Together, these findings suggest that ammonium phosphate stabilizes arrestin-3 against thermal decay through transient electrostatic interactions. Besides, the addition of DTT diminishes the  $T_m$  of mutant B33 by 5.7°C which could indicate the successful stabilization of arrestin by a disulfide bridge.

In the right graph of figure 33.B, the thermal decay curve of mutant B35 (blue dotted line), anticipated to tether the C-terminus to the polar core, is similar in intensity, shape and  $T_m$  (51.6°C) than that of WT arrestin-3 (51.7°C, in the first graph of figure 33.B). Interestingly, the addition of DTT to 50 mM HEPES seems to i) enhance the  $\beta$ -sheet signal at low temperatures, ii) disturb the 20 to 45°C range compared to WT arrestin-3 and iii) moderately diminish the  $T_m$  by 1.9°C, compared to the condition without DTT.

In conclusion, the thermal decay of WT arrestin-3 suggests that the protein cannot be fully denatured at high temperatures. In addition, the thermostability of two arrestin-3 mutants was investigated: mutant B33, anticipated to tether the N-domain and C-domain together in order to impede the intramolecular 20° rotation necessary for arrestin activation, and B35, a mutant supposed to anchor the C-tail to the polar core. Mutants B33 and B35 were selected because of their distinct trypsin digestion profiles upon addition of DTT (see figure 32.B). Here, a 10.7°C shift in  $T_m$  value was detected with mutant B33 upon addition of DTT (compared to 0.9°C with WT arrestin-3), potentially suggesting the presence of a disulfide bridge. This observation entails that impeding the 20° rotation in arrestin-3 contributes to the stabilization of the protein structure. With mutant B35, the addition of DTT more than doubled the  $\beta$ -sheet signal intensity at low temperatures, which coincides with the higher trypsin resistance detected for this mutant in the presence of DTT (figure 32.B, lower right panel). However,  $T_m$  values between the two oxidizing/reduced conditions (51.7°C and 48.8°C) are not significantly different for mutant B35. In other words, the overall protein stability is not impacted by DTT or the presence of a disulfide bridge. The  $\beta$ -sheet signal in low salt is dramatically enhanced with DTT, indicating a greater exposure of  $\beta$ -sheets in this condition.

### 3.7.3. Mass spectrometry

In order to probe the integrity and the crosslinking capability of purified proteins, arrestin-3 disulfide mutants were analyzed by mass spectrometry (LC-MS). A total of 3 conditions per mutant were analyzed (figures 35 and 36): the protein alone (further detailed in figure 34), the alkylated protein (IAA) and the reduced + alkylated protein (TCEP + IAA). Alkylation by IAA adds an exact mass of 57 Da to each free cysteine residue. The addition of reducing agent TCEP in the third condition aims to disrupt a potential disulfide bridge and free two additional cysteine residues that were not reactive in the protein+IAA condition. Stereotypical results of 6 mutants are exposed below in figures 35 and 36 and the rest of the mutant spectra in appendix 8 and 9.

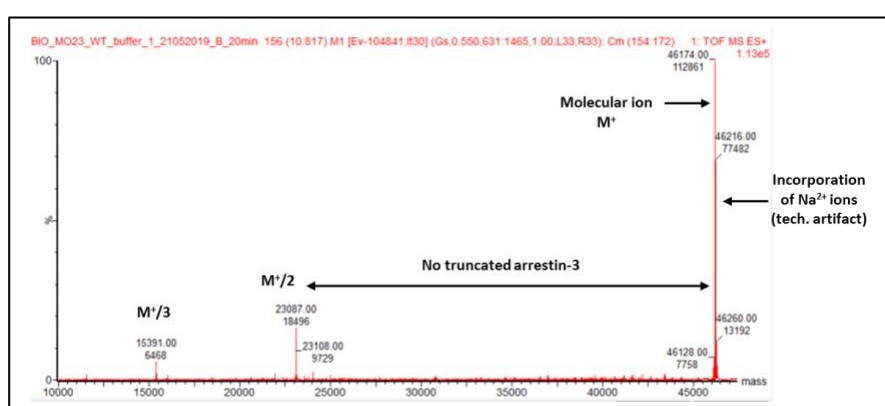


**Figure 34.** Deconvoluted spectrum of WT arrestin-3 in the “protein alone” condition (5 mM ammonium bicarbonate pH 7.0; 7.5 M guanidine; 0.1 M Tris-HCl; 1 mM EDTA). The molecular peak ( $M^+$ ) corresponds to the highest peak intensity detected, which happens to be the molecular weight in the deconvoluted spectrum. No truncated arrestin-3 or impurities are detected until the  $M^+/2$  and  $M^+/3$  species.

Firstly, purified proteins were proven exceptionally pure and accurate in mass as shown in figure 34 for WT arrestin-3. In fact, the measured molecular mass of WT arrestin-3 was only within 3 Da from the theoretical mass (46,174 Da vs. 46,177 Da respectively). The gap between experimental and theoretical mass never exceeded 6 Da throughout with WT arrestin-3 samples thus indicating optimal experimental conditions to pursue the LC-MS analysis. In addition, the  $M^+/2$  and  $M^+/3$  peaks in figure 34 corresponded to the other ionized forms of WT arrestin-3, which is typical of deconvoluted MS spectra.



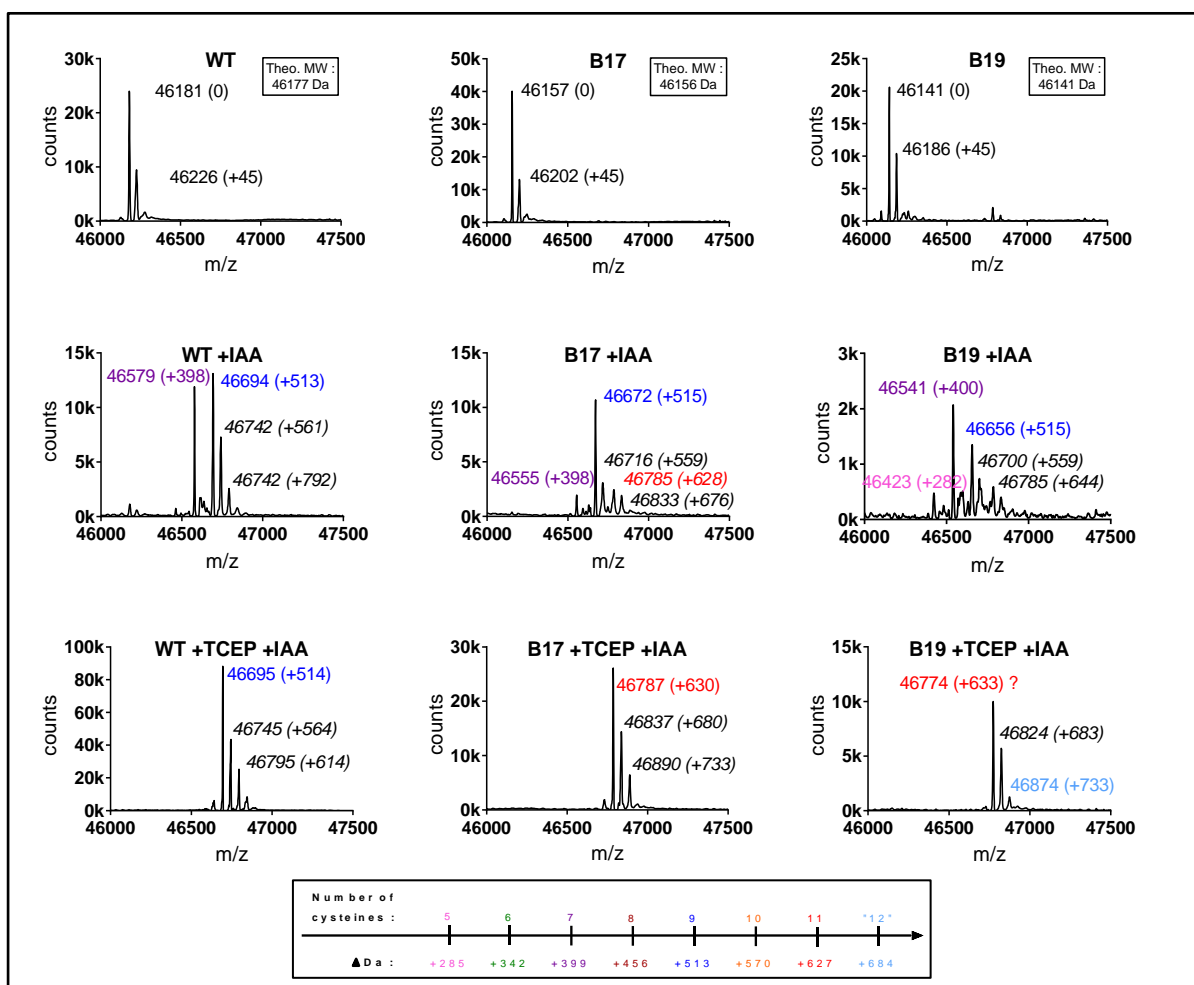


**Figure 35.** Deconvulated spectra of WT arrestin-3, B17 and B19 either i) alone (in 5 mM ammonium bicarbonate pH 7.0; 7.5 M guanidine; 0.1 M Tris-HCl; 1 mM EDTA), ii) +iodoacetamide (IAA) or iii) +IAA+ tris(2-carboxyethyl)phosphine (TCEP). Theo MW: theoretical molecular weight. Black labeled peaks: Na<sup>+</sup> incorporated species of arrestin-3 (technical artifacts).

In figure 34, the peaks 46,216 Da and 46,260 Da, found after the molecular ion (most intense peak at 46,174 Da; defined as 0 in each spectrum) were systematically found at +44 and +88 in all arrestin-3 samples (black labeled peaks in figure 35). They most likely represent the incorporation of two and four Na<sup>+</sup> ions by the larger arrestin molecule. These technical artifacts even “followed” the IAA-alkylated protein peak (+513 for 9 cysteines) at (+513 +44) and (+513 +88) respectively (black labeled peaks, middle section of figure 35). They were probably caused by an incomplete denaturation of arrestin, as also suggested in the residual  $\beta$ -sheet signature at high temperature by circular dichroism (see 3.7.2. *Thermal stability of arrestin-3 mutants by circular dichroism*).

In figure 35, peak intensities were not comparable from one spectrum to the other (in WT arrestin-3, maximal peak intensities were: 23,900 counts in the protein alone condition; 13,100 counts for the IAA condition and 88,200 counts for the IAA+TCEP condition) as variations resulted from different

ionization efficiencies. This phenomenon, called matrix effect, is well-known in mass spectrometry by electrospray in which the chemical environment of an analyte dramatically influences the ionization of the latter. For this reason, the interpretation of results can only be quantitative if restricted to the same spectrum or semi-quantitative if different spectra are compared.

Upon addition of IAA to WT arrestin-3 (left side of figure 35), the molecular peak (0) shifted to the right and revealed that 7 (7-cys, +398 Da) and 9 (9-cys, +513 Da) cysteines were successfully alkylated. In the IAA+TCEP condition of WT arrestin-3, the 7-cys species disappeared in favor of the 9-cys population: the presence of TCEP most likely promoted protein denaturation. As expected with WT arrestin-3, all nine native cysteines were free and therefore reacted with IAA. The addition of a reducing agent (TCEP, lower left spectrum of figure 35) essentially yielded to the same results with 9 free cysteines detected for WT arrestin-3. In mutant B17 (middle section of figure 35), the 7-, 9- and 11-cys species disappeared upon addition of TCEP in favor of a single 11-cys cysteine population in a reducing environment. Interestingly, mutant B17 was designed to only crosslink in an activated conformation (see 3.1.1. *Constrained arrestin-3 mutants and cloning*), which explained the non-negligible proportion of 11-cys adducts (the non-crosslinked population) in the IAA condition. Therefore, mass spectrometry data suggests that approximately 80% of mutant B17 crosslinked spontaneously, which entails that mutant B17 is able to adopt a potentially active conformation relatively often from the basal state. In mutant B19, the 5-, 7- and 9- alkylated species disappeared in favor of 11- and even 12-cys species in the presence of TCEP. However, there were only 11 cysteines present in arrestin-3 mutants (9 natives + 2 introduced by mutagenesis), therefore the 12<sup>th</sup> alkylated residue is probably a methionine, the second most reactive amino acid towards IAA<sub>114</sub>. This side reaction occurs at a slower pace and tend to emerge with increased IAA incubation time. For mutant B19 (right side of figure 35), the mass shift between the IAA condition (5-cys, 7-cys and 9-cys species) to IAA+TCEP condition (11-cys species) clearly indicates that a 2h incubation at room temperature (where mutant B19 was subjected to ambient oxidation in the absence of reducing agent) was sufficient to induce spontaneous disulfide bridge formation.

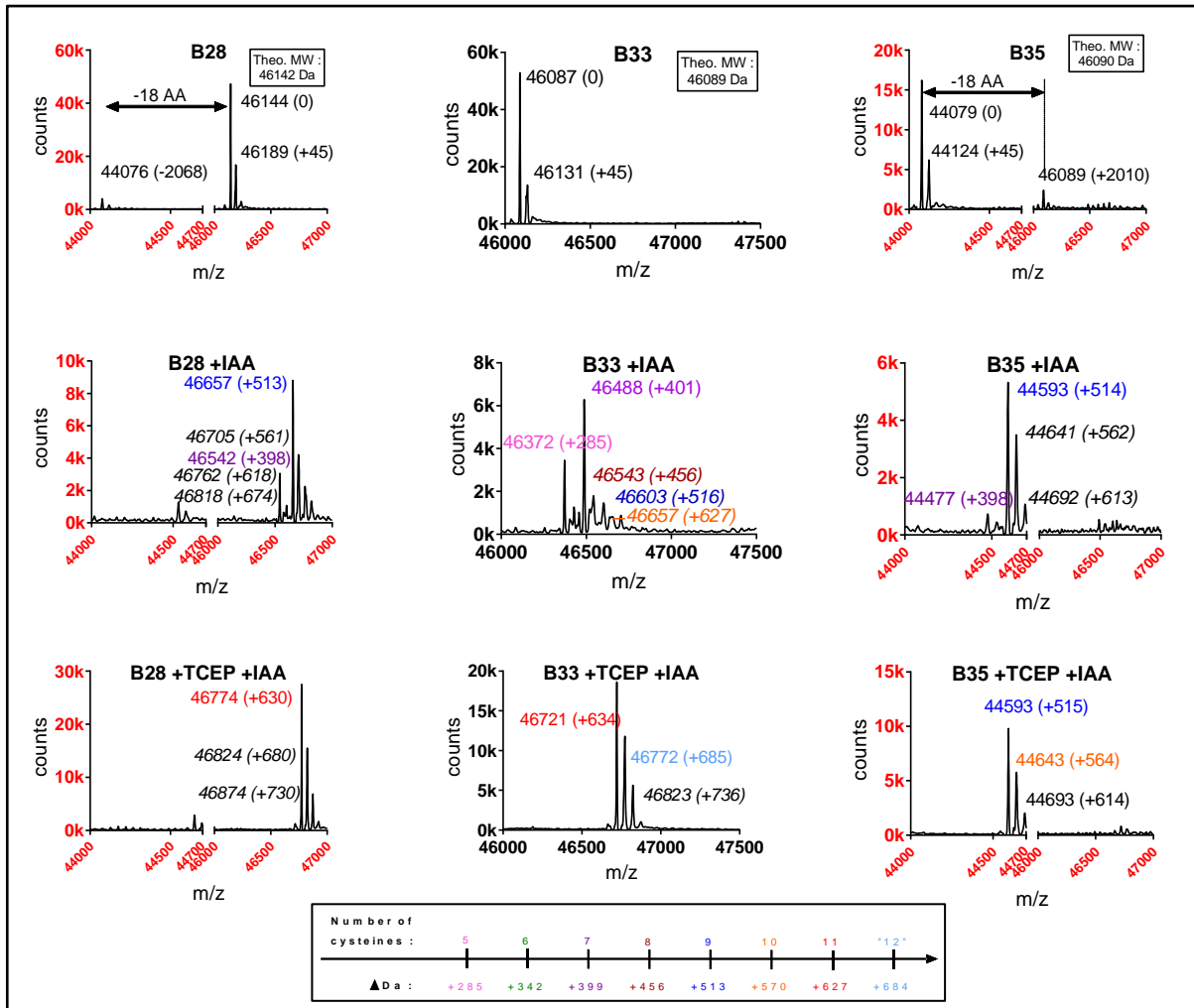


**Figure 36.** Deconvoluted spectra of arrestin-3 mutants B28, B33 and B35 either i) alone (in 5 mM ammonium bicarbonate pH 7.0; 7.5 M guanidine; 0.1 M Tris-HCl; 1 mM EDTA), ii) +iodoacetamide (IAA) or iii) +IAA+ tris(2-carboxyethyl)phosphine (TCEP). Theo MW: theoretical molecular weight. Black labeled peaks: Na<sup>+</sup> incorporated species of arrestin-3 (technical artifacts).

In figure 36, mutant B33 (middle section) exhibits the same spontaneous crosslinking ability as detected for mutant B19 (right side of figure 35): 5-, 7- and 9-cys species were transformed into 11- and 12-cys adducts upon addition of TCEP. For mutants B28 and B35 (left and right side of figure 36), unexpected peaks were detected at -2068 and -2010 Da, respectively. These peaks reflect an exact truncation of 17 amino acids from the C-terminus in both proteins. In addition, MS data reveal that one cysteine residue was clearly cut off from the main arrestin body in B35 as only the 9cys and 10cys species were detected in the TCEP condition (lower right spectrum in figure 36), although 11 cysteine were expected. This observation prompted a systematic quantification of the C-tail truncated variants for each following mutant.

The rest of the dataset of the mass spectrometry characterization of constrained mutants (mutants B14, B15, B16, B20, B21, B25, B26, B27, B30 and B34) can be found in appendix 8 and 9.

In summary, the crosslinking efficiency (calculated from peak intensities in the “protein +IAA” conditions) and C-tail truncation (peak intensities of the “protein alone” conditions) were estimated for each arrestin-3 mutants (table 7, see indicated equations). While estimations offer a certain perspective on mutant structure, caution must be taken with the interpretation of these calculations as they do not take into account the various intensities of peak intensities detected across samples, therefore various signal to noise ratios. Another limitation is the slower side-reaction of IAA with methionine residues (3 in WT arrestin-3) that generated a 12-cys species with mutant B19 (figure 35) and B33 (figure 36). For this reason, table 7 also reports the visual assessment of the peak shift to the right between the “protein+IAA” and the “protein +IAA+TCEP” conditions for each mutant. In addition, arrestin-3 mutants are either detected at  $\pm 6$  Da of their expected mass (WT, B15, B16, B17, B19, B21, B30, B33 and B34) or almost entirely truncated (B25, B27 and B35), with the exception of mutants B20, B26 and B28 that showed partial C-tail truncation (2% to 8%). Interestingly, all strongly truncated mutants have a cysteine near the polar core (B27, B35) or the three element interaction (B25). The moderately truncated ones (B20, B26, B28) only contain superficial cysteine substitution. In the case of B14, no peaks were detected near the expected molecular weight. The high capability of arrestin-3 mutants to form spontaneous disulfide bounds spontaneously is reflected by mutants B17, B19, B20, B21 and B28 with a crosslinking score higher than 75% only after a 2h incubation at room temperature.

Mutant name	Mutations	% crosslinking	% C-tail truncation	Peak shift : Disappearance of the 7 or 9cys peaks upon addition of TCEP
		$= 1 - \frac{10cys+11cys}{\Sigma(all\ cys\ species)}$	$= \frac{C-tail\ truncated\ variant}{(Molecular\ peak + C-tail\ truncated\ variant)}$	
WT	/	97%	1%	-
B14	R170C-L167C	NA	NA	-
B15	D298C-L167C	42%	0%	+++
B16	L69C-K293C	57%	1%	+++
B17	K293C-V168C	79%	1%	+++
B19	L69C-E146C	85%	0%	+++
B20	R66C-K139C	92%	8%	+++
B21*	D136C-Y250C	92%	4%	+++
B25	F391C-R26C	65%	98%	-
B26	L294C-Q131C	53%	6%	+
B27	R393C-D27C	73%	99%	+++
B28	L294C-K285C	77%	6%	+++
B30	K295C-Y404C	63%	2%	+
B33	F245C-F76C	92%	1%	+++
B34	F245C-Y64C	55%	2%	+
B35	R393C-H296C	73%	87%	-

**Table 7.** Proportions of crosslinked protein and C-tail truncated variants per mutant. B21\* mutant was detected with a His-Tag on, therefore estimations were calculated on the His-tagged version. C-tail truncated variant refers to a 18 aminoacid truncation from the C-terminus of arrestin-3 mutants. Columns are color-coded from low (green) to high values (red). The peak shift between the protein+IAA and protein+IAA+TCEP conditions can be assessed visually from figures 35/36 and appendix 8/9. NA: non applicable (no peak detected in the expected m/z range).

### 3.8. Phosphorylation state of PROS membrane preparations

The recruitment capability of arrestin 1/2/3 and arrestin-3 mutants to rhodopsin (embedded in rod outer segment (ROS) membranes, see protocol in 3.5.A *Preparation of ROS membranes*) was explored by centrifugal pull-downs. The phosphorylation state of membrane batches used for pull-down assays (ROS, phosphorylated ROS #1 and phosphorylated ROS #2) was assessed by mass spectrometry (figure 37 and table 8) and SDS-PAGE analysis (figure 38). For this, the 19 C-terminal amino acids of rhodopsin (DDEASTTVSKTETSQVAPA, MW= 1937.38 Da) of each batch was cleaved off by an endoprotease (AspN) so their phosphorylation state could be quantified by LC-MS.

As shown in the three spectra of figure 37,  $M_{+2}$  ionization species ( $1937.38 / 2 = 968.84$  Da) of the rhodopsin C-terminal peptide were the most ionized – therefore most detectable species – visible by MS spectra among others ionized forms ( $M_{+1}$ ,  $M_{+3}$ ,...). Experimental molecular weights of the different states of the C-terminal peptide were within <1 Da within expected molecular weights (968.84 Da for ROS, 969.36 Da for PROS #1 and 968.87 Da for PROS #2). A maximum of three phosphorylation sites induced by rhodopsin kinase were detected in PROS samples ( $I_1$ ,  $I_2$ ,  $I_3$  in figure 37, refer to the first peak of each peak cluster) and one constitutive phosphorylation ( $I_1$ ) in ROS membranes. Each cluster of peaks represent the natural isotope distribution engendered by carbon ( $^{12}C$ ,  $^{13}C$ ,  $^{14}C$ ) and nitrogen ( $^{14}N$  and  $^{15}N$ ) atoms. For the phosphorylation efficiency analysis (table 8), the first and highest peak of each cluster was chosen. Results indicate that PROS batch #1 is approximately 16% more phosphorylated than batch #2.

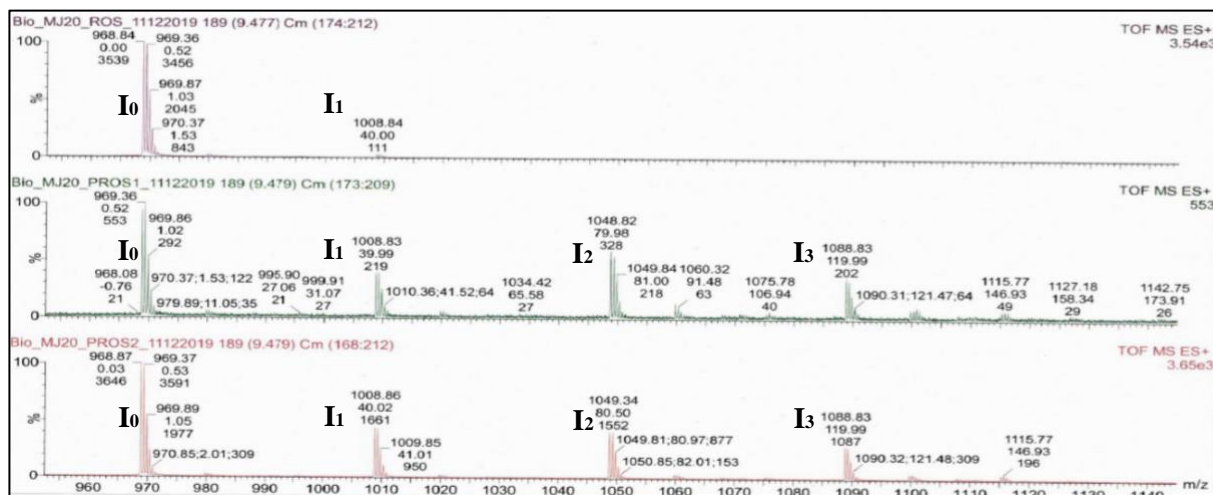


**Figure 37.** Mass spectrometry spectra of ROS (upper), PROS #1 (middle) and PROS #2 (lower) digested peptides (DDEASTTVSKTETSQVAPA). Data acquired by Alain Blanc (PSI). Molecular weight (MW) of the C-terminus peptide is 1937.38 Da. The  $M_{+2}$  species was by far the most visible ionization form of the peptide ( $1937.38 / 2 = 968.84$  Da,  $I_0$ ). The  $M_{+2}$  ionized species of mono- ( $I_1$ ), di- ( $I_2$ ) and tri- ( $I_3$ ) phosphate peptides were detected at 1008.8 Da, 1049.8 Da and 1068.8 Da respectively.

Sample	I <sub>0</sub> (0xPO <sub>3</sub> )	I <sub>1</sub> (1xPO <sub>3</sub> )	I <sub>2</sub> (2xPO <sub>3</sub> )	I <sub>3</sub> (3xPO <sub>3</sub> )	Average number of phosphate group per molecule of rhodopsin
ROS	3539	111	n. a.	n. a.	<b>0.03</b>
PROS #1	521	219	328	202	<b>1.17</b>
PROS #2	3646	1661	1552	1087	<b>1.01</b>

**Table 8.** Relative intensities of the unphosphorylated, mono-, di-, and tri-phosphate rhodopsin (C-terminal DDEASTTVSKTETSQVAPA peptide) per membrane batch. See equation for average number of phosphate group per molecule of rhodopsin in 3.4.2. *Phosphorylation state of PROS membrane preparation*. n. a.: non applicable.

As shown in figure 38, membrane samples containing C-terminal truncated rhodopsin in PROS batches #1 and #2 were run against undigested PROS batch #2. The apparition of bands at 30 kDa and 25 kDa after a 18h-long digestion by AspN clearly indicates that rhodopsin was cleaved. Nevertheless, the apparition of lower bands (red arrows in figure 38) around 5 and 10 kDa lower than full length rhodopsin (blue arrow, appearing at 35 kDa in SDS-PAGE due to SDS molecules bound to the neighboring phospholipids) contrasts with the expected band from C-terminal peptide cleavage (35-1.9 = 33.1 kDa) suggesting non-specific proteinase activity. In addition, an undigested portion of rhodopsin in PROS batch #2 but not in batch #1 indicate that rhodopsin might have a different conformation in the two batches.

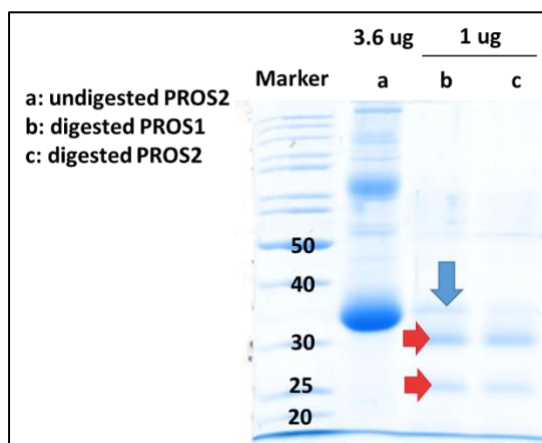


**Figure 38.** SDS-PAGE analysis of undigested PROS #2 (a) against AspN-digested PROS #1 and PROS#2 samples. M. : Marker with values in kDa. Blue arrow: undigested PROS #2 sample. Red arrows: AspN-digested products of rhodopsin.

In conclusion, PROS batch #1 appears to be 16% more phosphorylated than PROS batch #2. In addition, distinct AspN sensibilities among PROS #1 and PROS #2 digests suggest that rhodopsin in might be present in different conformations.

### 3.9. Centrifugal pull-downs

The recruitment of purified arrestins (bovine arrestin-1, human arrestin-2 and human arrestin-3) and arrestin-3 mutants was investigated against rhodopsin by centrifugal pull-downs as performed by *Kuhn et al., 1984*<sup>108</sup> and *Sommer et al., 2005*<sup>109</sup>. Rhodopsin is a light sensitive GPCR that can easily be manipulated *in vitro* in terms of phosphorylation state and overall activation. Arrestin-1 interactions with rhodopsin involve the so-called C-tail interaction<sup>81</sup> (with phosphate groups on the C-tail of activated rhodopsin), the membrane anchor<sup>84</sup> (with phospholipids surrounding the receptor) and the core-interaction<sup>34</sup> (with intracellular loops of rhodopsin), as detailed in *D.3. The GPCR-arrestin interface*. In this assay, rhodopsin was embedded in its native bovine rod outer segment (ROS) membranes and both rhodopsin and arrestin proteins were untagged. Upon mixing, arrestin/rhodopsin complexes were separated from the pool of unbound arrestin by centrifugation and entire pellets were run on SDS-PAGE gels. Bands corresponding to arrestin bound (50 kDa) to the receptor (33 kDa) were quantified by densitometry analysis (figure 39) and expressed relatively to the total amount of arrestin used (figure 40).

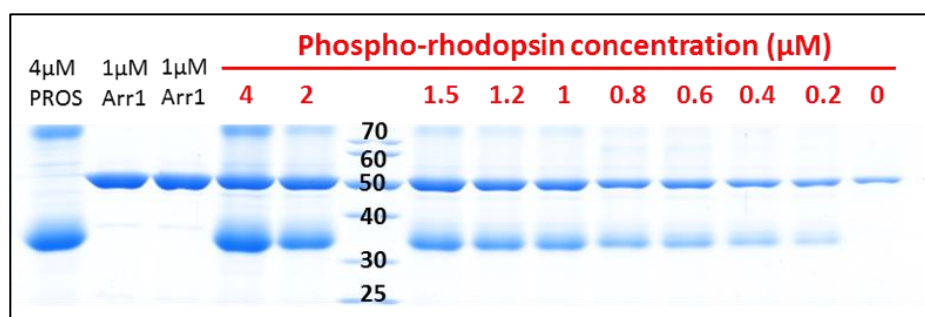


**Figure 39.** Titration of phosphorylated and light activated rhodopsin (PROS\*) from 0 to 4  $\mu\text{M}$  against 1  $\mu\text{M}$  arrestin-1 in 50 mM HEPES pH 7.0. Titrations were performed in a total volume of 40  $\mu\text{L}$ . Lane 1: 4  $\mu\text{M}$  of PROS\* alone. Lane 2 and 3: 4  $\mu\text{M}$  of arrestin-1 alone. Lane 4, 5 and 7 to 14: 1  $\mu\text{M}$  of arrestin-1 to a decreasing amount of PROS\*. Lane 6: Ladder in kDa.

#### 3.9.1. Salt screening on arrestin-3

The aim of salt titrations was to find the experimental conditions able to separate the arrestin-3/PROS complex (phosphorylated dark state rhodopsin interacting with arrestin only via the C-tail interaction and the membrane anchor) from the arrestin-3/PROS\* complex (phosphorylated and light-activated rhodopsin involving the C-tail interaction, the membrane anchor and the core interaction for a full arrestin engagement). In arrestin-1, the so-called pre-complex (arrestin-1/PROS) was reported to be more salt sensitive than the high affinity complex (arrestin-1/PROS\*)<sup>42</sup>. It is worth noting that salt sensitivity is not a strict measurement of affinity (defined as the combined forces of chemical interactions characterizing the association of two molecules), although the method takes advantage of

the dependency of arrestin–rhodopsin interactions on low ionic strength to measure an apparent complex stability. Here, ammonium phosphate, sodium chloride, magnesium chloride and potassium acetate were investigated as potential inhibitors of the complexes formed by arrestin-3 and four activated states of rhodopsin: non-phosphorylated ROS, ROS\* and their phosphorylated counterparts PROS and PROS\*. In this setup, the arrestin-3:rhodopsin ratio was fixed at 1 to 4  $\mu\text{M}$  in a total volume of 40  $\mu\text{L}$  and the PROS membrane batch #1 was used.

Under these conditions (figure 40), over 80% of arrestin-3 was bound to P-ROS\* (purple curve) at low salt concentrations (as indicated by  $B_{\text{max}}$  values of 0.93  $\mu\text{M}$  ( $(\text{NH}_4)_3\text{PO}_4$ ), 0.89  $\mu\text{M}$  (NaCl), 0.79  $\mu\text{M}$  ( $\text{MgCl}_2$ ) and 0.89  $\mu\text{M}$  ( $\text{CH}_3\text{COOK}$ )). At high salt concentrations, which is expected to obliterate arrestin-3 interaction with all functional forms of the receptor, approximately 10 to 15 % of arrestin-3 was still observed in the pellet following centrifugation. These levels of non-specific ‘pull-down’ are similar to those previously reported for arrestin-1<sup>116,118</sup>. With the exception of ammonium phosphate, known to be a potent inhibitor of arrestin-rhodopsin coupling<sup>116</sup>, recruitment of arrestin-3 to non-phosphorylated ROS (blue curves) and ROS\* (red curves) was significant at low salt concentrations yet effectively abolished at moderate NaCl,  $\text{MgCl}_2$ , and potassium acetate concentrations. Arrestin-3 binding to the non-phosphorylated and dark-state rhodopsin (ROS) cannot involve the C-tail interaction or the core interaction as rhodopsin is kept in its minimal activated state. Nevertheless, recruitment of arrestin-3 to ROS in moderate salt concentration suggests that constitutive membrane interactions might be at play. Additionally, ROS and ROS\* titration curves appear nearly identical in all four salt titrations, which indicates that arrestin-3 might does not interact with an activated core, in the absence of phosphorylations on the C-terminus of arrestin. In contrast, arrestin-3 binding to phosphorylated receptor (dark-state and light-activated; green and purple curves, respectively) was not affected by moderate salt concentrations. The presence of an activated rhodopsin core in PROS\* induced a minor increase in complex stabilization compared from arrestin-3/PROS (in NaCl titrations,  $\text{IC}_{50/\text{PROS}} = 235.9 \pm 10.7 \text{ mM NaCl}$  and  $\text{IC}_{50/\text{PROS}^*} = 441.9 \pm 23.4 \text{ mM NaCl}$  or a 1.87-fold increase in  $\text{IC}_{50}$  upon light activation). Other  $\text{IC}_{50}$  values also did not exceed a 2-fold increase upon light activation. These results contrast significantly with the reported salt-sensitivity of arrestin-1 binding to P-ROS versus P-ROS\*, in which a 10- (NaCl) to 100-fold ( $\text{MgCl}_2$ ) higher  $\text{IC}_{50}$  was observed for P-ROS\* compared to P-ROS<sup>115</sup>. Taken together, these observations suggest that a phosphorylated C-tail is important for arrestin-3 recruitment and that pre-complex formation can hardly be differentiated from the high affinity complex using salt.

In conclusion, all four salt titrations (figure 41) were poorly discriminative towards arrestin-3 recruitment to PROS and PROS\*. Ammonium phosphate and sodium chloride titrations were the most discerning strategies to separate the pre-complex formation from the high-affinity complex. Of those



two, sodium chloride titrations were retained in later experiments because its inhibition was less potent than ammonium phosphate, and a wider assay window should minimize day-to-day technical variations.

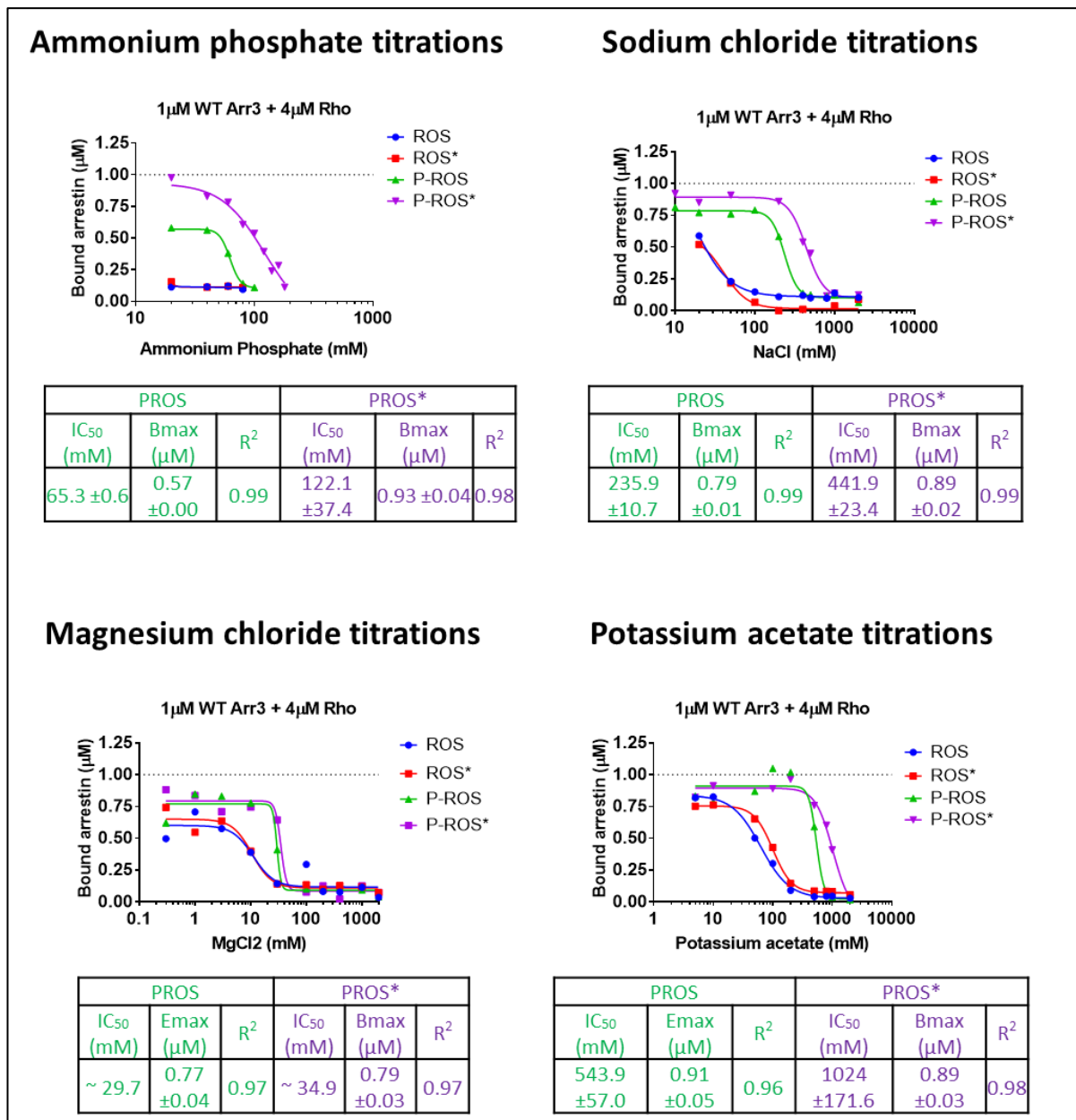


**Figure 40.** Salt titrations against 1  $\mu\text{M}$  of arrestin-3 mixed with 4  $\mu\text{M}$  of rhodopsin, in a total volume of 40  $\mu\text{L}$ . Rho: rhodopsin. ROS: unphosphorylated dark state rhodopsin. ROS\*: unphosphorylated light activated rhodopsin. PROS: phosphorylated dark state rhodopsin. PROS\*: phosphorylated light activated rhodopsin. IC<sub>50</sub>: half maximal inhibitory concentration. Bmax: maximal binding. R<sub>2</sub>: coefficient of determination. Data were fitted by a four parameter non-linear regression (see equation in 3.5.3. Data analysis).

### 3.9.2. Comparison of arrestin 1/2/3

In this section, the recruitment of WT arrestin-1, arrestin-2 and arrestin-3 to rhodopsin was investigated in pull-down assays by NaCl and receptor titrations similar to *Sommer et al., 2012*<sup>116</sup>. To

this day, three interfaces between arrestin-1 and rhodopsin have been identified: the C-tail interaction, the core interaction and the membrane anchor. The aim of this approach is to highlight potential differences in binding modes to various states of rhodopsin between arrestin-1, arrestin-2 and arrestin-3.

### 3.9.2.1. NaCl titrations

In the following pull-down experiment, the recruitment of arrestin-1, -2 and -3 to rhodopsin were compared in sodium chloride titrations with a fixed arrestin:rhodopsin ratio of 1 to 4  $\mu\text{M}$ , in a total volume of 40  $\mu\text{L}$ . The ROS membrane batch and PROS membrane batch #2 were used to screen various rhodopsin states: unphosphorylated dark-state (ROS) or light activated (ROS\*) rhodopsin and their phosphorylated counterparts (PROS and PROS\* respectively).

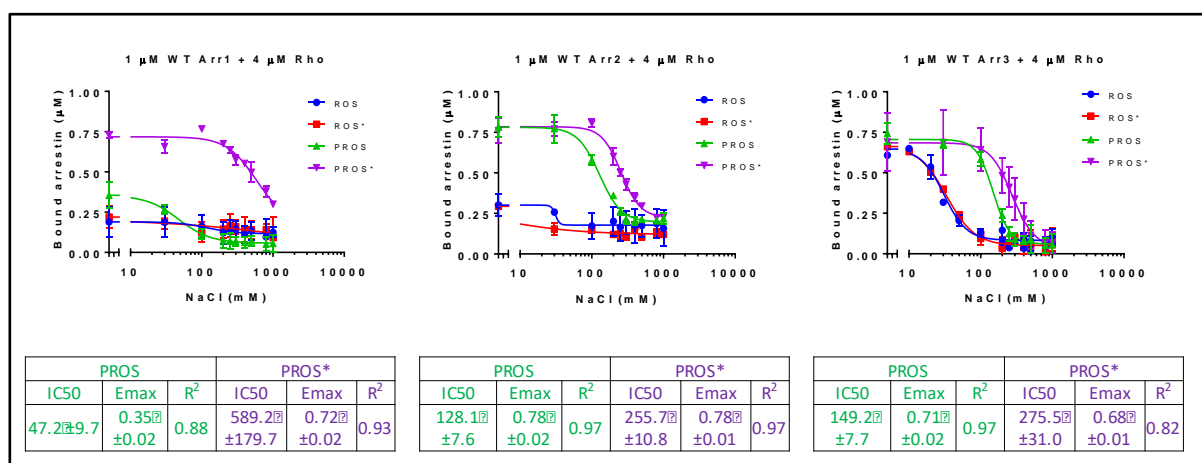


**Figure 41.** NaCl titrations against 1  $\mu\text{M}$  of arrestin-1, -2 or -3 mixed with 4  $\mu\text{M}$  of rhodopsin, in a total volume of 40  $\mu\text{L}$ . Pull-down assays were performed with: ROS (unphosphorylated dark state rhodopsin), ROS\* (unphosphorylated light activated rhodopsin), PROS (phosphorylated dark state rhodopsin) and PROS\* (phosphorylated light activated rhodopsin). Rho: rhodopsin. IC<sub>50</sub>: half maximal inhibitory concentration. Emax: maximal binding. R<sup>2</sup>: coefficient of determination. Data were fitted by a four parameter non-linear regression (see equation in 3.5.3. *Data analysis*).

For each arrestin (figure 41), ROS (blue) and ROS\* (red) titration curves are nearly identical suggesting that arrestins are not able to recognize an activated rhodopsin core in the absence of a phosphorylated C-terminus. In the case of arrestin-2 and arrestin-1, no or limited recruitment to ROS and ROS\* was detected in all salt concentrations. On the other hand, nearly all functional arrestin-3 (left panel) was pulled down with ROS and ROS\* at low salt concentrations. As shown in the third graph of figure 41, the arrestin-3/ROS (blue curve) or arrestin-3/ROS\* complexes (red) exhibit a higher salt sensitivity compared to the arrestin-3/PROS (green) or arrestin-3/PROS\* (purple) complexes. However, non-phosphorylated and dark-state rhodopsin (ROS, in blue) is in theory incapable to engage with arrestin-3 via the C-tail or the core interaction suggesting that arrestin-3 interacts non-specifically with the membrane phospholipids and not with the receptor directly. In the right table of figure 41, regression parameters of arrestin-1 binding with PROS and PROS\* reveal a 12-fold increase in IC<sub>50</sub>

values upon light activation (from  $47.2 \pm 9.7$  to  $589.2 \pm 179.7$  mM NaCl), which aligns with previous *in vitro* protein-protein interaction studies<sup>14</sup>. However, the PROS\*/PROS fold-change in IC<sub>50</sub> values was only of 2 (from  $128.1 \pm 7.6$  to  $255.7 \pm 10.8$  mM NaCl) and 1.8 (from  $149.2 \pm 7.7$  to  $275.5 \pm 31.0$  mM NaCl) for arrestin-2 and arrestin-3, respectively. The significant differences in fold-changes of IC<sub>50</sub> values upon illumination of arrestin/phosphorhodopsin complexes suggest that the relative importance of the three binding modes of arrestins to PROS\* or the plasma membrane (C-tail interaction, core interaction and membrane anchor) for complex stabilization is different for arrestin-1, -2 and -3. Finally, only 35% of arrestin-1 binds to PROS in absence of NaCl (green curve, first graph in figure 41) and this interaction is nearly abolished around 100 mM NaCl. In contrast, arrestin-2 and arrestin-3 couple with PROS (green curve in the last two panels) more efficiently as nearly 75% of arrestin-2 or -3 binds to the receptor in low salt and the interaction is abolished in the presence 300 mM NaCl. However, the high-affinity complex (arrestin/PROS\*) formed with arrestin-1 appears to be more stable (IC<sub>50</sub>=  $589.2 \pm 179.7$  mM NaCl) than with other arrestins (IC<sub>50</sub>=  $255.7 \pm 10.8$  mM NaCl for arrestin-2 and IC<sub>50</sub>=  $275.5 \pm 31.0$  mM NaCl for arrestin-3).

In conclusion, data suggest that membrane interactions might be more prominent with arrestin-3 in low salt conditions compared to arrestin-1 or -2. Secondly, the light-activation of phosphorhodopsin dramatically increases the stability of the arrestin-1/rhodopsin complex although this effect is more limited with arrestin-2 and arrestin-3. Finally, IC<sub>50</sub> values of NaCl titrations indicate that the arrestin-1/PROS\* complex is more stable than arrestin-2/PROS\* or arrestin-3/PROS\*.

### 3.9.2.2. Rhodopsin titrations

In this assay, three membrane preparations (ROS in figure 42.A, PROS #1 in figure 42.B and PROS #2 in figure 42.C) were titrated against 1  $\mu$ M of arrestin-1, arrestin-2 or arrestin-3 in pull-down assays. Receptor titrations were either performed in low salt (in the absence of NaCl) or 130 mM NaCl. According to *Gurevich et al., 1995*<sup>14</sup>, arrestin-1 binds primarily to phosphorylated and light activated rhodopsin (PROS\*) over the non-preferred forms of the receptor (ROS, ROS\* and PROS) whereas  $\beta$ -arrestins are less specific of PROS\* and form more stable complexes with non-preferred forms of rhodopsin than arrestin-1 does. Here, the objective was to assess the stoichiometry of arrestin/rhodopsin interactions.

On the left side of figure 42.A), titrations of ROS (blue) and ROS\* (red) against 1  $\mu$ M arrestin-1 show that no arrestin-1 is recruited to ROS or ROS\* in all salt concentrations. As previously suggested by NaCl titrations (see section 3.9.2.1.), the absence of bound arrestin-1 in low salt to ROS and ROS\* indicates that arrestin-1 does not bind to the membrane phospholipids as arrestin-2 and arrestin-3 do in these conditions (middle and right portions of figure 42). On the left side of figure 42.B) and 42.C)

PROS (green) titration curves reveal that approximately 40% of arrestin-1 is able to couple with unactivated phosphorhodopsin in low salt with both PROS membrane preparations. This interaction was nearly abolished in 130 mM NaCl. However, PROS\* (purple) appears to be stabilized by arrestin-1 at this salt concentration, which correlates with the high degree of specificity of arrestin-1 for PROS\* demonstrated by *Gurevich et al., 1995*<sup>14</sup>.

Interestingly, around 40% and 50% of arrestin-2 and arrestin-3 respectively were recruited to ROS and ROS\* membranes at a 1:4 arrestin to rhodopsin ratio (last data point). With arrestin-3, binding to ROS and ROS\* quickly saturated at a 1:1 ratio in low salt and this interaction almost disappeared in 130 mM NaCl. For PROS and PROS\* (figures 42.B and C, green and purple curves), a similar rapid saturation (at 1:2 for arrestin-2 and 1:1 for arrestin-3) of complex formation was detected in low salt. In fact, the nonlinear regression analysis applied to the PROS\* titrations suggested a stoichiometry of 1 molecule of arrestin-1 for 1 rhodopsin and 2 arrestin-3 for 1 rhodopsin. This observation suggests that arrestin-2 and especially arrestin-3 bind non-specifically to the phospholipids of ROS membranes and not to the receptor directly. At 130 mM NaCl and in both PROS batches, PROS and PROS\* titration curves can barely be differentiated with arrestin-2 and not at all with arrestin-3 due to the propensity of the C-tail interaction to drive the overall arrestin-rhodopsin interaction for the two proteins.

Titration curves in figure 42.B and 42.C reveal that 95% of arrestin-1 was pulled down by 4  $\mu$ M of PROS\* (purple curve) in low salt using the membrane batch #2 whereas only 75% of arrestin-1 was bound to 4  $\mu$ M of PROS\* using batch #1. Therefore, saturation appears to be reached at a 4-fold excess of light activated phosphorhodopsin with batch #2, but not with batch #1. This observation entails that rhodopsin in batch #1 either had reconverted to opsin through retinal release or that the receptor was partially denatured in the extraction process. Calculations derived from PROS\* titrations against 1  $\mu$ M of arrestin-1 in low salt resulted in K<sub>d</sub> values of 1.18  $\mu$ M (batch #1) and 808 nM (batch #2) which exceed the value of 365 nM derived from pull-down experiments performed by *Sommer et al., 2011*<sup>118</sup>. However, *Sommer et al., 2011*<sup>118</sup> used fluorescent probes, which *Lally et al., 2015*<sup>117</sup> stated to improve the quantification of arrestin/rhodopsin complexes compared to SDS-PAGE analysis, therefore affecting the apparent K<sub>d</sub> as well. The K<sub>d</sub> value of the PROS\*/arrestin-1 complex in the present pull-downs (808 nM) also exceeds the K<sub>d</sub> value derived from Extra MetaII experiments (20 nM according to *Pulvermüller et al., 1997*<sup>119</sup>) by a factor of 40. This discrepancy can be explained by the different temperatures used in pull-downs (20°C) and ExtraMetaII (2-10°C), as the decay of MetaII (the main signaling conformation of rhodopsin) is faster at higher temperatures, meaning that a significant amount of receptor decays in several minutes, before complete arrestin binding can be reached<sup>118</sup>. This effect is particularly true at conditions near the stoichiometric ratio of arrestin to rhodopsin, which are important determinants in the overall shape of the curve and for determination of the K<sub>d</sub><sup>118</sup>.

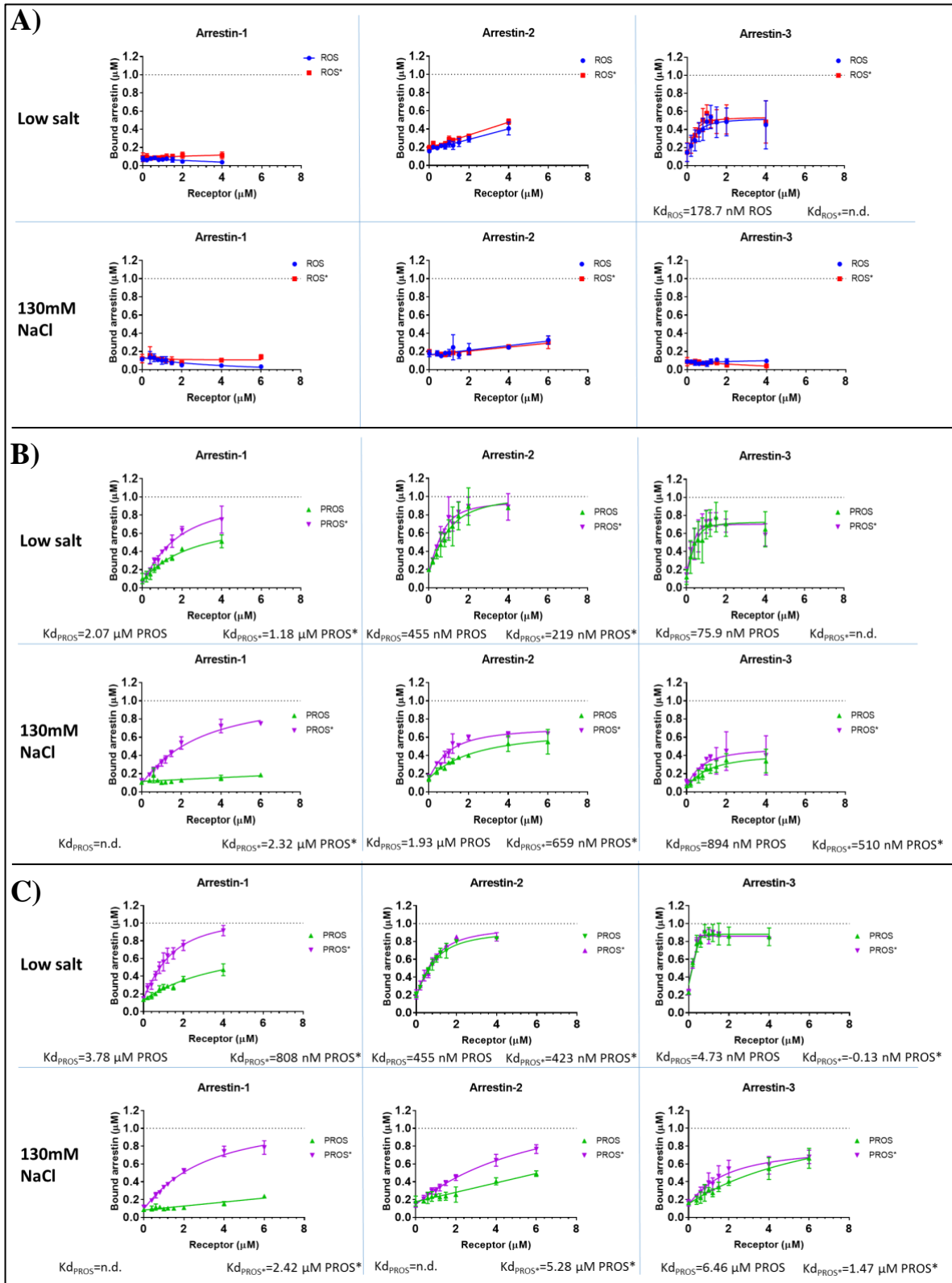


**Figure 42.** Rhodopsin titrations against 1  $\mu$ M of arrestin-1, -2 or -3 mixed in low salt (50 mM HEPES pH 7.0) or (130 mM NaCl, 50 mM HEPES pH 7.0) in a total volume of 40  $\mu$ L. Pull-down assays were performed with A) ROS membranes, B) PROS membrane batch #1 or C) PROS membrane batch #2 (see 3.5.1. Preparation of Rod Outer Segment membranes). ROS: unphosphorylated dark state rhodopsin. ROS\*: unphosphorylated light activated rhodopsin. PROS: phosphorylated dark state rhodopsin. PROS\*: phosphorylated light activated rhodopsin. Kd: constant of dissociation. n.d.: not determined. Data were fitted by a non-linear regression according to the stoichiometric saturation equation described in 3.5.3. Data analysis.

### 3.9.2.3. Influence of the 7-phosphopeptide on the arrestin/phosphorhodopsin complex

Crystal structures of p44/rhodopsin<sup>17</sup> and arrestin-2/V2Rpp<sub>31</sub> (V2Rpp being a peptidomimetic of the phosphorylated C-terminus of the vasopressin receptor 2) suggest that arrestins undergo an intramolecular 20-21° rotation between the N- and C-domains in order to recognize an activated GPCR core. Here, a phosphorylated peptide (7P) derived from the 19 residues of rhodopsin C-terminus<sub>120</sub> was used to verify the contribution of the C-tail interaction in arrestin-1, -2 and -3 binding with rhodopsin. In this pull-down assay, 1 μM of either arrestin-1, -2 or -3 was pre-incubated with increasing concentrations of the 7P peptide (0-200 μM) before 4 μM of rhodopsin was added.

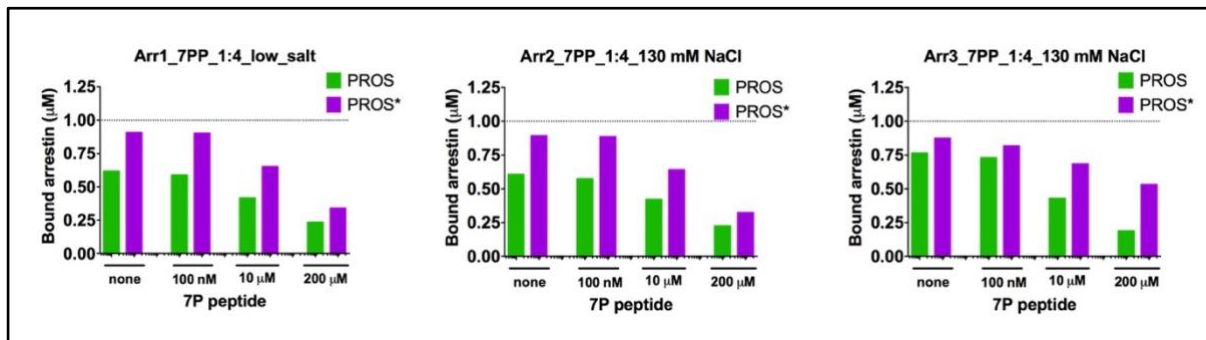


**Figure 43.** Influence of 7P, a peptidomimetic of phosphorylated C-terminal rhodopsin (7P peptide) on the recruitment of 1 μM of arrestin-1, -2 and -3 to 4 μM of dark state phosphorylated rhodopsin (PROS) or light activated phosphorylated rhodopsin (PROS\*, batch #2). Pull-down reactions were carried out in a total volume of 40 μL of either (50 mM HEPES pH 7.0) or (130 mM NaCl, 50 mM HEPES pH 7.0). Green bars: dark state phosphorylated rhodopsin (PROS). Purple bars: light activated phosphorylated rhodopsin (PROS\*).

Here, the 7P peptide successfully competed off arrestin recruitment to PROS (green bars) and PROS\* (purple bars), as shown in figure 43. As expected, this competition was found to be concentration-dependent but surprisingly affected arrestin members differently. In fact, arrestin-1 and -2 appeared less affected in PROS coupling than arrestin-3 (-63% binding for arrestin-1, -63% binding for arrestin-2 and -75% for arrestin-3 binding to PROS was detected between the 0 and the 200 μM 7P peptide conditions). The opposite is true for PROS\* association where -62% binding for arrestin-1, -64% binding for arrestin-2 and -39% binding for arrestin-3 to PROS\* was detected between the 0 and the 200 μM 7P peptide conditions.

In conclusion, the presence of the 7P peptide successfully competed off arrestin-1, -2 and -3 recruitment to PROS and PROS\*, highlighting the contribution of the C-tail interaction in these complexes. In addition, arrestin-3 seemed more sensitive to the competition by 7P peptide than arrestin-1 or arrestin-2 for the recruitment to PROS, yet less sensitive to the influence of 7P peptide for the recruitment to PROS\* compared to arrestin-1 and arrestin-2.

### 3.9.3. Arrestin-3 di-cysteine mutants: receptor titrations

In this section, the recruitment of structurally constrained mutants of arrestin-3 to rhodopsin was investigated in pull-down assays. The objective was to evaluate the relative importance of the 20-21° inter-domain rotation, the finger loop (located at the so-called central crest of arrestin) or the C-tail of arrestin-3 in recruitment to rhodopsin (see *D.3. The GPCR-arrestin interface*). For this, disulfide bridges have been introduced in arrestin-3 in order to restrict the flexibility of structural features involved in the recruitment to rhodopsin (see *3.1. Design of di-cysteine and glycine mutant arrestin-3*), as previously demonstrated by *Sommer et al., 2007*<sup>111</sup>. To ensure maximal intramolecular crosslinking, mutants were selected by mass spectrometry and incubated overnight in mild oxidizing conditions at 4°C. Pull-down reactions were carried out in optimal conditions to separate PROS from PROS\* coupling as discovered in *3.9.2.1. NaCl titrations*. These buffer conditions were 300 mM NaCl using PROS membrane batch #1 (figure 44 and 45) and 130 mM NaCl with PROS membrane batch #2 (figure 46). Overall, the recruitment of arrestin-3 mutants to PROS and PROS\* must be compared between the reduced (relaxed state of arrestin-3 mutants, in the presence of DTT) and oxidizing (constrained state of arrestin-3, in the absence of reducing reagent) conditions. Precautions must be taken with direct comparison between arrestin-3 mutants and WT arrestin-3 as cysteine mutations alone might affect arrestin recruitment.

Not surprisingly, DTT had little to no effect on WT arrestin-3 recruitment to PROS (green curve) and PROS\* (purple curve) as shown in figure 44 and 45. Arrestin-3 mutants B33, B19, B20 and B16 were all designed to restrict the finger loop movements (protein region from Y64 to L74), essential in arrestin-1 for the core interaction with PROS\*. Either the back of the finger loop sealed the upper central crest when linked to the C-loop (B33, F245C-F76C), or the finger loop was linked from the middle to the gate loop (B16, L69C-K293C), or was retained from the middle on the N-domain (B19, L69C-E146C) or finally stitched from the middle to the adjacent middle loop (B20, R66C-K139C). In all four mutants except B20, PROS\* coupling was greatly diminished in their constrained state compared to their relaxed state (tables in figures 44 and 45): -52% in B<sub>max</sub> values for B33, -54% in B<sub>max</sub> for B19 and -47% in B<sub>max</sub> for B16. In comparison WT arrestin-3 exhibited a reduction of 31% in B<sub>max</sub> value between the oxidized and reduced states. Disruption of the disulfide bridge by addition of DTT (relaxed state) restored a WT-like PROS\* binding profile (B<sub>max</sub>WT = 0.67 ± 0.05 μM PROS\*) in B33 (B<sub>max</sub>B33 = 0.75 ± 0.05 μM PROS\*), B19 (B<sub>max</sub>B19 = 0.52 ± 0.03 μM PROS\*) and B20 (B<sub>max</sub>B20 = 0.55 ± 0.08 μM PROS\*). However, a systematic decrease in PROS and PROS\* coupling is detected in mutant B16 (B<sub>max</sub>B16 = 0.38 ± 0.03 μM PROS\*) both in the relaxed and constrained states, probably from less tolerated cysteine mutations in terms of recruitment to rhodopsin.

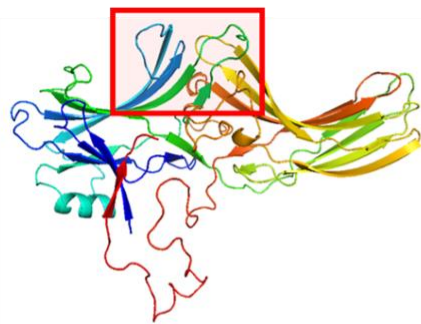
Due to the difficulty to separate PROS (green curves) from PROS\* (purple curves) arrestin-3 coupling (see 3.9.2.1. *NaCl titrations*), the recruitment of arrestin-3 mutants to dark-state PROS in 300 mM NaCl was hardly detected in B19, B20 and B16. Interestingly, PROS coupling with mutant B33 was increased in the presence of DTT ( $B_{\max_{B33,DTT}} = 0.49 \pm 0.03 \mu\text{M PROS}$ ) compared to the constrained state ( $B_{\max_{B33}} = 0.26 \pm 0.07 \mu\text{M PROS}$ ), which was more comparable to WT arrestin-3 ( $B_{\max_{WT}} = 0.21 \pm 0.03 \mu\text{M PROS}$ ).

Surprisingly, pre-activated mutant B17 where the gate loop is attached to the N-domain in an activated conformation did not lead to an increase in coupling to either PROS or PROS\*. On the contrary, the constrained state of B17 led to the abolition of PROS or PROS\* complex formation. Only in the relaxed state was PROS\* binding restored to WT-like levels ( $B_{\max_{B17}} = 0.42 \pm 0.06 \mu\text{M PROS*}$ ).

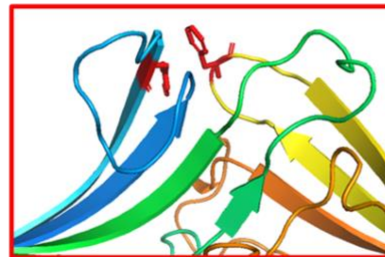
Preliminary receptor titrations on the PROS membrane batch #2 revealed that in 200 and 300 mM NaCl, WT arrestin-3 recruitment to PROS and PROS\* was either undistinguishable or abolished (data not shown). In light of this observation, 130 mM NaCl was chosen as the buffer condition to carry out receptor titrations with mutant B19 and B35 (C-tail truncated mutant from A392), despite no differentiation between PROS\* from PROS binding with WT arrestin-3 (figure 46). Surprisingly, the  $B_{\max}$  values of B19 for PROS binding nearly tripled from batch #1 ( $B_{\max_{B19,\#1}} = 0.09 \pm 0.03 \mu\text{M PROS*}$ ) to batch #2 ( $B_{\max_{B19,\#2}} = 0.30 \pm 0.05 \mu\text{M PROS*}$ ), despite the higher phosphorylation level in batch #1. Surprisingly, the lack of a distal C-tail (17 C-terminal residues) in B35, which normally inhibits arrestin activation therefore its recruitment with rhodopsin<sup>17,18</sup>, did not lead to a higher recruitment to either PROS or PROS\*, compared to WT arrestin-3. Therefore, the proximal C-tail must assume this function.

In conclusion, the various constrains applied in the central crest region revealed that the impairment of the 20-21° rotation (B33) led to the most drastic reduction in arrestin-3 coupling to PROS and especially PROS\*. Tethering the finger loop from the middle (B16 and B19) led to a decrease in arrestin-3 recruitment to PROS\*, whereas anchoring the finger loop to the adjacent middle loop (B20) did not significantly influence the core-interaction. Recruitment results on mutant B19 to rhodopsin with PROS batch #1 (most phosphorylated batch) were not reproduced using PROS batch #2 (less phosphorylated batch). Finally, pre-activated mutant B35 did not lead to an increased recruitment profile to PROS or PROS\* compared to WT arrestin-3, despite the partial deletion of the inhibitory C-tail towards arrestin activation<sup>17,18</sup>.





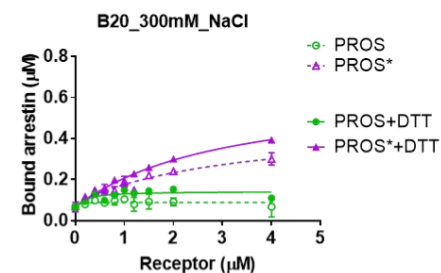
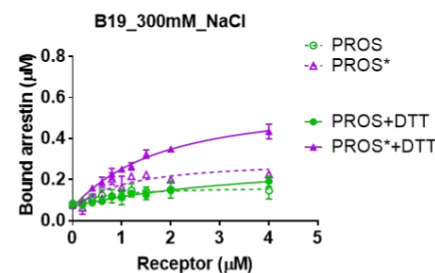
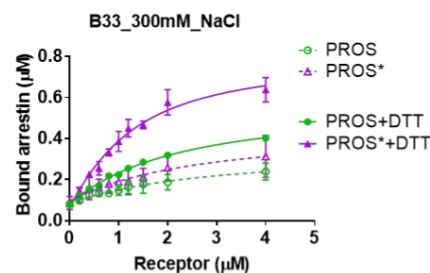
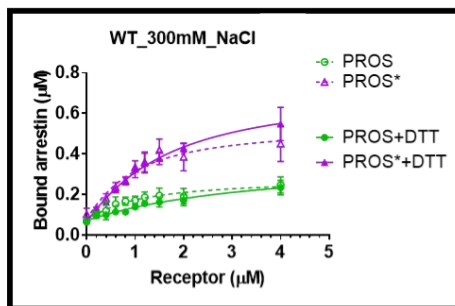
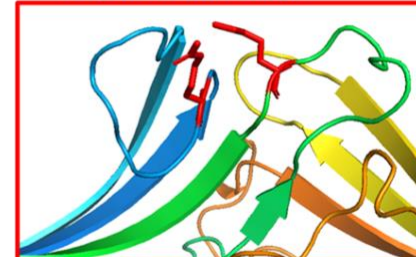
**B33 (F245C-F76C) :**  
Finger loop to C-loop



**B19 (L69C-E146C) :** Finger loop to N-domain



**B20 (R66C-K139C) :** Finger loop to Middle loop



WT	PROS	PROS*	PROS +DTT	PROS* +DTT	B33	PROS	PROS*	PROS +DTT	PROS* +DTT	B19	PROS	PROS*	PROS +DTT	PROS* +DTT	B20	PROS	PROS*	PROS +DTT	PROS* +DTT
<b>Bmax (μM)</b>	0.21 ±0.03	0.46 ±0.04	0.30 ±0.07	0.67 ±0.05	<b>Bmax (μM)</b>	0.26 ±0.07	0.36 ±0.13	0.49 ±0.03	0.75 ±0.05	<b>Bmax (μM)</b>	0.09 ±0.03	0.24 ±0.06	0.25 ±0.07	0.52 ±0.03	<b>Bmax (μM)</b>	N.A.	0.38 ±0.09	0.08 ±0.02	0.55 ±0.08
<b>Kd (μM)</b>	0.92 ±0.40	0.73 ±0.24	3.37 ±1.43	1.31 ±0.29	<b>Kd (μM)</b>	2.71 ±1.46	2.51 ±1.99	1.90 ±0.24	0.88 ±0.18	<b>Kd (μM)</b>	0.70 ±0.71	0.89 ±0.63	3.99 ±2.01	1.45 ±0.27	<b>Kd (μM)</b>	N.A.	2.88 ±1.41	0.16 ±0.18	2.52 ±0.77

**Figure 44.** Rhodopsin titrations (batch #1) against 1 μM of arrestin-3 mutants in 300 mM NaCl. Pull-down were carried out in a total volume of 40 μL. Green curves: dark state phosphorylated rhodopsin. Purple curve: light activated phosphorylated rhodopsin. Dotted lines: absence of DTT. Plain lines: +1 mM DTT. On arrestin-3 structure PDB 3P2D are highlighted the native residues mutated to cysteines in respective mutants. Data were fitted by the stoichiometric saturation non-linear regression (see equation in 3.5.3. *Data analysis*).

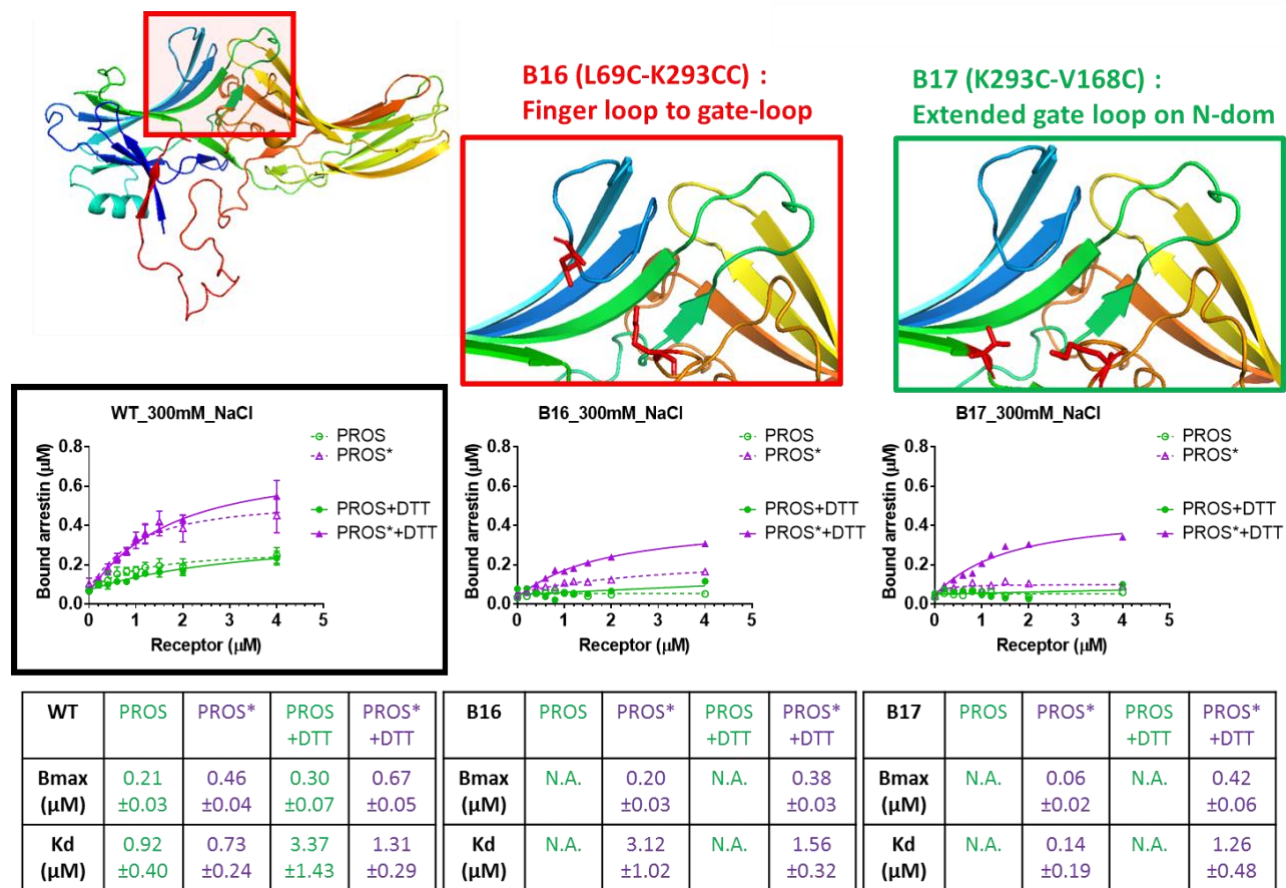


**Figure 45.** Rhodopsin titrations (batch #1) against 1  $\mu\text{M}$  of arrestin-3 mutants in 300 mM NaCl. Pull-down reactions were carried out in a total volume of 40  $\mu\text{L}$ . Green curves: dark state phosphorylated rhodopsin. Purple curve: light activated phosphorylated rhodopsin. Dotted lines: absence of DTT. Plain lines: +1 mM DTT. On arrestin-3 structure PDB 3P2D are highlighted the native residues mutated to cysteines in respective mutants. Data were fitted by the stoichiometric saturation non-linear regression (see equation in 3.5.3. *Data analysis*).

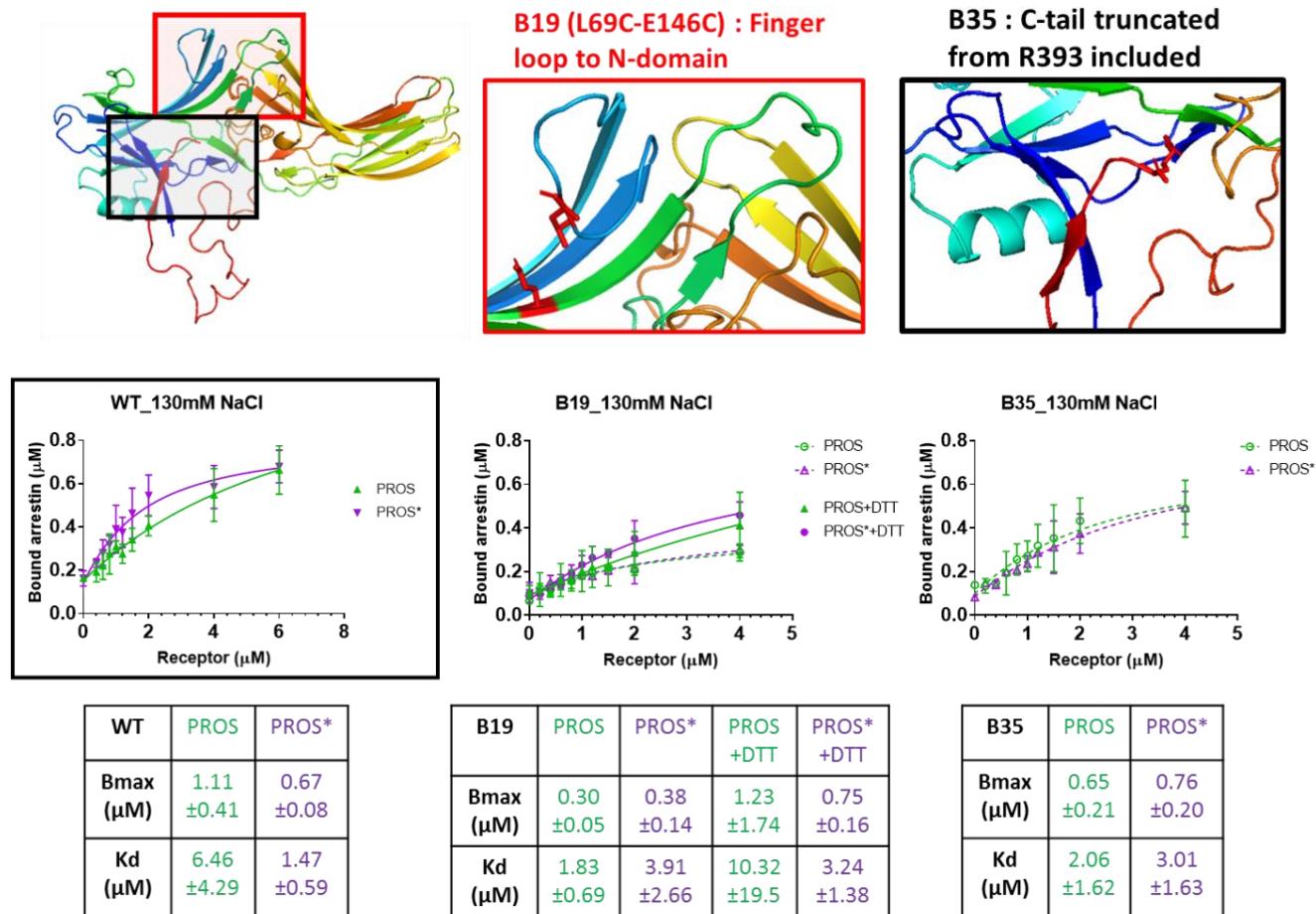


**Figure 46.** Rhodopsin titrations (batch #2) against 1  $\mu\text{M}$  of arrestin-3 mutants in 130 mM NaCl Pull-down reactions were carried out in a total volume of 40  $\mu\text{L}$ . Green curves: dark state phosphorylated rhodopsin. Purple curve: light activated phosphorylated rhodopsin. Dotted lines: absence of DTT. Plain lines: +1 mM DTT. On arrestin-3 structure PDB 3P2D are highlighted the native residues mutated to cysteines in respective mutants. Data were fitted by the stoichiometric saturation non-linear regression (see equation in 3.5.3. *Data analysis*).

## Discussion, chapter 3

In this chapter, the recruitment of arrestin 1/2/3 and constrained arrestin-3 mutants to rhodopsin was investigated by centrifugal pull-downs, as performed by *Kuhn et al., 1984*<sup>108</sup> and *Sommer et al., 2005*<sup>109</sup>. The objective of the study was to explore the different mechanisms involved in the recruitment of arrestins to four activated states of rhodopsin (dark-state ROS, light activated rhodopsin ROS\* and their phosphorylated counterparts PROS and PROS\*, respectively). In arrestin-3 mutants, constraints in the form of disulfide bridges were introduced to restrict movements of key structural features for the C-tail or the core interaction with GPCRs (see *D.3. The GPCR arrestin interface*). Guided by inactive arrestin-3 (PDB 3P2D) and pre-activated arrestin-1 (PDB 4J2Q) crystal structures, cysteine residues were optimally inserted for spontaneous crosslinking. In addition to functional pull-down assays, the structural integrity of arrestin-3 mutants was thoroughly characterized by mass spectrometry, circular dichroism and limited trypsinization. The arrestin-3 mutants used in pull-down assays were either i) restricting finger loop movements (an essential region from Y64 to L74 for the core interaction with GPCR, and located at the central crest of arrestin), ii) pre-activating arrestin-3 (mutant B17, K293C-V168C) or iii) were C-tail truncated (mutant B35, lacking 17 C-terminal amino acids). Among arrestin-3 mutants restricting finger loop movements: one mutant tethered the back of the finger loop to the C-loop in order to seal the upper central crest and impede the 20-21° intramolecular rotation necessary for arrestin activation (B33, F245C-F76C), one linked the middle of the finger loop to the gate loop (B16, L69C-K293C), one linked the middle of the finger loop on the N-domain (B19, L69C-E146C) or stitched the finger loop to the adjacent middle loop (B20, R66C-K139C).

### **Most purified proteins were structurally conserved and cysteine crosslinking was efficacious**

With the exception of mutant B14 and despite the constant double band profile observed in gels (figure 32), purified mutants of arrestin-3 appeared unequivocally pure by mass spectrometry (figure 34). Compared to WT arrestin-3, structural changes in mutants B33 and B35 were consistently observed across characterization experiments (limited trypsinization in figure 32, CD measurements in figure 33 and mass spectrometry in figure 36). For example, mutant B35 showed an unexpected C-tail truncation of 17 amino acids (identified by mass spectrometry, figure 36) that is very likely affecting the three-dimensional structure of the protein (higher sensitivity towards trypsinization in figure 32; modification of the  $\beta$ -sheet signature detected by CD measurements in figure 33). This observation strengthens the idea that other mutants that do not diverge from WT arrestin-3 in trypsin digests as well as in circular dichroism profile and with the expected mass by MS analysis, are more likely to adopt a similar conformation to WT arrestin-3. It is worth noting that limited trypsinization results differ from a similar

experiment published by *Mayer et al., 2019*<sup>81</sup>, where purified arrestin-3 appears as a single band compared to the double band detected in figure 32. In addition, arrestin-1 and arrestin-3 in *Mayer et al., 2019*<sup>81</sup> exhibit a similar trypsin sensitivity as opposed to the present study where arrestin-3 appeared more sensitive to trypsinization than arrestin-1.

Most importantly, mass spectrometry results confirmed the spontaneous ability of mutants to form disulfide bonds as previously shown by *Sommer et al., 2007*<sup>111</sup> where authors used the Ellman reagent (5,5'-dithiobis(2,2'-nitrobenzoic acid) to count the number of sulfhydryl groups per molecule of arrestin. Three arrestin-3 mutants (B25, B35 and B27) were more than 87% truncated from their C-terminus during *E. coli* expression, according to MS data (table 7). Interestingly, mutants B25, B35 and B27 share a cysteine located near the polar core or the three-element interaction which might indicate the cleaving site of (a) bacterial proteinase(s). Nevertheless, an ExPASy search did not lead to any particular enzyme. In addition, the introduction of cysteine residues in the periphery of the protein were generally better tolerated than in the core of arrestin: mutant B14 (R170C-D291C) and B18 (R170C-D27C) aimed to covalently reinforce the polar core but were not expressed in *E. coli*. For functional assays, arrestin-3 constrained mutants were let to incubate in oxidizing conditions overnight at 4°C before pull-down experiments, to ensure maximal crosslinking.

### **Arrestin-2 and arrestin-3 interact with phospholipids and PROS coupling is mainly C-tail driven**

As shown in figure 41 & 42, arrestin-1 is not recruited to non-phosphorylated states of the receptor ROS and ROS\* as previously reported by *Gurevich et al., 1995*<sup>14</sup>, whereas a significant amount of arrestin-2 and arrestin-3 appear to be recruited indiscriminately to ROS and ROS\* in low salt condition (blue and red curves in figure 41). The arrestin-2 and arrestin-3 interaction with ROS/ROS\* is abolished (for arrestin-3) or greatly diminished (for arrestin-2) in 130 mM NaCl (blue and red curves in figure 42). The 2-to-1 arrestin to rhodopsin stoichiometry in PROS\* titrations in low salt (purple curves in figure 42) suggest that arrestin-2 and -3 bind non-specifically to the phospholipids of the ROS membranes. Surprisingly, both salt and receptor titrations also show that arrestin-2 and arrestin-3 form complexes with phosphorylated rhodopsin of similar stability whether the receptor is kept in the dark (PROS, green curve, figure 41) or light activated (PROS\*, purple curve, figure 41). This observation was constant regardless of salts, membrane preparations or the fact that arrestin-2 and arrestin-3 were purified independently from one another. In addition, PROS binding seems more robust in NaCl titrations for arrestin-2 and arrestin-3 ( $E_{max}= 78\%$ ;  $IC_{50}= 128.1$  mM NaCl for arrestin-2 and  $E_{max}= 71\%$ ;  $IC_{50}= 149.2$  mM NaCl for arrestin-3) compared to arrestin-1 ( $E_{max}= 35\%$ ;  $IC_{50}= 47$  mM NaCl). Additionally, arrestin-2 and arrestin-3 are known to adopt their fully active conformation more spontaneously than arrestin-1 according to *Gurevich et al., 1995*<sup>14</sup> and *Kim et al., 2013*<sup>17</sup>. In the present

study, a similar observation was made by mass spectrometry on mutant B17, a mutant only able to form a disulfide bridge in its activated state, yet 79% of it was found in a constrained state in solution after two hours in oxidizing conditions.

A possible explanation for the differences in recruitment detected between arrestin-1 and arrestin-2/3 could be that first, phosphorylated rhodopsin creates negative charges around the membranes, thus pre-concentrating arrestins near the receptor via the low affinity C-tail interaction and the membrane anchor. At this stage, arrestin-1 could form the so-called pre-complex with rhodopsin (PROS/arrestin-1 complex) as suggested by *Kim et al., 2013*<sup>17</sup> among others. In the case of arrestin-2 and arrestin-3, it is possible that most proteins arrive at the membrane fully activated from spontaneous activation<sup>14,17</sup> (as shown with mutant B17 that maintains an activated state by extension of the gate loop on the N-domain). Either i) the contribution of the C-tail interaction and membrane anchor is greater in arrestin-2 and -3 compared to arrestin-1, or ii) arrestin-2 and arrestin-3 may engage also the cytosolic components of dark-state phosphorhodopsin (PROS), in addition to the phosphorylated C-tail exchange and the membrane interactions. Prior to light activation, most of arrestin-2 and arrestin-3 are already bound to the receptor in this medium-affinity state and the complex only gains a minor increase in stability upon light activation (green and purple curves, figure 41). Finally, the higher stability of the arrestin-1/PROS\* complex over the arrestin-2/PROS\* and arrestin-3/PROS\* complexes might simply be explained by the fact that arrestin-2 and arrestin-3 are not the physiological interacting partners of rhodopsin (tables in figure 41). Finally, the higher affinity of arrestin-3 for non-stimulated GPCRs and/or the phospholipids of physiological membranes might be linked to the classification of *Oakley et al., 2000*<sup>16</sup> (see *D.3. The GPCR-arrestin interface*) wherein arrestin-3 is the most promiscuous member of the arrestin family (compared to arrestin-1 and arrestin-2) towards class A and class B GPCRs.

### **Different phosphorylation states affect arrestin-3 recruitment and limitations of the MS analysis**

Arrestins are differently recruited to the two PROS membrane preparations (figure 42.B and 42.C). Using PROS batch #2 led to a higher arrestin recruitment of arrestin-1, arrestin-2 and arrestin-3 to PROS\* in low salt and in 130 mM (figure 42.C). Nevertheless, the higher sensitivity to salt detected in arrestin-2 and arrestin-3 recruitment with the PROS batch #2 compared to the batch #1 indicates that batch #2 is less phosphorylated than batch #1. The phosphorylation level of rhodopsin was assessed by LC-MS analysis of the AspN truncated C-terminus of the receptor, as described by *Lee et al., 2002*<sup>115</sup>. The LC-MS analysis revealed that batch #2 was 16% less phosphorylated than batch #1 (figure 37, table 8). If so, the incomplete recruitment of arrestin-1 with PROS membrane batch #1 in spite of the higher phosphorylation level suggests that rhodopsin experienced a retinal release and decayed back to opsin or that the receptor was partially denatured during extraction. Analysis by SDS-PAGE of digested

fractions of PROS membranes shows that the two receptors have different sensitivity towards AspN digestion and therefore might have a distinct conformation in membranes (figure 38).

Previous studies showed by gel filtration of rhodopsin/arrestin complexes<sup>121</sup> and electrophysiological measurements in mice expressing distinct phosphorylation states of rhodopsin<sup>122</sup>, that three phosphate groups are required for full arrestin recruitment and termination of rhodopsin signaling. According to *Vishnivetskiy et al., 2007*<sup>121</sup>, the presence of two phosphate groups per molecule moderately improves arrestin binding compared to receptors containing only one phosphate group, in which case almost no arrestin binding was detected. In addition, *Mendez et al., 2000*<sup>122</sup> showed in *in vivo* assays performed on transgenic mice, a sustained activation of mono- or di-phosphate rhodopsin compared to tri-phosphate rhodopsin, again indicating poor arrestin recruitment with less than three phosphate groups. Finally, crystal structures of arrestin binding with phosphopeptides<sup>31,82</sup> and the phosphorylation motif proposed by *Mayer et al., 2019*<sup>81</sup> (one phosphate group being required for proper placement of the distal C-terminus of rhodopsin onto arrestin and two additional phosphate groups for direct interaction with the arrestin N-domain) support this theory. In this thesis, the mass spectrometry data presented in section 3.8. *Phosphorylation sites of PROS membrane preparations* revealed that a significant amount of rhodopsin was not phosphorylated in PROS batches #1 and #2, and most importantly that receptors contained in average 1.17 and 1.01 phosphate groups respectively. However, pull-down results showed that receptors from both PROS membrane preparations were successfully able couple with arrestin. Taken together, it appears that rhodopsin in PROS membrane preparations were in fact phosphorylated enough to bind arrestin, despite the discrepancy of mass spectrometry results with *Mendez et al., 2000*<sup>122</sup> and *Vishnivetskiy et al., 2007*<sup>121</sup>. The most probable explanation is that the quantification of phosphorylated species of rhodopsin by mass spectrometry did not reflect the reality in PROS samples, perhaps due to a different ionization efficiency of each phosphorylated species.

### **Arrestin-3 di-cysteine mutants confirm finger loop residues involved in core-interaction**

The arrestin-3 mutants B33, B19 and B16 all tether the finger loop (sequence from Y64 to L74, involved in the core interaction): either from the back (F76C in B33), from the middle (L69C in B16 and B19) or from the proximal part (R66C in B20) of the finger loop (figures 44 and 45). Cysteine mutation R66C in mutant B20 is at least four amino acids away from residues directly interacting with the rhodopsin activated core: D70, L72, G73 and L74 (figure 7). Other mutations are only one amino acid away (L66C in B16 and B19) or directly on residues involved in core recognition (F245C on the C-loop for B33). In B33, the impairment is either caused by mutation F245C on the C-loop (directly interacting with ICL2) or obstruction of the central crest. In other words, PROS\* coupling with mutants preventing finger loop movements is only observed if mutations interfere with loop extension, seal the central crest or interfere directly with or in close proximity of residues engaged with an activated core.

As for PROS binding, it appears that only the complex formed with B33 is impaired in the constrained state which entails that full rotation of the N- and C-domains might either influence the C-tail release through allosteric coupling or that the rotation plays a role in dark state phosphorhodopsin binding independently from the C-tail. Surprisingly, pre-activated mutant B17 is not recruited to PROS\* in its constrained state (which should have been enhanced, in this case) but only after disruption of the disulfide bridge, indicating that the introduced constrain did not enable the intended conformation. Contrary to *Potter et al., 2002*<sup>39</sup>, C-tail truncated mutant B35 did not lead to an increased PROS or PROS\* stabilization compared to WT arrestin-3.



## CONCLUSION

It was long thought that the recruitment to GPCRs of all four arrestins operate in a similar manner due to their high structural and sequence similarity. However, recent studies suggested significant mechanistic and functional differences between the different arrestins. In particular, the molecular processes behind arrestin-2/3/4 recruitment and activation by GPCRs are not as well understood as for the arrestin-1. In this thesis, I aimed at filling this gap in knowledge and employed several experimental strategies to highlight the potential similarities and/or differences in the molecular mechanisms underlying the recruitment and activation of human arrestin-3 to several GPCRs.

### **Mapping the human arrestin-3 sequence for residues involved in the recruitment to the $\beta$ 2AR**

A large-scale recruitment screen of a library of 383 arrestin-3 single point alanine mutants to the  $\beta$ 2-adrenergic receptor was performed. Technical challenges using a novel split nanoluc arrestin-GPCR recruitment assay hampered the interpretation of the data from this screen. However, despite this caveat, several pivotal residues for receptor recruitment in arrestin-3 were identified, which seem to be conserved in both arrestin-1<sup>29</sup> and arrestin-3. The residues identified lie in the polar core of arrestin-3/arrestin-1 (D291A/D296A, D298A/D303, D28A/D30A) and in the three element interaction (I386A/F375A and L101A/L103A). The exchange of these residues with alanines led to an increase in the recruitment capability of the arrestins to their cognate GPCR (arrestin-3/  $\beta$ 2AR and arrestin-1/rhodopsin).

### **Engineering of arrestin-3 mutants that are strongly recruited to the $\beta$ 2AR and to variants of the $\beta$ 1-adrenergic receptor**

This thesis has been supported by the CTI project (#18540.1 IP-LPS) to help identify arrestin-3 proteins that could potentially be utilized for drug discovery purposes. Hence, arrestin-3 mutants with enhanced recruitment capabilities to a given GPCR were engineered and a subset of these arrestin-3 mutants have been submitted as the European patent application (EP19153159: “ $\beta$ -arrestin mutants”). Double and triple alanine mutants of arrestin-3 were generated with a focus on simultaneously disrupting the pivotal polar core and the three element interaction sites of arrestin-3. The recruitment capability of these arrestin-3 combined mutants was assessed against the  $\beta$ 2AR and variants of the  $\beta$ 1-adrenergic receptor. Both a double mutant A (I386A+T299A) and triple mutant B (I386A+T299A+R166A) of arrestin-3 were identified to display a significantly higher recruitment profile to the respective GPCRs than wild-type arrestin-3. Hence, these double and triple arrestin-3 mutants could represent novel tools i) for the stabilization of GPCRs in e.g. structural studies or ii) in drug discovery assays, in which an enhanced recruitment capability of such arrestins could improve drug screening efforts by, for instance, enhancing the assay window.

## **Recruitment of arrestin 1/2/3 and arrestin-3 constrained mutants to various activated states of rhodopsin in vitro**

The objective of the study was to explore the different mechanisms involved in the recruitment of arrestins to four activated states of rhodopsin (dark-state, light activated rhodopsin and their phosphorylated counterparts). The recruitment of arrestin-2 and arrestin-3 to phosphorylated and light activated rhodopsin (PROS\*) was found to be mainly driven by the C-tail interaction, compared to WT arrestin-1. In addition, significant non-specific membrane interactions to the rod outer segment membranes were detected in low salt condition for arrestin-2 and arrestin-3 compared to arrestin-1. In the second part of this study, disulfide bridges were introduced in arrestin-3 to restrict movement of key structural features for the C-tail or the core interaction with GPCRs. Guided by inactive arrestin-3 (PDB 3P2D) and pre-activated arrestin-1 (PDB 4J2Q) crystal structures, cysteine residues were optimally inserted for spontaneous crosslinking. In addition to functional pull-down assays, the structural integrity of arrestin-3 mutants was thoroughly characterized by mass spectrometry, circular dichroism and limited trypsin digestion. The main finding was that different levels of finger loop constrictions induced various degrees of arrestin-3 binding impairment to PROS\*. However, the most dramatic reduction in arrestin-3 recruitment to PROS\* was detected upon restriction of the 20-21° rotation (necessary for full arrestin activation and recognition of the rhodopsin core) induced by inter-domain crosslinking between the finger loop and the C-loop.

### **Perspectives**

In this thesis, I started to highlight similarities and differences in the recruitment mechanisms of arrestin-1, arrestin-2 and arrestin-3 to several members of class A GPCRs (rhodopsin,  $\beta$ 2AR,  $\beta$ 1AR). In particular, the studies described in chapter 3 of this thesis suggest profound recruitment differences between arrestin-2/3 and arrestin-1 to an activated GPCR, i.e. the phosphorylated and light activated rhodopsin. Future studies using experimental tools such as i) peptides mimicking the phosphorylated C-terminus of rhodopsin, ii) peptides mimicking heteromeric G proteins and iii) the characterization of additional constrained arrestin-3 mutants will continue to deepen our understanding of the intricacies of arrestin-3 recruitment to GPCRs.

## APPENDIX

- Plasmid #589 (AG10-B2AR-DS2-bArr2-EGFP<sub>95</sub>): human WT arrestin3-(GS)<sub>5</sub>-EGFP and human β2AR.

3' ATGGGGGAGAAACCCGGGACCAGGGTCTTCAAGAAGTCGAGCCCTAACTGCAAGCTCACCGTGTACTTGGGCAAGCGGG  
ACTTCGTAGATCACCTGGACAAAGTGGACCCTGTAGATGGCGTGGTGTCTGTGGACCCTGACTACCTGAAGGACCGCAAAGT  
GTTTGTGACCCTCACCTGCGCCTTCCGCTATGGCCGTGAAGACCTGGATGTGCTGGGCTTGTCTTCCGCAAAGACCTGTCA  
TCGCCACCTACCAGGCCTTCCCCCGGTGCCAACCACCCCGGCCCCACCCGCTGCAGGACCGGCTGTGAGGAAGCT  
GGGCCAGCATGCCCAACCCTTCTTCTTACCATAACCCAGAATCTTCCATGCTCCGTCACACTGCAGCCAGGCCAGAGGATA  
CAGGAAAGGCCTGCGCGTAGACTTTGAGACTTCGAGCCTTCTGTCTAAATCACTAGAAGAGAAAAGCCACAAAAGGAAT  
CTGTGCGGCTGGTGTACCGAAAAGTGCAGTTGCCCCGGGAGAAAAGCGGGTCTCGCCCTGGATGGGAACTCAAGCACGAGGACACCA  
CCTCATGTCTGACCGTCCCTGCACCTCGAGGCTTCCCTGGACAAGGAGCTGTACTACCATGGGGAGCCCTCAATGTAAT  
GTCCACGTACCAACAACCTCCACCAAGACCGTCAAGAAGATCAAAGTCTCTGTGAGACAGTACGCCGACATCTGCCTTCA  
GCACCGCCAGTACAAGTGTCTGTGGCTCAACTCGAACAAGATGACCAGGTATCTCCAGCTCCACATTCTGTAAGGTGTA  
CACCATAACCCCACTGCTCAGCGACAACCCGGGAGAAGCGGGTCTCGCCCTGGATGGGAACTCAAGCACGAGGACACCAA  
CCTGGCTTCCAGCACCATCGTGAAGGAGGGTGCCAACAAGGAGGTGCTGGGAATCCTGGTGTCTACAGGGTCAAGGTGAA  
GCTGGTGGTGTCTCGAGGCGGGGATGTCTCTGTGGAGCTGCCTTTTGTCTTATGCACCCCAAGCCCCACGCCACATCCCC  
TCCCCAGACCCAGTACCGCTCCGGAGACAGATGTCCCTGTGGACCAACCTCATTGAATTTGATACCAACTATGCCAC  
AGATGATGACATTGTGTTGAGGACTTTGCCCGGCTTCGGCTGAACGGGGATGAAGGATGACGACTATGATGATCACTCTGC  
GGTTCAGGTTCTGGTAGTGGATCCGGTAGTATGGTGTGCAAGGGCGAGGAGCTGTTACCGGGGTGGTGGCCATCTGGTGC  
AGCTGGACCGCGACGTAAACCGGCCAAAGTTACGCGTGTCCGGCGAGGGCGAGGGCGATGCCACCTACGGCAAGCTGACC  
TGAAGTTCATCTGCACCACCGGCAAGCTGCCCGTGCCTTGGCCACCCTCGTGACCACCCTGACCTACGGCGTGCAGTGCTC  
AGCCCTACCCCGACATGAAGCAGCAGACTTCTTCAAGTCCGCGATGCCGAAGGCTACGTCAAGGACCGGACACCAT  
TCTTCAAGGACGACGGCAACTACAAGACCCGCGCCGAGGTGAAGTTCGAGGGCGACACCCTGGTGAACCGCATCGAGTGA  
AGGGCATCGACTTCAAGGAGGACGGCAACATCCTGGGGCACAAGCTGGAGTACAACAGCCACAACGTCTATATCA  
TGGCCGACAAGCAGAAGAACGGCATCAAGGTGAAGTTCAGTCCGCCACAACATCGAGGACGGCAGCGTGCAGCTCGCCG  
ACCCTACCAGCAGAACACCCCATCGGGCAGCGCCCGTGTCTGCTGCCGACAACCACTACCTGAGCACCACGTCCGCCCT  
GAGCAAAGACCCCAACGAGAAGCGCGATCACATGGTCTGCTGGAGTTCGTGACCAGCCCGGGATCACTCTCGCATGGA  
CGAGCTGTACAAGTGA-5'

3' ATGGGGCAACCCGGGAACGGCAGCGCCTTCTGTGGACCCAATAGAAGCCATGCGCCGGACCACGACGTCACGCAGCA  
AAGGGACGAGGTGTGGTGGTGGGCATGGGCATCGTCTCATGCTCCTCATCGTCTGGCCATCGTGTGGCAATGTGCTGGTC  
ATCACAGCCATTGCCAAGTTCGAGCGTCTGCAGACGGTCAACCAACTTTCATCACTTCACTGGCCTGTGCTGATCTGGTCA  
GGGCTGGCAGTGGTGGCCTTTGGGGCCGCCATATTCTTATGAAAATGTGGACTTTGGCAACTTCTGGTGGAGTTTTGGA  
CTTCCATTGATGTGCTGTGCGTACGGCCAGCATTGAGACCTGTGCGTGATCGCAGTGGATCGCTACTTTGCCATTACTTCA  
CCTTTCAAGTACCAGAGCCTGTGACCAAGAATAAGGCCCGGGTGTATCATTCTGATGGTGTGGATTGTGTCAGGCCTTACCTC  
CTTCTTGGCCATTAGATGCAGTGGTACCGGGCCACCACAGGAAGCCATCAACTGCTATGCCAATGAGACCTGTGTGACT  
TCTTACGAACCAAGCCTATGCCATTGGCTTCTTCCATCGTGTCTTCTACGTTCCCTGGTGTATCATGGTCTTCTGCTACTCCA  
GGGTCTTTCAGGAGGCCAAAAGGCAGCTCCAGAAGATTGACAAATCTGAGGGCCGCTTCCATGTCCAGAACCTTAGCCAGGT  
GGAGCAGGATGGGCGGACGGGGCATGGACTCCGCAGATCTTCAAGTTCGCTTGAAGGAGCACAAGCCCTCAAGACGTT  
AGGCATCATGGGCACTTTCACCCTGTGCTGGCTGCCCTTTCATCGTTAACATTGTGCATGTGATGCCAGGATAACCTCAT  
CCGTAAGGAAGTTTACATCCTCCTAAATTGGATAGGCTATGTCAATTCTGGTTTCAATCCCTTATCTACTGCCGGAGCCAG  
ATTCAGGATTGCCTTCCAGGAGCTTCTGTGCCTGCGAGGTCTTCTTGAAGGCCTATGGGAATGGCTACTCCAGCAACGGC  
AACACAGGGGAGCAGAGTGGATATCAGTGGAAACAGGAGAAAGAAAATAAACTGCTGTGTGAAGACCTCCAGGCACGGA  
AGACTTTGTGGCCATCAAGGACTGTGCTAGCGATAACATTGATTACAAGGGAGGAATTGTAGTACAATGACTCACTG  
CTGTAATGA-5'

- Plasmid #444 (pcDNA3): EGFP-(KLTDI)-human WT arrestin3.

3' (EGFP sequence identical to #589)-TACAAGAAGCTTACCGATATCGGG-(arrestin-3 sequence identical to #589)-5'

- Plasmid #448 (pcDNA3): human β2AR-(GGSG)-Renilla luciferase 8.

3' (human β2AR sequence identical to #589) ACTCTGTGGATCCGGCATGGCTTCCAAGGTGTACGACCCCGAGC  
AACGCAAACGCATGATCACTGGCCTCAGTGGTGGGCTCGTGTGCAAGCAAATGAACGTGCTGGACTCCTTCACTCAACTACTA  
TGATTCCGAGAAGCACGCCGAGAACGCCGTGATTTTCTGATGGTAAACGCTACCTCCAGTACCTGTGGAGGCACGTCGTG  
CCTCACATCGAGCCCGTGGCTAGATGCATCATCCCTGATCTGATCGGAATGGGTAAGTCCGGCAAGAGCGGGAATGGTCTAT  
ATCGCCTCCTGGATCACTACAAGTACCTACCGCTTGGTTCGAGCTGTGAACCTTCCAAAGAAAATCATCTTTGTGGGCCAC  
GACTGGGGGGTGTCTTGGCCTTTCACTACGCCTACGAGCACAAGACAGGATCAAGGCCATCGTCCATATGGAGAGTGTG  
TGGACGTGATCGAGTCCGGACGAGTGGCCTGACATCGAGGAGGATATCGCCCTGATCAAGAGCGAAGAGGGCGAGAAAA  
TGGTGTGAGAAATAA-5'

- Plasmid #523 (pcDNA3): Receptor B6-(GGSG)-Renilla luciferase 8.

3' ATGGAGCTGTGTCGCGAGCAGTGGGAGGCGGGCATGAGCCTGTGATGGCCCTGGTGGTGTGCTCATCGTGGCCGGCAA  
CGTGTGGTGTATCGCGCCATCGGGCGCAGCAGCGGCTGCAGACGCTCAACACTTTCATCACTCGTGGCCTGCGCC  
GACCTGGTGTATGGGGTCTGGTGGTGCCTTCGGGGCCACGCTGGTGGTGGGGGCACTGGTGTGGGGCTCCTTCTCTG  
CGAGCTCTGGACATCGCTGGACGTGCTTTGCGTGACGGCAAGCATCGAGACCTTGTGCGTATCGCCATCGACCGCTACCTG

GCCATCACCTCTCCATTCCGCTACCAGAGCCTGATGACCAGGGCTCGGGCCAAGGTCATCATCTGCACCGTCTGGGCCATCTC  
 CGCTCTGGTCTCTTTCTGCCCATCATGATGCACTGGTGGCGGGACGAGGACCCTCAGGCGCTCAAGTGCTACCAGGACCCG  
 GGCTGCTGCGACTTTGTACCAACCGGGCTTACGCCATCGCCTCGTCCATCATCTCCTTCTACATCCCCCTCCTCATCATGAT  
 TTCGTGTACCTGCGGGTGTACCGGGAGGCCAAGGAGCAGATCAGGAAGATCGACCGCTGCGAGGGCCGGTTCTATGGCAGC  
 CAGGAGCAGCCGACGCCACCCCGCTCCCCAACACCAGCCATCTCGGCAACGGCCGTGCCAAGAGGAAGACGTCC  
 CGTGTATGGCCATGAGGGAAACAAAAGCTCTGAAGACATTGGGTATCATCATGCGGGGTGTTACCCCTCTGCTGGCTCCCTT  
 CTTCTGGTGAACATTGTCAACGTCTTCAACAGAGATCTGGTGGCGGACTGGCTCTTCGTTTTCTCAACTGGTTGGGCTACGC  
 CAACTCTGCTTTCAACCCCATCATCTACTGCCGACGCCAGACTTCCGTAAGGCCTTCAAGAGGCTGCTGCTTCCCCCGCA  
 AAGGTGACAGGCGGTGCACGCCGGCGGCCAACCCGCCCGCTGCCGGGGGCTTATCAGCACCCCTGGGCTCCCCTGAGCA  
 CAGCCCAGGGGGACGTGGTCCGACTGCAATGGGGGCACGCGGGGCGGCAGTGAGTCCAGCCTGGAGGAGACATAGCA  
 AAACATCCCGCTCGGAGTCCAAGATGCACCATCACCATCACCATGTGGATCCGGC-(renilla luciferase 8 sequence identical to  
 #448)-5'

- Plasmid #524 (pcDNA3): Receptor B44-(GSG)-Renilla luciferase 8.

3' ATGGGGGCCGAGCTGCTGTCGACGAGTGGGAGGCGGGCATGAGCCTGCTGATGGCCCTGGTGGTGTGCTCATCGTGGC  
 CGGCAACGTGTGGTGTGTCGCGCCATCGGGCGCACGACGGCTGCAGACGCTCACCACCTTTCATCACCTCGCTGGCC  
 TGCGCGACCTGGTGTGGGGCTGCTGGTGGTGCCTTTCCGGGCCACGCTGGTGGTGGCGGGGACCTGGCTGTGGGGCTCCT  
 TCCTTGCAGCTCTGGACATCGTGGACGTGCTTTGCGTGACGGCAAGCATCGAGACCTTGTGCGTATCGCCATCGACCGC  
 TACCTGGCCATCACCTCTCCATTCCGCTACCAGAGCCTGATGACCAGGGCTCGGGCCAAGGTATCATCTGCACCGTCTGGGC  
 CATCTCCGCTCTGGTCTCTTCTGCCATCATGATGCACTGGTGGCGGGACGAGGACCCTCAGGCGCTCAAGTGCTACCAGG  
 ACCCGGGTGTGCGACTTTGTACCAACCGGGCTTACGCCATCGCCTCGTCCATCATCTCCTTCTACATCCCCCTCCTCATCA  
 TGATTTCTGTACCTGCGGGTGTACCGGGAGGCCAAGGAGCAGATCAGGAAGATCGACCGCGCCAGCAAGAGGAAGACGT  
 CCCGTGTATGGCCATGAGGGAAACAAAAGCTCTGAAGACATTGGGTATCATCATGCGGGGTGTTACCCCTCTGCTGGCTCCC  
 TTTCTTCTGGTGAACATTGTCAACGTCTTCAACAGAGATCTGGTGGCGGACTGGCTCTTCGTTTTCTCAACTGGTTGGGCTA  
 CGCAAATCTGCTTTCAACCCCATCATCTACTGCCGACGCCAGACTTCCGTAAGGCCTTCAAGAGGCTGCTGCCTTCCCC  
 GCAAAGCTGACAGGCGGTGTGGATCCGGC-(renilla luciferase 8 sequence identical to #448)-5'

- Plasmid #601 (pET15b): (His)<sub>6</sub>-TEVsite-(GSG)-human arrestin-3 (optimized for E. coli expression).

3' ATGGGCAGCAGCCATCATCATCATCACGAAAACCTGTACTTCCAGGGTGGATCCGGTAAAAAGCCTGGCACC CGCT  
 TTTAAAGAAAGAGTAGCCCGAACTGCAAACTGACAGTGTATCTGGGCAAAACGCGACTTCGTGGACCATCTGGACAAGGTTGAT  
 CCTGTGGATGGCGTGGTGTGGTGGATCCGATTATCTGAAAGACCGCAAGGTGTTGTGACCCTGACCTGTGCCTTCCGTTA  
 TGGCCGTGAAGACCTGGATGTTCTGGGCTGAGCTTCCGTAAGATCTGTTATCGCCACCTACCAGGCCTTCCCGCCTGTT  
 CTAATCCCCCTCGCCGCTACACGTCTGCAGGATCGCCTGCTGCGCAAACTGGGCCAGCATGCACATCCGTTCTTCTTACC  
 ATCCCGCAAAACCTGCCGTGACGCTGACCTTACAGCCGGGCCCTGAGGATACCGCAAGGCATGCGGTGTGGATTTCGAAA  
 TTCGTGCCTTCTGCGCAAGAGTCTGGAGGAGAAAAGTCAACAAGCGCAACAGCGTGCCTGGTGTATCCGCAAAAGTCAATT  
 TGCCCTGAAAAGCCGGTCCGCAACCGAGCGCCGAAACCACACGCCATTTCTGATGAGTGACCGCAGCCTGCATCTGGAA  
 GCCAGCTGGACAAAGAGCTGTACTATCACGGCGAACCGCTGAATGTGAACGTTTATGTGACCAACAATAGCACAAAGACC  
 GTTAAGAAAATTAAGGTGAGTGTGCGCCAGTACGACAGATCTGTCTGTTAGTACCGCCAGTACAAAATGCCCTGTGGCAC  
 AGCTGGAACAGGATGATCAGGTGAGCCGAGTAGCACCTTTTGAAGGTGATACCATTACCCGCTGCTGAGTGACAATCG  
 CGAAAACGTTGGTCTGGCCCTGGATGGCAAGCTGAAACATGAGGACACCAACCTGGCAAGCAGCACCATCGTTAAAGAAGG  
 TGCAAAACAAAGAGGTGCTGGGTATCCTGGTGTGACTACCGGTTAAAGTGAAGCTGGTTGTTAGCCGCGGTGGCGATGTGAGC  
 GTGAACTGCCGTTTGTGCTGATGCACCCGAAGCCGATGACCATATTCCTTGCCTCGTCCGACAGCGCAGCACCTGAAA  
 CAGATGTCCGGTGGATACCAACCTGATTGAATTCGATACCAACTACGCAACCGACGACGACATCGTGTTCGAAGACTTTC  
 CGCTTACGCTGAAAGGCATGAAAGACGACGACTATGACGACCAGCTGTGTTAA-5'

**Appendix 1.** DNA sequences of plasmid #589 (human WT arrestin3-EGFP + human  $\beta$ 2AR.), #444 (EGFP-human WT arrestin3.), #448 (human  $\beta$ 2AR-Renilla luciferase 8), #523 (Receptor B6-Renilla luciferase 8), #524 (Receptor B44-Renilla luciferase 8), #601 (His-human arrestin-3).

<b>Basic settings</b>	
Measurement type:	Fluorescence (FI)
Microplate name:	GREINER 96 F-BOTTOM
<b>Endpoint settings</b>	
No. of flashes per well:	20
Scan mode:	spiral scan
Scan diameter [mm]:	6
<b>Optic settings</b>	
Optic module:	FI 485 520
Excitation:	485
Emission:	520
Gain:	300
Focal height [mm]:	4.1
<b>General settings</b>	
Top optic used	
Aperture spoon:	-
Reading direction:	bidirectional, horizontal left to right, top to bottom
Target temperature [°C]:	37

**Appendix 2.** Microplate reader settings for GFP measurements.

<b>Basic settings</b>				
Measurement type:	Luminescence			
Microplate name:	PE OptiPlate 96			
<b>Plate mode settings</b>				
No. of cycles:	169			
Cycle time [s]:	13			
Measurement interval time:	0.06			
<b>Optic settings</b>				
Optic module:	LUM plus			
Emission:	-			
Gain:	3600			
Focal height [mm]:	6			
Glow correction factor [%]:	0			
<b>Shaking settings</b>				
Shaking width [mm]:	4			
Shaking mode:	double orbital			
Additional shaking time:	1s after injection cycle(s)			
<b>Injection settings</b>				
Volume group	1	2	3	4
Volume of pump [μl]:	16	20	-	-
Used pump:	1	2	-	-
Pump speed [μl/s]:	150	150	-	-
Injection cycle:	5	56	-	-
<b>General settings</b>				
Top optic used				
To allow comparison of measurements with different measurement interval times values are normalized to 0.02 sec.				
Aperture spoon:	-			
Reading direction:	bidirectional, horizontal left to right, top to bottom			
Target temperature [°C]:	37			

**Appendix 3.** Microplate reader settings for the split nanluc assay.

### Cysless bovine arrestin-1 (yellow: native cysteines were mutated to alanine)

MKANKPAPNHVIFKKISRDKSVTIYLGKRDYIDHVERVEFVDGVVLDVPELVKGRVYVSLTCAFYRGQEDIDVM  
GLSFRRDLYFSQVQVFPVPGASGATTRLQESLIKKLGANTYFLLTFPDYLP<sup>C</sup>SVMLQPAPQDVGKSC<sup>C</sup>GVDFEIK  
AFATHSTDVEEDKIPKSSVRLLRKVKQHAPRDMGFPQRAEASWQFFMSDKPLRLAVLSLSKEIYYHGEPPIVTV  
VTNSTEKTVKKIKVLVEQVTNVVLYSSDYIKTVAAEEAQEKVPPNSLTKTLTLVPLLANNRERRGIALDGKIK  
HEDTNLASSTIIKEGIDKTVMGILVSYQIKVKLTVSGLLGELTSSEVATEVPFRLMHPQPEDPDTAKESFQDENF  
VFEEFARQNLKDAGEYKEEKTDQEAMDE

### Human arrestin-2

MGDKGTRVFKKASPNGKLTVYLGKRDVVDHIDLVDVDPVGVVLDVPEYLKERRVYVTLTCAFYRGREDLDVGLTF  
RKDLFVANVQSFPPAPEDKKPLTRLQERLIKKLGEHAYPFTFEIPPNLPCSVTLQPGPEDTGKACGVYEVKAF  
AENLEEKIHKRNSVRLVIRKVVQYAPERPGPQPTAETTRQFLMSDKPLHLEASLDKEIYYHGEPISVNVHVTNNTN  
KTVKKIKISVRQYADICLFNTAQYKCPVAMEEADDTVAPSSTFCVKYVTLTPFLANNREKRGLALDGKLGKHD  
ASSTLLREGANREILGIIVSYKVKVLLVSRGGLLDLASSDVAVELPFTLMHPKPKEEPHREVPENETPVD  
LIELDTNDDDIVFEDFARQLKGMKDDKEEEEDGTGSPQLNNR

### Human arrestin-3 (green: His(6)-tag; blue: residual TEV protease cleaving site, otherwise replaced by a methionine in nature)

MGSSHHHHHHENLYFQGGSGGKPKGTRVFKKSSPNCKLTVYLGKRDVVDHLDKVDVDPVGVVLDVDPDYLKDRKVFV  
TLTCAFYRGREDLDVGLSFRKDLFIATYQAFPPVNPPrPTRLQDRLLRKLQHAHPFFFTIPQNLPCSVTLQ  
PGPEDTGKACGVDFEIRAFCAKSLEEKSHKRNVRVIRKVVQFAPEKPGPQSAETTRHFMSDRSLHLEASLDK  
ELYHGEPLNVNVHVTNNTKTKVKKIKVSVRQYADICLFSTAQYKCPVAQLEQDDQVSPSSTFCVKYVTLTP  
NREKRGLALDGKLGKHDNLASSTIVKEGANKEVLGILVSYRVKVKLVSRGGDVSVELPFVLMHPKPHDHIPLP  
RPQSAAPETDVPVDTNLIIEFDNYATDDDIVFEDFARLRLKGMKDDDYDDQLC

### Human $\beta$ 2-adrenergic receptor

MGQPGNGSAFLLAPNGSHAPDHVDTQERDEVVVGMGIVMSLIVLAIIVFGNVLVIATAIKFERLQTVTNYFITSL  
ACADLVMLAVVPPFGAAHILMKMWTFGNFWCFWTSIDVLCVTASIE TLCVIAVDRIYFAITSPFKYQSLLTKNKA  
RVIIILMVIVSGLTSFLPIQMHWYRATHQEA INCYANETCCDFFTNQAYAIASSIVSFYVPLVIMVFVYSRVFQE  
AKRQLQKIDKSEGRFHVQNLQVEQDGRGTGHGLRRSSKFLCKEKKALKTLGIIMGTFTLCWLPFFIVNIVHVIQN  
LIRKEVYILLNWIGYVNSGFNPLIYCRSPDFRIAFQELLCRRSSLKAYNGYSSNGTGEQSGYHVEQEKENKL  
LCEDLPGTEDFVGHQGTVPDNDIDSQGRNCSTNDSLL

### Turkey $\beta$ 1-adrenergic receptor (blue: mutation C116L, N-terminal and C-terminal truncations found in receptor B6; green: additional mutation C358A, intracellular loop 3 and C-terminal truncations found in receptor B44)

MGDGWLPDPCGPHNRSGGGGATAAPTGSRQVSAELLSQWEAGMSLLMALVLLVAGNVLVIAAIGRTQRLQTL  
TNLFITSLACADLVMLLVVPPFGATLVVVRGTWLVGSLFCE<sup>C</sup>WTSLDVLCVTASIE TLCVIAIDRYLAITSPFRYQ  
SLMTRARAKVICTVWAI SALVSFLPIMMHWRDEDPQALKCYQDPGCCDFVTNRAYAIASSIISFYIPLLIMIF  
VYLRVYREAKEQIRKIDR<sup>C</sup>EGRFYGSQEQPPPLPOHQPILNGR<sup>A</sup>ASKRKT SRVMAMREHKALKTLGIIMGVFT  
LCWLPFFLVNIVNVFNRLVDPDLVFFVFNWLGANSANFPIIYCRSPDFRKA<sup>F</sup>KRL<sup>C</sup>FPKADRRLLH<sup>A</sup>GGQ<sup>P</sup>AP  
LPGGFISTLGSPEHSPGCTWSDCNGGTRGGSESSLEERH<sup>S</sup>SKTSRSE<sup>S</sup>KMEREK<sup>N</sup>ILAT<sup>T</sup>RFYCT<sup>F</sup>FLNG<sup>D</sup>KAV<sup>F</sup>C  
TVLRIVKLFEDATCTCPH<sup>T</sup>HK<sup>L</sup>KMK<sup>W</sup>RFK<sup>H</sup>Q<sup>H</sup>A

### Bovine rhodopsin

MNGTEGPNFYVFPFNSNKTGVVRSFPEAPQYYLAEWPQFSMLAAYMFLIMLGFPINFLTLYVTVQHKKLRTPNLN  
LLNLAVADLFMVFVGGFTTTLTSLHGYFVFGPTGCNLEGGFFATLGGIEALWLSLVLAIERVYVVKPMSNFRFGE  
NHAIMGVAFTWVMALACAAPLVGWSRYIPEGMQCSCGIDYYPHEETNNEFVIYMFVVFHFIIP<sup>L</sup>VI<sup>F</sup>FCY<sup>G</sup>Q  
LVFTVKEAAAQQQESATTQKAEKEVTRMVIIMVIAFLICWLPYAGVAFYIFTHQGSDFGPIFMTIPAFFAKTSAV  
YNPVIYIMMNKQFRNCMVTTLCCGKNPLGDDEASTTVSKTETSQVAPA

Appendix 4. Sequences of proteins in the split nanLuc, BRET and pull-down experiments.

<b>Basic settings</b>					
Measurement type:	Luminescence (dual emission)				
Microplate name:	PE OptiPlate 96				
<b>Plate mode settings</b>					
No. of cycles:	20				
Cycle time [s]:	90				
Measurement interval time [s]:	0.6				
<b>Optic settings</b>					
Optic module:	BRET 2 plus				
Emission A:	515-30				
Emission B:	410-80				
Gain A:	3600				
Gain B:	3600				
Focal height [mm]:	11				
Ratio multiplier:	10000				
Glow correction factor A [%]:	0				
Glow correction factor B [%]:	0				
<b>General settings</b>					
Top optic used					
Aperture spoon:	-				
Reading direction:	bidirectional, horizontal left to right, top to bottom				
Target temperature [°C]:	37				

**Appendix 5.** Microplate reader settings for BRET measurements.



Mutant	RAUC	SD if N=2	Exp (to WT)
G2A	2.94	NA	77%
E3A	2.98	1.02	71%
K4A	0.55	NA	85%
P5A	0.69	NA	92%
G6A	2.06	0.23	83%
T7A	1.96	0.52	82%
R8A	1.86	0.29	100%
V9A	NA	NA	NA
F10A	1.75	NA	51%
K11A	1.50	0.05	79%
K12A	3.89	1.27	45%
S13A	2.38	1.44	91%
S14A	1.51	0.04	96%
P15A	1.38	0.25	80%
N16A	2.37	0.54	64%
C17A	1.66	0.67	66%
K18A	0.66	NA	98%
L19A	2.15	1.08	35%
T20A	2.07	0.11	52%
V21A	3.00	0.48	39%
Y22A	6.00	5.78	44%
L23A	2.27	NA	34%
G24A	0.95	NA	98%
K25A	1.94	1.23	89%
R26A	3.63	1.94	39%
D27A	1.75	0.20	52%
F28A	2.83	1.09	39%
V29A	6.45	6.20	77%
D30A	1.15	0.12	69%
H31A	0.79	0.12	92%
L32A	2.98	0.04	56%
D33A	2.29	0.10	49%
K34A	NA	NA	NA
V35A	1.49	0.31	76%
D36A	3.66	0.67	19%
P37A	3.50	0.01	47%
V38A	4.57	1.80	29%
D39A	5.01	NA	32%
G40A	4.18	1.00	14%
V41A	4.22	2.28	27%
V42A	1.20	NA	68%
L43A	3.42	0.17	33%
V44A	3.22	0.19	32%
D45A	4.03	0.25	45%
P46A	NA	NA	NA
D47A	1.60	0.39	82%
Y48A	NA	NA	1%
L49A	3.38	1.55	48%
K50A	NA	NA	7%
D51A	3.13	1.02	63%
R52A	1.65	0.05	79%
K53A	NA	NA	NA
V54A	2.24	NA	75%
F55A	1.10	NA	52%
V56A	0.52	NA	66%
T57A	1.36	0.78	72%
L58A	NA	NA	NA
T59A	1.53	NA	90%
C60A	NA	NA	NA
A61G	1.80	NA	82%
F62A	NA	NA	NA
R63A	1.44	NA	68%
Y64A	1.63	NA	78%
G65A	NA	NA	NA
R66A	1.51	NA	88%
E67A	1.02	0.47	73%
D68A	1.86	1.04	51%
L69A	1.12	NA	59%

Mutant	RAUC	SD if N=2	Exp (to WT)
D70A	NA	NA	8%
V71A	0.69	0.25	79%
L72A	NA	NA	NA
G73A	0.70	NA	99%
L74A	0.50	NA	105%
S75A	0.77	NA	106%
F76A	0.98	0.55	94%
R77A	1.86	0.22	104%
K78A	3.49	1.76	65%
D79A	0.86	0.16	92%
L80A	NA	NA	NA
F81A	1.05	0.31	84%
I82A	0.69	0.20	93%
A83G	0.93	NA	106%
T84A	1.75	NA	106%
Y85A	1.33	NA	44%
Q86A	1.14	NA	78%
A87G	NA	NA	NA
F88A	0.95	NA	98%
P89A	NA	NA	3%
P90A	1.24	0.16	101%
V91A	0.44	NA	106%
P92A	1.41	0.17	81%
N93A	NA	NA	NA
P94A	NA	NA	101%
P95A	1.50	0.16	108%
R96A	0.76	0.16	109%
P97A	1.81	0.18	42%
P98A	0.84	0.04	122%
T99A	1.63	0.63	67%
R100A	3.57	0.88	82%
L101A	2.14	0.31	68%
Q102A	1.96	0.70	60%
D103A	1.32	0.07	80%
R104A	1.89	0.23	97%
L105A	2.70	NA	40%
L106A	1.58	0.16	75%
R107A	2.29	1.08	77%
K108A	2.09	NA	101%
L109A	3.36	NA	41%
G110A	NA	NA	NA
Q111A	2.81	0.02	82%
H112A	2.00	0.06	97%
A113G	NA	NA	NA
H114A	1.95	NA	66%
P115A	1.90	0.03	77%
F116A	1.10	NA	52%
F117A	3.84	0.28	73%
F118A	2.77	0.53	52%
T119A	1.82	0.66	106%
I120A	1.03	0.15	65%
P121A	0.86	NA	98%
Q122A	1.62	0.15	104%
N123A	1.52	0.63	99%
L124A	3.53	NA	42%
P125A	2.11	0.02	48%
C126A	0.82	0.15	94%
S127A	3.24	2.24	43%
V128A	1.98	NA	73%
T129A	NA	NA	NA
L130A	1.44	0.40	69%
Q131A	0.88	NA	111%
P132A	4.29	1.75	50%
G133A	0.74	NA	96%
P134A	1.47	NA	90%
E135A	1.38	0.46	106%
D136A	1.59	0.08	92%
T137A	0.70	0.15	56%

Mutant	RAUC	SD if N=2	Exp (to WT)
G138A	1.49	0.61	109%
K139A	1.20	0.65	96%
A140G	2.54	1.30	71%
C141A	2.06	1.20	85%
G142A	1.46	NA	75%
V143A	NA	NA	NA
D144A	3.71	0.76	70%
F145A	1.99	0.27	33%
E146A	3.48	NA	14%
I147A	2.90	0.34	26%
R148A	1.33	NA	89%
A149G	1.51	NA	70%
F150A	1.09	NA	74%
C151A	1.66	NA	81%
A152G	1.49	0.32	96%
K153A	1.20	0.02	102%
S154A	1.70	0.46	82%
L155A	1.50	0.00	107%
E156A	2.12	0.38	85%
E157A	1.57	0.43	89%
K158A	1.69	0.11	74%
S159A	0.54	NA	96%
H160A	1.91	0.40	90%
K161A	NA	NA	2%
R162A	NA	NA	7%
N163A	1.04	0.21	116%
S164A	1.13	0.10	106%
V165A	NA	NA	NA
R166A	2.12	NA	70%
L167A	0.89	NA	87%
V168A	1.65	0.44	103%
I169A	1.40	0.14	59%
R170A	0.89	NA	51%
K171A	0.86	0.05	101%
V172A	8.76	0.27	47%
Q173A	1.04	0.02	98%
F174A	0.86	0.13	97%
A175G	1.96	0.15	83%
P176A	1.55	0.41	72%
E177A	8.70	1.66	203%
K178A	0.86	NA	80%
P179A	1.18	0.08	94%
G180A	1.34	0.19	106%
P181A	1.08	0.08	104%
Q182A	1.52	0.24	90%
P183A	1.71	0.80	82%
S184A	1.30	0.28	116%
A185G	1.84	0.20	92%
E186A	NA	NA	91%
T187A	1.04	NA	96%
T188A	1.41	0.52	92%
R189A	NA	NA	112%
H190A	1.37	0.21	112%
F191A	1.54	0.59	85%
L192A	0.98	0.10	110%
M193A	0.98	0.01	105%
S194A	1.54	0.37	108%
D195A	3.68	1.03	79%
R196A	0.66	NA	102%
S197A	1.97	0.67	81%
L198A	1.92	NA	40%
H199A	1.59	0.01	74%
L200A	1.30	0.12	76%
E201A	0.96	NA	97%
A202G	66.22	NA	30%
S203A	0.75	NA	68%
L204A	2.17	0.36	67%
D205A	1.57	0.27	75%

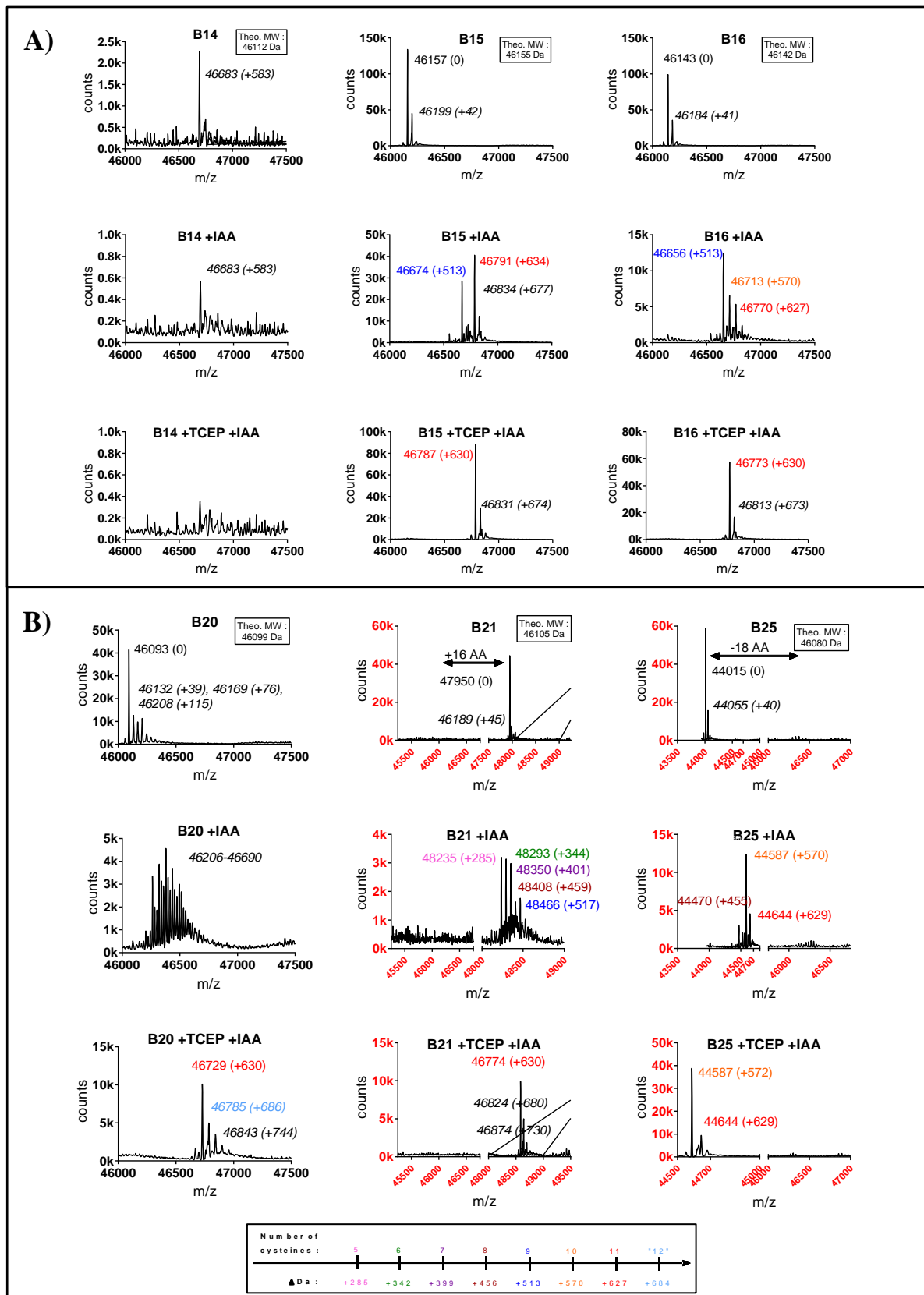
**Appendix 6.** Ratios RAUC (see 1.2.3. Data analysis) analyzed from kinetic traces in the split nanluc assay (from mutant G2A to L208A). SD: standard deviation when N=2. Exp: GFP signal compared to WT. NA: non applicable.

Mutant	RAUC	SD if N=2	Exp (to WT)
K206A	2.30	0.25	39%
E207A	1.45	NA	70%
L208A	2.08	0.67	87%
Y209A	1.70	0.68	55%
Y210A	3.05	1.04	67%
H211A	0.47	NA	76%
G212A	1.17	NA	44%
E213A	2.25	0.63	57%
P214A	1.48	0.64	74%
L215A	1.11	0.40	63%
N216A	1.59	0.24	73%
V217A	1.89	0.53	40%
N218A	1.04	0.14	88%
V219A	1.80	0.07	37%
H220A	1.50	0.29	72%
V221A	1.60	0.30	74%
T222A	1.54	0.38	77%
N223A	3.70	NA	32%
N224A	1.49	NA	78%
S225A	1.41	0.17	67%
T226A	1.29	0.18	83%
K227A	0.68	0.05	88%
T228A	NA	NA	80%
V229A	1.48	0.19	52%
K230A	1.12	0.05	65%
K231A	1.04	0.08	74%
I232A	NA	NA	3%
K233A	1.00	0.11	77%
V234A	NA	NA	51%
S235A	1.16	0.03	79%
V236A	1.65	0.07	60%
R237A	NA	NA	4%
Q238A	NA	NA	5%
Y239A	1.47	0.06	55%
A240G	2.72	0.73	34%
D241A	1.72	0.20	65%
I242A	2.69	1.00	53%
C243A	1.05	NA	34%
L244A	1.46	0.20	65%
F245A	NA	NA	NA
S246A	1.13	0.07	68%
T247A	NA	NA	91%
A248G	1.79	0.02	38%
Q249A	0.85	NA	58%
Y250A	1.17	NA	72%
K251A	2.06	NA	51%
C252A	2.14	0.79	69%
P253A	3.40	3.54	91%
V254A	0.68	NA	77%
A255G	1.53	NA	50%
Q256A	1.48	0.56	68%
L257A	2.15	0.45	52%
E258A	NA	NA	3%
Q259A	1.60	0.06	63%
D260A	6.48	NA	45%
D261A	0.70	NA	108%
Q262A	1.90	0.14	57%
V263A	0.69	NA	77%
S264A	0.68	NA	79%
P265A	NA	NA	73%
S266A	1.82	0.03	63%
S267A	1.41	0.44	71%
T268A	1.01	NA	85%
F269A	0.89	NA	75%
C270A	1.40	NA	60%
K271A	2.96	NA	43%
V272A	0.84	NA	108%
Y273A	69.26	67.64	17%

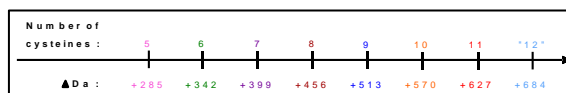
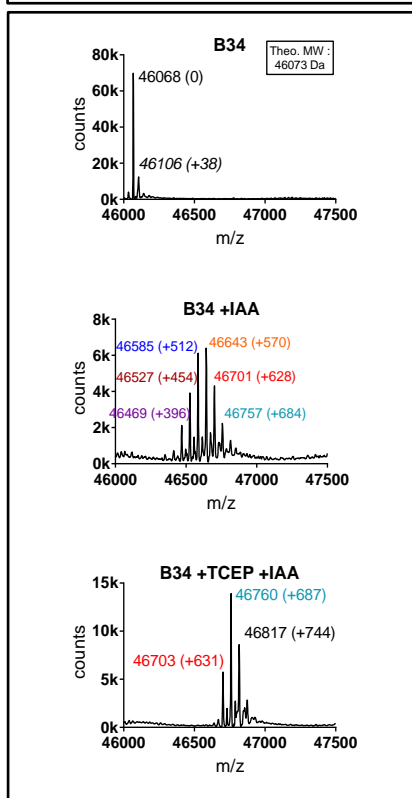
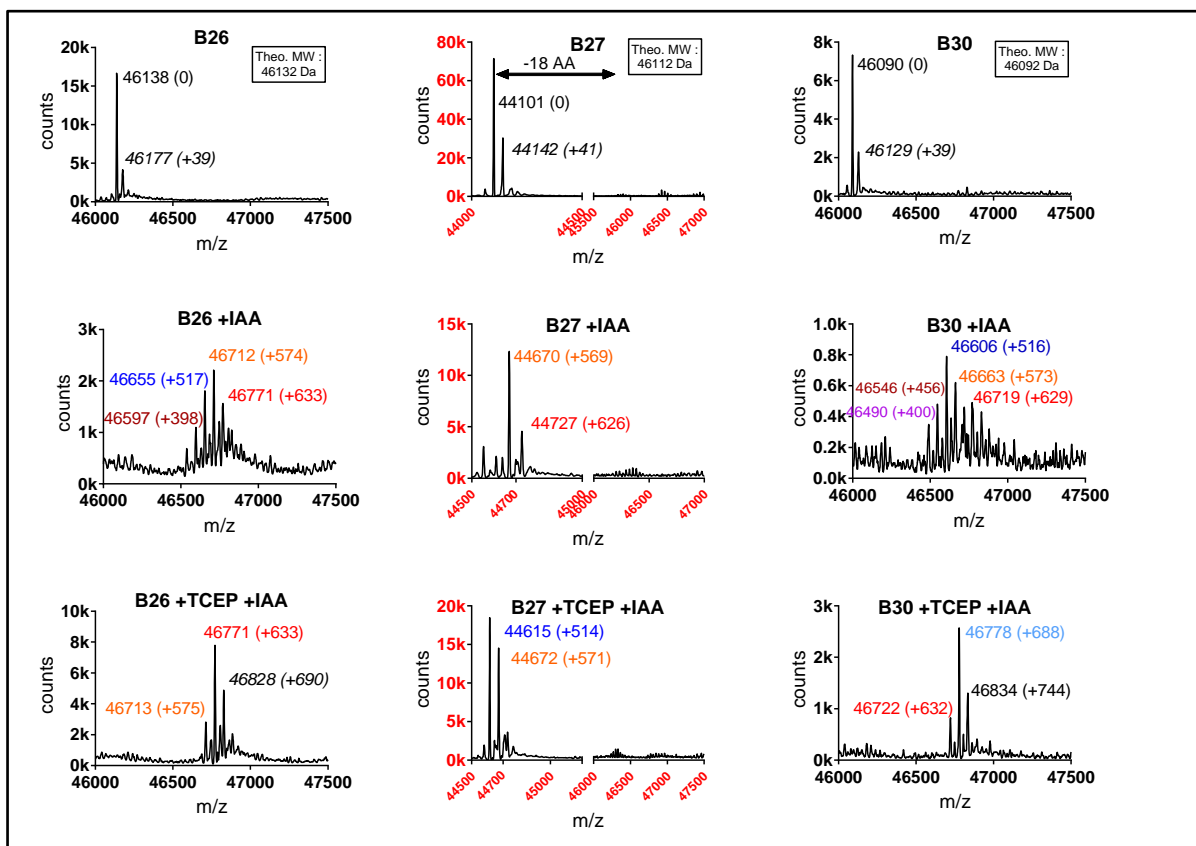
Mutant	RAUC	SD if N=2	Exp (to WT)
T274A	3.07	1.64	52%
I275A	1.31	0.07	61%
T276A	3.84	NA	34%
P277A	2.35	NA	43%
L278A	5.48	5.73	46%
L279A	1.22	NA	74%
S280A	1.31	NA	82%
D281A	1.15	NA	97%
N282A	0.76	NA	91%
R283A	1.30	NA	79%
E284A	1.53	NA	83%
K285A	0.87	NA	84%
R286A	1.52	0.03	76%
G287A	0.84	NA	79%
L288A	1.42	NA	55%
A289G	2.36	NA	39%
L290A	0.68	NA	88%
D291A	2.31	NA	51%
G292A	3.40	NA	55%
K293A	1.09	NA	79%
L294A	0.80	NA	86%
K295A	NA	NA	4%
H296A	3.23	NA	50%
E297A	1.08	NA	73%
D298A	2.07	NA	88%
T299A	2.70	NA	77%
N300A	1.25	0.34	81%
L301A	0.89	0.13	65%
A302G	2.44	NA	40%
S303A	0.28	0.05	141%
S304A	1.09	NA	60%
T305A	1.77	NA	53%
I306A	1.33	0.18	41%
V307A	1.01	NA	97%
K308A	0.80	NA	100%
E309A	0.56	NA	97%
G310A	1.16	0.23	109%
A311G	2.82	NA	97%
N312A	1.38	0.19	88%
K313A	1.09	0.57	111%
E314A	NA	NA	NA
V315A	0.90	0.05	109%
L316A	0.97	NA	99%
G317A	0.54	0.03	113%
I318A	1.01	0.06	69%
L319A	2.09	0.22	94%
V320A	1.36	0.02	63%
S321A	0.81	0.08	103%
Y322A	0.87	0.15	55%
R323A	0.44	0.03	132%
V324A	NA	NA	49%
K325A	NA	NA	NA
V326A	NA	NA	NA
K327A	1.69	0.01	29%
L328A	NA	NA	89%
V329A	1.52	NA	28%
V330A	0.86	0.08	101%
S331A	1.61	0.06	95%
R332A	0.52	NA	117%
G333A	1.11	0.05	97%
G334A	0.60	NA	42%
D335A	0.91	0.02	99%
V336A	1.07	0.24	106%
S337A	NA	NA	NA
V338A	1.67	NA	55%
E339A	0.72	0.08	85%
L340A	NA	NA	53%
P341A	1.37	0.17	50%

Mutant	RAUC	SD if N=2	Exp (to WT)
F342A	2.07	0.06	42%
V343A	4.76	NA	42%
L344A	NA	NA	NA
M345A	0.55	0.07	106%
H346A	1.21	0.30	96%
P347A	1.45	0.26	92%
K348A	1.11	0.16	85%
P349A	0.72	NA	111%
H350A	2.19	0.13	63%
D351A	2.37	NA	32%
H352A	2.37	NA	88%
I353A	0.65	NA	101%
P354A	0.65	NA	99%
L355A	4.21	NA	81%
P356A	0.68	NA	84%
R357A	20.88	NA	96%
P358A	2.08	NA	55%
Q359A	14.53	NA	83%
S360A	1.03	NA	73%
A361G	NA	NA	84%
A362G	16.43	NA	72%
P363A	0.55	NA	95%
E364A	0.88	NA	76%
T365A	0.68	NA	92%
D366A	5.45	NA	86%
V367A	NA	NA	93%
P368A	9.11	NA	69%
V369A	1.27	0.68	93%
D370A	3.56	3.41	73%
T371A	3.37	2.96	80%
N372A	0.52	NA	91%
L373A	4.79	NA	70%
I374A	2.28	NA	71%
E375A	0.65	NA	88%
F376A	4.97	NA	77%
D377A	5.04	NA	57%
T378A	NA	NA	NA
N379A	0.69	NA	80%
Y380A	2.86	NA	70%
A381G	0.66	NA	87%
T382A	1.14	NA	99%
D383A	2.29	0.65	93%
D384A	NA	NA	71%
D385A	2.24	0.62	92%
I386A	3.13	1.62	60%
V387A	3.27	0.31	84%
F388A	NA	NA	NA
E389A	3.09	0.52	98%
D390A	1.40	NA	60%
F391A	1.56	NA	54%
A392G	0.72	NA	75%
R393A	0.93	NA	89%
L394A	0.72	NA	89%
R395A	1.55	0.53	96%
L396A	0.56	NA	87%
K397A	1.19	0.08	92%
G398A	2.78	0.44	56%
M399A	1.22	0.15	101%
K400A	1.36	NA	77%
D401A	1.98	0.90	90%
D402A	3.02	1.64	71%
D403A	3.13	0.61	90%
Y404A	8.61	8.70	62%
D405A	1.55	0.09	92%
D406A	2.24	0.44	87%
Q407A	1.95	0.70	92%
L408A	1.86	0.05	88%
C409A	0.74	NA	53%

**Appendix 7.** Ratios RAUC (see 1.2.3. Data analysis) analyzed from kinetic traces in the split nanluc assay (from mutant K206A to C409A). SD: standard deviation when N=2. Exp: GFP signal compared to WT. NA: Non applicable.



**Appendix 8.** Deconvoluted spectra of A) arrestin-3 mutants B14, B15, B16 and B) B20, B21 and B25 either i) alone (in 5 mM ammonium bicarbonate pH 7.0; 7.5 M guanidine; 0.1 M Tris-HCl; 1 mM EDTA), ii) +iodoacetamide (IAA) or iii) +IAA+ tris(2-carboxyethyl)phosphine (TCEP). Theo MW: theoretical molecular weight. Black labeled peaks: Na<sup>+</sup>-incorporated species of arrestin-3 (technical artifacts).



**Appendix 9.** Deconvoluted spectra of arrestin-3 mutants B26, B27, B30 and B34 either i) alone (in 5 mM ammonium bicarbonate pH 7.0; 7.5 M guanidine; 0.1 M Tris-HCl; 1 mM EDTA), ii) +iodoacetamide (IAA) or iii) +IAA+ tris(2-carboxyethyl)phosphine (TCEP). Theo MW: theoretical molecular weight. Black labeled peaks: Na<sup>+</sup> incorporated species of arrestin-3 (technical artifacts).

## REFERENCES

1. Vaudry, H. MOLECULAR EVOLUTION OF GPCRS: What we know and what the future holds. *J. Mol. Endocrinol.* **52**, E1–E2 (2014).
2. Zhou, X. E., Melcher, K. & Xu, H. E. Understanding the GPCR biased signaling through G protein and arrestin complex structures. *Curr. Opin. Struct. Biol.* **45**, 150–159 (2017).
3. Fredriksson, R., Lagerström, M. C., Lundin, L.-G. & Schiöth, H. B. The G-Protein-Coupled Receptors in the Human Genome Form Five Main Families. Phylogenetic Analysis, Paralogon Groups, and Fingerprints. *Mol. Pharmacol.* **63**, 1256–1272 (2003).
4. Nakamichi, H. & Okada, T. Crystallographic Analysis of Primary Visual Photochemistry. *Angew. Chem. Int. Ed.* **45**, 4270–4273 (2006).
5. Ishchenko, A. *et al.* Toward G protein-coupled receptor structure-based drug design using X-ray lasers. *IUCrJ* **6**, 1106–1119 (2019).
6. Birnbaumer, L. The discovery of signal transduction by G proteins. A personal account and an overview of the initial findings and contributions that led to our present understanding. *Biochim. Biophys. Acta* **1768**, 756–771 (2007).
7. Du, Y. *et al.* Assembly of a GPCR-G Protein Complex. *Cell* **177**, 1232–1242.e11 (2019).
8. Rasmussen, S. G. F. *et al.* Structure of a nanobody-stabilized active state of the  $\beta$  2 adrenoceptor. *Nature* **469**, 175–180 (2011).
9. Schönege, A.-M. *et al.* Evolutionary action and structural basis of the allosteric switch controlling  $\beta$ 2AR functional selectivity. *Nat. Commun.* **8**, (2017).
10. Shen, Y. *et al.* D2 Dopamine Receptor G Protein-Biased Partial Agonists Based on Cariprazine. *J. Med. Chem.* **62**, 4755–4771 (2019).
11. Rasmussen, S. G. F. *et al.* Crystal structure of the  $\beta$  2 adrenergic receptor–Gs protein complex. *Nature* **477**, 549–555 (2011).
12. DeVree, B. T. *et al.* Allosteric coupling from G protein to the agonist-binding pocket in GPCRs. *Nature* **535**, 182–186 (2016).

13. Wang, J., Gareri, C. & Rockman, H. A. G-Protein–Coupled Receptors in Heart Disease. *Circ. Res.* **123**, 716–735 (2018).
14. Gurevich, V. V. *et al.* Arrestin Interactions with G Protein-coupled Receptors DIRECT BINDING STUDIES OF WILD TYPE AND MUTANT ARRESTINS WITH RHODOPSIN,  $\beta$ 2-ADRENERGIC, AND  $m_2$  MUSCARINIC CHOLINERGIC RECEPTORS. *J. Biol. Chem.* **270**, 720–731 (1995).
15. Vishnivetskiy, S. A. *et al.* Few Residues within an Extensive Binding Interface Drive Receptor Interaction and Determine the Specificity of Arrestin Proteins. *J. Biol. Chem.* **286**, 24288–24299 (2011).
16. Oakley, R. H., Laporte, S. A., Holt, J. A., Caron, M. G. & Barak, L. S. Differential Affinities of Visual Arrestin,  $\beta$ Arrestin1, and  $\beta$ Arrestin2 for G Protein-coupled Receptors Delineate Two Major Classes of Receptors. *J. Biol. Chem.* **275**, 17201–17210 (2000).
17. Kim, Y. J. *et al.* Crystal structure of pre-activated arrestin p44. *Nature* **497**, 142–146 (2013).
18. Granzin, J. *et al.* Crystal Structure of p44, a Constitutively Active Splice Variant of Visual Arrestin. *J. Mol. Biol.* **416**, 611–618 (2012).
19. Palczewski, K. *et al.* Characterization of a truncated form of arrestin isolated from bovine rod outer segments. *Protein Sci. Publ. Protein Soc.* **3**, 314–324 (1994).
20. Beaufrais, A. *et al.* A new inhibitor of the  $\beta$ -arrestin/AP2 endocytic complex reveals interplay between GPCR internalization and signalling. *Nat. Commun.* **8**, (2017).
21. Breit, A., Lagacé, M. & Bouvier, M. Hetero-oligomerization between  $\beta$ 2- and  $\beta$ 3-Adrenergic Receptors Generates a  $\beta$ -Adrenergic Signaling Unit with Distinct Functional Properties. *J. Biol. Chem.* **279**, 28756–28765 (2004).
22. Mende, F. *et al.* Translating biased signaling in the ghrelin receptor system into differential in vivo functions. *Proc. Natl. Acad. Sci. U. S. A.* **115**, E10255–E10264 (2018).
23. Altschul, S. F. *et al.* Gapped BLAST and PSI-BLAST: a new generation of protein database search programs. *Nucleic Acids Res.* **25**, 3389–3402 (1997).
24. Altschul, S. F. *et al.* Protein Database Searches Using Compositionally Adjusted Substitution Matrices. *FEBS J.* **272**, 5101–5109 (2005).

25. Vishnivetskiy, S. A. *et al.* How Does Arrestin Respond to the Phosphorylated State of Rhodopsin? *J. Biol. Chem.* **274**, 11451–11454 (1999).
26. Granzin, J., Stadler, A., Cousin, A., Schlesinger, R. & Batra-Safferling, R. Structural evidence for the role of polar core residue Arg175 in arrestin activation. *Sci. Rep.* **5**, 15808 (2015).
27. Hirsch, J. A., Schubert, C., Gurevich, V. V. & Sigler, P. B. A Model for Arrestin's Regulation: The 2.8 Å Crystal Structure of Visual Arrestin. *Cell* **97**, 257–269 (1999).
28. Gurevich, V. V. The Selectivity of Visual Arrestin for Light-activated Phosphorhodopsin Is Controlled by Multiple Nonredundant Mechanisms. *J. Biol. Chem.* **273**, 15501–15506 (1998).
29. Vishnivetskiy, S. A. *et al.* An Additional Phosphate-binding Element in Arrestin Molecule IMPLICATIONS FOR THE MECHANISM OF ARRESTIN ACTIVATION. *J. Biol. Chem.* **275**, 41049–41057 (2000).
30. Schröder, K., Pulvermüller, A. & Hofmann, K. P. Arrestin and Its Splice Variant Arr1–370A(p44) MECHANISM AND BIOLOGICAL ROLE OF THEIR INTERACTION WITH RHODOPSIN. *J. Biol. Chem.* **277**, 43987–43996 (2002).
31. Shukla, A. K. *et al.* Structure of active  $\beta$ -arrestin1 bound to a G protein-coupled receptor phosphopeptide. *Nature* **497**, 137–141 (2013).
32. Scheerer, P. & Sommer, M. E. Structural mechanism of arrestin activation. *Curr. Opin. Struct. Biol.* **45**, 160–169 (2017).
33. Chen, Q. *et al.* Structural basis of arrestin-3 activation and signaling. *Nat. Commun.* **8**, (2017).
34. Kang, Y. *et al.* Crystal structure of rhodopsin bound to arrestin by femtosecond X-ray laser. *Nature* **523**, 561–567 (2015).
35. Latorraca, N. R. *et al.* Molecular mechanism of GPCR-mediated arrestin activation. *Nature* **557**, 452–456 (2018).
36. Carter, J. M., Gurevich, V. V., Prossnitz, E. R. & Engen, J. R. Conformational Differences Between Arrestin2 and Pre-activated Mutants as Revealed by Hydrogen Exchange Mass Spectrometry. *J. Mol. Biol.* **351**, 865–878 (2005).

37. Kim, D. K., Yun, Y., Kim, H. R., Seo, M.-D. & Chung, K. Y. Different conformational dynamics of various active states of  $\beta$ -arrestin1 analyzed by hydrogen/deuterium exchange mass spectrometry. *J. Struct. Biol.* **190**, 250–259 (2015).
38. Development of a BRET2 Screening Assay Using  $\beta$ -Arrestin 2 Mutants - Milka Vrecl, Rasmus Jorgensen, Azra Pogačnik, Anders Heding, 2004.  
<https://journals.sagepub.com/doi/abs/10.1177/1087057104263212>.
39. Potter, R. M., Key, T. A., Gurevich, V. V., Sklar, L. A. & Prossnitz, E. R. Arrestin Variants Display Differential Binding Characteristics for the Phosphorylated N-Formyl Peptide Receptor Carboxyl Terminus. *J. Biol. Chem.* **277**, 8970–8978 (2002).
40. Ostermaier, M. K., Peterhans, C., Jaussi, R., Deupi, X. & Standfuss, J. Functional map of arrestin-1 at single amino acid resolution. *Proc. Natl. Acad. Sci.* **111**, 1825–1830 (2014).
41. Hanson, S. M. *et al.* Differential interaction of spin-labeled arrestin with inactive and active phosphorhodopsin. *Proc. Natl. Acad. Sci. U. S. A.* **103**, 4900–4905 (2006).
42. Sommer, M. E., Farrens, D. L., McDowell, J. H., Weber, L. A. & Smith, W. C. Dynamics of Arrestin-Rhodopsin Interactions LOOP MOVEMENT IS INVOLVED IN ARRESTIN ACTIVATION AND RECEPTOR BINDING. *J. Biol. Chem.* **282**, 25560–25568 (2007).
43. Szczepek, M. *et al.* Crystal structure of a common GPCR-binding interface for G protein and arrestin. *Nat. Commun.* **5**, (2014).
44. Prokop, S. *et al.* Differential manipulation of arrestin-3 binding to basal and agonist-activated G protein-coupled receptors. *Cell. Signal.* **36**, 98–107 (2017).
45. Evolving Concepts in G Protein-Coupled Receptor Endocytosis: The Role in Receptor Desensitization and Signaling | Pharmacological Reviews.  
<http://pharmrev.aspetjournals.org/content/53/1/1>.
46. Goodman, O. B. *et al.*  $\beta$ -Arrestin acts as a clathrin adaptor in endocytosis of the  $\beta$  2 -adrenergic receptor. *Nature* **383**, 447–450 (1996).
47. Krupnick, J. G., Goodman, O. B., Keen, J. H. & Benovic, J. L. Arrestin/Clathrin Interaction LOCALIZATION OF THE CLATHRIN BINDING DOMAIN OF NONVISUAL ARRESTINS TO THE CARBOXYL TERMINUS. *J. Biol. Chem.* **272**, 15011–15016 (1997).



48. Kang, D. S. *et al.* Structure of an Arrestin2-Clathrin Complex Reveals a Novel Clathrin Binding Domain That Modulates Receptor Trafficking. *J. Biol. Chem.* **284**, 29860–29872 (2009).
49. Laporte, S. A., Oakley, R. H., Holt, J. A., Barak, L. S. & Caron, M. G. The Interaction of  $\beta$ -Arrestin with the AP-2 Adaptor Is Required for the Clustering of  $\beta$ 2-Adrenergic Receptor into Clathrin-coated Pits. *J. Biol. Chem.* **275**, 23120–23126 (2000).
50. Laporte, S. A., Miller, W. E., Kim, K.-M. & Caron, M. G.  $\beta$ -Arrestin/AP-2 Interaction in G Protein-coupled Receptor Internalization IDENTIFICATION OF A  $\beta$ -ARRESTIN BINDING SITE IN  $\beta$ 2-ADAPTIN. *J. Biol. Chem.* **277**, 9247–9254 (2002).
51. Lee, S.-J., Xu, H., Kang, L.-W., Amzel, L. M. & Montell, C. Light Adaptation through Phosphoinositide-Regulated Translocation of Drosophila Visual Arrestin. *Neuron* **39**, 121–132 (2003).
52. Peterson, Y. K. & Luttrell, L. M. The Diverse Roles of Arrestin Scaffolds in G Protein–Coupled Receptor Signaling. *Pharmacol. Rev.* **69**, 256–297 (2017).
53. Pierce, K. L., Luttrell, L. M. & Lefkowitz, R. J. New mechanisms in heptahelical receptor signaling to mitogen activated protein kinase cascades. *Oncogene* **20**, 1532–1539 (2001).
54. Dangi, S., Chen, F. M. & Shapiro, P. Activation of extracellular signal-regulated kinase (ERK) in G2 phase delays mitotic entry through p21CIP1. *Cell Prolif.* **39**, 261–279 (2006).
55. Meng, D. *et al.* MEK1 Binds Directly to  $\beta$ Arrestin1, Influencing Both Its Phosphorylation by ERK and the Timing of Its Isoprenaline-stimulated Internalization. *J. Biol. Chem.* **284**, 11425–11435 (2009).
56. Hanson, S. M. *et al.* Arrestin mobilizes signaling proteins to the cytoskeleton and redirects their activity. *J. Mol. Biol.* **368**, 375–387 (2007).
57. Coffa, S. *et al.* The Effect of Arrestin Conformation on the Recruitment of c-Raf1, MEK1, and ERK1/2 Activation. *PLOS ONE* **6**, e28723 (2011).
58. McDonald, P. H. *et al.*  $\beta$ -Arrestin 2: A Receptor-Regulated MAPK Scaffold for the Activation of JNK3. *Science* **290**, 1574–1577 (2000).
59. Kyriakis, J. M. & Avruch, J. Mammalian MAPK Signal Transduction Pathways Activated by Stress and Inflammation: A 10-Year Update. *Physiol. Rev.* **92**, 689–737 (2012).

60. Song, X., Raman, D., Gurevich, E. V., Vishnivetskiy, S. A. & Gurevich, V. V. Visual and Both Non-visual Arrestins in Their “Inactive” Conformation Bind JNK3 and Mdm2 and Relocalize Them from the Nucleus to the Cytoplasm. *J. Biol. Chem.* **281**, 21491–21499 (2006).
61. Crépieux, P. *et al.* A Comprehensive View of the  $\beta$ -Arrestinome. *Front. Endocrinol.* **8**, (2017).
62. Wu, N. *et al.* Arrestin binding to calmodulin: a direct interaction between two ubiquitous signaling proteins. *J. Mol. Biol.* **364**, 955–963 (2006).
63. Wang, P., Wu, Y., Ge, X., Ma, L. & Pei, G. Subcellular Localization of  $\beta$ -Arrestins Is Determined by Their Intact N Domain and the Nuclear Export Signal at the C Terminus. *J. Biol. Chem.* **278**, 11648–11653 (2003).
64. Milano, S. K., Kim, Y.-M., Stefano, F. P., Benovic, J. L. & Brenner, C. Nonvisual Arrestin Oligomerization and Cellular Localization Are Regulated by Inositol Hexakisphosphate Binding. *J. Biol. Chem.* **281**, 9812–9823 (2006).
65. Hoepfner, C. Z., Cheng, N. & Ye, R. D. Identification of a Nuclear Localization Sequence in  $\beta$ -Arrestin-1 and Its Functional Implications. *J. Biol. Chem.* **287**, 8932–8943 (2012).
66. Mo, W. *et al.* Nuclear  $\beta$ -Arrestin1 Functions as a Scaffold for the Dephosphorylation of STAT1 and Moderates the Antiviral Activity of IFN- $\gamma$ . *Mol. Cell* **31**, 695–707 (2008).
67. Kang, J. *et al.* A Nuclear Function of  $\beta$ -Arrestin1 in GPCR Signaling: Regulation of Histone Acetylation and Gene Transcription. *Cell* **123**, 833–847 (2005).
68. Gregorio, G. G. *et al.* Single-molecule analysis of ligand efficacy in  $\beta$ 2AR-G-protein activation. *Nature* **547**, 68–73 (2017).
69. Gurevich, V. V. & Gurevich, E. V. GPCR Signaling Regulation: The Role of GRKs and Arrestins. *Front. Pharmacol.* **10**, (2019).
70. He, Y. *et al.* Molecular assembly of rhodopsin with G protein-coupled receptor kinases. *Cell Res.* **27**, 728–747 (2017).
71. Komolov, K. E. *et al.* Structural and Functional Analysis of a  $\beta$ 2-Adrenergic Receptor Complex with GRK5. *Cell* **169**, 407–421.e16 (2017).

72. Farrens, D. L., Altenbach, C., Yang, K., Hubbell, W. L. & Khorana, H. G. Requirement of Rigid-Body Motion of Transmembrane Helices for Light Activation of Rhodopsin. *Science* **274**, 768–770 (1996).
73. Pan, L., Gurevich, E. V. & Gurevich, V. V. The Nature of the Arrestin·Receptor Complex Determines the Ultimate Fate of the Internalized Receptor. *J. Biol. Chem.* **278**, 11623–11632 (2003).
74. Li, L. *et al.* G Protein-coupled Receptor Kinases of the GRK4 Protein Subfamily Phosphorylate Inactive G Protein-coupled Receptors (GPCRs). *J. Biol. Chem.* **290**, 10775–10790 (2015).
75. Rankin, M. L. *et al.* The D1 Dopamine Receptor Is Constitutively Phosphorylated by G Protein-Coupled Receptor Kinase 4. *Mol. Pharmacol.* **69**, 759–769 (2006).
76. Xiao, K. & Sun, J. Elucidating structural and molecular mechanisms of  $\beta$ -arrestin-biased agonism at GPCRs via MS-based proteomics. *Cell. Signal.* **41**, 56–64 (2018).
77. Nobles, K. N. *et al.* Distinct Phosphorylation Sites on the  $\beta$ 2-Adrenergic Receptor Establish a Barcode That Encodes Differential Functions of  $\beta$ -Arrestin. *Sci. Signal.* **4**, ra51 (2011).
78. Ren, X.-R. *et al.* Different G protein-coupled receptor kinases govern G protein and  $\beta$ -arrestin-mediated signaling of V2 vasopressin receptor. *Proc. Natl. Acad. Sci. U. S. A.* **102**, 1448–1453 (2005).
79. Kim, J. *et al.* Functional antagonism of different G protein-coupled receptor kinases for  $\beta$ -arrestin-mediated angiotensin II receptor signaling. *Proc. Natl. Acad. Sci. U. S. A.* **102**, 1442–1447 (2005).
80. Zidar, D. A., Violin, J. D., Whalen, E. J. & Lefkowitz, R. J. Selective engagement of G protein coupled receptor kinases (GRKs) encodes distinct functions of biased ligands. *Proc. Natl. Acad. Sci.* **106**, 9649–9654 (2009).
81. Mayer, D. *et al.* Distinct G protein-coupled receptor phosphorylation motifs modulate arrestin affinity and activation and global conformation. *Nat. Commun.* **10**, (2019).
82. Zhou, X. E. *et al.* Identification of Phosphorylation Codes for Arrestin Recruitment by G Protein-Coupled Receptors. *Cell* **170**, 457-469.e13 (2017).

83. Beyrière, F. *et al.* Formation and Decay of the Arrestin-Rhodopsin Complex in Native Disc Membranes. *J. Biol. Chem.* **290**, 12919–12928 (2015).
84. Lally, C. C. M., Bauer, B., Selent, J. & Sommer, M. E. C-edge loops of arrestin function as a membrane anchor. *Nat. Commun.* **8**, 14258 (2017).
85. Marion, S., Oakley, R. H., Kim, K.-M., Caron, M. G. & Barak, L. S. A  $\beta$ -Arrestin Binding Determinant Common to the Second Intracellular Loops of Rhodopsin Family G Protein-coupled Receptors. *J. Biol. Chem.* **281**, 2932–2938 (2006).
86. Peterhans, C., Lally, C. C. M., Ostermaier, M. K., Sommer, M. E. & Standfuss, J. Functional map of arrestin binding to phosphorylated opsin, with and without agonist. *Sci. Rep.* **6**, (2016).
87. Nuber, S. *et al.*  $\beta$ -Arrestin biosensors reveal a rapid, receptor-dependent activation/deactivation cycle. *Nature* **531**, 661–664 (2016).
88. Charest, P. G. & Bouvier, M. Palmitoylation of the V2 Vasopressin Receptor Carboxyl Tail Enhances  $\beta$ -Arrestin Recruitment Leading to Efficient Receptor Endocytosis and ERK1/2 Activation. *J. Biol. Chem.* **278**, 41541–41551 (2003).
89. Charest, P. G., Terrillon, S. & Bouvier, M. Monitoring agonist-promoted conformational changes of  $\beta$ -arrestin in living cells by intramolecular BRET. *EMBO Rep.* **6**, 334–340 (2005).
90. Grundmann, M. *et al.* Lack of beta-arrestin signaling in the absence of active G proteins. *Nat. Commun.* **9**, (2018).
91. Nguyen, A. H. *et al.* Structure of an endosomal signaling GPCR–G protein– $\beta$ -arrestin megacomplex. *Nat. Struct. Mol. Biol.* **26**, 1123–1131 (2019).
92. NanoLuc Complementation Reporter Optimized for Accurate Measurement of Protein Interactions in Cells | ACS Chemical Biology.  
<https://pubs.acs.org/doi/10.1021/acscchembio.5b00753>.
93. Breton, B. *et al.* Multiplexing of Multicolor Bioluminescence Resonance Energy Transfer. *Biophys. J.* **99**, 4037–4046 (2010).
94. Haider, R. S. *et al.* Arrestin-1 engineering facilitates complex stabilization with native rhodopsin. *Sci. Rep.* **9**, (2019).

95. Mansouri, M., Ehsaei, Z., Taylor, V. & Berger, P. Baculovirus-based genome editing in primary cells. *Plasmid* **90**, 5–9 (2017).
96. Sun, D. *et al.* AAScan, PCRdesign and MutantChecker: A Suite of Programs for Primer Design and Sequence Analysis for High-Throughput Scanning Mutagenesis. *PLOS ONE* **8**, e78878 (2013).
97. NanoBiT® PPI Starter Systems. <https://ch.promega.com/products/protein-interactions/live-cell-protein-interactions/nanobit-ppi-starter-systems/>.
98. Dixon, A. S. *et al.* NanoLuc Complementation Reporter Optimized for Accurate Measurement of Protein Interactions in Cells. *ACS Chem. Biol.* **11**, 400–408 (2016).
99. Kobayashi, H., Picard, L.-P., Schönege, A.-M. & Bouvier, M. Bioluminescence resonance energy transfer–based imaging of protein–protein interactions in living cells. *Nat. Protoc.* **14**, 1084–1107 (2019).
100. Namkung, Y. *et al.* Functional selectivity profiling of the angiotensin II type 1 receptor using pathway-wide BRET signaling sensors. *Sci. Signal.* **11**, eaat1631 (2018).
101. Hoffmann, C., Leitz, M. R., Oberdorf-Maass, S., Lohse, M. J. & Klotz, K.-N. Comparative pharmacology of human beta-adrenergic receptor subtypes - characterization of stably transfected receptors in CHO cells. *Naunyn. Schmiedebergs Arch. Pharmacol.* **369**, 151–159 (2004).
102. Zheng, C., Tholen, J. & Gurevich, V. V. Critical role of the finger loop in arrestin binding to the receptors. *PLoS ONE* **14**, (2019).
103. Gurevich, V. V., Gurevich, E. V. & Uversky, V. N. Arrestins: structural disorder creates rich functionality. *Protein Cell* 1–18 (2018) doi:10.1007/s13238-017-0501-8.
104. Yang, F. *et al.* Phospho-selective mechanisms of arrestin conformations and functions revealed by unnatural amino acid incorporation and <sup>19</sup>F-NMR. *Nat. Commun.* **6**, 8202 (2015).
105. Warne, T., Serrano-Vega, M. J., Tate, C. G. & Schertler, G. F. X. Development and crystallization of a minimal thermostabilised G protein-coupled receptor. *Protein Expr. Purif.* **65**, 204–213 (2009).
106. Meger, B., Zimmermann, M., Waldhoer, M., Berger, P. & Ostermaier, M. ‘β arrestin mutants’ EP5657EP00. (2019).

107. Krasel, C. *et al.* Dual Role of the  $\beta$ 2-Adrenergic Receptor C Terminus for the Binding of  $\beta$ -Arrestin and Receptor Internalization. *J. Biol. Chem.* **283**, 31840–31848 (2008).
108. Kühn, H., Hall, S. W. & Wilden, U. Light-induced binding of 48-kDa protein to photoreceptor membranes is highly enhanced by phosphorylation of rhodopsin. *FEBS Lett.* **176**, 473–478 (1984).
109. Sommer, M. E., Smith, W. C. & Farrens, D. L. Dynamics of Arrestin-Rhodopsin Interactions ARRESTIN AND RETINAL RELEASE ARE DIRECTLY LINKED EVENTS. *J. Biol. Chem.* **280**, 6861–6871 (2005).
110. Gurevich, V. V. & Benovic, J. L. Cell-free expression of visual arrestin. Truncation mutagenesis identifies multiple domains involved in rhodopsin interaction. *J. Biol. Chem.* **267**, 21919–21923 (1992).
111. Sommer, M. E., Farrens, D. L., McDowell, J. H., Weber, L. A. & Smith, W. C. Dynamics of Arrestin-Rhodopsin Interactions LOOP MOVEMENT IS INVOLVED IN ARRESTIN ACTIVATION AND RECEPTOR BINDING. *J. Biol. Chem.* **282**, 25560–25568 (2007).
112. Vishnivetskiy, S. A., Baameur, F., Findley, K. R. & Gurevich, V. V. Critical role of the central 139-loop in stability and binding selectivity of arrestin-1. *J. Biol. Chem.* **288**, 11741–11750 (2013).
113. Greenfield, N. J. Using circular dichroism spectra to estimate protein secondary structure. *Nat. Protoc.* **1**, 2876–2890 (2006).
114. Krüger, R., Hung, C.-W., Edelson-Averbukh, M. & Lehmann, W. D. Iodoacetamide-alkylated methionine can mimic neutral loss of phosphoric acid from phosphopeptides as exemplified by nano-electrospray ionization quadrupole time-of-flight parent ion scanning. *Rapid Commun. Mass Spectrom.* **19**, 1709–1716 (2005).
115. Lee, K. A., Craven, K. B., Niemi, G. A. & Hurley, J. B. Mass spectrometric analysis of the kinetics of in vivo rhodopsin phosphorylation. *Protein Sci.* **11**, 862–874 (2002).
116. Sommer, M. E., Hofmann, K. P. & Heck, M. Distinct loops in arrestin differentially regulate ligand binding within the GPCR opsin. *Nat. Commun.* **3**, 995 (2012).

117. Lally, C. C. M. & Sommer, M. E. Quantification of Arrestin–Rhodopsin Binding Stoichiometry. in *Rhodopsin: Methods and Protocols* (ed. Jastrzebska, B.) 235–250 (Springer New York, 2015). doi:10.1007/978-1-4939-2330-4\_16.
118. Sommer, M. E., Hofmann, K. P. & Heck, M. Arrestin-Rhodopsin Binding Stoichiometry in Isolated Rod Outer Segment Membranes Depends on the Percentage of Activated Receptors. *J. Biol. Chem.* **286**, 7359–7369 (2011).
119. Pulvermüller, A. *et al.* Functional Differences in the Interaction of Arrestin and Its Splice Variant, p44, with Rhodopsin. *Biochemistry* **36**, 9253–9260 (1997).
120. Kisselev, O. G., Downs, M. A., McDowell, J. H. & Hargrave, P. A. Conformational Changes in the Phosphorylated C-terminal Domain of Rhodopsin during Rhodopsin Arrestin Interactions. *J. Biol. Chem.* **279**, 51203–51207 (2004).
121. Vishnivetskiy, S. A. *et al.* Regulation of Arrestin Binding by Rhodopsin Phosphorylation Level. *J. Biol. Chem.* **282**, 32075–32083 (2007).
122. Mendez, A. *et al.* Rapid and Reproducible Deactivation of Rhodopsin Requires Multiple Phosphorylation Sites. *Neuron* **28**, 153–164 (2000).

# CURRICULUM VITAE

## **Benoît Meger**

Laboratory of Biomolecular Research

Paul Scherrer Institute

OFLG/124

CH-5232 Villigen PSI

Telefon: +41 56 310 28 74

E-Mail: [benoit.meger@psi.ch](mailto:benoit.meger@psi.ch)

Date of birth: 29<sup>th</sup> August 1992

Nationality: French

## EDUCATION

---

- **Pharm.D.**, *Université Montpellier, France, 2010-2016*
- **MSc. in Biotechnology**, *Université Montpellier, France, 2014-2016*

## WORK EXPERIENCE

---

- **Master Thesis**, *Novartis, Basel, Switzerland, Feb 2016 – Jul 2016*  
Project: « Development of a mass spectrometry imaging technique for preclinical PK in vitro studies »
- **Research Intern**, *Pennington Biomedical Proteomics Group, UCD, Dublin, Ireland, Apr 2015 – Aug 2015*  
Project: « Development of an LC-MS method for the discovery serum biomarkers of confined prostate cancer »
- **Hospital intern**, *Laboratoire de Protéomique clinique, IBRM, Montpellier, France*  
*Sep 2014 – Mar 2015*  
Project: « Novel dried blood spot immunoassays for the discovery of biomarkers of the frailty syndrome »
- **Research intern**, *Plateforme de Protéomique Clinique, Sys-Diag Biorad, Montpellier, France,*  
*Jun 2014 – Jul 2014*  
Project: « Validation of predictive biomarkers of diabetic nephropathy in a pending patent application »
- **Research Intern**, *Centre de Pharmacologie et d'Innovation dans le Diabète, CNRS,*  
*Montpellier, France, Mar 2014 – Apr 2014*  
Project: « Protein-Protein interaction study of the pancreatic n-NOS, a potential anti-diabetes target »



- **Pharmacist**, *Pharmacie des Sables, Aigues-Mortes, France, Jun 2013 – Aug 2013 / Jun 2012 – Aug 2012 / Jun 2011 – Aug 2011*

## HONORS AND SKILLS

---

- **European patent application**  
“ $\beta$ -arrestin mutants” EP19153159, Benoit Meger, Maria Waldhoer, Martin Konrad Ostermaier, Philipp Berger, Mirjam Zimmermann, *Jan 2019*
- **Poster prize**, *GPCR symposium 2017, Zürich Area, Switzerland*  
« Comprehensive approach for the development of novel arrestin-3 biosensors tracking GPCR biased signaling »
- **COST Fellowship**, *European Proteomics Association (EuPA) Fellowship for Educational Program, Milan, Italy, Sep 2014 – Mar 2015*
- **Erasmus fellowship**, *Europe Coaching Association, Dublin, Ireland, Apr 2015 – Aug 2015*

## CERTIFICATIONS

---

- **Good pharmacovigilance practice training**, *ETH Zürich, Switzerland, Feb 2019*
- **Good clinical practice training for investigators and study teams**, *Swiss Tropical and Public Health Institute, Basel, Switzerland, Dec 2019*
- **Signal detection and causality assessment in pharmacovigilance**, *Uppsala Monitoring Center, Nov 2018*
- **Statistical reasoning and algorithms in pharmacovigilance**, *Uppsala Monitoring Center, Nov 2018*